Investigation into the Functions of Sumoylation in Yeast

Clare Lewis

Thesis submitted for the degree of Doctor of Philosophy

Faculty of Medical Sciences

Institute for Cell and Molecular Biosciences

Newcastle University

September 2016

Declaration

I certify that this thesis is my own work, except where acknowledged, and has not been previously submitted for a degree or any other qualification at this or any other university.

Abstract

Small ubiquitin modifier (SUMO) is a ubiquitin-like modification that regulates many fundamental processes in eukaryotes such as DNA damage and repair, cell cycle, stress responses and gene expression. Sumoylation is essential for viability in the model organisms *Saccharomyces cerevisiae*, *Drosophila melanogaster, Caenorhabditis elegans*, and is embryonic lethal in mice. Conversely, sumoylation is dispensable for growth in the fission yeast *Schizosaccharomyces pombe*. High throughput proteomic approaches have detected many sumoylated substrates in a large number of cellular processes, however, the biological function of sumoylation in many of these processes, as well as the essential processes in *S. cerevisiae* and mammals, have not been elucidated.

To gain insight into the biological functions of sumoylation in eukaryotes, we aimed to take advantage of the viability of sumoylation mutants and large scale deletion collections available in *S. pombe* to study the process via a high throughput genetic screening. Although the sumoylation mutants studied were found unsuitable for genetic screening, characterisation of the cell cycle defects observed in the mutants revealed that cells lacking sumoylation exhibited abnormal expression of cell cycle dependant genes. The gene transcripts affected by lack of sumoylation are normally regulated by a conserved family of forkhead transcription factors, and this study indicates that sumoylation acts specifically to repress forkhead dependant gene expression. A conserved forkhead transcription factor homolog in human cells has been previously identified as a sumoylated substrate, but the effect of sumoylation on the activity of the transcription factor was unclear. Our data therefore suggests that sumoylation may be a conserved negative regulator of cell cycle regulated gene transcription in eukaryotes.

To further increase our understanding of sumoylation, a high throughput screening approach was used in *S. cerevisiae*. The SUMO encoding gene, *SMT3*, is essential in *S. cerevisiae*, hence a hypomorphic *smt3* allele was screened against a genomic library of mutants. Excitingly, through this approach, we identified that perturbation of highly conserved cytoskeleton proteins, involved in filamentous actin (F actin) dynamics and tubulin, suppressed the slow growth defect associated with misregulated sumoylation. This novel observation suggests that a major role of sumoylation in eukaryotes is in cytoskeleton regulation.

Aberrant sumoylation is implicated in many disease states, such as cancer, pathogenic infection, and neurodegenerative disease. Furthermore, forkhead transcription factors have been implicated in human cancers, and F actin dynamics are often misregulated in cancer and viral and bacterial infection. Thus, understanding the mechanism of sumoylation underpinning these processes have potential impacts for human health.

Acknowledgements

I would firstly like to thank my supervisor, Brian Morgan, for his enthusiasm and cheer throughout this project, for bringing the well needed data-optimism to my data-pessimism, and allowing me to make this project my own. I would also like to acknowledge the Newcastle Biomedical Research Centre for funding this research.

I would also like to thank Peter Banks and Adrian Blackburn in the High Throughput Facility at Newcastle University for the use of the robotics for the SGA analysis in this thesis, as well catering for the many requests for yeast strains over the course of this study.

In addition, I would like to thank all the supervisors and members of the Quinn, Veal, and Whitehall labs, past and present, for discussion and ideas throughout this project. Special thanks to Alison, Ellen, Csénge, Lewis, Melanie, Faye M., Pippa, Johny, Alex, Zoe and Faye C., for being the best bunch of people to work with. A little extra special mention goes to Heather, the better half of Cleather, as I'm not sure I would have even passed my BSc without your organisational skills.

Finally, a huge thank you to my family - Mam, Dad, and Jess - for listening to my kitchen-based laboratory analogies much longer than most would. I couldn't have done this without your support over the years, and the belief that I can do it (no matter how much I try to convince you otherwise). Remember, even carrots have DNA!

Table of Contents

Abbreviations

·OH	Hydroxyl radicals
A. thalania	*Arabidopsis thalania*
APC/C	Anaphase promoting complex/cyclosome
APP	Amyloid precursor protein
BSA	Bovine serum albumin
C. albicans	*Candida albicans*
CDK	Cyclin Dependant Kinase
C. elegans	*Caenorhabditis elegans*
CCT	Chaperonin Containing TCP-1
CELO	Chicken embryo lethal orphan
D. melanogaster	*Drosophila melanogaster*
DAmP	Decreased Abundance by mRNA Perturbation
DAPI	4',6-diamidino-2-phenylindole
DIC	Differential Interference Contrast
DMSO	Dimethyl sulfoxide
E. coli	*Escherichia coli*
EBV	Epstein-Barr virus
EDTA	Ethylenediaminetetraacetic acid
EMM	Edinburgh minimal medium
ESM	Enriched sporulation media
F actin	Filamentous actin
G actin	Globular actin
gDNA	Genomic DNA
GO	Gene Ontology
GIS	Genetic Interaction Score
H. sapiens	*Homo sapiens*
H_2O_2	Hydrogen peroxide
HAdV5	Human adenovirus serotype 5
HCSM	Hydrophopic cluster motif
HGPS	Hutchinson Guilford Progeria Syndrome
HMW	High molecular weight
HR	Homologous Recombination
HRP	Horseradish peroxidase
HSFs	Heat shock factors
HU	Hydroxyurea
IP	Immunoprecipitation
LLO	Listeriolysin O
MAPK	Mitogen-activated protein kinase
MBF	MluI cell cycle box-Binding Factor
MCB	MluI cell Cycle Box
MCC	Mitotic checkpoint complex
MMS	Methyl methanesulfonate
NDSM	Negatively charged amino acid dependant motif
NEM	N-Ethylmaleimide

NHEJ	Non-Homologous End Joining
O_2^-	Superoxide
PCB	Pombe cell cycle Box
PCR	Polymerase chain reaction
PDSM	Phosphorylation dependant motif
PEG	Polyethylene glycol
PFO	Perfingolysin
PLY	Pneumolysin
PML-NBs	Promyelocytic leukaemia protein nuclear bodies
PMSF	Phenylmethane sulfonyl fluoride
qRT-PCR	Qualitative real-time polymerase chain reaction
ROS	Reactive oxygen species
S. cerevisiae	*Saccharomyces cerevisiae*
S. pombe	*Schizosaccharomyces pombe*
SAC	Spindle assembly checkpoint
SD	Synthetic dextrose
SD/MSG	Synthetic dextrose/monosodium glutamate
SDS	Sodium dodecyl sulfate
SGA	Synthetic Genetic Array
SIM	SUMO interaction motif
SSR	SUMO stress response
STUbL	SUMO Targeted Ubiquitin Ligase
TBS	Tris Buffered Saline
TBZ	Thiabendazole
TCA	Trichloroacetic acid
TE	Tris EDTA
ts	Temperature sensitive
Ubl	Ubiquitin-like modifier
UV	Ultraviolet
YE5S	Yeast extract 5 supplements
YFG	Your Favourite Gene
YPD	Yeast extract peptone dextrose

List of Figures

List of Tables

Chapter One: Introduction

1.1 Protein Modification by the Small Ubiquitin like Modifier SUMO

Post translational modification of proteins, such as phosphorylation, acylation, glycosylation, or acetylation allows cells to modify the activity of protein targets. Addition or removal of a chemical moiety can alter the activity, stability, or subcellular location of a protein substrate, allowing broadening of the range of functionality beyond the initial amino acid sequence. Further to the smaller chemical post translational modifications that a cell may utilise, there is also a subset of post translational modifiers which are themselves small proteins. This family of proteins are the Ubiquitin-like modifiers (Ubls), which share similarity to the founding member ubiquitin. Addition of these small protein moieties to target proteins leads to the formation of branched proteins. Due to the increased interaction surface provided by a small protein versus a small chemical moiety such as phosphorylation, these branched proteins provide a large scope of potential changes in functionality. One such protein modifier is the Small Ubiquitin like Modifier (SUMO). Since the initial discovery of SUMO, it has been found to have many roles in protein localisation and activation, and is linked to the regulation of key cellular processes including gene transcription, cell cycle regulation, DNA damage and repair and stress responses (Singh *et al.*, 2012).

1.1.1 SUMO - Part of the Ubiquitin-like Modifier Family

After the discovery of the founding member ubiquitin, many other Ubl protein modifiers, like SUMO, have been identified in eukaryotes (Table 1.1). Members of the Ubl family share a number of common characteristics. Firstly, Ubls are generally conjugated to their target substrates via a conserved E1 activation, E2 conjugation and E3 ligase enzyme pathway (Figure 1.1) (Jentsch and Pyrowolakis, 2000). Secondly, while the amino acid sequence conservation between Ubl members is surprisingly low, they share a similar 3D globular β-grasp structure, termed a "ubiquitin fold" (Figure 1.2) (Jentsch and Pyrowolakis, 2000). Thirdly, most Ubls are translated as an immature precursor that requires processing at a conserved C-terminal diglycine motif before they can be conjugated to targets (Figure 1.2). Despite the similarities described above, individual Ubl members have unique characteristics, highlighting the diversity of the family. For instance, the ubiquitin system encodes a large number of E1, E2 and E3 enzymes in comparison to the other Ubl proteins (Table 1.1). In contrast, the Ubl Urm1 is conjugated to its targets without an E2 or E3 enzyme (Table 1.1). Furthermore, Urm1 is translated with the C-terminal diglycine motif already exposed, meaning it does not undergo proteolytic cleavage before conjugation (Figure 1.2). The autophagy proteins (Atg3, 5, 7, 8, 10 and 12 in yeast) form two interconnected Ubl signalling pathways, where the conjugation of the Ubl Atg12 to Atg5 creates a new E3 ligase (Otomo *et al.*, 2013).

Ubl	E1	E2	E3	Targets	Cellular Roles
Ubiquitin	Uba1 (~16 in mammalian cells) (Kouranti *et al.*, 2010)	Ubc1-13 (~40 in mammalian cells) (Metzger *et al.*, 2012)	~80 in yeast (~600 in mammalian cells) (Metzger *et al.*, 2012)	Many	Mono ubiquitination – chromatin remodelling, endocytosis K48 linkages – target for protein degradation K63 linkages – postreplicative repair (Komander, 2009)
Smt3 (SUMO-1, SUMO-2/3)	Aos1/Uba2 (SAE1/UBA2)	Ubc9	Siz1, Siz2, Mms21, Zip3 (15 identified in mammalian cells) (Watts, 2013)	Many	DNA damage and repair, cell cycle progression, transcriptional regulation, stress responses
Rub1 (NEDD8)	Uba3/Ula1 (UBA3/AppBp1)	Ubc12 (UBE2M)	Many	Cullin subunits of ubiquitin E3 ligases	Meiosis to mitosis transition
Urm1	Uba4 (MOCS3)	-	-	Many	Nutrient sensing, stress responses, sulphur donation (Goehring *et al.*, 2003)
Atg12	Atg7	Atg10	-	Atg5	Autophagy (Otomo *et al.*, 2013)
Atg8 (LC3 family)	Atg7	Atg3	Atg12~Atg5	Phosphatydylethylamine	Autophagy (Otomo *et al.*, 2013)

Table 1.1: The Ubl family members share common conjugation pathway, but have diverse cellular roles and targets. The conjugation pathways and target substrates of ubiquitin and the Ubl members SUMO (Smt3 in *S. cerevisiae*), NEDD8 (Rub1 in *S. cerevisiae*), Urm1, Atg8 and Atg12. Examples of the known cellular roles of the Ubl are indicated. *S. cerevisiae* enzymes are shown, and mammalian homologs included in brackets. Modified from figure in (Jentsch and Pyrowolakis, 2000).
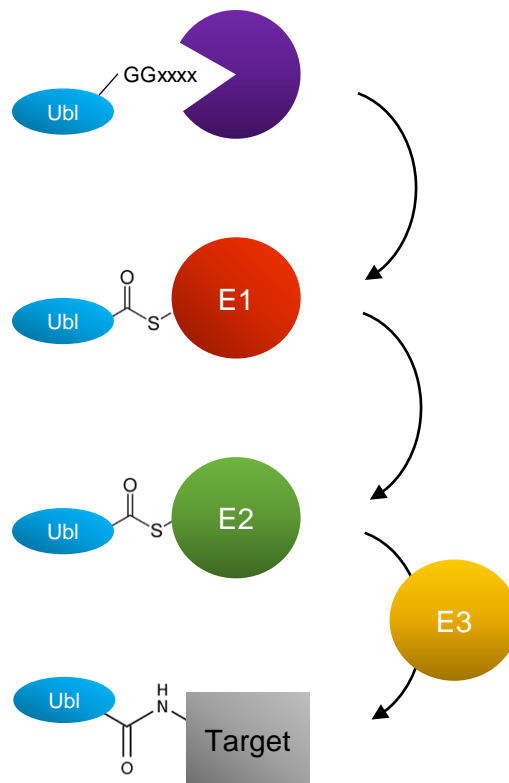
Figure 1.1: Ubiquitin and the Ubl proteins are conjugated to protein substrates via a conserved enzymatic pathway. Ubl proteins are commonly processed at a diglycine motif before activation by an E1 activating enzyme. The activated Ubl is then transferred to the E2 conjugating enzyme, and the Ubl finally conjugated via an E3 ligase.

```
Smt3       MSDSEVNQEAKPEVK--PEVKPETHINLKVS-DGSSEIFFKIKKT--------------T
SUMO-1     MSDQ----EAKPSTEDLGDKKEGEYIKLKVIGQDSSEIHFKVKMT--------------T
SUMO-2     MADE----KPKE----GVKTENNDHINLKVAGQDGSVVQFKIKRH--------------T
SUMO-3     MSEE----KPKE----GVKTE-NDHINLKVAGQDGSVVQFKIKRH--------------T
Ubiquitin  -----------------------MQIFVKTLTGKTITLEVESS--------------D
Urm1       ----------------------MVNVKVEFLGGLDAIFGKQRVHKIKMDKEDPVTVGD
Rub1       ------------------------MIVKVKTLTGKEISVELKES--------------D
                                   : : *       .     . :

Smt3       PLRRLM----------EAFAKRQGKEMDSLRFLYDGIRIQADQTPEDLDMEDNDIIEAHR
SUMO-1     HLKKLK----------ESYCQRQGVPMNSLRFLFEGQRIADNHTPKELGMEEEDVIEVYQ
SUMO-2     PLSKLM----------KAYCERQGLSMRQIRFRFDGQPINETDTPAQLEMEDEDTIDVFQ
SUMO-3     PLSKLM----------KAYCERQGLSMRQIRFRFDGQPINETDTPAQLEMEDEDTIDVFQ
Ubiquitin  TIDNVK----------SKIQDKEGIPPDQQRLIFAGKQLEDGRTLSDYNIQKESTLHLVL
Urm1       LIDHIVSTMINNPNDVSIFIEDDSIRPGIITLINDTDW--ELEGEKDYILEDGDIISFTS
Rub1       LVYHIK----------ELLEEKEGIPPSQQRLIFQGKQIDDKLTVTDAHLVEGMQLHLVL
             : .:          .   . :.        :          : :.   :

Smt3       EQIGGATY*--------
SUMO-1     EQTGGHST*--------
SUMO-2     QQTGGVY*---------
SUMO-3     QQTGGVPESSLAGHSF*
Ubi        RLRGGN*----------
Urm1       TLHGG*-----------
Rub1       TLRGGN*----------
```

Figure 1.2: Sequence homology of ubiquitin and Ubl proteins. Protein sequence alignment of Smt3, human SUMO-1/2/3, ubiquitin, Urm1. Atg12 amino acid sequence is unrelated to ubiquitin, so it not included here. The N-terminal extension conserved across SUMO proteins is indicated in orange. The conserved diglycine motif found in Ubls is indicated in green. Modified from (Jentsch and Pyrowolakis, 2000).

4

While most Ubls are conjugated to other proteins, the action of the Atg12~Atg5 E3 ligase targets the autophagy Ubl Atg8 (member of the LC3 family in mammals) to the phospholipid phosphatydylethylamine (Otomo *et al.*, 2013) (Table 1.1).

Sumoylation has been found to be an essential process in most eukaryotic model organisms. Loss of sumoylation in the nematode worm *Caenorhabditis elegans*, fruit fly *Drosophila melanogaster* and mice is embryonic lethal due to errors in chromosomal segregation (Jones *et al.*, 2002; Nacerddine *et al.*, 2005; Talamillo *et al.*, 2008). Furthermore, in budding yeast *Saccharomyces cerevisiae*, most genes involved in the SUMO pathway are essential for cell viability (Dieckhoff *et al.*, 2004). This is similar to ubiquitin, where the gene encoding the sole E1 activation enzyme *UBA1* is essential (Giaever *et al.*, 2002). In contrast, the other Ubl genes *URM1*, *RUB1*, *ATG8* and *ATG12* are non-essential in *S. cerevisiae* (Giaever *et al.*, 2002). Interestingly, however, sumoylation is not essential for viability in the fission yeast *Schizosaccharomyces pombe* and the opportunistic fungal pathogen *Candida albicans* (Tanaka *et al.*, 1999; Leach *et al.*, 2011). However, both *S. pombe* and *C. albicans* cells deficient in sumoylation exhibit poor growth and cell morphology defects.

Although SUMO is conserved across eukaryotes, organisms contain variable numbers of SUMO encoding genes. For example, *C. elegans* (*smo-1*), *D. melanogaster* (*smt3⁺*), *S. cerevisiae*, (*SMT3*) and *S. pombe* (*pmt3⁺*) all contain one copy of a SUMO encoding gene. There are many more SUMO encoding genes in the plant model system *Arabidopsis thalania*, which encodes 8 copies of the SUMO gene (*AtSUM1-7*, *9*) (Kurepa *et al.*, 2003). Furthermore, humans express 4 SUMO homologs, SUMO-1, -2, -3 and -4. SUMO-1 protein is most similar to the yeast proteins (Tanaka *et al.*, 1999; Takahashi *et al.*, 1999). SUMO-2 and SUMO-3 have 96% amino acid identity to each other (and are often referred to as SUMO-2/3 in literature), but only have 46% identity with SUMO-1 (Watts, 2013). Additionally, differing conjugation dynamics and cellular targets of SUMO-1 and SUMO-2/3 suggests that the two proteins are from distinct families (Saitoh and Hinchey, 2000). SUMO-4 does not appear to be able to be covalently conjugated to targets, as it cannot be processed from the immature precursor (Owerbach *et al.*, 2005). Like most other Ubl proteins, SUMO is produced as an immature precursor, that requires processing at a diglycine motif before it can be conjugated (Figure 1.2) (see section 1.1.3). Comparison of SUMO amino acid sequences to the other Ubl family members also reveals a unique N-terminal tail conserved in SUMO proteins (Bayer *et al.*, 1998) (Figure 1.2).

1.1.2 SUMO Conjugation

Like many members of the Ubl family, the pathway to SUMO conjugation follows the E1, E2 E3 ligation pathway. The conjugation (and subsequent removal) of SUMO from cellular targets in budding yeast is shown in Figure 1.3. For the *S. cerevisiae, S. pombe* and mammalian homologs of conjugation enzymes, see Table 1.2.

1.1.2.1 The Sumoylation Consensus Motif

Alignment of acceptor lysine residues of known SUMO-1 targets in mammalian cells revealed the presence of a simple consensus sequence for sumoylation, ψ-K-x-D/E, where ψ is a large hydrophobic residue, K is the acceptor lysine, x is any amino acid, and D/E is aspartic or glutamic acid. (Rodriguez *et al.*, 2001; Sampson *et al.*, 2001). However, it is estimated that ~75% of SUMO substrates occur within consensus motifs, thus sumoylation of a non-consensus motif is not an uncommon event (Xu *et al.*, 2008a). Furthermore, due to the very simple nature of the consensus motif, not all consensus motifs found within the proteome are sumoylated.

Interestingly, variants of the simple consensus sequence have been identified in mammalian cells. One example is the phosphorylation dependant motif (PDSM) Ψ-K-x-E-x-x-S-P, where the phosphorylation of the serine residue downstream of the consensus motif increases the sumoylation of the substrate (Hietakangas *et al.*, 2006). A further extended variant of the consensus motif is the negatively charged amino acid-dependant sumoylation motif (NDSM), where acidic amino acids within the 10 residues downstream of the consensus motif of a substrate increases the efficiency of sumoylation (Yang *et al.*, 2006). Increased sumoylation of NDSM containing substrates is dependent upon a corresponding positively charged region of Ubc9, suggesting that the basic patch on Ubc9 electrostatically binds the negatively charged NDSM region (Yang *et al.*, 2006). As both the PDSM and NDSM introduce a negative charge to the region immediately downstream to the target lysine, it would suggest that the PDSM consensus motif also recruits Ubc9 in this manner.

Most recently, due to improvement in mass spectrometry protocols, two new variants of the sumoylation consensus motif were identified. Firstly, the inverted sumoylation motif, E/D-x-K-ψ, where the consensus is reversed. Secondly, the hydrophobic cluster motif (HCSM) ψ-ψ-ψ-K-x-D/E, in which the hydrophobic amino acid found in the original consensus is extended by a further two residues (Matic *et al.*, 2010; Impens *et al.*, 2014). These consensus sequences have been less well characterised in how they affect the efficiency of sumoylation.
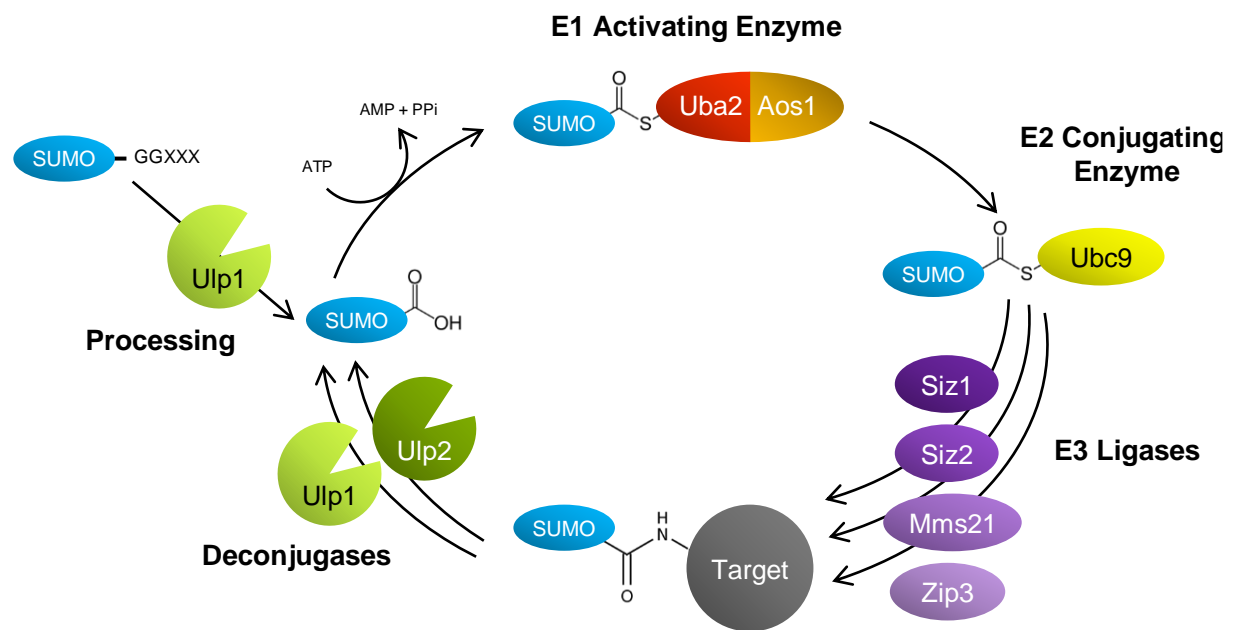
Figure 1.3: Pathway of SUMO conjugation in *S. cerevisiae*. SUMO is processed by the Ulp1 protease at a conserved C terminal diglycine motif to expose the carboxyl group of the terminal glycine. The SUMO then forms a thioester bond between the catalytic cysteine of the Uba2 subunit of the E1 activating heterodimer Aos1/Uba2 via an ATP dependant reaction. SUMO is then transferred to a cysteine residue in the E2 conjugating enzyme Ubc9. Ubc9 alone can modify identified targets, but most sumoylation requires the action of an E3 ligase of which there are 3 known in *S. cerevisiae*: Siz1, Siz2, Mms21 and Zip3. SUMO can be removed from its substrates by the deconjugases Ulp1 and Ulp2, which are specific to individual targets. Adapted from (Geiss-Friedlander, 2007).

Protein	*S. cerevisiae*	*S. pombe*	Mammalian
SUMO	Smt3	Pmt3	SUMO-1 SUMO-2 SUMO-3 SUMO-4
SUMO deconjugases	Ulp1	Ulp1	SENP-1 SENP-2 SENP-3 SENP-5
	Ulp2	Ulp2	SENP-6 SENP-7
	-	-	DeSI-1 USPL1
SUMO activating enzyme (E1)	Aos1 Uba2	Rad31/Uba4 Fub2/Uba2	SAE1 SAE2
SUMO conjugating enzyme (E2)	Ubc9	Ubc9/Hus5	Ubc9
SUMO ligase (E3)	Siz1 Siz2	Pli1	PIAS1 PIAS3 (PIAS3, PIAS3L) PIAS2 (PIASxα, PIASxβ) PIAS4 (PIASγ, PIASyE6-)
	Mms21	Pli2/Nse2	MMS21/NSE2
	Zip3	-	-
	-	-	RanBP2 HDAC4 HDAC7 Pc2 Topors KAP1 co-repressor Fus

Table 1.2: SUMO conjugation pathway enzymes and their homologs in *S. cerevisiae, S. pombe* and mammalian cells*. Isomers from alternate splicing are shown in brackets. Adapted from (Watts, 2013).

1.1.2.2 E1 Activation

Once processed, SUMO is then activated by an E1 activating enzyme. In most other Ubl conjugation pathways this is normally a monomer (Hochstrasser, 2000), however in the sumoylation pathway this activation is completed by a heterodimer of two essential subunits, Aos1 and Uba2 (Johnson *et al.*, 1997). Alignment of the domain structures of *S. cerevisiae* Aos1 and Uba2 with the monomeric ubiquitin E1 Uba1 suggested that Aos1 and Uba2 would function together as a heterodimer to activate Smt3 (Johnson *et al.*, 1997). Indeed, similarly to ubiquitin activation, Aos1/Uba2 uses ATP to adenylate the processed C-terminal diglycine of Smt3, which is then used to form a high energy thioester intermediate between Smt3 and the catalytic cysteine (Cys177 in *S. cerevisiae*) within the E1 domain of Uba2 (Johnson *et al.*, 1997). The E1 then catalyses the transfer of the activated Smt3 thioester onto the E2 conjugating enzyme, Ubc9. The interaction of the E1 and E2 is mediated by a ubiquitin fold domain within the C terminus of Uba2, and the N terminus of Ubc9 (Wang *et al.*, 2010). The loss of the ubiquitin fold domain of Uba2 is lethal in *S. cerevisiae*, potentially due to the loss of this interaction and the subsequent failure of Smt3 being passed to Ubc9 (Lois and Lima, 2005). Interestingly, sumoylation of Uba2 has been detected in mammalian cells, which inhibits the ability of the SUMO thioester to be transferred from the E1 enzyme to the E2 (Truong *et al.*, 2012).

1.1.2.3 E2 Conjugation

Unlike ubiquitination, which has many E2 conjugation enzymes, Ubc9 is the only E2 of the SUMO modification pathway identified to date in eukaryotes (Table 1.2) (Figure 1.3). Furthermore, like many sumoylation components, *UBC9* essential in *S. cerevisiae* (Seufert *et al.*, 1995; Johnson and Blobel, 1997; Dieckhoff *et al.*, 2004). Interestingly, the strain background appears to be linked to Ubc9 function, encoded by *hus5*[+], in *S. pombe* (for ease I will refer to *hus5*[+] as its alias *ubc9*[+] for the remainder of this study). In particular, two studies found *ubc9*[+] to be essential (al-Khodairy *et al.*, 1995; Kim *et al.*, 2010), whereas other publications indicated the *ubc9*[+] gene to be non-essential (Hayles *et al.*, 2013). If *pmt3*[+] and *ubc9*[+] do indeed have differing phenotypes, this could suggest a sumoylation-independent role for Ubc9 in *S. pombe*. In both *S. pombe* and *S. cerevisiae,* Ubc9 was found to localise predominantly in the nucleus (Griffiths *et al.*, 1995; Srikumar *et al.*, 2013). In mammalian cells, there are two cellular pools of Ubc9; one Ubc9 pool is bound to the cytosolic face of the nuclear pore complex by RanBP2 (Saitoh *et al.*, 2002), and another Ubc9 pool is located in the cytoplasm, which can shuttle to the nucleus via the RanGTP-regulated nuclear import protein Importin13 (Grunwald and Bono, 2011).

As described above (see section 1.1.2.2), the ubiquitin fold domain of the E1 Aos1/Uba2 complex interacts with the N terminus of the E2 Ubc9 (Wang *et al.*, 2010). This interaction allows the SUMO thioester to be transferred from the E1 enzyme to the catalytic cysteine of Ubc9 (Cys93 in *S. cerevisiae*). Indeed, further support for the importance of the N-terminal of Ubc9 for E1-E2 interaction is indicated by studies of site mutants within the N terminus of *S. cerevisiae* Ubc9, which were found to reduce Ubc9~Smt3 thioester formation by weakening the interaction of the E1 and E2 *in vitro* (Bencsath *et al.*, 2002).

For ubiquitination to occur, many combinations of E2 and E3 ligases can be employed to gain target specificity (Table 1.1). Although most sumoylation events require an E3 ligase *in vivo* (see section 1.1.2.4), sumoylation is unusual among ubiquitin and the Ubls in that the E2 can sumoylate target proteins directly. Studies suggest that this is in part due to direct Ubc9 interaction with the consensus motif. For example, mutation of residues of the surface surrounding Cys93 in Ubc9, that are in direct contact with the sumoylation consensus motif, reduces the sumoylation of a wide array of sumoylation targets in mammalian cells, including RanGAP1, p53, IκBα, c-Jun and E2-25K (Bernier-Villamor *et al.*, 2002; Lin *et al.*, 2002; Pichler *et al.*, 2005). Furthermore, the modification of Ubc9 can influence target specificity. For instance, autosumoylated Ubc9 has been detected in a variety of proteomic studies in both *S. cerevisiae* and mammalian cells (Wohlschlegel *et al.*, 2004; Zhou *et al.*, 2004; Denison *et al.*, 2005; Knipscheer *et al.*, 2008). One study into the role of Ubc9 autosumoylation in mammalian cells identified Lys14 as a site for sumoylation (Knipscheer *et al.*, 2004). This study showed that autosumoylation of Ubc9 changed subsequent sumoylation of sumoylation targets, depending if these targets contained sumo interaction motifs, or SIMs (see section 1.1.5). Although Ubc9 autosumoylation is also detected in *S. cerevisiae*, the site of sumoylation does not appear to be conserved. Systematic mutational analysis of lysine residues within *S. cerevisiae* Ubc9 demonstrated that Lys153 is the major sumoylation site of Ubc9 (Ho *et al.*, 2011). Sumoylation of Lys157 was also detected, but it was found to modified at a relatively lower level than Lys 153 (Ho *et al.*, 2011). Interestingly, loss of the K153R/K157R modification sites of Ubc9 increased the *in vivo* sumoylation of septins, well characterised sumoylation targets in *S. cerevisiae* (see section 1.2.2.3) (Ho *et al.*, 2011). The authors proposed that sumoylation of Ubc9 inhibited the interaction between Ubc9 and cellular targets, and this was a negative feedback mechanism to prevent excessive sumoylation (Ho *et al.*, 2011). Further study into Ubc9 sumoylation in *S. cerevisiae* revealed that sumoylated Ubc9 was defective in formation of the Ubc9~Smt3 thioester *in vitro* (Klug *et al.*, 2013).

1.1.2.4 E3 Ligases

In ubiquitination, more E2 enzymes are available than E1 enzymes, and more E3 ligases than E2 enzymes, allowing increasing specificity through the conjugation pathway (Table 1.1). It is

therefore striking how the SUMO pathway has far fewer identified E3 ligases in comparison. To date, only 4 have been identified in *S. cerevisiae*; Siz1, Siz2, Mms21 and Zip3; and 2 in *S. pombe;* Pli1 and Nse2; all of which are Siz-PIAS-RING (SP-RING) domain ligases (Table 1.2). Humans encode 4 SP-RING ligase genes, PIAS-1,2,3 and 4, which also undergo alternate splicing (Table 1.2). Human cells also express other SUMO E3 ligases which lack the canonical SP-RING domain, such as the nucleoporin Nup358/RanBP2 (Pichler *et al.*, 2002), the histone deacetylases HDAC4 (Gregoire and Yang, 2005) and HDAC7 (Gao *et al.*, 2008), the polycomb-group protein Pc2 (Kagey *et al.*, 2003), and the topoisomerase I-binding protein Topors (Table 1.1) (Weger *et al.*, 2005). These highlight the higher complexity of the sumoylation system in mammalian systems. However, as there are no apparent homologs in yeast, these will not be discussed at length here.

The SUMO ligases Siz1 and Siz were identified in *S. cerevisiae* in screens for suppressors of an *ulp2* mutant (Strunnikov *et al.*, 2001). The Siz proteins were successfully identified as SUMO E3 ligases, as sequence alignment revealed RING-like domains found in ubiquitin E3 ligases (Johnson and Gupta, 2001; Takahashi *et al.*, 2001b). Indeed, like the RING domain ubiquitin E3 ligases, Siz/PIAS-RING (SP-RING) ligases act as a scaffold to bind the target and Ubc9 in position for optimal conjugation of SUMO to target substrates (Yunus and Lima, 2009). Similarity between Siz1 and Siz2 is mostly found at the N terminus over the SAP domains and the SP-RING domain (42% amino acid sequence identify over ~470 amino acids of the N-terminus), but the C-terminals convey very little sequence similarity (Johnson and Gupta, 2001). Interestingly, in contrast to the other genes within the sumoylation pathway, both *SIZ1* and *SIZ2* are not essential in *S. cerevisiae* (Johnson and Gupta, 2001). Furthermore, *siz1*Δ and *siz2*Δ single mutants have no obvious phenotypes or growth defects. (Johnson and Gupta, 2001). However, the *siz1*Δ *siz2*Δ double mutant displays a mass reduction in global sumoylation along with an apparent G_2/M delay, and slower growth, particularly at cold temperatures (Johnson and Gupta, 2001; Chen *et al.*, 2005). The molecular basis of these defects in not well understood, although it has been shown that some of the *siz1*Δ *siz2*Δ associated growth defects are due to the increased copy number of the endogenous 2µm plasmid (Chen *et al.*, 2005). Global analysis of Smt3 conjugation revealed that Siz1 and Siz2 mostly sumoylate separate substrates, with ~25% overlap between targets (Makhnevych *et al.*, 2009; Srikumar *et al.*, 2013). However, most likely due to the ability of Ubc9 to bind to consensus motifs without an E3 ligase, both Siz1 and Siz2 both recognise and sumoylate the same targets in *in vitro* reconstitution experiments (Takahashi *et al.*, 2003), raising the question of how these proteins discriminate targets *in vivo*. Studies of the domains within the SP-RING ligases have provided insight into this.

The Siz-PIAS E3 ligases contain four domains, which are conserved from the *S. cerevisiae* E3 ligases Siz1 and Siz2, the *S. pombe* E3 ligase Pli1 and the human PIAS proteins (the example PIAS1 is shown) (Figure 1.4). An N-terminal SAP domain has been shown to bind DNA in the human E3 PIAS1 (Okubo *et al.*, 2004). The PINIT domain was identified in PIAS E3 ligases in higher eukaryotes by a proline, isoleucine, asparagine, isoleucine, threonine motif (hence "PINIT" domain), and this conserved region in the Siz-PIAS E3 ligases confers a degree of substrate specificity (Yunus and Lima, 2009; Mautsa *et al.*, 2011; Duval *et al.*, 2003; Mautsa *et al.*, 2011). The SP-RING domain is required for SUMO ligase activity in all SUMO E3 ligases discovered in *S. cerevisiae*, including the E3 ligases Mms21 and Zip3 (Zhao and Blobel, 2005; Cheng *et al.*, 2006). Most SP-RING E3 ligases contain a SIM motif (see section 1.1.4), positioned downstream of the SP-RING domain. Siz1 contains a unique C-terminal, which is important for bud neck localisation. It is of note that Mms21 and Zip3 do not contain SAP or PINIT domains. This is most likely because these E3 ligases are part of a protein complex, and as such the protein complex helps target the E3 ligases to targets.

In *S. cerevisiae*, much of sumoylation target specificity is dictated by the differing intracellular localisation of Siz1 and Siz2. Siz1 resides in the nucleus, but upon completion of mitosis is exported from the nucleus to sumoylate cytoplasmic targets, such as the septins at the bud neck (Makhnevych *et al.*, 2007) (see section 1.2.2.3). The cell cycle nuclear export requires the C-terminal domain unique to this ligase (Reindle *et al.*, 2006). However, mutations in the SAP, PINIT or SP-RING domain mutants of mammalian PIAS3L cause the E3 to lose nuclear localisation (Duval *et al.*, 2003). This suggests it is not the direct DNA binding of the ligase, but correct target sumoylation provided by targeting through the SAP domain, that promotes nuclear accumulation of the SP-RING ligases (Duval *et al.*, 2003). Conversely, Siz2 is only detected within the nucleolus, a site within the nucleus for ribosome biogenesis and assembly (Srikumar *et al.*, 2013). Furthermore, the highly variable PINIT domain also is important in substrate specificity. For example, the helicase PCNA is sumoylated by both Siz1 and Siz2, but at differing sites (Pfander *et al.*, 2005; Parker *et al.*, 2008). Indeed, the Siz1 PINIT domain increased the sumoylation of PCNA, and structural studies revealed that the PINIT domain bound to PCNA (Reindle *et al.*, 2006; Yunus and Lima, 2009).
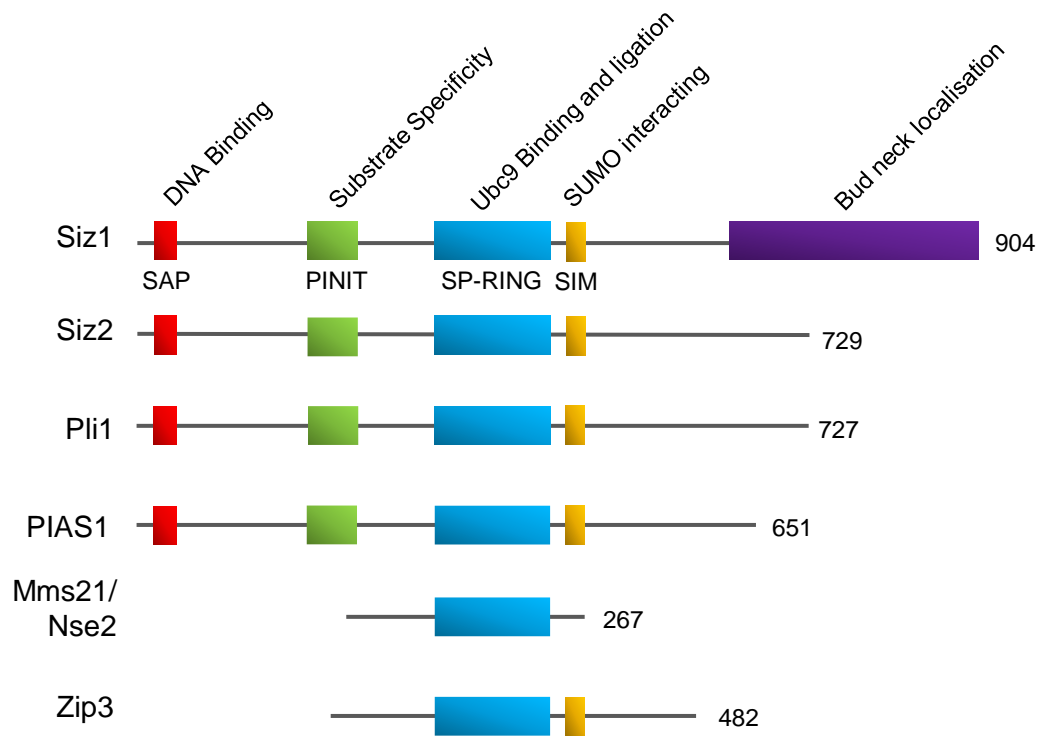
Figure 1.4: Domain structure of the SP-RING containing SUMO E3 ligases. Domain structures of the E3 ligases Siz1, Siz2, Mms21 and Zip3 from *S. cerevisiae*, Pli1 from *S. pombe*, and the human PIAS1. SAP DNA binding domains are indicated in red. The PINIT domains, required for substrate specificity, are indicated in green. The SP-RING domains, required for Ubc9 binding and target sumoylation, are indicated in blue. SIM domains, which bind to SUMO moieties, are indicated in yellow. The bud neck localisation domain unique to Siz1 is indicated in purple.

The other E3 ligases, Mms21 and Zip3, were identified more recently. Mms21 functions as part of the Smc5/6 (Structural Maintenance of Chromosomes) complex in *S. cerevisiae*, which is essential for the correction of toxic recombination intermediates (Zhao and Blobel, 2005). Interestingly, while complete deletion of this gene is required for viability, mutant Mms21 lacking a SP-RING domain can support growth, suggesting the sumoylation it performs is not essential (Zhao and Blobel, 2005). Furthermore, while sumoylation is non-essential in *S. pombe*, the Mms21 homolog Nse2 is required for growth, further suggesting that sumoylation is not the essential role. It is therefore likely that the essential cellular role of Mms21 is in supporting the structure of the Smc5/6 complex. Following the discovery of Mms21 as an E3 ligase, Zip3 was uncovered as another Smt3 E3 ligase in *S. cerevisiae.* During meiosis a large protein complex, named the synaptonemal complex, forms along the length of homologous sister chromatids (Cheng *et al.,* 2006). This complex is thought to aid in DNA recombination and chiasma formation by scaffolding the chromatids together and by recruitment of necessary factors. Zip3 was found to globally sumoylate proteins along the length of the synaptonemal complex (Cheng *et al.*, 2006). Moreover, these Smt3-modified proteins are likely to interact with the major synaptonemal complex protein Zip1, aiding the formation of this complex during meiosis (Cheng *et al.*, 2006). As both Mms21 and Zip3 form part of a protein complexes, the surrounding proteins within the complexes could aid in recruiting the E3 ligases to the target substrates, negating the need for the SAP or PINIT domains of the other ligases (Figure 1.4).

1.1.3 SUMO Deconjugation

SUMO is a mostly transient modification that is rapidly removed from its targets by deconjugase enzymes. In *S. cerevisiae*, there are 2 known deconjugases, Ulp1 and Ulp2. Alignment of the 621 residue Ulp1 and 1,034 reside of Ulp2 protein sequence revealed sequence similarity within a 200 amino acid region containing the catalytic triad of histidine, aspartate and cysteine, termed the Ulp domain (Li and Hochstrasser, 1999). However, sequence similarity is rather low between these two deconjugases, with only 27% identity between the Ulp domain and virtually none throughout the rest of the proteins (Kroetz *et al.*, 2009). Ulp1 was identified in *S. cerevisiae* by a biochemical screen for proteins with Smt3 cleaving activity (Li and Hochstrasser, 1999). Ulp1 is essential for the processing of immature Smt3, as it was identified that Ulp2 lacks the C-terminal hydrolase activity required to remove the amino acids following the diglycine motif of Smt3 (Li and Hochstrasser, 2000). Interestingly, like Smt3, Ulp1 was also found to be essential for passing the G_2-M boundary unless large amounts of mature Smt3-GG were expressed in the cells (Li and Hochstrasser, 1999). However, *ulp1Δ* mutant cells expressing mature Smt3 still grew extremely poorly, suggesting that deconjugation as well as conjugation of Smt3 is essential for cell cycle progression in *S. cerevisiae* (Li and Hochstrasser, 1999). Furthermore, deletion of both Siz1 and Siz2 (but not Mms21) rescued the poor growth phenotype of *ulp1Δ* mutant cells,

suggesting that the removal of the bulk of Smt3 conjugates, rather than a specific subset of targets, is the main function of Ulp1 within cells (de Albuquerque *et al.*, 2016). The *ULP2* gene was identified in *S. cerevisiae* as a high copy suppressor of a temperature sensitive allele of the E1 activating enzyme *uba1* (Schwienhorst *et al.*, 2000). Unlike Ulp1, Ulp2 is dispensable for growth, but is temperature sensitive and thus cannot grow at 37°C in *S. cerevisiae* (Schwienhorst *et al.*, 2000). In mammalian cells there are 6 identified SUMO deconjugase enzymes, SENP-1-4, 6-7 (Hay, 2007). The small number of SUMO deconjugation enzymes is in contrast to the ubiquitin system, where there are ~100 deubiquitinases identified in human cells (Hickey *et al.*, 2012). The SENP proteins can be classified into 3 main families (Yeh, 2009). The first family containing SENP-1 and SENP-2, are efficient at removing all the mammalian SUMO isoforms (SUMO-1-3). The second family contains SENP-3 and SENP-5 which preferentially remove SUMO-2/3 from substrates. The final family, SENP-6 and SENP-7, also preferentially remove SUMO-2/3 from substrates. SENP-1 appears to be the main C-terminal hydrolase for SUMO-1, as mice embryos with non-functional SENP-1 also show a reduction in processed SUMO-1 (Cheng *et al.*, 2007). However, SENP-2 can also process SUMOs, but it has a preference for SUMO-2 in biochemical assays (Reverter and Lima, 2004). This suggests further complexity in SUMO processing in high eukaryotes compared to yeast. To this end, new SUMO deconjugase enzymes have been recently identified with low sequence similarity to the SENPs in mammalian cells, which have no obvious homologs in yeast (Hickey *et al.*, 2012). These novel SUMO deconjugases, DE-SI1/2 and USPL1, could specifically cleave SUMO from substrates *in vitro*, but their function *in vivo* is not well characterised (Hickey *et al.*, 2012).

Like the Siz ligases, the two Ulps in *S. cerevisiae* have almost completely different intracellular targets, with less than 10% substrate overlap (Srikumar *et al.*, 2013). Furthermore, the subcellular localisation of Ulp1 and Ulp2 appear to give rise to specificity. Ulp1 localises to the nuclear pore via an interaction of the N-terminal domain of Ulp1 with the karyopherins Kap121 and Kap95-Kap60 and the nuclear pore complex (NPC) (Takahashi *et al.*, 2000; Makhnevych *et al.*, 2007; Srikumar *et al.*, 2013). This interaction is then transiently lost during mitosis, when Ulp1 relocates to desumoylate the septins at the bud neck (Makhnevych *et al.*, 2007) (see section 1.2.2.3). In contrast, Ulp2 is constitutively located within the nucleus and nucleolus (Srikumar *et al.*, 2013). Furthermore, the nuclear localisation sequences in the N-terminal domain of Ulp2 are essential for its function (Kroetz *et al.*, 2009), suggesting Ulp2 only targets proteins in the nucleus. As such, overexpression of full length Ulp1 which localised to the nuclear pore does not improve the increased benomyl and temperature sensitivity associated with *ulp2Δ* mutant cells (Li and Hochstrasser, 2003). However, expression of Ulp1 lacking the signal for the NPC rescues the *ulp2Δ* phenotypes, also leading to an apparent global reduction of the high molecular weight Smt3 conjugates observed in *ulp2Δ* mutant cells (Li and

Hochstrasser, 2003). These initial observations suggest that Ulp1 tethering to the NPC prevents excessive desumoylation throughout the nucleoplasm. Interestingly however, recent studies in *S. cerevisiae* expressing the same NPC Ulp1 localisation mutant found that while indeed the sumoylation of many nuclear Ulp2 substrates decreased, the sumoylation levels of some Ulp2 targets actually increased (de Albuquerque *et al.*, 2016). The reason for this was unclear, however this result indicates that feedback mechanisms exist to detect aberrant sumoylation, and thus shift the homeostasis of SUMO conjugation. A key role of Ulp2 appears to be in the disassembly of SUMO chains. This was first indicated as expression of a mutant form of SUMO which cannot form chains (*Smt3^{allR}*) in *ulp2Δ* mutant cells supresses the temperature and hydroxyurea (HU) sensitivity of the mutant strain, showing the growth defects of the strain are most likely due to the accumulation of SUMO chains (Bylebyl *et al.*, 2003). Furthermore, biochemical studies have shown that Ulp2 binds chains of 3 or more Smt3 molecules *in vivo*, then sequentially trims the last Smt3 from the chain, further cementing a role in Smt3 chain processing (Eckhoff and Dohmen, 2015).

1.1.4 SUMO Interaction Motifs

As SUMO provides a complex interaction surface, proteins can bind to sumoylated substrates non-covalently via SUMO interacting motifs (SIMs) (Minty *et al.*, 2000; Song *et al.*, 2004; Hecker *et al.*, 2006). The first identified SIM was discovered in a yeast 2 hybrid screen for SUMO-1 interacting proteins (Minty *et al.*, 2000). Of the SUMO-1 interacting proteins isolated, a subset contained a conserved sequence of ψ-ψ-x-S-x-S-D/E-D/E-D/E, where ψ is a large hydrophobic amino acid, and x is any amino acid (Minty *et al.*, 2000). Interestingly, the S-x-S-D/E-D/E motif in the centre of the SIM is also a repeated casein kinase II site (S-x-x-E/D) suggesting phosphorylation could regulate these interactions (Minty *et al.*, 2000). Indeed, a study has shown that the phosphorylation of the serine residues in the SIM increases the binding of SUMO to the SIM (Stehmeier and Muller, 2009). Subsequent studies of SIM motifs also highlighted a requirement for a hydrophobic core of amino acids in the pattern (V/I/L)-(V/I/L)-x-(V/I/L) or (V/I/L)-x-(V/I/L)-(V/I/L), forming a β-strand which can position between the hydrophobic cleft formed by an α-helix and a β-strand in SUMO (Gao *et al.*, 2005). Most recently, a study into the strings of SIM motifs in the SUMO targeted ubiquitin ligase (STUbL) RNF4 used to bind SUMO chains (see section 1.1.5) identified a novel SIM (V/I/L/F/Y)-(V/I)-D-L-T, which is often the first SIM within a string of hydrophobic type SIMs (Sun and Hunter, 2012). Interestingly, this novel SIM was found to be the most crucial in binding the chain of SUMOs, suggesting it drives the recognition of the entire SUMO chain (Sun and Hunter, 2012). These data together suggest the emerging picture that proteins could have tailored SIM components to elicit the type of SUMO interaction required. Interestingly, all SIMs thus far only recognise one face of SUMO, while ubiquitin is recognised by many surfaces (Seet *et al.*, 2006).

1.1.5 Polysumoylation

Although most studies of sumoylation are of the conjugation of its monomeric form, SUMO, like ubiquitin, can form polymeric chains. As discussed previously, SUMO has an extended N-terminal "tail" compared to ubiquitin and other Ubls (Bayer *et al.*, 1998). Within the N-terminal tail are sumoylation consensus motifs, which can accept other SUMO monomers to form polymeric structures. In *S. cerevisiae*, the main linkage is through Lys15 (Bencsath *et al.*, 2002; Bylebyl *et al.*, 2003). In mammalian cells only the SUMO-2/3 isoform can form polymeric chains, through Lys11 (Tatham *et al.*, 2001). In *S. cerevisiae*, expression of a mutant form of Smt3 which contained no lysine residues for conjugation (*Smt3^{allR}*) was acutely sensitive to HU and MMS, and was defective in many processes such as chromatin organisation and stress induced gene transcription (Srikumar *et al.*, 2013). Similarly, Pmt3 chains are required for replication arrest in *S. pombe*, demonstrated by the HU sensitivity of mutants lacking the chain forming N-terminal lysine residues (*pmt3^{K14,30R}*) (Skilton *et al.*, 2009).

One particular function of poly-SUMO chains is to allow cross-talk between ubiquitin and sumoylation. The SUMO targeted ubiquitin ligases (STUbLs) are ubiquitin E3s which contain many SIMs. The multiple SIMs within STUbLs bind poly-SUMO chains (Sun and Hunter, 2012), and subsiquently ubiquitinate them, often leading to proteasomal degradation of the ubiquitinated target. In *S. cerevisiae* there are two major STUbLs, the heterodimer Slx5/8, and the Uls1(Uzunova *et al.*, 2007). In *S. pombe*, there are proteins functionally similar to Slx5, Rfp1 and Rfp2, and one Slx8 subunit (Prudden *et al.*, 2007). In mammalian cells, the only STUbl idnetified to date is RNF4, which functions like the Slx5/8 dimer (Galanty *et al.*, 2012).

1.2 Roles and Regulation of Sumoylation

1.2.1 Regulation of Transcription

Transcription factors can either promote or repress transcription of a gene, as transcriptional activators or repressors, respectively. For transcription factors to exert an effect on transcription, they need to be localised in the nucleus to effectively bind to the target DNA and stabilise or block the recruitment of other factors such as transcriptional machinery, chromatin remodelling complexes or other transcriptional regulators. Thus, effecting any of these processes, or indeed the stability of a transcription factor itself, will influence the functionality of the transcription factor. The studies outlined here, as well as others, established the consensus that sumoylation acts as a general inhibitor of transcription. The mechanisms described below are outlined in Figure 1.5.

One of the first understood roles of SUMO was in the regulation of IκBα (inhibitor of nuclear factor κB alpha), an inhibitor of the stress regulated transcription factor NFκB. Sumoylation of Lys21 prevented the ubiquitination of the same residue, preventing ubiquitin mediated

proteaosomal degradation (Desterro *et al.*, 1998). Thus, IκBα can still inhibit the transcription factor NFκB, reducing transcription. Another transcription factor, Atf7, was found to be sumoylated at Lys118, and mutation of this sumoylation site increased association of the Atf7 with its target gene promoter (Hamard *et al.*, 2007). Atf7 provides an example of sumoylation effecting dynamics of nuclear localisation of a transcription factor. Although the final nuclear localisation of a SUMO-Atf7 fusion protein was similar to wild type Atf7, this reduced the rate of Atf7 uptake into the nucleus in time lapse experiments (Hamard *et al.*, 2007). Although the fusion protein is not equivalent to the *in vivo* sumoylated form, this data suggested that the SUMO moiety was increasing the rate of nuclear uptake. Another mechanism by which sumoylation can regulate the function of transcription factors is by the recruitment of other factors. Sumoylation of a transcription factor, Elk-1 recruits the histone-deacetylase HDAC-2, thus reducing histone acetylation levels, which are a marker of transcriptionally active chromatin (Yang and Sharrocks, 2004). Interestingly, phosphorylation of Elk-1 by MAP kinase, activated by a variety of cell stresses, also specifically reduced the sumoylation of Elk-1.1 compared to other known sumoylation targets (Yang *et al.*, 2003), via action of the desumoylase SENP-1 (Witty *et al.*, 2010), providing evidence of cross talk between various stress response pathways leading to a sumoylation dependant change in transcription.
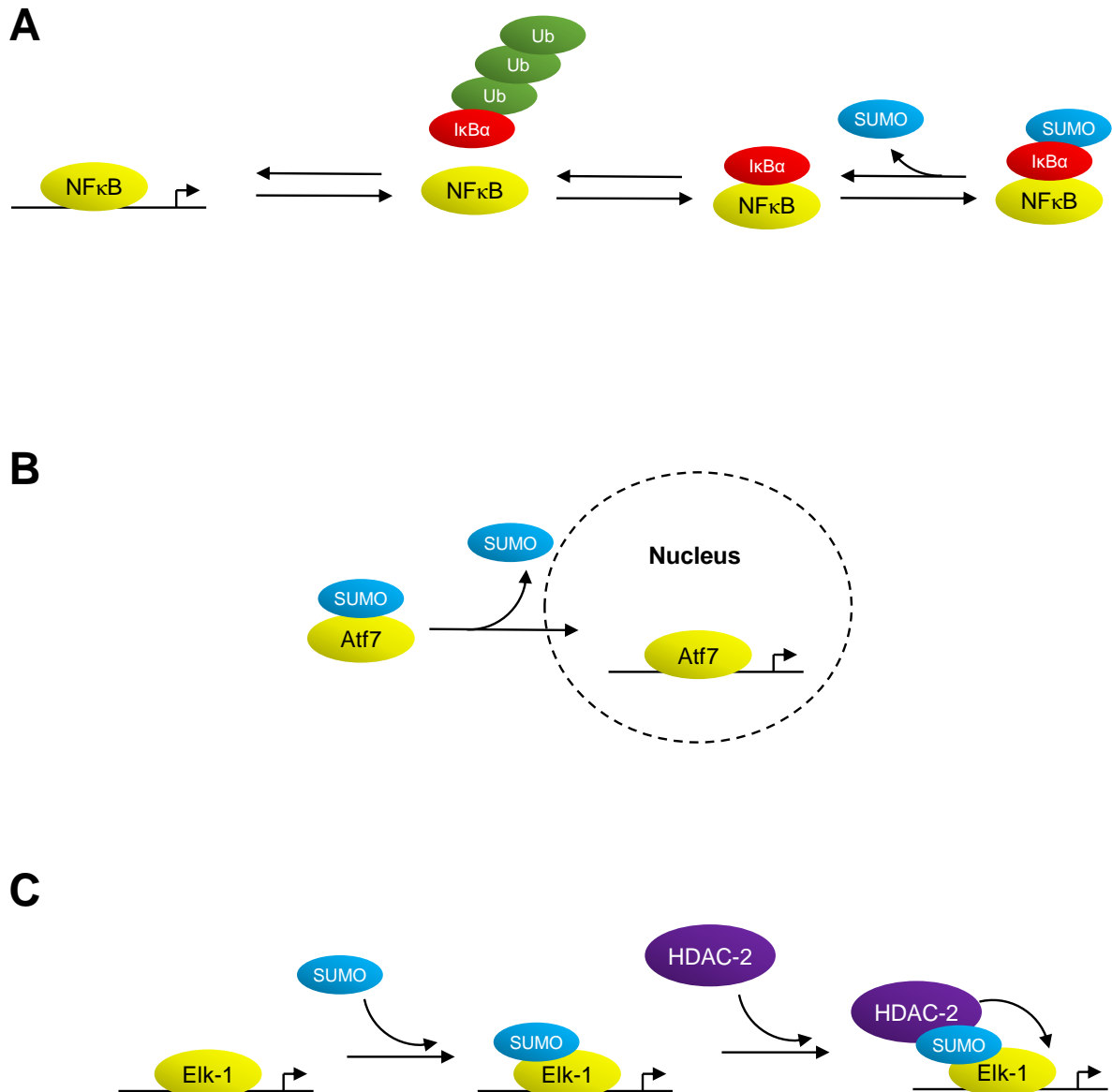
Figure 1.5: Mechanisms in which sumoylation can regulate transcriptional regulation.
A) Stabilisation: sumoylation of the inhibitor of the transcription factor NFκB, IκBα, stabilises the inhibitor by preventing ubiquitin mediated degradation (Desterro *et al.*, 1998). B) Localisation: sumoylation of the transcription factor Atf7 inhibits the import of Atf7 into the nucleus (Hamard *et al.*, 2007). C) Factor recruitment: sumoylation of the transcription factor Elk-1, recruits the histone deacetylase HDAC-2, decreasing transcription via histone modification (Yang and Harrocks, 2004).

The forkhead transcription factor, FoxM1, is highly expressed in many tumours (Wierstra, 2013), and a target of sumoylation (Myatt *et al.*, 2014; Schimmel *et al.*, 2014). In a normal cell cycle, FoxM1 is important for the expression of cell cycle-regulated genes during G_2-M-phases of the cell cycle, and for the expression of various homologous recombination and DNA double strand break repair genes, such as *RAD51* (Zhang *et al.*, 2012). Interestingly, the current data investigating the function of SUMO modified FoxM1 are conflicting. One study demonstrated that the sumoylation of FoxM1 occurs at mitosis, and is induced by treatment of cells with the spindle poisons nocodozole and cancer drug paclitaxel, which both slow growth at the G_2-M boundary (Myatt *et al.*, 2014). Furthermore, using FoxM1-Ubc9 fusion constructs, it was revealed that expression of an otherwise wild type form of FoxM1, fused to Ubc9 to induce sumoylation of FoxM1 by proximity, passed through mitosis slowly, suggesting the sumoylated form of FoxM1 slows mitotic progression (Myatt *et al.*, 2014). Consistent with this hypothesis, expression of a FoxM1-Ubc9 fusion construct lacking identified sumoylation residues on FoxM1 (K201R, K218R, K460R, K478R and K495R) appeared to have no effect on the time to proceed through mitosis (Myatt *et al.*, 2014). Furthermore, they found that the FoxM1-Ubc9 fusion localised to the cytoplasm, and accelerated the anaphase promoting complex/cyclosome (APC/C) mediated degradation of the transcription factor, thus delaying mitotic progression (Myatt *et al.*, 2014) (see section 1.2.2). Conversely, the unsumoylated form was nuclear and had increased resistance to degradation (Myatt *et al.*, 2014). Paradoxically, another study showed that the sumoylation of FoxM1 increased its transcriptional activity, by reducing the interaction of the repressor domain with the activator domain of FoxM1 (Schimmel *et al.*, 2014). It is interesting that sumoylation is generally considered a negative inhibitor of The paper finding an inhibitory role for FoxM1 sumoylation found it to be modified by SUMO-1 and not SUMO-2/3 (Myatt *et al.*, 2014), in contrast to the other which looked at SUMO-2 (Schimmel *et al.*, 2014), which could suggest that SUMO-1 and SUMO-2/3 modification of FoxM1 at different lysine residues have different cellular outcomes.

1.2.2 Sumoylation in Cell Cycle

The cell division cycle is a highly regulated, consecutive process. Controlled cell division ensures that genetic material is accurately replicated and inherited to the new daughter cell. Genetic instability that can arise upon aberrant cell division is often identified in cancers. Due to the importance of this cellular process, many of the regulatory mechanisms are conserved from yeast to man. In eukaryotes, the cell division cycle proceeds through 4 steps: gap phase 1 (G1), S-phase, gap phase 2 (G2), and mitosis (M-phase). During the gap phases, the cell reads environmental and internal cues prior to commitment to the next stages. In *S. cerevisiae* the major cell cycle commitment step occurs at G1, where the cell must be above a critical size, and have enough cellular resources to proceed with the initiation of DNA synthesis in S-phase (Forsburg and Nurse, 1991). Subsequently, at G2, complete DNA synthesis must have

occurred before the cell can proceed with mitosis and the division of the genetic material, and in *S. pombe*, G2 is the main step for critical size determination (Forsburg and Nurse, 1991). The chromosomes condense at the beginning of mitosis (prophase), followed by the aligning of the chromatids to the metaphase plate (metaphase) via mitotic spindles binding to the chromatids and to the spindle bodies found at the cell ends. Paired chromatids are then pulled to the opposite cell ends during anaphase. This event is then followed by cytokinesis, where the constriction of the cell membrane and cell wall at the division site completes cell division, resulting in two cells.

1.2.2.1 Sumoylation in Anaphase

During the many regulatory processes of the cell cycle, protein modifications are utilised to alter protein stability and regulate transcriptional cues to allow cell cycle progression. A highly conserved mechanism to regulate the cell cycle is by the levels of cyclins (Mendenhall and Hodge, 1998). The master regulator of cell cycle progression in *S. cerevisiae*, the cyclin dependant kinase (CDK) Cdc28 (Cdc2 in *S. pombe*), is an essential serine/threonine kinase, which phosphorylates key targets throughout the cell cycle allowing cell cycle progression (Mendenhall and Hodge, 1998). Cdc28 is present during all stages of the cell cycle in *S. cerevisiae.* Therefore, the cell cycle-regulated activation of Cdc28 is achieved in part by the binding of a cell cycle-regulated cyclin protein (Mendenhall and Hodge, 1998; Vermeulen *et al.*, 2003). Each cyclin is maintained at low levels by transcriptional regulation, localisation, or by targeted ubiquitination and degradation, until the levels of cyclins are allowed to rise, activating Cdc28 and allowing cell cycle progression. In *S. cerevisiae* there are 3 cyclins which regulate early cell cycle progression through G_1-S-phase (Cln1-3), and 6 B-type cyclins which regulate cell cycle progression through S-phase to mitosis (Clb1-6). Within the cell cycle there are 'checkpoints', which regulate the cyclins and other targets, to arrest the cell cycle if conditions are not correct to proceed. The regulation of cyclins ensures that the cell cycle proceeds in a forward manner, and furthermore, the regulation of cyclin levels by 'checkpoints' prevents the cell cycle progressing until such a time to do so. In particular, sumoylation mutants in *S. cerevisiae* appear to have defects in the regulation of the checkpoint from metaphase to anaphase, termed the spindle assembly checkpoint (SAC), which I will discuss here. For further information of cell cycle regulation, I direct the reader to the following reviews: (Mendenhall and Hodge, 1998; Flynn and Zou, 2011; Johnson and Skotheim, 2013).

The SAC is one of the regulatory checkpoints throughout the cell cycle, which prevents the missegregation of chromatids at anaphase. Chromatids have two kinetochores at the centromere, which bind to the mitotic spindles. The SAC ensures that, prior to anaphase, both kinetochores of paired chromatids have bipolar attachment to spindles from opposite sides of the cell. Unattached kinetochores, or a lack tension between the two chromatids, produces a

signal which prevents anaphase. Many of the SAC proteins, Mps1, Mad1, Mad2, Mad3 (BubR1), Bub1 and Bub3 were identified in genetic screens in *S. cerevisiae* as mutants which did not arrest after treatment with microtubule depolymerisation drugs benomyl or benzimidazole (Hoyt *et al.*, 1991; Li and Murray, 1991). The SAC genes are highly conserved in eukaryotes, however only Mps1 is essential for cell viability in *S. cerevisiae* (Li and Murray, 1991). This could suggest that during normal circumstances, chromatids in wild type cells generally achieve biorientation without requirement of the checkpoint. The proteins Mad1 and Mad2 only bind to unattached kinetochores. Mad1 remains bound, but Mad2 is found in two cellular pools (De Antoni *et al.*, 2005). One pool is bound to the kinetochore, while another pool cycles between bound and unbound. The binding of Mad1 to Mad2 induces a conformational change in Mad2 from an 'open' to 'closed' state. The 'closed' state Mad2 is able to change the confirmation of 'open' soluble Mad2 to 'closed' state, thus allowing the signal of unattached kinetochores to be propagated (De Antoni *et al.*, 2005). 'Closed' Mad2, as well as Mad3, Bub3 and Cdc20 form the mitotic checkpoint complex (MCC), a protein complex which inhibits anaphase. The MCC causes inhibition of ubiquitin E3 ligase activity of the APC/C, thus preventing the APC/C ubiquitination targeted degradation of B-type cyclins Clb2 and Clb5 (Shirayama *et al.*, 1999; Wasch and Cross, 2002; Peters, 2006). Another important target of the APC/C is the securin Pds1 (Cut2 in *S. pombe*) (Nasmyth and Haering, 2005; Peters, 2006). To ensure sister chromatids remain paired until anaphase, the chromatids are held together by a protein structure called cohesin. Cohesin is a ring like structure formed by Smc1, Smc3, Scc1, and Scc3 in *S. cerevisiae* (Nasmyth and Haering, 2005). Seperase, Esp1, is a protease which degrades the Scc1 subunit of cohesin, thus allowing sister chromatids to separate in anaphase (Shirayama *et al.*, 1999; Nasmyth and Haering, 2005; Peters, 2006). Pds1 inhibits Esp1, preventing Scc1 degradation and sister chromatid separation, until the APC/C is activated and degrades Pds1 (Peters, 2006).

Studies in yeast have highlighted the role of *SMT3* in cell cycle regulation at this cell cycle point. The SUMO gene was identified in *S. cerevisiae* as a high-copy suppressor of *mif2,* a gene encoding a centromere protein important for kinetochore formation (*SMT3*, Suppressor of Mif-Two) (Meluh and Koshland, 1995). The SUMO E2 Ubc9 was found to be required for the degradation of the APC/C target cyclins Clb2 and Clb5, and depletion of Ubc9 led to an arrest as large budded cells with a short metaphase spindle (Seufert *et al.*, 1995). This led to the proposal that Ubc9 was a ubiquitin E2 enzyme that acted with the APC/C ubiquitin ligase (Seufert *et al.*, 1995). However, later Ubc9 was actually identified as the E2 enzyme for SUMO in *S. cerevisiae* (Tatham *et al.*, 2001; Bencsath *et al.*, 2002). Analysis of a temperature sensitive allele of *SMT3, smt3-331*, found that Smt3 function was essential for chromosome segregation (Biggins *et al.*, 2001). In this study, Smt3 was found to localise to the chromosomes, and incubation of *smt3-331* expressing cells at the non-permissive temperature

caused a G$_2$/M arrest with short spindles (Biggins *et al.*, 2001). The arrest was not due to the activation of the SAC, as deletion of Mad2 in the *smt3-331* mutant cells did not allow spindle elongation (Biggins *et al.*, 2001). Further study confirmed that *UBC9* and *SMT3* were required for the rapid degradation of the APC/C targets securin Pds1 and Clb2, again even in the absence of the SAC (Dieckhoff *et al.*, 2004). Interestingly, this study found that deletion of Pds1 allowed spindle elongation in a subset of Ubc9 depleted cells, suggesting part of the metaphase block defect was due to the inability to degrade Pds1 (Dieckhoff *et al.*, 2004). However, many cells which were able to elongate the microtubule spindles in the absence of Pds1 had poorly segregating DNA masses; additionally, a fraction of *pds1Δ ubc9Δ* cells were still unable to elongate their microtubules (Dieckhoff *et al.*, 2004), suggesting that sumoylation still plays other important roles in anaphase. Furthermore, to investigate if Smt3 is required to remove cohesive structures between sister chromatids, or to segregate the sister chromatids to the opposite spindle poles, the *smt3-331* mutant strain was incubated at the non-permissive temperature in the presence of the microtubule depolymerising drug nocodazole (Biggins *et al.*, 2001). In the absence of the spindle assembly checkpoint, the chromatids drifted apart. This suggests that the chromatids are not cohesively bound together, and that the defect could be due to the inability for the spindles to elongate (Biggins *et al.*, 2001). The deconjugation of Smt3 is also critical for cell cycle progression in *S. cerevisiae*, as Ulp1 deficient cells also stall in G$_2$/M even when provided with mature Smt3 protein (Li and Hochstrasser, 1999). Ulp1 localisation is also regulated during mitosis in *S. cerevisiae*, where Ulp1 transiently relocates to the bud neck (see section 1.2.2.1). The mechanism of many of these events still requires elucidating.

In *S. pombe*, cells lacking Pmt3 and Ubc9 are viable, but they grow at a much slower rate than wild type, with an elongated cell morphology, indicative of cell cycle delay (Tanaka *et al.*, 1999; al-Khodairy *et al.*, 1995). *pmt3⁻* cells were also found to be extremely sensitive to the spindle depolymerisation drug tetrabenazine (TBZ), and exhibited a much higher rate of minichromosome loss than wild type cells (Tanaka *et al.*, 1999). As expected, loss of Ubc9 in *S. pombe* also leads to cell cycle defects (al-Khodairy *et al.*, 1995). As well as the long cell morphology observed in *pmt3⁻* mutant cells, *ubc9⁻* mutant cells also showed spindle elongation defects (al-Khodairy *et al.*, 1995). Furthermore, localisation studies of Pmt3 fused to GFP revealed Pmt3 localised primarily in the nucleus in *S. pombe* (Tanaka *et al.*, 1999). In particular, GFP-Pmt3 signal showed cell cycle regulated co-localisation with the spindle pole bodies during G$_1$ and after anaphase, which was transiently lost during metaphase (Tanaka *et al.*, 1999). This co-localisation is similar to the localisation of the centromeres, which associate with the spindle pole bodies during the majority of the cell cycle, except for metaphase, suggesting that Pmt3 has roles at the centromere in *S. pombe*. The deconjugation of Pmt3 in *S. pombe* is also important for cell cycle regulation. *S. pombe* lacking Ulp1 also show nuclear

defects such as misplaced nuclei, and cell morphology defects such as misshapen or multiseptate cells (Taylor *et al.*, 2002). Ulp1 localisation is also regulated by cell cycle in *S. pombe*, where Ulp1 is localised to the nuclear periphery during most of the cell cycle, and is shuttled into the nucleus at mitosis (Taylor *et al.*, 2002). However, what substrates are targeted by Pmt3, and subsequently removed by Ulp1 in the *S. pombe* cell cycle is unclear.

1.2.2.2 S. cerevisiae septin sumoylation

The septins Cdc3, Cdc11, and Shs1 were the first SUMO targets identified in *S. cerevisiae* (Johnson and Blobel, 1999; Takahashi *et al.*, 1999). Septins are conserved cytoskeletal guanosine-nucleotide binding proteins, which polymerise into filaments, with roles in the formation of cytokinetic rings (Barral and Kinoshita, 2008). In *S. cerevisiae*, the septin proteins Cdc3, Cdc10, Cdc11, Cdc12, and Shs1 form a collar-like structure at the bud neck, binding to the membrane via phosphatidylinositide binding domains in the N-terminus (Casamayor and Snyder, 2003). The most predominately sumoylated septin in *S. cerevisiae* is Cdc3, which contains 4 sumoylated lysine residues within its N-terminus, while in contrast Shs1 contains two sites and Cdc11 one site, all located within their C-terminal regions (Takahashi *et al.*, 1999; Johnson and Blobel, 1999). Sumoylation of the *S. cerevisiae* septins is a cell-cycle regulated event, as the majority of septin sumoylation occurs during mitosis, appearing to be localised to the mother side of the septin ring (Johnson and Blobel, 1999).

Studies have elucidated sumoylation of septins during mitosis is achieved by cell cycle-regulated localisation of the Siz1 E3 ligase, and the Ulp1 deconjugase (see Figure 1.6) (Johnson and Blobel, 1999; Takahashi *et al.*, 2001a; Makhnevych *et al.*, 2007). During interphase, Siz1 is imported into the nucleus via the importin Kap95 (Makhnevych *et al.*, 2007). In mitosis, Siz1 becomes phosphorylated (Takahashi *et al.*, 2001b), and this modification coincides with its export from the nucleus via the exportin Kap142/Msn5, which often exports phosphorylated substrates (Makhnevych *et al.*, 2007). Once in the cytoplasm, Siz1 then localises to the septin ring where it aids the sumoylation of the septins Cdc3, Cdc11 and Shs1 (Johnson and Blobel, 1999). Interestingly, preventing Siz1 nuclear export in mitosis by loss of Msn5 causes Siz1 protein levels actually drop. This feedback mechanism was shown to be via targeted degradation following ubiquitination by the STUbL Slx5/8 (Westerbeck *et al.*, 2014). Septin sumoylation is transient, as the SUMO moieties which are conjugated to the septins are subsequently removed at the end of mitosis (Johnson and Blobel, 1999). The desumoylation of the septins is via action of the Ulp1 deconjugase. As previously stated, (see section 1.1.3), Ulp1 is bound to the nuclear pore complex during most of the cell cycle in *S. cerevisiae*, via interactions with the karyopherins Kap121 and Kap95-Kap60 (Takahashi *et al.*, 2000). Ulp1 is imported into the nucleus by Kap95-Kap60, and is then sequestered to the nuclear pore by a non-canonical interaction between Kap121 and the nuclear pore protein

Nup53 (Makhnevych *et al.*, 2007). Interestingly, by impeding this interaction in *nup53* mutant cells, the desumoylation of septins is delayed, suggesting the timely release of Ulp1 from the NPC is crucial for the prompt desumoylation of the septins (Makhnevych *et al.*, 2007).

Despite the studies of the elegant sumoylation and desumoylation mechanism of septin sumoylation in *S. cerevisiae*, the cellular function of septin sumoylation is still unclear. As the sumoylation of Cdc3 occurs on lysines within the membrane binding N-terminal it was proposed that the sumoylation of Cdc3 could promote the dissociation of the septin rings from the membrane, whereas the modification of Shs1 and Cdc11 provide a more signalling role (Takahashi *et al.*, 2008). However, there appears to be little to no phenotype associated with the lack of sumoylation of septins in *S. cerevisiae*. This was illustrated by analysis of a triple septin mutant lacking all sumoylated lysine residues (*cdc3^{K4,11,30,63R} cdc11^{K412R} shs1^{K426,437R}*) (Johnson and Blobel, 1999). While mutation of these sites appeared to prevent all septin sumoylation, and removed most of the SUMO visible at the bud neck at mitosis, the cells behaved like wild type, with no change in growth rate or sensitivities to stresses (Johnson and Blobel, 1999). One phenotype which was observed was the septin mutant cells appeared accumulate septin rings after division (Johnson and Blobel, 1999), however *uba2* and *ubc9* temperature sensitive mutants did not also accumulate extra septin rings at either the permissive or non-permissive temperature (Johnson and Blobel, 1999).
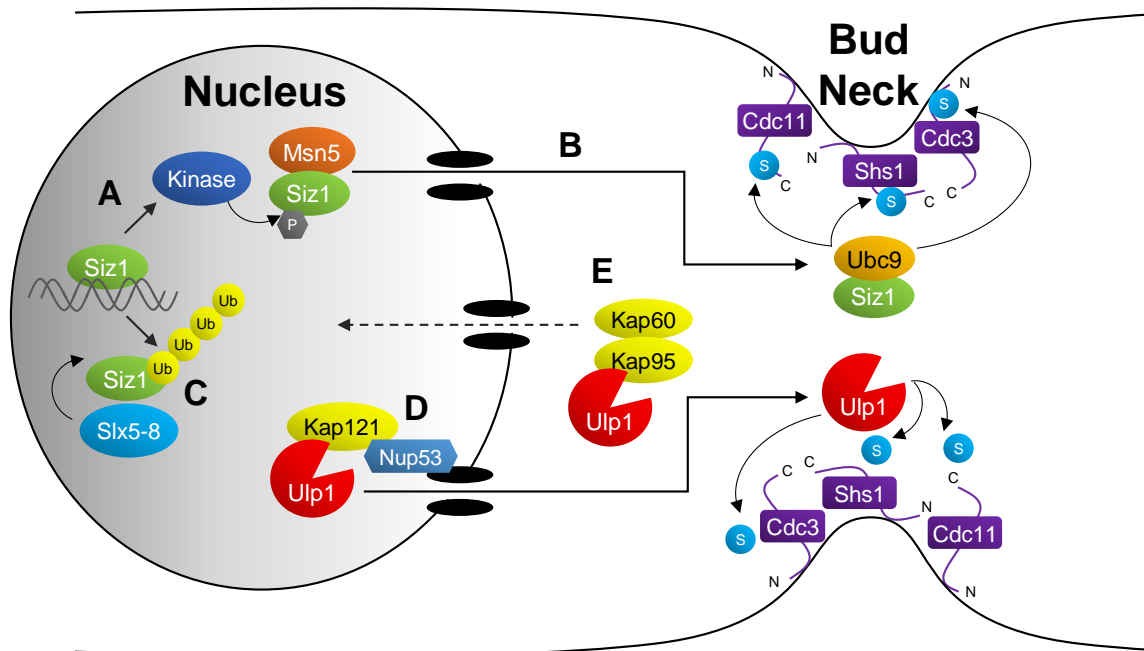
Figure 1.6: Cell cycle-regulated septin sumoylation in *S. cerevisiae*. A) During interphase, Siz1 stays bound to DNA and maintained in the nucleus. During mitosis, Siz1 becomes phosphorylated and this modification is hypothesised to allow nuclear export via Msn5. B) Siz1 then becomes localised at the bud neck and sumoylates the septins. Cdc3 is sumoylated at the N-terminus, which interacts with the membrane, where Cdc11 and Ssh1 are sumoylated on the C terminus which are exposed into the bud neck. C) Any Siz1 that does not leave the nucleus during M-phase is degraded in a Slx5-8 dependant manner. D) Ulp1 is maintained at the nuclear pore by non-canonical interactions with the karyopherin Kap121, which is tethered to the nuclear pore by Nup53. Upon completion of anaphase, the interaction of Ulp1 with the nuclear pore is lost, and Ulp1 localises to the bud neck to desumoylate the septins. E) Ulp1 is transported back into the nucleus by Kap60-Kap95. Cdc3 is sumoylated at the N terminus, which interacts with the membrane, where Cdc11 and Ssh1 are sumotylated on the C terminus which are exposed into the bud neck. Figure adapted from (Takashi *et al.*, 2008).

This is puzzling when it is considered that septins are one of the most abundantly sumoylated substrates in the cell (Johnson and Blobel, 1999; Takahashi *et al.*, 1999). Significantly, the sumoylation of septins is also species specific. Septins are also sumoylated in *D. melanogaster* (Shih *et al.*, 2002), and interactions between the human septins and SUMO machinery have been detected (Nakahira *et al.*, 2010). Interestingly, although similar to *S. cerevisiae*, Smt3 is found to localise to the mother side of the bud neck and hyphal septa in *C. albicans*, the septins themselves are not targeted for sumoylation (Martin and Konopka, 2004). However, Smt3 modified proteins were found to interact with the *C. albicans* septin Cdc11, suggesting a conserved role for SUMO at the bud neck in these organisms. Thus, the links to septin and bud neck associated proteins and sumoylation (if indeed there are any) still remains enigmatic. It remains possible that sumoylation of septins is an off target effect of the dynamic changes in sumoylation during the cell cycle. Alternatively, the sumoylation of the septins could provide a localised pool for other targets nearby. Interestingly, the role of SUMO in regulating the cytoskeleton, other than in the case of septin sumoylation described in these above studies, is thus far unknown.

1.2.3 The SUMO Stress Response (SSR)

Sumoylation has long been known to respond to many types of stress, commonly producing a global change in sumoylation (Lewicki *et al.*, 2015). Indeed, global sumoylation changes often allow the modification of many proteins within one pathway or complex, termed the "SUMO cloud", which can be identified in many cellular pathways from DNA damage regulation to septin sumoylation, described below (Johnson and Blobel, 1999; Psakhye and Jentsch, 2012; Chen *et al.*, 2016). There are many reasons why a cell would potentially want to sumoylate many proteins within a pathway. One hypothesis is that many sumoylation events within many components are required to amplify many weak SUMO-SIM interactions to promote the assembly of a complex (Psakhye and Jentsch, 2012). Secondly, with logic similar to the hypothesis above, as the SSR often induces global sumoylation changes, it could be that some proteins which are not targets of the sumoylation wave will be inappropriately sumoylated. Perhaps the requirement of sumoylation of many components within target complexes allows some flexibility in incorrect signal being relayed. Reliance upon a single sumoylation event during waves of a potentially messy signal could propagate unwanted signals.

1.2.3.1 Sumoylation in DNA Damage

When DNA damage occurs, it must be sensed and appropriate repair mechanisms employed to ensure genome stability. Indeed, a wide range of DNA repair mechanisms exist to repair lesions. Many have been identified in yeast by genetic epistasis studies of strains unable to survive ionising radiation or UV, such nucleotide excision repair (the RAD3 epistasis group), homologous recombination (the RAD52 epistasis group) and the post replication repair (RAD6)

pathway, as well as the mismatch and base excision repair pathways (Hanawalt, 2015; Cipolla *et al.*, 2016; Himmels and Sartori, 2016). Unsurprisingly, given the important roles of DNA damage repair, these pathways are highly conserved in eukaryotes, often allowing parallels to be drawn from the yeast studies. Although the roles of the proteins encoded by these genes on their respective pathways are well understood, less is known about how the cell selects the appropriate repair mechanism to utilise, and how this links with the timing and location of the specific lesion. Interestingly, initial studies of sumoylation enzymes revealed many mutants had increased sensitivity to genotoxic agents. For example, the *S. pombe ubc9*[+] gene was initially identified in a screen for mutants with increased sensitivity to HU (*hus5*[+] HydroxyUrea Sensitive) (al-Khodairy *et al.*, 1995). Similarly, *pmt3*[+] mutants display increased sensitivity to UV and HU (Tanaka *et al.*, 1999). In *S. cerevisiae*, mutations of the genes encoding SUMO conjugation and deconjugation enzymes, *UBC9* (Hoege *et al.*, 2002), *ULP1* (Li and Hochstrasser, 1999), *ULP2* (Li and Hochstrasser, 2000), *SIZ1*, *SIZ2*, (Cremona *et al.*, 2012) and *MMS21* (Zhao and Blobel, 2005) display increased sensitivity to UV or drug induced DNA damage, or replication stress. As outlined in the studies below, sumoylation appears crucial in the regulation of DNA repair during replication and homologous recombination, during both normal cellular growth and genotoxic stress. Consistent with these observations, many DNA damage and repair components are sumoylated, either at steady state or during chronic DNA damage induced by MMS treatment (Burgess *et al.*, 2007; Cremona *et al.*, 2012; Psakhye and Jentsch, 2012)

If the replication fork encounters either DNA lesions after damage, endogenous lesions such as bound proteins or transcriptional machinery, or if dNTPs become depleted, the replication fork stalls (Zeman and Cimprich, 2014). However, the helicase continues to unwind the DNA helix at the replication fork, leading to the accumulation of ssDNA, which is susceptible to unstable homologous recombination (Zeman and Cimprich, 2014). As such, the ssDNA produced by the replication machinery during normal replication and at stalled replication forks is covered by the RPA complex, which is composed of 3 subunits Rfa1-3 in *S. cerevisiae* (Brill and Stillman, 1991). However, persistent stalled replication forks can collapse (Zeman and Cimprich, 2014). However, repairing a DNA lesion by excising it from the ssDNA produced during replication poses the risk that a double strand break could occur which could lead to much more toxic chromosomal rearrangements. Thus the cell has specific repair pathways for damage encountered during replication, mediated by the ubiquitin enzymes Rad6 (E2) and Rad18 (E3). The role of SUMO modification of the sliding clamp PCNA Pol30 is well characterised in *S. cerevisiae*. PCNA is a processivity factor for DNA polymerase, but also acts as a molecular signal platform for interacting proteins and modifications during replication. PCNA is shown to be modified by ubiquitin and SUMO at Lys164, and a minor sumoylation site at Lys127 (Pfander *et al.*, 2005; Parker *et al.*, 2008). The modifications and outcomes of

PCNA modification by SUMO, are outlined in Figure 1.7. Lys164 sumoylation of Pol30 is dependent on Siz1, whereas Lys127 sumoylation was only abolished in a *siz1Δ siz2Δ* mutant suggesting Siz2 is essential for sumoylation for the minor site (Parker *et al.*, 2008). PCNA is sumoylated throughout normal S-phase, coinciding with the loading of PCNA onto DNA (Pfander *et al.*, 2005). Interestingly, sumoylation of PCNA can also recruit the ubiquitin E3 Rad18 via a SIM motif within Rad18, signalling for DNA damage repair (Parker and Ulrich, 2012). This could suggest that the sumoylation of DNA loaded PCNA is prerequisite for DNA damage induced ubiquitination, thus DNA repair pathways can only be activated by clamps actively on DNA (García-Rodríguez *et al.*, 2016) (Figure 1.7). Furthermore, during normal S-phase, mono-sumoylation of PCNA at Lys164 recruits the DNA helicase Srs2 to the replication fork, via SIM and PCNA interaction domains within Srs2 (Armstrong *et al.*, 2012) (Figure 1.7). The recruited Srs2 then resolves recombinogenic Rad51 filaments from ssDNA at the replication fork (Krejci *et al.*, 2003; Veaute *et al.*, 2003) (Figure 1.7). This suggests a role for SUMO in the prevention of unwanted homologous recombination under unstressed conditions.

In conditions of genotoxic stress, sumoylation of DNA damage proteins increases, suggesting sumoylation is important for repair of DNA damage as well maintaining steady state conditions. One example is the RPA subunit Rfa1, which is sumoylated after MMS treatment in *S. cerevisiae* (Burgess *et al.*, 2007; Cremona *et al.*, 2012). Recent studies have revealed that upon replication fork stalling, the excess ssDNA and RPA complex formation recruits Siz2 to the sites of DNA damage (Chung and Zhao, 2015). The recruitment of Siz2 is crucial for DNA damage-induced sumoylation of other DNA damage proteins, such as Rad52 and of RPA itself (Chung and Zhao, 2015). Furthermore, PCNA sumoylation increases during treatment with lethal levels of MMS (Hoege *et al.*, 2002). Recent data in *S. cerevisiae* has shown that in response to DNA damage, the helicase Srs2 is targeted for ubiquitination and degradation by the STUbL Slx5/8 (Urulangodi *et al.*, 2015). Thus reduced Srs2 levels at the replication fork allows the accumulation of Rad51 filaments, promoting homologous recombination to repair the lesion (Urulangodi *et al.*, 2015). Interestingly in *S. pombe* neither the sumoylation of PCNA, nor the SIM within the Srs2 homolog, is conserved (Frampton *et al.*, 2006). This could suggest that *S. pombe* does not use sumoylation of PCNA for DNA damage regulation. However, Lys164 sumoylation is conserved in higher eukaryotes which could indicate that the *S. cerevisiae* mechanisms of PCNA sumoylation are conserved in mammals (Gali *et al.*, 2012). Another role for PCNA sumoylation has been identified in *S. cerevisiae*, where sumoylation of
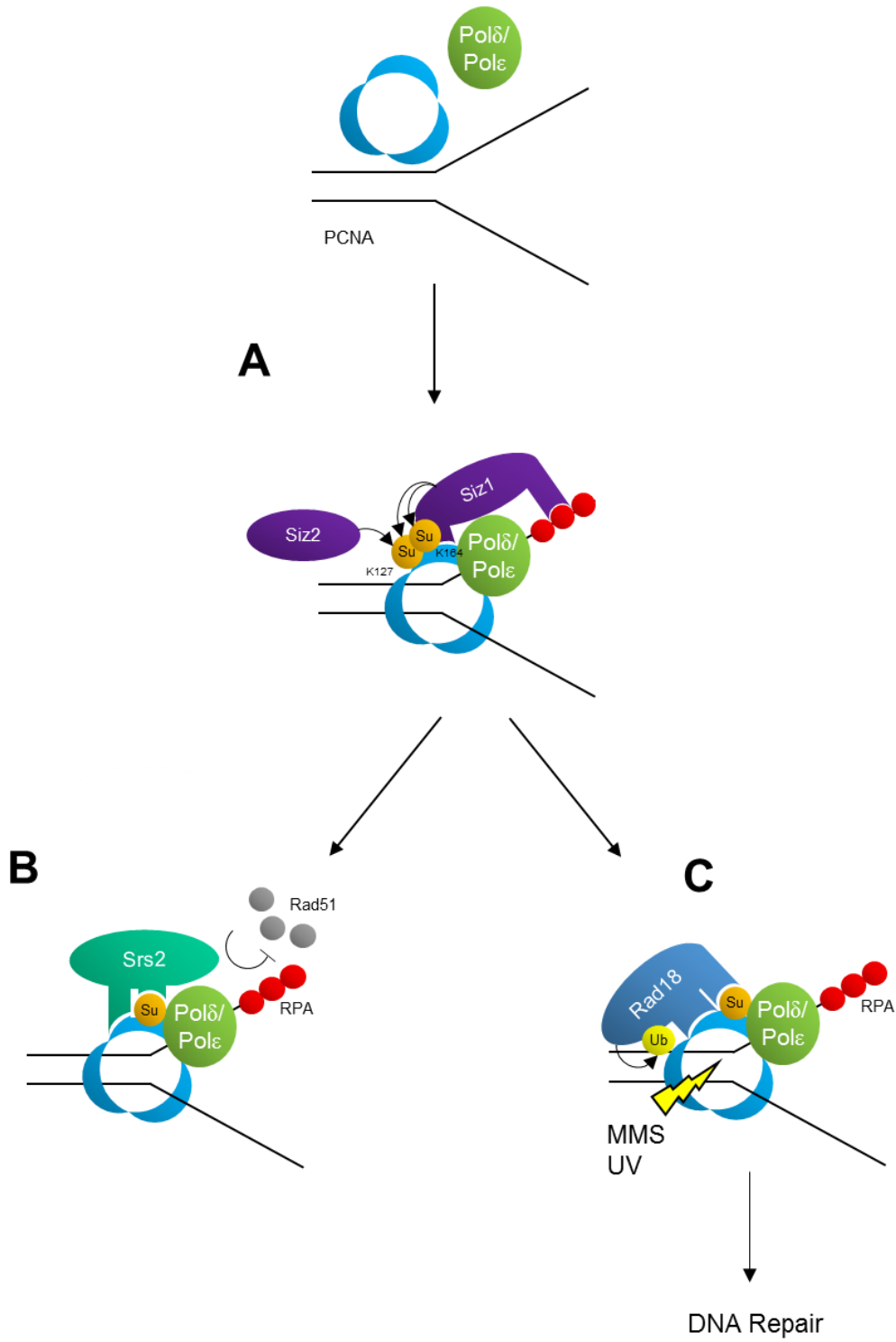
Figure 1.7: Sumoylation modification of PCNA in *S. cerevisiae*. PCNA is a trimer, so many combinations of modifications can exist on one PCNA molecule. A) Upon loading of PCNA to the DNA, PCNA is sumoylated on the major sumoylation site Lys164 and the minor site Lys127. B) Under normal conditions, sumoylation of Lys164 recruits the helicase Srs2, which removes recombinogenic Rad51 filaments from the single stranded DNA, allowing replacement with RPA. C) Following DNA damage, PCNA can be modified by ubiquitin on Lys64, by the recruitment of the ubiquitin E3 ligase Rad18, by a SIM motif in Rad18. This signals for DNA damage repair. Image adapted from (Sale, 2012).

PCNA increases cohesion between sister chromatids during S-phase via the cohesin establishing protein Eco1 (Moldovan *et al.*, 2006). Interestingly, genetic data revealed that sumoylation at the minor site Lys127 appears to be the most important site for this interaction (Moldovan *et al.*, 2006). DNA double strand breaks can be introduced following incorrect repair of a lesion at the replication fork, by replication fork collapse following persistent stalling, or by endogenous stress such as ionising radiation. DNA double strand breaks are repaired by two mechanisms; either non-homologous end joining (NHEJ) or by homologous recombination (HR). NHEJ requires resection of the damaged DNA ends and ligation. However, HR allows error free repair by use of an identical or similar DNA template, normally a sister chromatid, as a template to resynthesize damaged DNA from an undamaged template. This is completed by resection of the damaged end via the Mre11-Rad50-Xrs2 (MRN complex in mammalian cells) complex, and the resected strand invades the sister chromatid by Rad51 and Rad52. Following DNA synthesis from the sister chromatid, the homologous recombination intermediates from strand invasion are resolved, leading to the repaired strand. Sumoylation appears to have roles at all steps of HR, from end resection, to Rad51-Rad52 filament formation, and the resolving of intermediates following HR. Initial end DNA resection of damaged breaks via the MRX complex is reduced in *ubc9-1* mutant cells, suggesting that sumoylation is important for the initiation of DNA resection (Cremona *et al.*, 2012). Rad52 is sumoylated after DNA damage by Siz2 in *S. cerevisiae* (Sacher *et al.*, 2006), and sumoylation of the Rad52 homologs in *S. pombe* and mammalian cells is conserved (Ho *et al.*, 2001). It has been shown that sumoylation of Rad52 aids the recruitment of Rad51 to ssDNA, via a SIM within Rad51 (Bergink *et al.*, 2013). Interestingly, sumoylation appears to play a role in spatial separation of different repair mechanisms, by the recruitment of persistent DNA damage and stalled replication forks to the nuclear pore to SUMO machinery localised there, such as Slx5/8 and Ulp1 (Nagai *et al.*, 2008). Indeed, sumoylation of Rad52 was shown to be important for nuclear pore localisation of stalled replication forks (Su *et al.*, 2015). However, the reason for the nuclear pore movement is unclear.

Once the damaged DNA has been repaired by the DNA polymerases following strand invasion, the resulting recombination intermediates, known as Holliday junctions, need to be resolved to produce the final repaired DNA. The importance of SUMO in the resolving of recombination is indicated by the accumulation of homologous recombination mediates in *ubc9-1* and E3 ligase *mms21* mutants (Branzei *et al.*, 2006). One complex of importance in the resolution of recombination intermediates is the Structural Maintenance of Chromosomes 5 and 6 (Smc5/6) complex (Murray and Carr, 2008). The Smc5-6 is formed of 8 subunits; Smc5, Smc6 and six non-Smc element (Nse) subunits, Nse1-6, including the SUMO E3 ligase Nse2/Mms21 in *S. cerevisiae* or Nse2 in *S. pombe* (Murray and Carr, 2008; Andrews *et al.*, 2005; Branzei *et al.*, 2006). This complex is essential to resolve recombination events caused by endogenous

replication stress, as the accumulation of toxic recombination in Smc5/6 mutant cells leads to failure to complete chromatid separation in anaphase (Branzei *et al.*, 2006; Choi *et al.*, 2010). Interestingly, the Nse2/Mms1 E3 ligase subunit is also essential in both *S. cerevisiae* and *S. pombe* (McDonald *et al.*, 2003; Zhao and Blobel, 2005). However, the E3 ligase activity is only essential when the cells are treated with DNA damaging agents (Zhao and Blobel, 2005; Andrews *et al.*, 2005). This suggests that the essentiality of the Nse2/Mms21 subunit is due to a structural role within the Smc5/6 complex. Nse2/Mms21 sumoylates mostly chromatin bound targets, which are coupled with the loading of Smc5-6 onto DNA (Bermudez-Lopez *et al.*, 2015). Thus the DNA binding capacity of the Smc5-6 complex negates the fact that Nse2/Mms21 does not contain a DNA binding motif like the other E3 ligases (Figure 1.4). A sumoylation target of Smc5/6 complex is the Sgs1-Top3-Rmi1 (STR) complex, which is important for resolving crossovers from recombination, suggesting misregulation of the STR complex is leading to the toxic recombination intermediates in Smc5/6 complex lacking cells (Bonner *et al.*, 2016). Indeed, sumoylation appears to regulate the function of the STR, as sumoylation deficient *sgs^{2K3R}* mutants accumulate toxic recombination intermediates (Lu *et al.*, 2010). Interestingly, Sgs1 is also a target of the STUbL Slx5-8, whose directed ubiquitination appears to influence the localisation of Sgs1, highlighting the signalling roles of the STUbLs. (Bohm *et al.*, 2015).

DNA damage regulation is the most well studied stress response regulated by SUMO, however global sumoylation changes occur from many other stresses.

1.2.3.2 Heat Shock

Most organisms have an optimum growth temperature at which cellular proteins function normally. Above this temperature, in the condition of heat shock, cellular proteins are prone to misfolding, unfolding, or aggregation, which can prove toxic to cells (Saibil, 2013). Global sumoylation due to heat shock has been shown to increase in mammalian cells by two mechanisms (Figure 1.8). Firstly, when mammalian cells are treated with heat stress, the E1 component, SAE2, is desumoylated (Truong *et al.*, 2012). Sumoylation of Uba2 reduces enzymatic activity of the E1, by preventing transfer of activated SUMO to the E2 Ubc9. Therefore, the desumoylation of Uba2 upon heat shock leads to a global increase in sumoylation (Truong *et al.*, 2012) (Figure 1.8 A). As well as an increase of SUMO conjugation during heat shock, a parallel decrease in desumoylation by SENPs also occurs. It has been demonstrated in mammalian cells that all the SENPs, with the notable exception of SENP-6, are denatured by heat stress, leading to increased sumoylation (Pinto *et al.*, 2012) (Figure 1.8 B).
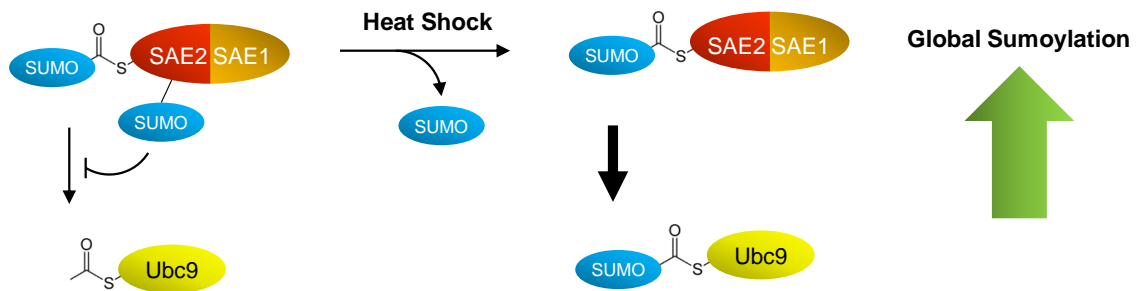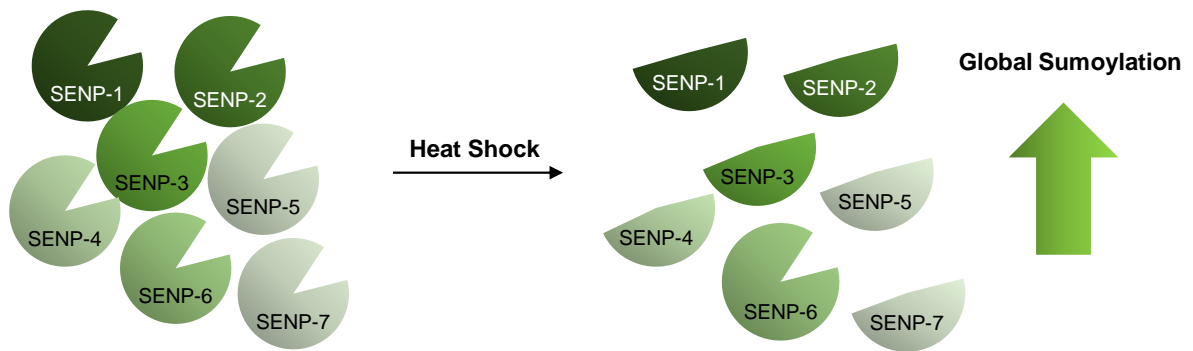
Figure 1.8: Heat shock leads to an increase in global sumoylation by two mechanisms.
A) The desumoylation of SAE2 after heat shock allows increased transfer of causes an increase in global sumoylation (Truong *et al.*, 2012). B) Upon heat shock of mammalian cells, the SUMO deconjugase enzymes become denatured, with the exception of SENP-6. This leads to an increase in global sumoylation (Pinto *et al.*, 2012).

This appears to be specific to the SENP proteins, as deubiquitinases appeared to be insensitive to heat (Pinto *et al.*, 2012). A target candidate during the global sumoylation changes is the heat shock transcription factors (HSFs). These transcription factors induce the expression of heat shock proteins, molecular chaperones which aid in the folding of misfolded proteins following heat shock (Pirkkala *et al.*, 2001). HSF1 and HSF4 were both found to be sumoylated in mammalian cells and interestingly, HSF1 was found to be sumoylated on Lys298 following phosphorylation of Ser303 in a heat stress dependant manner (Hietakangas *et al.*, 2006). Interestingly, this sumoylation event of HSF1 coincided with localisation of HSF1 to stress granules in the nuclei (Hietakangas *et al.*, 2006).

C. albicans lacking the SUMO gene *SMT3* have many increased stress sensitivities, one such stress being growth in high temperatures, suggesting a role for *SMT3* in the response to heat shock (Leach *et al.*, 2011). Interestingly, in contrast to mammalian cells, *C. albicans* show reduction of high molecular weight conjugates during heat shock at 42°C (Leach *et al.*, 2011). Interestingly, upon screening sumoylation targets from cells exposed to heat shock, sumoylation of many heat shock proteins were increased (Hsp60, Ssb1, Ssc1, and Hsp104). Furthermore, mutation of Lys357 within the SUMO consensus motif within Hsp104 produced similar heat sensitivities to *smt3/smt3* mutant cells, suggesting that the sumoylation of Hsp104 is critical in the *C. albicans* heat shock response (Leach *et al.*, 2011).

1.2.3.3 Hypoxia

Another stress which has been shown to affect global sumoylation is the metabolic stress of hypoxia. Interestingly, treatment of mammalian cells *in vitro* with low oxygen conditions increases expression levels SUMO-1 (Comerford *et al.*, 2003), and this was also verified *in vivo* in mouse brains (Shao *et al.*, 2004). Indeed, two studies of induced cerebral ischemia in mice, used as a model for strokes, saw increased global SUMO conjugation of SUMO-2/3 (Yang *et al.*, 2008). Furthermore, sumoylation of both SUMO-1 and SUMO-2/3 is increased in hibernating ground squirrels, a model of reduced blood flow and energy consumption, due to increased Ubc9 expression during hibernation (Lee *et al.*, 2007). However, attempts to elucidate if the sumoylation events were due to the hypothermia or the hypoxia induced by hibernation was unclear, as indeed a level of global sumoylation was induced by temperature reduction in human cells (Lee *et al.*, 2007). However, the temperatures used were less physiologically relevant in human cell lines compared to the ground squirrels (4°C), as survival mechanisms for hibernation in the ground squirrels will most likely be extremely organism specific.

1.2.3.4 Osmotic Stress

Osmotic stress is the condition of a rapid change in the solute concentration of a cells environment. Osmotic stress results in rapid water flux across membranes and changes in intracellular ion concentration. In *S. cerevisiae,* changes in environmental osmolarity are sensed by two transmembrane sensors Sho1 and Sln1, triggering a signalling cascade which ultimately leads to the activation of the mitogen-activated protein kinase (MAPK) Hog1 (Chen and Thorner, 2007). A recent study into the response of sumoylation to osmotic stress revealed that a Siz1 dependant accumulation of poly-Smt3 chains occur upon osmotic stress conditions (Irqeba *et al.*, 2014). Interestingly, the MAPK Hog1 was revealed to control the level and persistence of these poly-Smt3 chains, thus preventing the accumulation of poly-SUMO chains after osmotic stress (Irqeba *et al.*, 2014). However, the Hog1 dependant limitation of poly-Smt3 chains was not dependent on new protein synthesis, suggesting that Hog1 was acting independently of transcriptional activation (Irqeba *et al.*, 2014). Another study identified global increases in sumoylation after cationic and osmotic stress by $NaCl_2$ and KCl, as well as osmotic stress by sorbitol *S. cerevisiae* (Lewicki *et al.*, 2015). In agreement with the previous study into osmotic induced sumoylation, this study also identified Siz1, as well as Ulp2, as the sumoylation pathway components that mediated the SSR response. Furthermore, this study also found that de novo protein synthesis was not required for the SSR response (Lewicki *et al.*, 2015). Interestingly, however, this study identified that active transcription was required for the response, and found that many factors involved in transcription were sumoylated in the osmotic SSR, such as chromatin remodellers and Pol II-associated elongation factors (Lewicki *et al.*, 2015). It is therefore interesting to note that the poly sumoylation mutant ($smt3^{allR}$) was identified as having aberrant stress response transcription (see section 1.1.5), suggesting that the role of the SSR, at least in the case of osmotic stress, could be due to stress induced changes in transcription via poly-Smt3 chain formation.

1.2.3.5 Oxidative Stress

Oxidative stress is the condition of high levels of reactive oxygen species (ROS) such as hydroxyl radicals ($\cdot OH$), superoxide (O_2^-), and hydrogen peroxide (H_2O_2). High levels of ROS can cause damage to lipids, protein and DNA. ROS such as are produced endogenously during respiration, but can also arise from the environment, and are detoxified by abundant ROS scavenging enzymes to prevent cellular damage (Veal *et al.*, 2007). Evidence of the involvement of sumoylation pathway enzymes in sensing levels of ROS was first indicated by a study in mammalian cells (Bossis and Melchior, 2006). The pKa of most cysteine residues in proteins is normally too high to allow their oxidation by ROS, but some catalytic cysteines have a lower pKa, allowing oxidation. An example of such reactive cysteine residues are the catalytic cysteines of the E1 subunit SAE2, E2 UBC9 and SENPs, which are sensitive to

oxidation by H_2O_2 (Figure 1.9). When cells are treated with low H_2O_2 (1 mM), a disulphide was found to form between the catalytic cysteine residue of SAE2 (Cys173) and the catalytic cysteine residue of Ubc9 (Cys93) (Bossis and Melchior, 2006). The oxidation of the E1 and E2 enzymes prevented protein sumoylation, and as a consequence led to a decrease in global sumoylation (Figure 1.9 A). Conversely, although SAE2/Uba2 and Ubc9 were still oxidised, eatment with high levels of H_2O_2 lead to an increase in sumoylation levels (Bossis and Melchior, 2006). The basis for the increase in sumoylation was not elucidated, but it was proposed that the catalytic cysteine residues of the SENPs were oxidised, preventing desumoylation of substrates. Indeed, further research revealed there was differential oxidation of the mammalian SENP proteins upon exposure to oxidative stress (Xu *et al.*, 2008b). Disulphide dimers of SENP-1 were demonstrated to form in the presence of 20 mM H_2O_2, involving the catalytic Cys603 and another Cys613 residue (Xu *et al.*, 2008b) (Figure 1.9 B). However, the cysteine residues of SENP-2 were oxidised to the sulphinic (-SOOH) and sulphonic (-SOOOH) forms, leaving SENP-2 in monomeric form (Xu *et al.*, 2008b) (Figure 1.9 B). Interestingly, the dimerization of SENP-1 was reversible, as desumoylase activity was recovered upon treatment with the reducing agent dithiothreitol (Xu *et al.*, 2008b). However, SENP-2 was oxidised irreversibly at the same concentration (Xu *et al.*, 2008b). Furthermore, treatment of the fungal pathogen *C. albicans* to H_2O_2 led to an increase in sumoylated substrates (Leach *et al.*, 2011). This is particularly relevant in the case of pathogenic *C. albicans*, as evasion of host immune systems requires resistance to ROS during the respiratory burst following phagocytosis (Dantas Ada *et al.*, 2015).
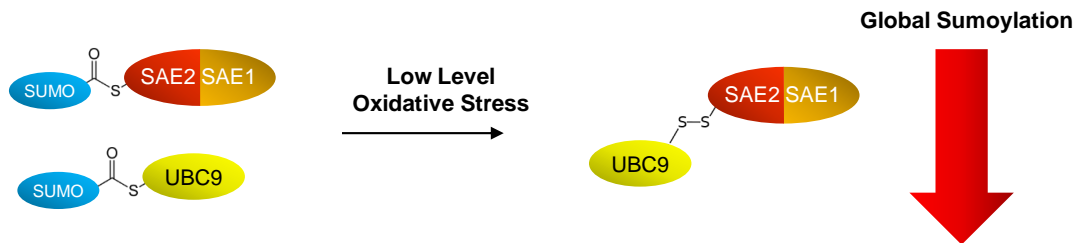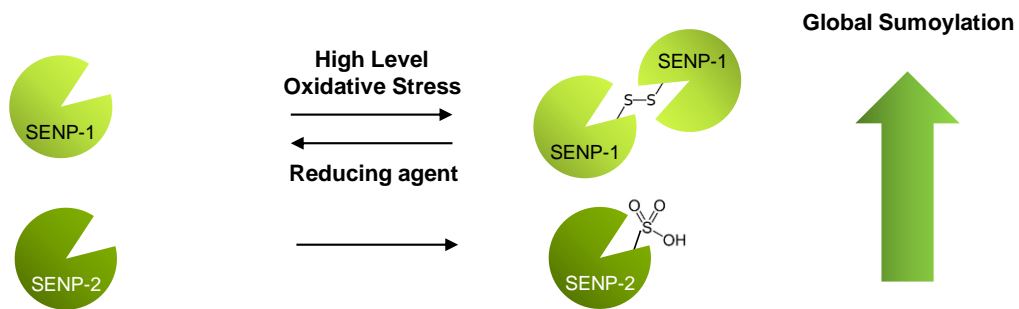
Figure 1.9: Oxidative stress levels are sensed by the differential oxidation of the sumoylation E1 and E2 and deconjugation enzymes. A) During low level H_2O_2 treatment (1 mM), a disulphide forms between the catalytic cysteines between the E1 SAE2 (Cys173) and the E2 UBC9 (Cys93), reducing global sumoylation (Bossis and Melchoir, 2006). B) During high level H_2O_2 treatment (20 mM), SENP-1 forms a dimer between the catalytic cysteine Cys603 and another cysteine Cys613. This dimerization is reversible in the presence of the reducing agent DTT. At 20 mM H_2O_2 SENP-2 is oxidised irreversibly. These events lead to an increase in global sumoylation (Xu *et al.*, 2008b).

1.3 Genome wide screens

As described above, directed approaches in yeast and mammalian cells have identified many functions of sumoylation in a diverse range of cellular processes. However, many of the sumoylation events occur as a global sumoylation event, as shown by sumoylation dynamics in the SSR.

1.3.1 Proteomics to Discover Sumoylated Proteins

Many early studies used *in vitro* sumoylation assays to confirm protein sumoylation (Takahashi *et al.*, 1999; Takahashi *et al.*, 2001), however, using this method to identify sumoylation targets has caveats. Ubc9 can bind and sumoylate consensus sequences alone (Bernier-Villamor *et al.*, 2002; Lin *et al.*, 2002; Pichler *et al.*, 2005), and E3 ligases can lack specificity *in vitro* reactions (Takahashi *et al.*, 2003), therefore artefactual sumoylation events are likely to occur when substrates and the conjugation machinery are expressed in amounts which may never occur in the cell due to different localisation. Moreover, many sumoylation events may require previous modifications, e.g., phosphorylation (Hietakangas *et al.*, 2006) (see section 1.1.2.1), so this will not be seen *in vitro*. Therefore, confirmation of *in vitro* sumoylation does by no means verify that this occurs *in vivo*. Thus, proteomics of *in vivo* sumoylation are much more appropriate in the detection of sumoylated substrates. However, mass spectrometry of sumoylated proteins is demanding, as sumoylated proteins can be modified at very low levels, and sumoylated substrates are particularly vulnerable to deconjugation during protein extraction due to the high activity of deconjugase enzymes (Eifler and Vertegaal, 2015a). Furthermore, ubiquitin is also more suited for MS analysis to detect target lysine residues, as trypsin digestion of ubiquitinated substrates leaves a small diglycine adduct. However, digestion of sumoylated substrates leaves a larger adduct which makes identification of the sumoylated lysine residue more difficult (Eifler and Vertegaal, 2015a). Therefore, some methods require exogenous enrichment of sumoylated substrates by ectopic over expression of SUMO, or heat shock can be used (Zhao *et al.*, 2004; Leach *et al.*, 2011, Blomster *et al.*, 2009). Although others use either SUMO specific antibodies (Becker *et al.*, 2013), or cells lines with stable epitope tagged expression of SUMOs (Vertegaal *et al.*, 2004), without the confirmation of sumoylation occurring on a lysine motif, it is difficult to determine if these are SUMO interacting partners or sumoylated substrates without biochemical data (Filosa *et al.*, 2013). Due to the extremely high number of hits these global arrays often provide, many cannot validate all sumoylation hits. Thus, although sumoylation proteomic data provides a rich resource for researchers, they are limited in the insight which can be gained. For instance, a crucial yet transient sumoylation event may not be picked up in mass spectrometry analysis. Furthermore, abundance of sumoylation on a target does not correlate with importance of function, as observed with the *S. cerevisiae* septins (see section 1.2.2.2). Also, the cellular

response to such a sumoylation event is unknown, making selection of appropriate substrates to research further difficult. Therefore, genetic approaches can prove a powerful tool for elucidating sumoylation.

1.3.2 Genetic Interaction Studies in Yeast

Genetic interaction is the phenomenon where the phenotype associated with the mutation of a gene is either suppressed or aggravated by a mutation of a different loci. When the phenotype of a mutant is aggravated by the presence of another genetic mutation, which is unexpectedly more severe than the summation of the respective single mutant phenotypes, the gene pair are said to negatively interact. In the extreme case of this, the presence of the two mutations leads to cell death, and these genes are synthetically lethal. Conversely, if the phenotype of a mutant is suppressed by the presence of another mutation, the two genes are said to have a positive genetic interaction. Genetic interaction studies can then infer biological function to the original mutants. Gene pairs which negatively interact or are synthetically lethal imply that the two genes function in the same biological role, but in different cellular pathways. Thus, the loss of both pathways towards the similar biological process then leads to a more extreme phenotype or cell death, as loss of one pathway can no longer compensate for the other. The case of positive genetic interaction can indicate that one gene is negatively regulating a biological process, and the loss of regulation is detrimental for cell growth. Therefore, removal of the aberrant biological process by mutation then synthetically rescues the single mutant. In yeast, study of genetic interaction can be completed on a genome wide scale, termed a synthetic genetic array (Tong *et al.*, 2001). This powerful technique can use libraries of genetic mutants to infer biological functions to a mutation, down to single genes within genetic pathways.

Global genetic interactions of SUMO have been previously completed in *S. cerevisiae* and *S. pombe* (Makhnevych *et al.*, 2009; Costanzo *et al.*, 2010; Ryan *et al.*, 2012). The only screen in *S. pombe*, and one of the screens in *S. cerevisiae*, were global epistasis map screens. In the case of the *S. pombe* screen, a *pmt3Δ* strain was used in the library that was crossed with ~953 query strains (Ryan *et al.*, 2012). However, *ubc9Δ* was not included in this screen.

1.4 Dysregulation of Sumoylation in Disease States

Given the lethality associated with the loss of sumoylation in many organisms, it is not surprising that there is a growing body of evidence that deregulation of sumoylation could be linked to various disease states.

1.4.1 Cancer

SUMO appears to have tumour promoting roles in different cancers. For example, over expression of Ubc9 occurs in ovarian (Ryan *et al.*, 2012), colon and prostate cancers (Moschos *et al.*, 2010), and in breast, head and neck, and lung cancers (Wu *et al.*, 2009). Furthermore, lung cancer cells stably overexpressing of Ubc9 in a mouse model showed increased metastasis ability, suggesting over expressed Ubc9 promotes cell invasion (Li *et al.*, 2013). Indeed, Ubc9 is the most highly expressed protein in melanoma infiltrated lymph nodes, strongly suggesting metastasis requires high levels of Ubc9 (Moschos *et al.*, 2007). Consistent with the tumour promotion role of sumoylation, lower expression of SAE1, the human SUMO E1, was indicative of breast cancer tumours which would metastasise later than others (Kessler *et al.*, 2012). However, SUMO removal is also likely to have tumour promoting functions, as elevated levels of the deconjugase SENP-1 is observed in prostate cancer cells, and reduction of SENP1 in prostate cancer cell lines show decreased cell viability (Wang *et al.*, 2015).

Interestingly, SUMO also directly modifies proteins encoded by various oncogenes (the term used for genes involved in cell proliferation which are often deregulated or mutated in cancers). For example, the transcription factor c-Myc is one of the most frequently upregulated oncogenes in many cancer types, upregulated by amplification, gain of function mutation, gain in protein stabilisation or over expression (Beroukhim *et al.*, 2010). Interestingly, sumoylation was found to be essential for the transcriptional programme of c-Myc, as knock down of the SAE2 E1 subunit in c-Myc overexpressing cell lines lead to mitotic catastrophe, while the same knock down of SAE2 in cells expressing normal levels of c-Myc did not (Kessler *et al.*, 2012). However, how sumoylation regulates c-Myc is not well understood. Recent studies identified that sumoylation of c-Myc promoted degradation via RNF4, the Slx5/8 homolog in mammals (Gonzalez-Prieto *et al.*, 2015). Interestingly, a recent study showed that the sumoylation of another Myc family member, n-Myc, is increased upon heat shock and proteasome inhibition (Sabo *et al.*, 2014). This could suggest that n-Myc is a targeted by the heat shock SSR. Furthermore, the increase in n-Myc sumoylation upon proteasome inhibition is consistent with c-Myc RNF4 promoted degradation (Gonzalez-Prieto *et al.*, 2015). This could suggest a role for sumoylation and degradation of the Myc family proteins. Thus, while essential for c-Myc function, the role for sumoylation in the regulation of Myc family members is unclear. However, the specific effect of sumoylation knockdown on c-Myc overexpressing cancers could provide an interesting avenue for drug targetting.

1.4.2 Ageing and Neurodegerative Diseases

Sumoylation has also been linked to the premature ageing disease, Hutchinson Guilford Progeria Syndrome (HGPS). HGPS causes rapid ageing in children, and patients with the disease often die from disease associated with arterial hardening at age 13 (Ding and Shen,

2008). Nuclear lamins are proteins which form nuclear lamina, providing structure to the nucleus as well as other functions (Gruenbaum and Foisner, 2015). In HGPS, a sporadic genetic mutation in the nuclear lamin A gene LMNA causes a premature lamin called progerin to accumulate in the nuclear membrane, but how this causes the disease state is unknown. Recently a study of fibroblasts of HGPS patients revealed that Ubc9 is mislocalised to the cytoplasm (Kelley *et al.*, 2011). Furthermore, the same group found that the Ubc9 localisation disruption was due to progerin producing reactive oxygen species (ROS) which disrupted the nuclear-cytoplasmic Ran gradient, thereby lowering the nuclear concentration of Ubc9 by reduced import (Datta *et al.*, 2014). However, whether disruption of Ubc9 localisation by ROS could have an influence in HGPS is unknown.

Alzheimer's disease is an incurable neurodegerative disease that begins as a gradual decline in memory recall, leading to eventual loss of bodily functions. The cause of Alzheimer's is poorly understood, but one theory is the cognitive decline is due to the production of tau protein aggregates, and of $A\beta$ aggregates from the amyloid precursor protein (APP) forming in neurons (Armstrong, 2013). Interestingly, SUMO-3 protein levels were found to be increased in the brains of patients with Alzheimer's disease (Li *et al.*, 2003), and conversely the levels of SENP-3 were down regulated (Weeraratna *et al.*, 2007). The APP that is processed to form $A\beta$ aggregates in Alzheimer's disease is also known to be sumoylated, and interestingly the modification of APP decreases the formation of $A\beta$ aggregates, although the mechanism is unknown (Zhang and Sarge, 2008). Furthermore, the microtubule associated protein tau has been shown to be modified by SUMO on Lys340 in cell lines (Dorval and Fraser, 2006). Interestingly, upon proteasome inhibition the levels of ubiquitinated tau increased, while the levels of sumoylated tau decreased (Dorval and Fraser, 2006). This suggests Lys340 residue is also modified by ubiquitin, and ubiquitination promotes tau degradation. However, this study was completed in a kidney cell line, so this would be interesting to see if this modification could be detected in a neuronal cell line. The regulation of sumoylation in neurodegenerative diseases is still a relatively new topic, but the role of SUMO in $A\beta$ aggregates and tau degradation would be of interest to study to elucidate the cause of this disease, and provide potential for future therapeutics.

1.4.3 Pathogenic Infection

1.4.3.1 Viral Infection

Given the roles of sumoylation in cell stress responses, it is perhaps unsurprising that the sumoylation pathway is heavily implicated with infection. In mammalian cells, promyelocytic leukaemia protein nuclear bodies (PML-NBs) appear as 'nuclear dots' enriched with the principal component, PML protein. PML-NBs are implicated in a wide range of processes,

such as transcription, cell-cycle control, DNA damage and repair and apoptosis (Cheng and Kao, 2012; Sahin *et al.*, 2014), and have been identified as important regulators of the cellular response to invasion of viral pathogens (Everett and Chelbi-Alix, 2007). Furthermore, SUMO is understood to be a key regulator of PML-NB function, with many of the proteins within PML-NBs sumoylated and contain SIMs (Van Damme *et al.*, 2010; Cheng and Kao, 2012). For example, upon poliovirus infection, sumoylation of PML recruits p53 to the PML-NBs, and subsequently induces apoptosis of the infected cell (Pampin *et al.*, 2006). Interestingly, viruses have developed methods of altering the host sumoylation systems to their advantage. For example, the avian adenovirus chicken embryo lethal orphan (CELO) virus produces a protein, Gam-1, which inhibits host sumoylation in a two pronged approach by interrupting the E1-E2 in the SUMO conjugation pathway, as well as targeting the E1 and E2 enzymes for proteaosomal degradation (Boggio *et al.*, 2004; Boggio *et al.*, 2007). Additionally, viruses produce proteins that share similarities with SUMO system components to enable them to target PML-NBs. For example, the human herpes simplex virus produces the ICP0 protein which acts as a STUbL to ubiquitinate sumoylated proteins, including the PML-NB components to promote their degradation (Muller and Dejean, 1999). This causes a decrease in global sumoylation, and dispersal of PML-NBs (Muller and Dejean, 1999). In addition, the human adenovirus serotype 5 (HAdV5) E1B-55K protein acts as a SUMO E3 ligase to sumoylate p53, causing eviction of p53 from the nucleus, thereby preventing p53 recruitment to the nuclear PML-NBs and subsequent apoptosis (Pennella *et al.*, 2010). However, not all connections between viral infection and SUMO are linked to PML-NB dysregulation and dispersal. Indeed, the Epstein-Barr virus (EBV) uses host sumoylation systems to sumoylate its own viral transcription factor BZLF1 (Murata *et al.*, 2010). The sumoylated BZLF1 then represses the transcription of genes within the viral genome, by recruiting host histone deacetylase complexes to the viral genome (Murata *et al.*, 2010). As well as those listed here, many other DNA and RNA human viruses such as papillomaviridae, poxviridae and retroviridae have been shown to influence or interact with the SUMO system (Wimmer *et al.*, 2012).

1.4.3.2 Bacterial Infection

As well as viruses, virulent bacteria also target the SUMO system to their advantage. For example, the human pathogen *Listeria monocytogenes* produces the Listeriolysin O (LLO) protein, a pore forming toxin crucial for its virulence (Hamon *et al.*, 2012). Significantly, LLO was found to promote the proteasomal degradation of Ubc9 in *L. monocytogenes* infected HeLa cells, reducing global sumoylation levels (Ribet *et al.*, 2010). This effect on Ubc9 levels was found to be promoted by other pore forming toxins from the bacteria *Clostridium perfringens* (Perfingolysin O, PFO) and *Streptococcus pneumoniae* (Pneumolysin, PLY) (Ribet *et al.*, 2010). The researchers demonstrated that the LLO induced global reduction in

sumoylation was advantageous for *L. monocytogenes* due to inhibition of a TNF-β-dependant immune response (Ribet *et al.*, 2010). However, it could not be confirmed that this was a direct effect of LLO on sumoylation, or it was another off target effect of the LLO toxin. Another pathogenic bacterial species, Yersinia, has been shown to effect host SUMO conjugate levels (Orth *et al.*, 2000; Zhou *et al.*, 2005). Both *Yersinia pseudotuberculosis* and *Yersinia enterocolitica* produce a cysteine protease, YopJ, which shows structural similarity to Ulp1 (Orth *et al.*, 2000; Zhou *et al.*, 2005). Indeed, YopJ has SUMO deconjugating activity against SUMO-1 modified proteins, as well as ubiquitinated proteins (Orth *et al.*, 2000; Zhou *et al.*, 2005). While the sumoylated substrates targeted by YopJ have not been identified, interestingly, the NFκB inhibitor IκBα was deubiquitinated by YopJ (Zhou *et al.*, 2005). This prevented the activation of NFκB signalling, like SUMO modification of IκBα. These studies show that many pathogens use sumoylation to evade host immune defences, however, more could be understood about the targets of these global sumoylation changes which occur upon pathogenic infection.

1.5 Summary and Aims

Sumoylation is a well conserved protein modification with roles in many cellular processes, from cell cycle regulation, DNA damage and repair, transcription and stress responses. As such, aberrant sumoylation has implications for human health and disease. Proteomic data has shown that targets are sumoylated in a wide array of cellular processes, however the biological relevance of many sumoylation events is unknown. Therefore, the aim of this study was to take advantage of the viability of sumoylation mutants in the organism *S. pombe*, and use high through put genetic screening strategies to aid the understanding of the biological processes regulated by sumoylation.

Chapter Two: Materials and Methods

2.1 *S. pombe* and *S. cerevisiae* Yeast Strains

The *S. pombe* strains used in this study were derived from the CHP428 background strain (h^+ *ade6-M210 his7-336 leu1-32 ura4-D18*) or the Bioneer strain background derived from the diploid host strain SP286 (h^+/h^+ *ade6-M210/ade6-M216 ura4-D18/ura4-D18 leu1-32/leu1-32*). The *S. cerevisiae* strains used in this study are derived from BY4741 strain background (*MATa his3Δ1 leu2Δ0 met15Δ0 ura3Δ0*). *S. pombe* strains are outlined in Table 1, and *S. cerevisiae* strains are outlined in Table 2.

2.2 Yeast Techniques

2.2.1 *S. pombe* Growth Conditions

S. pombe strains were grown in YE5S rich media (0.5% [w/v] yeast extract, 3% [w/v] glucose, 225 mg/L adenine hemisulphate, L-histidine, uracil, L-Lysine monochloride and L-Leucine) or EMM media (3 g/L potassium hydrogen phthalate, 2.2 g/L Na_2HPO_4, 5 g/L NH_4Cl, 2% [w/v] glucose, 20 ml/L salt solution [50x stock [52.5 g/L $MgCl_2.6H_2O$, 735 µg/L $CaCl_2.2H_2O$, 50 g/L KCl, 2 g/L $NaSO_4$], 1 ml/L vitamins [1 g/L pantothenic acid, 10 g/L nicotinic acid, 10 g/L inositol, 10 mg/L biotin], 0.1 ml/L minerals [5 g/L boric acid, 4 g/L MnSO4, 4 g/L $ZnSO_4.7H_2O$, 2 g/L $FeCl_2.6H_2O$, 0.4 g/L molybdic acid, 1 g/L KI, 0.4 g/L $CuSO_4.5H_20$, 10 g/L citric acid]) supplemented with the appropriate amino acids and nucleotides as outlined previously (Moreno *et al.*, 1991) (all supplied by Sigma-Aldrich). To repress expression from *nmt41$^+$* promoters in pREP41 plasmids, EMM was supplemented with 15 µM thiamine. Solid media was made with the above components supplemented with 2% (w/v) bacto-agar. Strains were grown at 30°C unless otherwise stated.

2.2.2 *S. cerevisiae* Growth Conditions

S. cerevisiae strains were grown in YPD rich media (1% [w/v] yeast extract, 2% [w/v] Bacto-Peptone, 2% [w/v] glucose), or minimal SD media (0.67% [w/v] Bacto-Yeast nitrogen base without amino acids (Difco), 2% glucose). Where appropriate, SD was supplemented with L-Histidine hydrochloride (10 mg/L), L-Leucine (20 mg/L), Uracil (8 mg/L), L-Lysine hydromonochloride (30 mg/L) and L-Methionine (10 mg/L) (all supplied by Sigma). G418 antibiotic (Formedium) was supplemented at 400 µg/ml and clonNAT (WERNER BioAgents) supplemented at 100 µg/ml. Media used during SGA analysis is described in section 2.2.7.1. Strains were grown at 30°C unless otherwise stated. For YPD or SD solid agar the media was supplemented with 2% (w/v) bacto-agar. Strains were grown at 30°C unless otherwise stated.

ID	Genotype	Source
RB9	*h^+/h^- fkh2Δ::ura4/fkh2$^+$ ade6-M210/ade6-M216 his7-366/his7-366 leu1-32/leu1-32 ura4-D18/ura4-D18*	(Bulmer *et al.*, 2004)
CHP428	*h^+ ade6-M210 his7-366 leu1-32 ura4-D18*	Gift from Charlie Hoffman
CHP429	*h^- ade6-M216 his7-366 leu1-32 ura4-D18*	Gift from C. Hoffman
CL49	*h^+/h^+ pmt3Δ::KanMX4/pmt3$^+$ ade6-M210/ade6-M216 ura4-D18/ura4-D18 leu1-32/leu1-32*	(Kim *et al.*, 2010)
CL53	*h^+/h^+ ubc9Δ::KanMX4/ubc9$^+$ ade6-M210/ade6-M216 ura4-D18/ura4-D18 leu1-32/leu1-32*	(Kim *et al.*, 2010)
CL109	*h^+/h^- fkh2Δ::ura4$^+$/fkh2$^+$ ubc9Δ::KanMX4/ubc9$^+$ ade6-M210/ade6-M216 his7-366/his7-366 leu1-32/leu1-32 ura4-D18/ura4-D18*	This study
CHP428/ CHP429	*h^+/h^- ade6-M210/ade6-M216 his7-366/his7-366 leu1-32/leu1-32 ura4-D18/ura4-D18*	Gift from Charlie Hoffman
CL363	*h^+/h^- fkh2-3PK::ura4$^+$/fkh2$^+$ pmt3Δ::KanMX4/pmt3$^+$ ade6-M210/ade6-M216 his7-366/his7-366 leu1-32/leu1-32 ura4-D18/ura4-D18*	This study
CL370	*h^+/h^- pmt3Δ::KanMX4 ade6-M210/ade6-M216 his7-366/his7-366 leu1-32/leu1-32 ura4-D18/ura4-D1*	This study
CL76	*h^+ ade6-MX ura4-D18 leu1-32*	This study
FP66	*h^+ leu1-32 ura4-D18 ade6-MX yox1Δ::KanMX4*	(Purtil *et al.*, 2011)
JB355	*h^+ leu1-32 ura4-D18 ade6-MX sep1Δ::ura4$^+$*	(Zilahi *et al.*, 2000)

Table 2.1: *S. pombe* **strains used in this study**. If the *ade6* allele is unknown, this is indicated by *ade6-MX.*

ID	Genotype	Source
CL90	*MATa his3-DAmP::KanMX his3Δ1 leu2Δ0 ura3Δ0 met15Δ0*	(Breslow *et al.,* 2008)
CL91	*MATa uba2-DAmP::KanMX his3Δ1 leu2Δ0 ura3Δ0 met15Δ0*	(Breslow *et al.,* 2008)
CL92	*MATa smt3-DAmP::KanMX his3Δ1 leu2Δ0 ura3Δ0 met15Δ0*	(Breslow *et al.,* 2008)
CL93	*MATa aos1-DAmP::KanMX his3Δ1 leu2Δ0 ura3Δ0 met15Δ0*	(Breslow *et al.,* 2008)
CL94	*MATa ulp1-DAmP::KanMX his3Δ1 leu2Δ0 ura3Δ0 met15Δ0*	(Breslow *et al.,* 2008)
CL95	*MATa ulp2-DAmP::KanMX his3Δ1 leu2Δ0 ura3Δ0 met15Δ0*	(Breslow *et al.,* 2008)
CL100	*MATa smt3-DAmP::NatMX his3Δ1 leu2Δ0 ura3Δ0 met15Δ0*	*This study*
CL106	*MATα lyp1Δ::HphMX::LEU2 can1Δ::STE2pr-Sp_his5 his3Δ1 leu2Δ0 ura3Δ0 met15Δ0*	*Newcastle University High throughput service*
CL107	*MATa smt3-DAmP::NatMX lyp1Δ::HphMX::LEU2 can1Δ::STE2pr-Sp_his5 his3Δ1 leu2Δ0 ura3Δ0 met15Δ0*	*This study*
CL163	*MATa siz2Δ::KanMX smt3-DAmP::NatMX lyp1Δ::HphMX::LEU2 can1Δ::STE2pr-Sp_his5 his3Δ1 leu2Δ0 ura3Δ0 met15Δ0*	*This study*
CL207	*MATa cct8-DAmP::KanMX smt3-DAmP::NatMX lyp1Δ::HphMX::LEU2 can1Δ::STE2pr-Sp_his5 his3Δ1 leu2Δ0 ura3Δ0 met15Δ0*	*This study*
CL211	*MATa cct3-DAmP::KanMX smt3-DAmP::NatMX lyp1Δ::HphMX::LEU2 can1Δ::STE2pr-Sp_his5 his3Δ1 leu2Δ0 ura3Δ0 met15Δ0*	*This study*
CL227	*MATa siz1Δ::KanMX smt3-DAmP::NatMX lyp1Δ::HphMX::LEU2 can1Δ::STE2pr-Sp_his5 his3Δ1 leu2Δ0 ura3Δ0 met15Δ0*	*This study*
BY4741	*MATa his3Δ1 leu2Δ0 ura3Δ0 met15Δ0*	*David Lydall*
CL237	*MATa smt3-DAmP::NatMX arp2-DAmP::KanMX his3Δ1 leu2Δ0 ura3Δ0 met15Δ0 lyp1Δ::HphMX::LEU2 can1Δ::STE2pr-Sp_his5*	*This study*
CL238	*MATa smt3-DAmP::NatMX arp3-DAmP::KanMX his3Δ1 leu2Δ0 ura3Δ0 met15Δ0 lyp1Δ::HphMX::LEU2 can1Δ::STE2pr-Sp_his5*	*This study*
CL239	*MATa smt3-DAmP::NatMX arc35-DAmP::KanMX his3Δ1 leu2Δ0 ura3Δ0 met15Δ0 lyp1Δ::HphMX::LEU2 can1Δ::STE2pr-Sp_his5*	*This study*
CL244	*MATa slx8Δ::KanMX his3Δ1 leu2Δ0 ura3Δ0 met15Δ0*	*Newcastle University High throughput service*
CL253	*MATa siz1Δ::KanMX his3Δ1 leu2Δ0 ura3Δ0 met15Δ0*	*Newcastle University High throughput service*
CL254	*MATa cct8-DAmP::KanMX his3Δ1 leu2Δ0 ura3Δ0 met15Δ0*	(Breslow *et al.,* 2008)
CL259	*MATa cct3-DAmP::KanMX his3Δ1 leu2Δ0 ura3Δ0 met15Δ0*	(Breslow *et al.,* 2008)
CL260	*MATa siz2Δ::KanMX his3Δ1 leu2Δ0 ura3Δ0 met15Δ0*	*Newcastle University High throughput service*
CL268	*MATa arc35-3HA::KanMX his3Δ1 leu2Δ0 ura3Δ0 met15Δ0*	*This study*
BY4742	*MATa his3Δ1 leu2Δ0 ura3Δ0 met15Δ0*	*Gift from David Lydall*
CL280	*MATa ulp1-DAmP::KanMX smt3-DAmP::NatMX lyp1Δ::HphMX::LEU2 can1Δ::STE2pr-Sp_his5 his3Δ1 leu2Δ0 ura3Δ0 met15Δ0*	*This study*
CL284	*MATa ulp2-DAmP::KanMX smt3-DAmP::NatMX lyp1Δ::HphMX::LEU2 can1Δ::STE2pr-Sp_his5 his3Δ1 leu2Δ0 ura3Δ0 met15Δ0*	*This study*

CL340	MATa arp2-DAmP::KanMX his3Δ1 leu2Δ0 ura3Δ0 met15Δ0	*Newcastle University High throughput service*
CL341	MATa arp3-DAmP::KanMX his3Δ1 leu2Δ0 ura3Δ0 met15Δ0	*Newcastle University High throughput service*
CL342	MATa arc35-DAmP::KanMX his3Δ1 leu2Δ0 ura3Δ0 met15Δ0	*Newcastle University High throughput service*
CL376	MATa tub3Δ::KanMX his3Δ1 leu2Δ0 ura3Δ0 met15Δ0	*Newcastle University High throughput service*
CL380	slx8Δ::KanMX arc35-DAmP::KanMX his3Δ1 leu2Δ0 ura3Δ0 lysX metX	*This study*
CL445	MATa smt3-DAmP::NatMX tub3Δ::KanMX his3Δ1 leu2Δ0 ura3Δ0 met15Δ0 lyp1Δ::HphMX::LEU2 can1Δ::STE2pr-Sp_his5	*This study*
CL474	MAT? arc35-3HA:KanMX smt3-DAmP::NatMX his3Δ1 leu2Δ0 ura3Δ0 met15Δ0	*This study*
CL480	MATa tub2-DAmP::KanMX his3Δ1 leu2Δ0 ura3Δ0 met15Δ0	*Newcastle University High throughput service*
CL486	MATa tub2-DAmP::KanMX smt3-DAmP::NatMX his3Δ1 leu2Δ0 ura3Δ0 met15Δ0 lyp1Δ::HphMX::LEU2 can1Δ::STE2pr-Sp_his5	*This study*

Table 2.2: *S. cerevisiae* strains used in this study. If the presence of a marker has not been verified it is indicated by X. If the mating type of the strain is unknown it is indicated by *MAT?*.

2.2.3 S. pombe Genomic DNA (gDNA) Extraction

gDNA was extracted from *S. pombe* by pelleting 100 µl of stationary phase cells at 2000 rpm for 3 minutes. The cells were resuspended in 1 ml nH$_2$O, pelleted again for 1 minute at 9000 rpm, then resuspended in 200 µl breakage buffer (10 mM Tris-HCl [pH 8], 1 mM EDTA, 100 mM NaCl, 1% [w/v] SDS, 2% [v/v] Triton X-100). Cells were ribolysed for 20 seconds after the addition of 400 µl of glass beads and 200 µl phenol:chloroform:isoamyl alcohol (25:24:1, pH 7.4) (Fisher BioReagents). Another 500 µl of breakage buffer were added then the sample vortexed, and pelleted at 9000 rpm for 5 minutes. The supernatant was added to 50 µl of 3 M sodium acetate and 1 ml 100% ethanol, then placed at -20°C for 30 minutes to precipitate DNA. After precipitation, the sample was then spun for 15 minutes at 13000 rpm to collect gDNA. After washing in 70% ethanol, the supernatant was removed and gDNA resuspended in 100 µl dH$_2$O.

2.2.4 S. cerevisiae gDNA Extraction

gDNA was extracted from *S. cerevisiae* by a protocol previously described (Hoffman and Winston, 1987). *S. cerevisiae* cells were grown to saturation in 10 ml of YPD and collected at 3000 rpm for 3 minutes. The pellet was resuspended in 200 µl of detergent lysis buffer (2% [v/v] Triton X-100, 1% [w/v] SDS, 100 mM NaCl, 10 mM Tris-HCl [pH 8], 1 mM EDTA). 200 µl of phenol:chlorophorm:isoamyl alcohol (25:24:1; pH 7.4) and 200 µl of glass beads were added and the cells lysed for 1 minute using a Mini Beadbeater (Biospec Products). After addition of 200 µl of TE (10 mM Tris-HCl [pH 7.4], 1 mM EDTA [pH 8]), the aqueous layer was separated

by centrifugation at 13000 rpm for 3 minutes. The aqueous upper layer was transferred into a fresh eppendorf. 1 ml of ice cold 100% ethanol was added and the precipitated DNA collected by centrifugation for 5 minutes at 13000 rpm at 4°C. The DNA was resuspended in TE (pH 8) solution containing 75 µg/ml RNase A (Sigma-Aldrich), and incubated at 37°C for 5 minutes to degrade RNA. The DNA was then precipitated for a final time in 100% ice cold ethanol plus 40 mM ammonium acetate, and collected by centrifugation for 5 minutes at 13000 rpm at 4°C. The pellet was dried and finally resuspended in 50 µl TE (pH 8).

2.2.5 Yeast Transformations

2.2.5.1 S. pombe Lithium Acetate Transformation

DNA was introduced into *S. pombe* using the LiAc method described previously (Moreno *et al.*, 1991). 50 ml of *S. pombe* cells were grown to an OD_{595nm} ~0.4, and pelleted at 2000 rpm for 2 minutes. The cells were washed in 1 ml of sterile dH_2O, and resuspended in 1 ml LiAc/TE (0.1 M LiAc [pH 7.5], 10 mM Tris-HCl [pH 7.5], 1 mM EDTA). 100 µl of cell suspension were mixed with 20 µg of salmon sperm DNA (Ambion) and ~0.1-1 µg of transforming DNA. After 10 minutes at room temperature, 260 µl of LiAc/TE/PEG (0.1 M LiAc [pH 7.5], 10 mM Tris-HCl [pH 7.5], 1 mM EDTA, 50% [w/v] PEG-4000) were added to the transformation mixture. The transformation reaction was incubated at 30°C for 30-60 minutes with agitation. Following incubation, 43 µl of 100% DMSO were added, and the reaction then incubated at 42°C for 5 minutes to heat shock the cells. The cells were then washed in 1 ml of dH_2O, resuspended in 200 µl of dH_2O and plated onto appropriate selective EMM media. The plates were incubated for 3-5 days at 30°C until colonies formed. For G418 selection, the cells were plated onto YE5S, incubated for 2-3 days at 30°C, then replica plated onto YE5S supplemented with G418, then incubated again at 30°C. Plates were incubated for 3 days, then G418 resistant colonies selected.

2.2.5.2 S. cerevisiae Lithium Acetate Transformation

DNA was introduced into *S. cerevisiae* cells as previously described (Schiestl and Gietz, 1989). 50 ml of mid-log phase growing cells (~3 x 10^7 cells) were pelleted at 2000 rpm for 3 minutes, washed with an equal volume of sterile water, and pelleted again. Cells were resuspended in 1 ml LiAc/TE (0.1 M LiAc, 10 mM Tris-HCl [pH 7.4], 1 mM EDTA [pH 8]). 200 µl of cells were added to 50 µg of salmon sperm DNA (Ambion) 0.1-10 µg of transforming DNA. 1.2 ml of LiAc/TE/PEG solution (0.1 M LiAc, 10 mM Tris-HCl [pH 7.4], 1 mM EDTA [pH 8], 40% [w/v] PEG-4000) were added and thoroughly mixed. The transformation mix was then incubated at 30°C with agitation for 30 minutes. Cells were heat shocked at 42°C for 15 minutes, then pelleted at 7000 rpm for 30 seconds. Cells were resuspended in 150 µl sterile water and plated onto appropriate selective media. Selection plates were incubated for 3-5 days at 30°C to

allow growth of transformants. For G418 and clonNAT selection of KanMX and NatMX strains, the transformation mixture was split over 2 YPD plates and grown for 2 days at 30°C. The resulting lawns were replica plated using a wooden block with Wattman filter paper onto 2 YPD plates supplemented with G418 or clonNAT, then incubated for a further 3 days at 30°C.

2.2.6 Strain Construction

2.2.6.1 Gene Deletion in S. pombe

Gene deletion in *S. pombe* is outlined in Figure 2.1. *S. pombe h⁺/h⁺* diploids containing a heterozygous KanMX4 replacement of each gene were purchased from Bioneer (Kim *et al.*, 2010). To move the cassette into the CHP428 strain, the *yfgΔ::KanMX4* cassette was amplified by PCR (see section 2.3.1.1) from the gene locus with including an additional 100 bp upstream and downstream from the deletion cassette. To increase the amount of cassette available for transformation, the cassette was cloned into pGEM-T (Promega) by TA cloning, and the resulting plasmid digested with EcoRI to drop out the cassette. The cassette was separated agarose gel electrophoresis, and the DNA extracted (see section 2.3.4). The cassette was then transformed into an *h⁺/h⁻* diploid strain, and plated onto YE5S. After incubation at 30°C for 2-3 days, the lawn was replica plated onto YE5S containing G418, and colonies obtained after another 2-3 day incubation. Correct integration of the deletion cassette was confirmed by a gene specific primer (Ubc9delF or Pmt3delF), and a KanMX cassette specific primer (Kan909R) (see section 2.3.1).

2.2.6.2 Antibiotic Marker Switching in S. cerevisiae

To switch the KanMX markers for NatMX marker in *S. cerevisiae*, a NatMX cassette containing plasmid, pAG25 (gift from P. Banks) was first digested with NsbI restriction enzyme, and the 1 kb NatMX cassette separated by agarose gel electrophoresis, and the DNA extracted from the agarose (see section 2.3.4). The NatMX cassette was then introduced into the *smt3-DAmP::KanMX* strain (CL92) by LiAc transformation method (see section 2.2.5.2). Antibiotic resistance switching at the correct locus was confirmed by sensitivity of cells to G418 and resistance to clonNAT, and by PCR.

2.2.6.3 ARC35 Epitope Tagging in S. cerevisiae

N terminal 3-HA epitope tagging of Arc35 expressed from the normal chromosomal locus was achieved by a method described previously (Longtine *et al.*, 1998). The strategy used is outlined in Figure 2.3. Briefly, oligonucleotide primers with homology to pFA6a-3HA-KanMX, and with homology to the sequence located directly upstream and downstream of the *ARC35* stop codon (Arc35HAtagF and Arc35HAtagR), were used to amplify a tagging cassette conferring G418 resistance.

Diploid *h⁺/h⁺*

PCR amplifies 100 bp up and downstream of
yfgΔ::KanMX4 and yfg⁺. The *yfgΔ::KanMX4* cassette
is cloned into pGEM®-T by TA cloning

EcoRI   *yfgΔ::KanMX4*   EcoRI

pGEM®-T is digested with EcoRI,
and fragment introduced into
CHP428/CHP429 diploid by LiAc
transformation

yfgΔ::KanMX4

The cassette integrates the
yfg⁺ gene locus by homologous
recombination.

Diploid *h⁺/h⁻*

yfg⁺

yfg⁺

Strain is checked by PCR using internal
KanMX primer and downstream primer

Diploid *h⁺/h⁻*

yfgΔ::KanMX4

yfg⁺

pmt3⁺/pmt3Δ   *ubc9⁺/ ubc9Δ*

− + + MW − +

2000
1500
1000
750
500

250

←~1600 bp

Strain is sporulated and the
haploid mutant obtained by
dissection.

Haploid   *yfgΔ::KanMX4*

51

Figure 2.1: Schematic diagram of gene deletion in *S. pombe*. Your favourite gene (*yfg⁺*) indicates gene to be deleted, which in this study is either *pmt3⁺* or *ubc9⁺*. The *yfg*Δ::*KanMX4* deletion cassette was amplified by PCR from deletion strain (Bioneer Corp.).   This was achieved using oligonucleotide primers located 100 bp upstream (pmt3delF or Ubc9delF) and 100 bp downstream (pmt3delR and Ubc9delR). The *yfg*Δ::*KanMX4* deletion cassette (1.7 kb) was extracted from the wildtype amplified cassette *yfg⁺* (900 bp) and cloned into the pGEM®-T vector via TA cloning, and the cassette sequenced using T7 and SP6 oligonucleotide primers. To introduce the deletion cassette into a CHP428/CHP429 diploid, the pGEM®-T vector was digested with EcoRI restriction enzyme, to drop out the *yfg*Δ::*KanMX4* deletion cassette.   The deletion cassette was introduced into diploid strains of *S. pombe* by LiAc transformation. Heterozygous diploids were selected by resistance to G418. Successful integration of the *yfg*Δ::*KanMX4* cassette at the *yfg⁺* locus was verified by PCR using oligonucleotide primers which anneal to the 3' end of KanMX (Kan909F) and upstream of *yfg⁺* (pmt3delF and Ubc9delF). Diploids were sporulated on appropriate EMM media plates for 3 days, and spores dissected to gain haploid sergeants. Haploids were verified by G418 resistance.
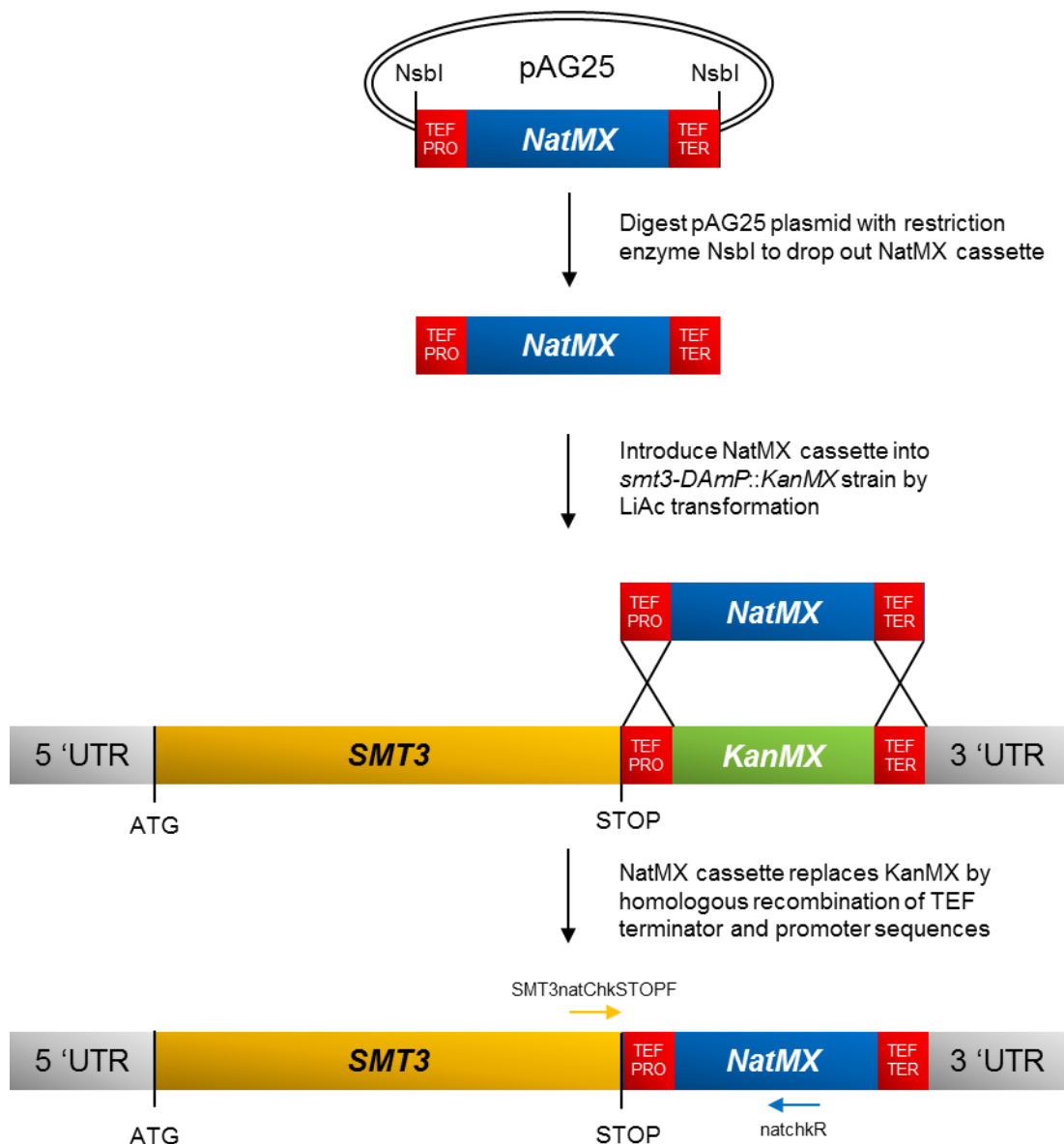
Figure 2.2: Schematic diagram of switching KanMX antibiotic marker with NatMX marker in *smt3-DAmP* strain. The plasmid pAG25 containing the NatMX marker sequence was digested with the restriction enzyme NsbI which drops out the NatMX cassette including the TEF promoter and terminator sequences in MX marker cassettes. The NatMX cassette was then introduced into the *smt3-DAmP::KanMX* strain by LiAc transformation. The NatMX cassette integrates at the KanMX marker within the *smt3-DAmP::KanMX* allele, directed by homology from the TEF promoter and terminator sequences. Colonies are selected by resistance to clonNAT, sensitivity to G418. Positive integrants at the *smt3-DAmP* loci are checked by PCR.
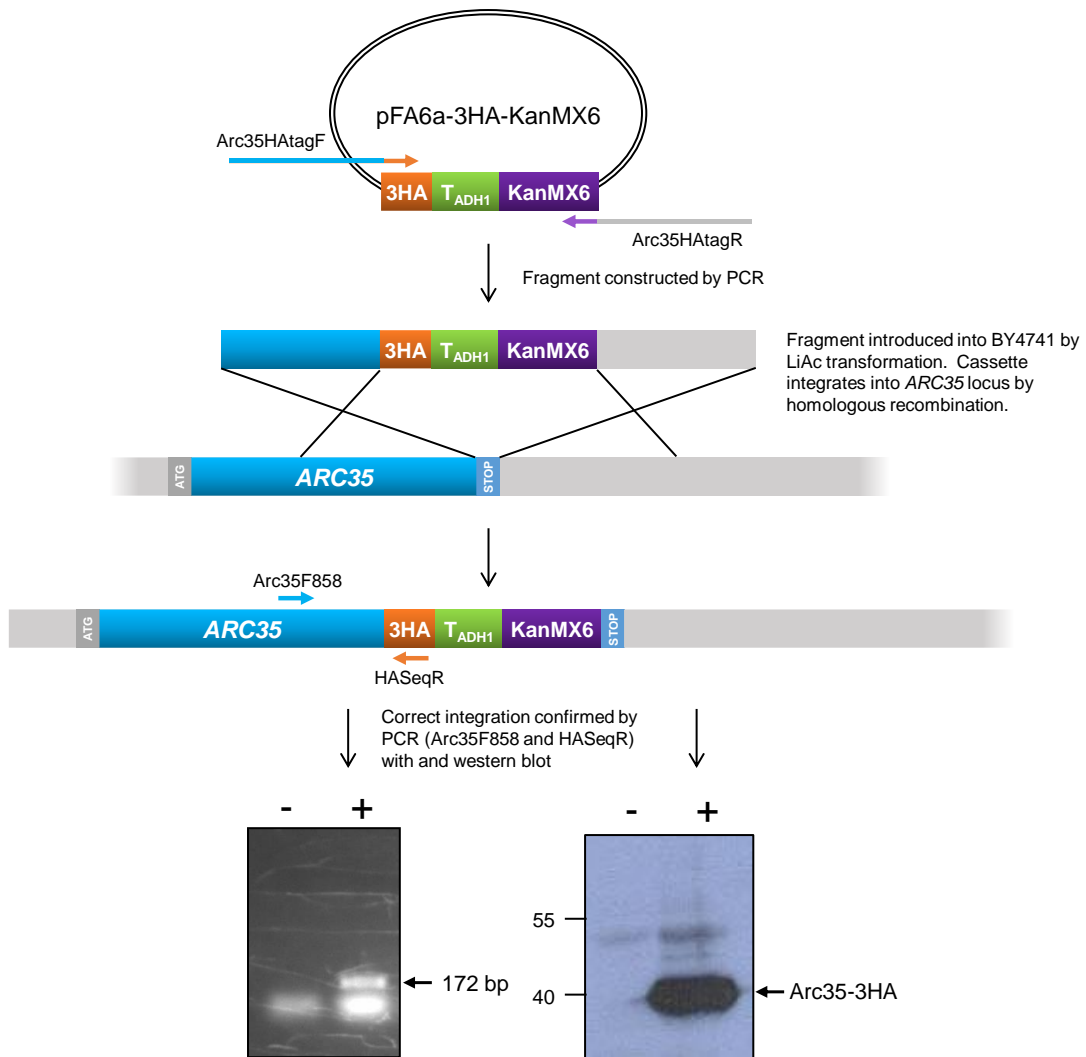
Figure 2.3: Schematic diagram of tagging Arc35 with 3HA epitope at its normal chromosomal locus. The oligonucleotide primer Arc35HATagF contains 40 bp of homology to the sequence located immediately upstream from the *ARC35* stop codon, and 20 bp of homology to the HA epitope sequence in the pFA6a-3HA-KanMX6 plasmid. The oligonucleotide primer Arc35HAtagR has 40 bp of homology to the sequence located immediately downstream of the *ARC35* stop codon, and 20 bp of homology to the sequence within the KanMX6 cassette of the pFA6a-3HA-KanMX6 plasmid. The HA tagging cassette is amplified via PCR (see section 2.3.1). The cassette is then introduced into BY4741 by LiAc transformation (see section 2.2.5.2). The cassette then integrates at the *ARC35* chromosomal locus, targeted by the 80 bp of homology introduced by Arc35HAtagF and Arc35HAtagR. The integration of the cassette replaces the *ARC35* stop codon with the 3HA tag. The 3HA tag is terminated by the T_{ADH1} is the terminator from the alcohol dehydrogenase *ADH1* gene in *S. cerevisiae*. Transformants were plated onto YPD, and the lawn allowed to grow for 2 days at 30°C. The lawn was then replica plated onto YPD + G418 plates and incubated at 30°C for 2 days. Resulting G418 resistant colonies were streaked onto YPD containing G418 twice more to ensure G418 resistance. G418 positive colonies were checked by PCR to ensure correct integration using Arc35F858 and HASeqR (see section 2.3.1). Successful epitope tagging was then confirmed by western blotting (see section 2.4.2).

2.2.6.4 S. cerevisiae Mating and Tetrad Dissection

Strains of opposite mating types were crossed on YPD media for 24 hours, and diploids selected using appropriate markers. A small amount of diploids freshly grown on YPD agar were added to 2 ml sporulation medium (1% [w/v] potassium acetate, L-Histidine hydrochloride [2.5 mg/ml], L-Leucine [5 mg/ml], Uracil [2 mg/ml], L-Lysine hydromonochloride [2.5 mg/ml] and L-Methionine [2.5 mg/ml]), and incubated for 7 days at 30°C to induce sporulation. 100 μl of sporulated cells were pelleted, resuspended in 50 μl of 5% [v/v] glusulase (PerkinElmer) and incubated at 30°C for 30 minutes to digest cell walls. This solution was then gently mixed with 300 μl of YPD medium, and 20 μl were pipetted onto a YPD plate. Tetrads containing 4 spores were then manipulated using a dissector (Singer Instruments) and the plates incubated at 30°C for 2-3 days.

2.2.6.5 S. pombe Sporulation and Tetrad Dissection

S. pombe h^+/h^+ diploids were sporulated by the introduction of the *ura4*$^+$ marked pON177 plasmid by LiAc transformation (Styrkarsdottir *et al.*, 1993) (see section 2.2.5.1). *ura*$^+$ colonies were allowed to grow and sporulate by incubation at 30°C on the selective EMM transformation plate for 5-7 days until asci were observed microscopically. h^+/h^- strains were sporulated by growth on EMM agar for 3-5 days at 30°C, until asci were observed microscopically. Sporulated diploids were mixed with 100 μl sterile dH$_2$O, and 20 μl pipetted onto a YE5S plate. Asci were manipulated using a dissector (Singer), and incubated at 37°C for 3-4 hours until the cell wall had broken down. Individual spores from each ascus were then separated, and allowed to grow for 4 days at 30°C, then patched onto YE5S + G418 to identify positive mutants. Strains were confirmed by PCR using an internal KanMX primer (Kan909R) and a primer targeting to a region 200 bp upstream of the start site of the gene deletion (see section 2.3.1).

2.2.7 Synthetic Genetic Array in S. cerevisiae

2.2.7.1 SGA Media

Media used during the SGA procedure are as follows. Enriched sporulation media (ESM) supplemented with G418 (1 g/L yeast extract, 0.05% [w/v] glucose, 1% [w/v] potassium acetate, 12.5 mg/L histidine, 62.5 mg/L leucine, 12.5 mg/L lysine, 12.5 mg/L uracil, 50 mg/L G418). Meiotic progeny were selected on SD/MSG (1.7 g/L yeast nitrogen base w/o ammonium sulphate, 1 g/L monosodium glutamate, 2 g/L amino nucleic acid drop-out power, 20 g/L bacto agar), as ammonium sulphate inhibits G418 and clonNAT selection. The appropriate amino acids were not included in the drop out powder to select for *MAT*a haploids harbouring the query and library mutations.

Amino nucleic acid drop-out power recipe for robotic media:

Adenine	3 g/L
Alanine	2 g/L
Arginine	**2 g/L**
Asparagine	2 g/L
Aspartic acid	2 g/L
Cysteine	2 g/L
Glutamic acid	2 g/L
Glutamine	2 g/L
Glycine	2 g/L
Histidine	**2 g/L**
Inositol	2 g/L
Isoleucine	2 g/L
Leucine	**10 g/L**
Lysine	**2 g/L**
Methionine	2 g/L
Para-aminobenzoic acid	0.2 g/L
Phenylalanine	2 g/L
Proline	2 g/L
Serine	2 g/L
Threonine	2 g/L
Tryptophan	2 g/L
Tyrosine	2 g/L
Uracil	2 g/L
Valine	2 g/L

Amino acids which are dropped out during the SGA process are highlighted in bold.

To all media used in the SGA, canavanine was supplemented at 50 µg/ml, thialysine was supplemented at 50 µg/ml, G418 supplemented at 200 µg/ml, hygromycin supplemented at 300 µg/ml, and clonNAT supplemented at 100 µg/ml.

2.2.7.2 SGA Process

All *S. cerevisiae* strains in the gene deletion and essential gene DAmP allele collection used in the cross were in the BY4741 strain background. The *MATα smt3-DAmP::NatMX* strain (CL100) was constructed to contain *NatMX* at the *SMT3* locus using a strategy outlined in Figure 2.3. The resulting *smt3-DAmP::NatMX* (CL100) strain was then crossed with a *MATα* strain containing SGA markers *lyp1Δ::HphMX::LEU2, can1Δ::STE2pr-Sp_his5* (AR3) (markers allow selection of *MATa* meiotic progeny via the *MATa* specific *STE2* promoter). The resulting query strain (CL107) was then cultured overnight in YPD at 30°C, and spread onto YPD clonNAT plates, for 2 days at 30°C until a lawn formed. The following manipulations were then conducted using a BM3 robot (S&P Robotics). The resulting lawn was repinned onto YPD

clonNAT using a 1536 pinned tool, and grown at 30°C for 2 days to form 1536 colonies. The deletion collection of 4291 single deletion mutants and 842 DAmP allele strains (Synthetic Deletion Library Version 4 (SDLV4)(Tong and Boone, 2006; Breslow *et al.*, 2008)) were also pinned onto 18 YPD + G418 plates in a 384-format, resulting in 384 individual mutant strains per plate. After incubation at 30°C for two days, the resulting 18 YPD + G418 384-format plates were repinned to the 1536 format on YPD + G418, to allow 4 replicates of each of the 384 mutant strains, and grown for 2 days at 30°C. All 18 1536-format mutant collection plates were then crossed with the 1536-format *smt3-DAmP* query strain on YPD for 24 hours at 30°C, forming 4 replicate crosses. Diploids were then selected on YPD + G418 + clonNAT plates at 30°C for 36 hours. Resulting diploids were then sporulated on enriched sporulation media (ESM) + G418 for 5 days at 23°C. Sporulation of diploids was confirmed visually, and the resulting spores were sequentially pinned onto the following media to allow selection of *MAT*a *smt3-DAmP yfgΔ* and *yfg-DAMP* and haploid segregants:

SD/MSG - Histidine/Arginine/Lysine +canavanine/thialysine (Repinned to this media twice)

SD/MSG - Histidine/Arginine/Lysine +canavanine/thialysine/G418

SD/MSG - Histidine/Arginine/Lysine/Leucine +canavanine/thialysine/G418/hygromycin

SD/MSG - Histidine/Arginine/Lysine/Leucine
   +canavanine/thialysine/G418/hygromycin/clonNAT

Each of these repinnings were grown at 30°C for 2-3 days. The resulting colonies on plate 4 are the final strains. The plates were photographed during the SGA process using a robotic plate imager (SPImager, S&P Robotics), and compared to a control SGA without the *smt3-DAmP::NatMX* allele but containing the *NatMX*, *HphMX*, *LEU2* and *can1Δ::STE2pr-Sp_his5* markers (reference SGA0003). Colony growth images were compared to give each cross a Genetic Interaction Score (GIS) using COLONYZER image analysis software (Lawless *et al.*, 2010).

2.2.8 Sensitivity Analysis of Yeast

S. cerevisiae and *S. pombe* cells were grown to exponential phase, and cells/ml calculated using a Coulter counter. Cells were diluted either to 5×10^6 cells/ml *(S. pombe)*, or 4.5×10^5 cells/ml (*S. cerevisiae*). 5-fold serial dilutions of these cultures were spotted onto indicated agar plates using a 48 pin tool (Sigma). When UV sensitivity was assessed the cells were treated with the appropriate UV dose by a Stratalinker. Plates were incubated at the appropriate temperature for 3-7 days.

2.2.9 RNA Extraction

S. pombe and *S. cerevisiae* cells were grown in 50 ml YE5S (*S. pombe*) or YPD (*S. cerevisiae*) until mid-log phase and subjected to centrifugation at 3000 rpm for 3 minutes to harvest cells. The cell pellet was washed in 1 ml dH$_2$O, transferred to a screw top eppendorf, and cells pelleted at 6000 rpm. Cells were snap frozen in liquid nitrogen then stored at -80°C. Prior to extraction samples were thawed on ice. The pellet was then resuspended in 750 µl TES (0.1 M Tris-HCl, 100 mM EDTA [pH 8.0], 0.5% [w/v] SDS), and 750 µl acidic phenol:chloroform (5:1) (Sigma-Aldrich) added immediately and vortexed. Samples were incubated for 1 hour at 65°C and vortexed every 10 minutes for 10 seconds. Samples were then cooled for 1 minute on ice, vortexed for 20 seconds then subjected to centrifugation at 6000 rpm for 15 minutes at 4°C. 700 µl of supernatant were added to 700 µl acidic phenol:chloroform (5:1) inverted to mix, and spun for 5 minutes at 14000 rpm (4°C). 700 µl of the upper phase were added to 700 µl phenol:chloroform:isoamyl alcohol (25:24:1), inverted and spun again. 500 µl of upper phase were transferred to a 2 ml eppendorf, and 1.5 ml 100% ethanol and 50 µl 3 M sodium acetate (pH 5.2) added. RNA was left to precipitate at -80°C for 1 hour, or overnight at -20°C. After pelleting for 10 minutes at 13000 rpm, the RNA was washed in 70% ethanol. Once dry the resulting pellet was resuspended in 100 µl of RNAse-free dH$_2$O, incubated for 10 minutes at room temperature to allow the pellet to dissolve, and then stored at -80°C. 5 µl of sample were analysed on an agarose gel to check for degradation, and then RNA was cleaned up using the RNA Clean and Concentrator-25 kit (Zymo Research). 5 µg of RNA was DNase-treated using Precision DNase (PrimerDesign) for 30 minutes at 30°C, and then the enzyme heat-killed for 5 minutes at 55°C. The resulting RNA was stored at -80°C until use.

2.2.10 Trichloroacetic acid (TCA) Protein extraction

TCA extraction was used for both *S. pombe* and *S. cerevisiae* protein extractions. 7 ml of mid-log phase growing cells were mixed with 7 ml ice cold 20% (w/v) TCA and pelleted at 3000 rpm for 1 minute. The resulting cell pellets were immediately snap frozen in liquid nitrogen. Once thawed, pellets were resuspended in 200 µl 10% (w/v) TCA, and cells broken in 750 µl of chilled glass beads by 6x 15 seconds in a bead beater, with 1 minute on ice between each vortex. 500 µl 10% (w/v) TCA were added to lysed cells and proteins spun through into a new eppendorf. Precipitated proteins were pelleted by centrifugation at 13000 rpm for 10 minutes at 4°C. The pellet was washed 3 times in 200 µl acetone. When dry, the pellet was resuspended in 50 µl TCA buffer (100 mM Tris-HCl [pH 8], 1 mM EDTA [pH 8], 1% [w/v] SDS). To stabilise SUMO conjugates, the TCA buffer was supplemented with 12.5 mM N-ethylmaleimide (NEM) to inhibit SUMO deconjugase enzymes, and other proteases were inhibited with 0.5 mg/ml PMSF, 1 µg/ml leupeptin, and 1 µg/ml pepstatin. Final protein concentrations were determined using the Pierce BCA Protein Assay Kit (Thermo Scientific) following the manufacturer's instructions.

2.2.11 DNA Content Analysis

S. cerevisiae cells were grown overnight in 5 ml YPD then diluted back in YPD in the morning and grown to mid-log phase. 4.5×10^6 of cells were pelleted for 2 minutes at 3000 rpm, washed in H_2O, and pelleted again. Cells were then fixed in 1 ml 70% ethanol and stored at $4^{\circ}C$ overnight. Cells were sonicated for 5 seconds and pelleted at 13000 rpm for 1 minute. After washing with 800 µl 50 mM sodium citrate (pH 7.2), the cell pellet was resuspended in 500 µl RNase A solution (50 mM sodium citrate [pH 7.2], 0.25 mg/ml RNaseA) and incubated at $37^{\circ}C$ overnight. 50 µl of proteinase K (20 mg/ml) (Ambion) were added and cells incubated for 1 hour at $50^{\circ}C$. Cell were sonicated for 5 seconds to break up clumps and incubated with 500 µl of Sytox Green solution (50 mM sodium citrate [pH 7.2], 4 µM Sytox Green [LifeTechnologies]) for 1 hour at room temperature in the dark. DNA content analysis was performed using a FACSCanto™ II flow cytometer (BD Life Sciences) using DIVA software for data analysis (BD Life Sciences).

2.2.12 Yeast Immunofluorescence

2.2.12.1 S. pombe Immunofluorescence

Immunofluorescence of *S. pombe* was carried out as previously described (Hagan, 2000). 9 ml of mid-log phase growing cells were incubated with 1 ml 37% (w/v) formaldehyde solution (Sigma-Aldrich) for 30 minutes at room temperature. Cells were pelleted at 2000 rpm for 2 minutes, washed in 1 ml PEM (0.1 mM PIPES [pH 6.9], 1 mM EDTA [pH 8], 1 mM $MgCl_2$), and pelleted again at 6000 rpm for 1 minute. The 1 ml PEM wash was repeated 3 times, then cells were resuspended in 1 ml PEMS (0.1 mM PIPES [pH 6.9], 1 mM $MgCl_2$, 1.2 M sorbitol) containing 0.5 mg/ml zymolyase 20T (ICN Biomedicals), and incubated for 70 minutes at $37^{\circ}C$ with gentle agitation. Cells were pelleted at 6000 rpm for 1 minute, then resuspended in 1 ml PEMS and 100 µl 10% (v/v) Triton X-100. Cells were incubated at room temperature for 1 minute, pelleted and then washed 3x with 1 ml PEM. After resuspending cells in 1 ml PEMBAL (0.1 M lysine, 1% [w/v] BSA, 0.1% NaN_3, 1x PEM) cells were incubated at room temperature for 30 minutes to block non-specific binding. Cells were pelleted at 6000 rpm for 1 minute, resuspended in 200 µl 1:1000 anti-PK antibody, and incubated overnight at room temperature. After removal of the anti-PK antibody cells were washed 3x in 1 ml PEMBAL, resuspended in 200 µl PEMBAL containing 1:200 dilution of Alexa-Fluor® 594 conjugated anti-mouse antibody (Molecular Probes) and incubated at room temperature for 1 hour. Cells were pelleted and washed 3x in 1 ml PEMBAL, and applied to a pre-coated poly-lysine microscope slide. When dry, slides were placed in $-20^{\circ}C$ methanol for 6 minutes, then $-20^{\circ}C$ acetone for 1 minute, and mounted with VECTASHIELD® mounting medium containing 4′,6-diamidino-2-phenylindole (DAPI) (Vector Laboratories Inc.). White light images were captured by differential interference contrast (DIC). To visualise fluorescence, Alexa-Fluor® 594 conjugates were excited at 495

nm, and DAPI at 358 nm. Images were collected using an Axioscope (Zeiss) 63x oil immersion lens, and analysed using Axiovision software or ImageJ software.

2.2.12.2 S. cerevisiae Immunofluorescence

S. cerevisiae cells were fixed and stained in a method described previously, but with modifications outlined below (Kilmartin and Adams, 1984). Cells were grown to a density of 4-8 x10^6 cells/ml in YPD at 30°C. For each staining, 1 ml of 37% (w/v) formaldehyde (Sigma-Aldrich) was added directly to 9 ml of cells in YPD medium, and the cells were fixed for 10 minutes at room temperature with shaking. Cells were collected at 2000 rpm for 3 minutes, and resuspended in 0.1 M KPO$_4$ (pH 7.4) plus 3.7% (w/v) formaldehyde, and fixed for a further 50 minutes. After fixing the cells were pelleted at 2000 rpm for 3 minutes, washed in 1 ml 0.1 M KPO$_4$ (pH 7.4), and collected at 7000 rpm for 1 minute. After a further 2 washes with 0.1 M KPO$_4$ (pH 7.4), the cells were washed with 1 ml 0.1 M KPO$_4$ (pH 7.4) plus 1.2 M sorbitol, and finally resuspended in 1 ml KPO$_4$ plus 1.2 M sorbitol. Cell walls were removed by adding 1 µl of 14.3 M β-mercaptoethanol and a final concentration of 10 µg/ml zymolyase 20T (ICN Biomedicals) for 5-10 minutes. Cells were pelleted at 7000 rpm for 1 minute, resuspended in 1 ml 0.1 M KPO$_4$/1.2 M sorbitol/0.1% (v/v) Triton X-100, and incubated at room temperature for 1 minute. Cells were washed twice in 0.1 M KPO$_4$ plus 1.2 M sorbitol, and blocked for 30 minutes at room temperature in 0.5 ml of PBS-BSA (0.05 M KPO$_4$, 0.015 M NaCl$_2$ [pH 7.4], 1% [w/v] BSA, 0.2% [w/v] NaN$_3$). Cells were then probed overnight at room temperature with 100 µl anti-TAT1 antibody in PBS-BSA, at a dilution of 1:50. Cells were washed 3x in 1 ml PBS-BSA, and resuspended in 200 µl of 1:200 Alexa-Fluor® 594 conjugated anti-mouse antibody. After a 1-hour incubation at room temperature in the dark, the cells were then washed 3x in 1 ml PBS-BSA. To double stain actin, the cells were resuspended in 200 µl of PBS-BSA plus 5 µl of 6.6 µM methanol stock Alexa-Fluor® 488 conjugated phalloidin (Molecular Probes), giving a final concentration of 0.165 µM. The cells were incubated for one more hour at room temperature in the dark, washed once in 1 ml of PBS-BSA and mounted onto poly-lysine coated slides and topped with mounting medium (1x PBS [pH 7.4], 90% Glycerol [v/v]). White light images were captured by DIC. If DNA was to be visualised, the cells were mounted using VECTASHIELD® mounting medium plus DAPI (Vector Laboratories Inc.). To visualise fluorescence, Alexa-Fluor® 488 conjugates were excited at 495 nm, Alexa-Fluor® 594 conjugates at 581 nm, and DAPI at 358 nm. Images were collected using an Axioscope (Zeiss) 63x oil immersion lens. Image analysis was completed using Axiovision software, or ImageJ software (outlined below).

To image actin and tubulin staining throughout the cell, Z stacks were obtained (25 stacks, 0.250 µm distance between each image). The resulting Z stacks were viewed by maximum

projection on ImageJ, or for clearer images deconvoluted using Axiovision software, using the iterative algorithm.

To quantify actin and tubulin staining, cells from all strains within the experiment were stained and acquired together using the same exposure times between each image, ensuring the fluorescence recorded remained below saturation levels of detection. Fluorescence was quantified using ImageJ-Fiji software (Schindelin *et al.*, 2012), using a corrected cell fluorescence method used previously (Karpova *et al.*, 1998; Gavet and Pines, 2010). Nonspecific binding of phalloidin conjugates for actin cytoskeleton fluorescence quantification has been shown to be virtually nil in previous studies, and slice through one focal plane sufficient to gain quantification of the entire actin cytoskeleton in *S. cerevisiae* (Karpova *et al.*, 1998). Empirical studies of total fluorescence from both z stacked images and single focal plane images were completed using our data to ensure there were no differences in quantification. The area of the cell was selected, and the integrated density measured (giving the mean pixel value of the area). Background removal was completed per cell by quantifying the integrated density of three surrounding background areas of the cell. This value of average background signal was subtracted from the cell value, to give the mean fluorescence value for each cell. All mean fluorescence values for all the unbudded cells in each biological replicate cells were then averaged, and the ratio to the wildtype control was calculated per experiment. All microscope data was quantified from at least 2 independent biological replicates, unless otherwise stated.

2.3 Molecular Biology Techniques

2.3.1 Polymerase Chain Reaction (PCR) Reagents

DNA was amplified from templates using either Phusion® High-Fidelity Polymerase (NEB) (see section 2.3.1.1) or DreamTaq Green DNA Polymerase (see section 2.3.1.2). Primers used for PCR are outlined in Table 2.3.

2.3.1.1 Phusion High Fidelity (NEB)

For cloning and DNA sequencing reactions where DNA proofreading was required, Phusion® High-Fidelity Polymerase (NEB) was used to amplify DNA. Typical reaction conditions were as follows: 0.5 µl Phusion® polymerase (0.02 U), 0.1-1 ng template DNA, 0.5 µl forward and reverse primer (10 µM), 0.5 µl dNTP mix (10 mM), 1.5 µl $MgCl_2$ (1.5 mM), 10 µl 5x Phusion HF buffer, up to 50 µl with sterile dH_2O. The reactions were placed in a thermocycler with the following conditions:

Step 1: Initial Denaturation   2 minutes at 94°C

Step 2: Denaturation   30 seconds at 94°C

Step 3: Annealing   15-30 seconds at 52-60°C

Step 4: Extension   30-120 seconds at 72°C

Step 5: Final Extension   10 minutes at 72°C

Step 2-4 were cycled 35 times.

2.3.3.2 DreamTaq Green DNA polymerase (Thermo Scientific)

For check PCR reactions, DreamTaq Green PCR was used (Thermo Scientific), with the following conditions: 0.5 µl DreamTaq polymerase (0.2 U), 5 µl DreamTaq Green buffer, 0.1-1 ng template DNA, 0.5 µl forward and reverse primer (10 µM), 0.5 µl dNTP mix (10 mM), up to 50 µl with sterile dH_2O. The reactions were placed in a thermocycler with the following steps:

Step 1: Initial Denaturation   10 minutes at 94°C

Step 2: Denaturation   30 seconds at 94°C

Step 3: Annealing   15-30 seconds at 52-60°C

Step 4: Extension   30-120 seconds at 72°C

Step 5: Final Extension   10 minutes at 72°C

Step 2-4 were cycled 35 times.

Primer Name	Sequence (5'-3')	Primer use (Figure)
Arc35F858	CAT-AAA-GTG-CTC-TAA-AGC-C	Check Arc35-3HA epitope tagging (Figure 2.3)
Arc35HAtagF	CAG-ACA-ACA-GGC-AAG-AAG-AAC-CTT-CAC-CGG-TAG-AAA-GAT-TGT-CTA-CCG-GAT-CCC-CGG-GTT-AAT-TAA	Construction of Arc35-3HA epitope tagged strain (Figure 2.3)
Arc35HAtagR	TTT-TTT-AGT-TAT-AAC-CCT-TTT-TAC-GGA-TTC-TTA-CGT-ACT-TAT-TTA-ATC-TTT-GAA-TTC-GAG-CTC-GTT-TAA-AC	Construction of Arc35-3HA epitope tagged strain (Figure 2.3)
HASeqR	TGA-GCA-GCG-TAA-TCT-GGA-ACG	Check HA epitope tagging (Figure 2.3)
Kan909R	ATC-ACG-CTA-ACA-TTT-GAT-TAA-AAT-AG	Check KanMX cassette integrations (Figure 2.1)
natchkR	GAA-CAC-CTT-GGT-CAG-GGG	Check KanMX to NatMX switch (Figure 2.2, 4.4)
pmt3delF	CGT-AGC-TTT-AAG-ACA-CAA-CTA	Amplify *pmt3* locus (Figure 2.1, 3.1)
pmt3delR	GCA-GGC-AGG-CAA-TAA-CGT-TT	Amplify *pmt3* locus (Figure 2.1, 3.1)
SMT3natChk STOPF	CCT-GAA-GAT-TTG-GAC-ATG-G	Check KanMX to NatMX switch (Figure 2.2, 4.4)
SP6	ATT-TAG-GTG-ACA-CTA-TAG-AA	DNA sequencing of pGEM-T® plasmids (Figure 3.1)
T7	TAA-TAC-GAC-TCA-CTA-TAG-GG	DNA sequencing of pGEM-T® plasmids (Figure 3.1)
Ubc9delF	CAT-TCT-GTC-TCG-CTT-GCC-CCT-A	Amplify *ubc9* locus (Figure 2.1, 3.1)
Ubc9delR	CGA-CTT-GTG-AAA-CCG-CTA-AT	Amplify *ubc9* locus (Figure 2.1, 3.1)

Table 2.3: Primers used for PCR in this study ordered alphabetically, with brief description of use and in which figure the primers feature. All primers supplied by Sigma Aldrich, with the exception of SP6 and T7, supplied by GATC Biotech for DNA sequencing of pGEM-T® plasmids.

2.3.2 Escherichia coli Transformation and Plasmid Isolation

Plasmids were propagated by introducing them into *E. coli* SURE competent cells (Agilent Technologies) (e14⁻ [McrA⁻] Δ*[mcrCB-hsdSMR-mrr]171 endA1 gyrA96 thi-1 supE44 relA1 lac recB recJ sbsC umuC*::Tn5 [Kanʳ] *uvrC* [F'*proAB lac1ᵍZΔM15* Tn*10* [Tetᴿ]]) using the CaCl₂ transformation method described previously (Maniatis, 1983). *E. coli* containing plasmids conferring ampicillin resistance were grown in LB media (2% [w/v] bacto tryptone, 1% [w/v] bacto yeast extract, 1% [w/v] NaCl [pH 7.2]), containing 0.1 mg/ml ampicillin (Sigma-Aldrich). GenElute Plasmid miniprep kit (Sigma-Adrich) was used to isolate plasmid DNA, following manufacturer's instructions.

2.3.3 Restriction Enzyme Digestion and DNA Ligation

DNA was digested using the relevant restriction enzymes following manufacturer's instructions (Thermoscientifc). DNA was ligated using T4 DNA ligase according to manufacturer's instructions (Promega).

2.3.4 DNA Analysis and Clean up

For analysis of DNA, DNA products were separated on a 0.8-1.2% (w/v) agarose gel in TAE buffer (40 mM Tris acetate, 1 mM EDTA [pH 8]). DNA was extracted using the QIAquick gel extraction kit (QIAGEN), or precipitated by ethanol. DNA concentrations were determined using a Nanodrop spectrophotometer (Labtech). DNA sequencing reactions were completed by GATC Biotech.

2.4 Biochemical Techniques

2.4.1 Smt3 Immunoprecipitation (IP)

To IP Smt3-conjugated proteins, protein extracts were collected as described previously (Sung *et al.*, 2008). 100 ml of mid-log phase cells (OD_{660nm} ~0.5 cells) were collected at 2000 rpm for 3 minutes, washed in 1 ml PBS, and snap frozen in liquid nitrogen. Cells were immediately resuspended in ice cold lysis buffer (20 mM Tris–HCl [pH 7.5], 1 mM EDTA, 1 mM PMSF, 1 μg/ml leupeptin, 1 μg/ml pepstatin, 10 mM freshly dissolved NEM). Cells were disrupted by bead beating 6x for 15 seconds, with 1 minute on ice between each vortex. Insoluble cell debris was pelleted for 15 minutes at 13000 rpm in a prechilled centrifuge. The supernatant was removed, and the lysate clarified at 13000 rpm for 5 minutes. The protein concentration of the whole cell lysate was assayed using coomassie reagent. The Smt3 IP reaction performed was similar to a method described previously (Sung *et al.*, 2013). 300 μg of total protein from whole cell lysates were immunoprecipitated in a total volume of 300 μl. 1% input was removed, 20 μl protein A/G plus beads (Santa Cruz) were added, and the IP reaction rotated overnight at 4°C. 3 μg of anti-Smt3 antibody were added, and the IP rotated for 1 hour at 4°C. Unbound proteins were removed by pelleting the beads at 2000 rpm for 5 minutes at 4°C, and washing the beads 4x in 1 ml wash buffer (20 mM Tris–HCl [pH 7.5], 1 mM EDTA, 150 mM NaCl, 0.2% [v/v] NP40, 1 mM PMSF, 1 μg/ml leupeptin, 1 μg/ml pepstatin, 10 mM freshly dissolved NEM). After a final wash step in 1 ml wash buffer without NP40, the beads were resuspended in 12 μl 4x non-reducing sample buffer (0.5% [w/v] bromophenol blue, 10% [w/v] SDS, 625 mM Tris-HCl [pH 6.8], 50% [v/v] glycerol), boiled for 5 minutes at 100°C, and pelleted at 13000 rpm for 3 minutes. The sample was removed from the beads, and 1 μl β-mercaptoethanol was added to samples to aid denaturation of anti-Smt3 antibody before blotting. Samples were analysed by western blotting (see section 2.4.2). HA epitope tagged proteins were detected by probing with an anti-HA primary antibody, and 1:2000 HRP conjugated protein G as a secondary detection (Table 2.4).

2.4.2 Western Blotting

To prepare protein samples for analysis, 4x sample buffer (0.5% [w/v] bromophenol blue, 10% [w/v] SDS, 625 mM Tris-HCl [pH 6.8], 50% [v/v] glycerol, 10% [v/v] β-mercaptoethanol) was added to samples before denaturation at 100°C for 3 minutes. 20 µg of proteins were analysed on 10% or 13% SDS-polyacrylamide gels. Separated proteins were transferred onto Protran nitrocellulose transfer membrane (Amersham) for 120 minutes at 400 mA, and blocked for non-specific binding by incubating in 10% (w/v) BSA in 1xTBST (1 mM Tris-HCl [pH 8], 15 mM NaCl, 0.01% [v/v] Tween-20) for 30 minutes. The membrane was incubated at 4°C overnight with the indicated primary antibody. Antibodies were diluted in 5% (w/v) BSA in 1xTBST, and (dilutions shown in Table 2.4). The membrane was washed 4x in 1xTBST, and then incubated for an hour at room temperature with 1:2000 HRP-conjugated secondary antibody diluted in 5% (w/v) BSA in 1xTBST. After 4x washes in 1xTBST, proteins were then visualised using an ECL+ Chemiluminescent kit (GE Healthcare) and scanned on a Typhoon FLA 9500 (GE Healthcare). Images were analysed using ImageQuantTL software. To reprobe nitrocellulose membranes with another antibody, membranes were stripped by a 30-minute incubation at 50°C with stripping buffer (2% SDS [w/v], 62.5 mM Tris-HCl [pH 6.7], 100 mM β-mercaptoethanol). Blots were washed in 1x TBST thoroughly, then blocked again in 10% BSA (w/v) in 1xTBST before reprobing.

Antibody (1º/2º)	Manufacturer/Source	Dilution Western Blot	Dilution Immunofluorescence	Raised in
Anti-HA (1º)	Thermoscientific (26183)	1:1000	-	Mouse
Ant-PK (1º)	Serotec	-	1:1000	Mouse
Anti-Arp3 (1º)	Santa Cruz Biotechnology (sc-36625)	1:1000		Mouse
Anti-Smt3 (1º)	Abcam (ab14405)	1:500	-	Rabbit
Anti-β-Act1 (1º)	GeneTex (GTX109639)	1:2000	-	Mouse
Anti-Skn7 (1º)	(Morgan *et al.*, 1997)	1:1000	-	Rabbit
Anti-α-Tubulin (TAT1) (1º)	Cancer Research UK	1:200	1:50	Mouse
Anti-Mouse-HRP (2º)	Sigma Aldrich (A9044)	1:2000	-	-
Anti-Rabbit-HRP (2º)	Sigma Aldrich (A0545)	1:2000	-	-
Natural Protein-G HRP (2º)	Abcam (ab7460)	1:5000	-	-
Anti-Mouse Alexa-Fluor® 488 (2º)	Invitrogen (A-11001)	-	1:200	Goat
Anti-Mouse Alexa-Fluor® 594 (2º)	Invitrogen (A-11005)	-	1:200	Goat

Table 2.4: Antibodies used in this study. Catalogue numbers are indicated in brackets if applicable.

2.4.3 Quantitative Reverse Transcriptase-PCR (qRT-PCR)

qRT-PCR was performed using Precision OneStep qRT-PCR Mastermix with SYBR Green (Primer Design) following manufacturer's instructions, with the following 2 step cycle:

Step 1: Reverse transcription   10 minutes at 55ºC

Step 2: Enzyme Activation   8 minutes at 95ºC

Step 3: Denaturation   10 seconds at 95ºC

Step 4: Data collection   60 seconds at 60ºC

Step 3 and 4 were cycled 50 times.

SYBR Green detection was recorded using a Rotor Gene 6000 Real-Time PCR machine. Melt curves were collected during cycling, and final PCR products analysed by 1.2% agarose gel electrophoresis to check target amplification. Primers used for *S. pombe* and *S. cerevisiae* qRT-PCR shown in Table 5 and Table 6 respectively.

Primer Name	DNA Sequence (5'-3')
ace2F	TGC-GAT-CAT-GGA-CTT-GAC-AT
ace2R	GGA-ATC-ATG-CTC-GGT-GAC-TT
act1F	GGC-ATC-ACA-CTT-TCT-ACA-ACG
act1R	GAG-TCC-AGG-ACG-TAT-CCA-GTG
cdc15F	GGA-GAC-CCA-CTT-CTC-CCT-TC
cdc15R	GTG-CCT-CTC-CAA-CAG-AAA-GC
cdc18F	TTG-CAG-CTT-CAA-GTG-GTG-AC
cdc18R	TTG-GCT-CAT-AGC-AGA-TGT-CG
fkh2F	GGT-CGA-TTG-TGC-CTG-AAT-TT
fkh2R	TGT-CCT-TCA-TTT-TCG-GAA-GG
plo1F	TGC-AGC-TCG-TAA-ATC-CAC-TG
plo1R	TGC-CAT-CCC-GAT-TTT-AAG-AG
spo12F	CAC-AAT-TCA-GCC-ATT-GCA-TC
spo12R	TTT-TCT-GTC-TGG-ACG-CTT-TG

Table 2.5: *S. pombe* **primers used for qRT-PCR in this study.**

Primer Name	DNA Sequence (5'-3')
ACT1F	GCC-TTC-TAC-GTT-TCC-ATC-CA
ACT1R	GGC-CAA-ATC-GAT-TCT-CAA-AA
AOS1F	AAG-ATG-TTG-GCC-AAT-GGA-AG
AOS1R	TGC-ATT-TCT-GTA-GCC-ACG-AC
ARP3F	CCC-AAT-TTG-TGG-TGG-AAA-AC
ARP3R	CAA-TAG-GGC-AAG-CCT-GGA-TA
CCT8F	TGA-AGT-GGT-TCC-TCG-TAC-CC
CCT8R	TTT-TTC-GTT-GCA-AGC-ATG-TC
SAC7F	TGG-ACC-CCA-AAG-AAT-ACG-AG
SAC7R	CGA-ATC-GGA-TGA-GGT-GAT-CT
SMT3F	GGT-CAA-GCC-AGA-AGT-CAA-GC
SMT3R	TCC-AAA-TCT-TCA-GGG-GTC-TG
TUB2F	CCG-ATC-CAA-GAA-ACG-GTA-GA
TUB2R	ACC-CTT-GAG-GAG-CGA-CAG-AA
UBA2F	CTG-CTG-CGA-ACA-TAA-GGT-CA
UBA2R	CTG-CTG-CGA-ACA-TAA-GGT-CA
UBC6F	GAA-GCC-ACG-ACA-GGA-TCA-AT
UBC6R	ATC-CCC-CTC-ATC-CAA-TTT-TC
ULP1F	TTG-AAC-AAT-CCC-TCC-GAG-TC
ULP1R	CAA-AAT-TGC-GAG-GTT-CGT-TT
ULP2F	GAC-GAG-GGC-TAA-GCA-GTT-TG
ULP2R	TTG-GGA-CTA-GAT-TGG-CGT-TC

Table 2.6: *S. cerevisiae* **primers used for qRT-PCR in this study.**

Chapter Three: The Roles of Sumoylation in Late Cell Cycle Gene Expression

3.1 Introduction

Sumoylation is an essential process in many model organisms, such as *S. cerevisiae*, *C. elegans*, *D. melanogaster*, and mice (Jones *et al.*, 2002; Dieckhoff *et al.*, 2004; Nacerddine *et al.*, 2005; Talamillo *et al.*, 2008). However, there are notable organisms in which sumoylation is not required for viability, such as the fission yeast *S. pombe* and the opportunistic fungal pathogen *C. albicans* (Tanaka *et al.*, 1999; Leach *et al.*, 2011). Currently, the mechanisms underlying the species specific roles of sumoylation are unknown. Recent advances in sumoylation detection via high throughput proteomic screens have shown the plethora of biological processes in which sumoylation is involved in. While these studies are informative, the detection of sumoylation does not always correlate to sumoylation events which are most important for cell growth. For example, the *S. cerevisiae* septins are one of the most abundantly sumoylated targets in the cell, yet loss of septin sumoylation has little effect on growth (Johnson and Blobel, 1999). Genetic screening in yeast can provide insight into complex biological processes, and as such have been used to map global genetic interactions in both *S. cerevisiae* and *S. pombe* (Costanzo *et al.*, 2010; Ryan *et al.*, 2012). Thus we aimed to take advantage of the viability of sumoylation mutants, and available genetic libraries, to investigate the biological processes of sumoylation.

There is conflicting data regarding the essential role of SUMO, and the sumoylation conjugation pathway enzymes in *S. pombe*. In particular, the loss of SUMO (*pmt3*[+]) gene in *S. pombe* is reported to result in viable cells (Tanaka *et al.*, 1999; Kim *et al.*, 2010; Hayles *et al.*, 2013). In contrast, the essentiality of the sole sumoylation pathway E2 enzyme Ubc9 in *S. pombe* varies between two different studies (al-Khodairy *et al.*, 1995; Kim *et al.*, 2010; Hayles *et al.*, 2013). Furthermore, the essentiality of *ubc9*[+] was recorded differently in two publications using strains from the same deletion collection (Kim *et al.*, 2010; Hayles *et al.*, 2013). Ubc9 is the sole sumoylation E2 enzyme identified in model organisms studied to date, including *S. pombe*, and consequently all Pmt3 modifications should be conjugated through this enzyme. Therefore, loss of either Pmt3 or Ubc9 mutants should theoretically result in same phenotypes. On the other hand, if *pmt3Δ* and *ubc9Δ* mutants do behave differently, then this could suggest that Ubc9 has novel roles in addition to its role as the sumoylation pathway E2. However, no studies have directly compared the phenotypes of the *pmt3Δ* and *ubc9Δ* deletion strains. Thus the aims of this chapter were to ascertain the essentiality of the *pmt3*[+] and *ubc9*[+] genes in *S. pombe*, with the aim of setting up the strains for a high throughput synthetic genetic array (SGA) analysis.

3.2 Results

3.2.1 ubc9Δ and pmt3Δ Haploids are Viable, and have Cell and Nuclear Morphology Defects

Previous studies have found differing viabilities for the *pmt3*[+] and *ubc9*[+] genes in *S. pombe*. To investigate this, heterozygous diploid deletion strains were purchased from Bioneer. The deletion loci from both *pmt3Δ::KanMX4/pmt3*[+] (CL49) and *ubc9Δ::KanMX4/ubc9*[+] (CL53) diploids from the deletion collection were analysed prior to investigation to ensure both gene loci were completely deleted. Hence, the *pmt3Δ::KanMX* and *ubc9Δ::KanMX4* cassettes were amplified by PCR, the deletion cassettes isolated from the wild type cassettes, and the DNA sequences obtained (Figure 3.1). Analysis of the DNA sequence confirmed that the entire open reading frames of *pmt3*[+] and *ubc9*[+] were replaced by KanMX4 at the respective locus.

Having confirmed the gene deletions, the phenotypes associated with *pmt3Δ* and *ubc9Δ* mutants were determined. Firstly, the spore viabilities from dissection of *pmt3Δ::KanMX4/pmt3*[+] (CL49) and *ubc9Δ::KanMX4/ubc9*[+] (CL53) heterozygote diploids were compared. However, *S. pombe* diploid strains formed from crossing haploids of opposite mating types (plus mating type, *h*[+]; minus mating type, *h*[-]) are very unstable and undergo meiosis easily. Hence, the parental diploids used to create the *S. pombe* deletion collection are actually homozygotic for the plus mating type (*h*[+]/*h*[+]) so only the plus mating type information is expressed. Consequently, these diploid strains are unable to sporulate. Hence to achieve sporulation of *h*[+]/*h*[+] *pmt3Δ::KanMX4/pmt3*[+] and *ubc9Δ::KanMX4/ubc9*[+] diploids, a *ura4*[+] marked plasmid harbouring the minus mating information was introduced into both the strains (kind gift from Nielsen, O., University of Copenhagen) (Styrkarsdottir *et al.*, 1993; Kim *et al.*, 2010). Sporulated *ura*[+] diploids were then dissected and the resulting haploid colonies were analysed for G418 resistance (Figure 3.2 A). Significantly, G418 resistant colonies were identified from dissections of both *pmt3Δ::KanMX4/pmt3*[+] and *ubc9Δ::KanMX4/ubc9*[+] heterozygous diploid asci (Figure 3.2 A). G418 resistance segregated 2:2 with slow growth and, importantly, the G418 resistant colonies from both *pmt3Δ::KanMX4/pmt3*[+] and *ubc9Δ::KanMX4/ubc9*[+] strains were similarly sized, suggesting similar growth defects (Figure 3.2 A). This initial analysis suggested that *pmt3Δ* and *ubc9Δ* haploid mutants are in fact viable, and that similar growth defects are associated with the loss of either gene. Interestingly, however, the viable spore germination frequency varied between the *pmt3Δ* and *ubc9Δ* strains (Figure 3.2 A). The frequency of inviable spores derived from the *pmt3Δ::KanMX4/pmt3*[+] strain was higher compared to *ubc9Δ::KanMX4/ubc9*[+] (35% vs 9%) (Figure 3.2 A). By inferring the genotypes of inviable strains, the *pmt3Δ::KanMX4/pmt3*[+] strains not only had reduced viability of *pmt3Δ* spores, but also wild type spores (Figure 3.2 A, red circles).

.
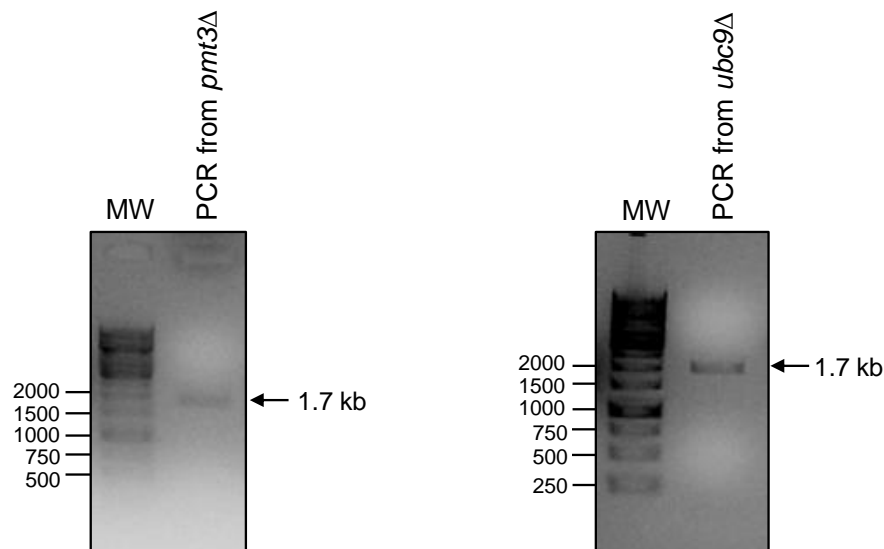
Figure 3.1: Deletion of wild type *pmt3⁺* and *ubc9⁺* loci. *pmt3Δ::KanMX4* and *ubc9Δ::KanMX4* loci were amplified by PCR using ORF specific primers (pmt3delF/pmt3delR and Ubc9delF/Ubc9delR) which bind upstream and downstream of the respective gene loci. Amplification of the *pmt3Δ::KanMX4* and *ubc9Δ::KanMX4* deletion loci were predicted to produce a 1658 bp and 1694 bp product respectively, while *pmt3⁺* and *ubc9⁺* loci were predicted to amplify a 857 bp and 1155 bp product respectively. *pmt3Δ::KanMX4* and *ubc9Δ::KanMX4* PCR products were cloned into the pGEM-T vector, and the DNA sequenced to verify that the whole open reading frames of *pmt3Δ* and *ubc9Δ* were replaced with KanMX4 (data not shown). MW indicates molecular weight marker (1 kb gene ruler, Fermentas).

A

pmt3Δ

Viable, G418 Resistant

Inviable, G418 Resistance Inferred

Inviable, G418 Sensitivity Inferred

Large Colony, 37%
Inviable, 35%
Small Colony, 28%

ubc9Δ

Large Colony, 47%
Inviable, 9%
Small Colony, 44%

B

	30°C	20°C	37°C	20°C (10 days)	15°C (10 days)
Wild type					
pmt3Δ/pmt3+					
ubc9Δ/ubc9+					
pmt3Δ					
ubc9Δ					
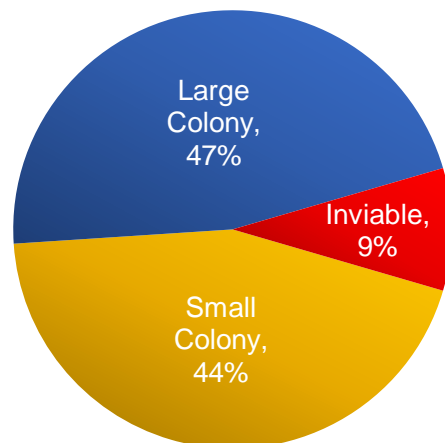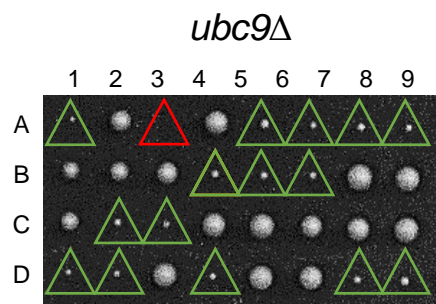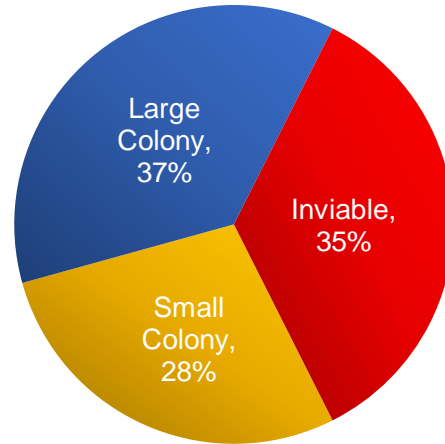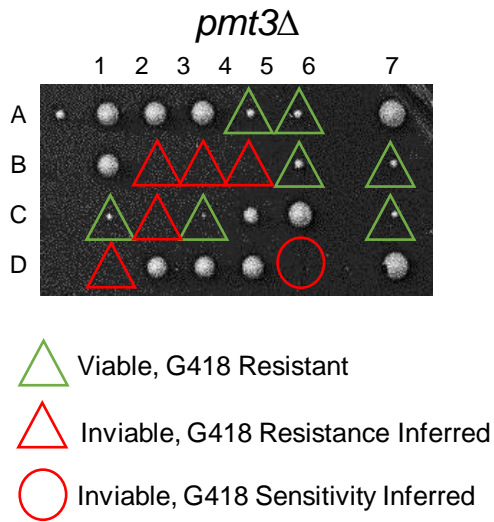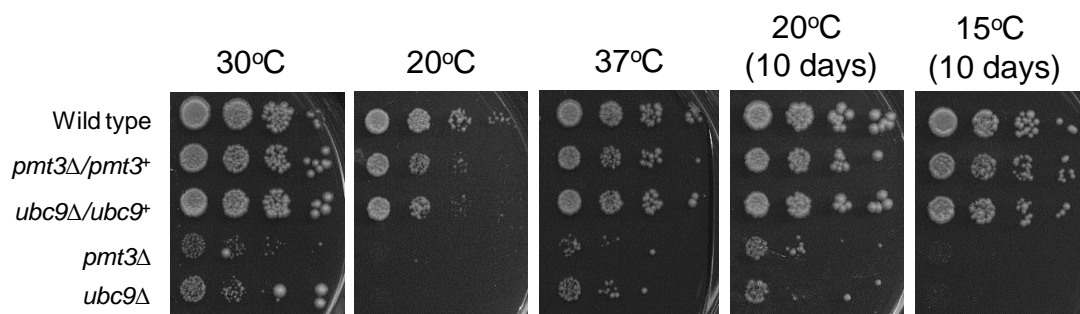
Figure 3.2: *pmt3Δ* and *ubc9Δ* haploid mutants are viable, and exhibit slow growth defects. A) *S. pombe* heterozygote diploids *pmt3Δ::KanMX4/pmt3⁺* (CL49) and *ubc9Δ::KanMX4/ubc9⁺* (CL53) cells were sporulated by the introduction of the pON177 plasmid (Nielsen. O, 1993). The resulting asci were dissected, and the spores incubated for 4 days at 30°C. Numbers represent individual asci dissections, and A-D haploid spores from each ascus. G418 resistant colonies are indicated by green triangles, inferred G418 resistant inviable spores are indicated by red triangles, and inferred G418 sensitive spores are indicated by red circles. Spore viability from *pmt3Δ::KanMX4/pmt3⁺* and *ubc9Δ::KanMX4/ubc9⁺* strains were counted from all viable spores, 124 and 144 respectively, and percentage viability shown in pie charts. B) 10 fold serial dilutions of wild type (CL76), *pmt3Δ::KanMX4/pmt3⁺* (CL49), *ubc9Δ::KanMX4/ubc9⁺* (CL53), *pmt3Δ* (parent CL49) and *ubc9Δ* (parent CL53) strains were spotted onto YE5S media and incubated at the indicated temperature for 5 or 10 days as stated.

The basis of this difference in spore viability between the *pmt3Δ::KanMX4*/*pmt3*[+] strain compared to *ubc9Δ*::*KanMX4*/*ubc9*[+] is unclear. This could suggest that half dose levels of Pmt3 in the diploid strain prior to sporulation negatively impacts spore viability. Nonetheless, the major conclusion from these data is that both the *pmt3Δ* and *ubc9Δ* haploids are viable. Furthermore, when the growth of viable *pmt3Δ* and *ubc9Δ* mutants were compared at different temperatures, similar growth characteristics were observed (Figure 3.2 B). Previous analysis of a *pmt3* mutant strain had shown temperature sensitivity at 37°C (Tanaka *et al.*, 1999). However, this result does not appear consistent with our haploid strains, as temperature sensitivity is not apparent in either the *pmt3Δ* or *ubc9Δ* strain (Figure 3.2 B), suggesting strain background differences. Interestingly however, the *pmt3Δ* and *ubc9Δ* haploid mutants also exhibited slower growth in cold conditions, a phenotype which has not been previously described (Figure 3.2 B). In conclusion, we have confirmed that both the *pmt3Δ* and *ubc9Δ* haploid strains are viable, and grow similarly. This suggests that they are indeed phenotypically similar. Hence there is no evidence that Ubc9 has any cellular functions outside of Pmt3 conjugation. It was also noted during the characterisation of the strains that both *pmt3Δ* and *ubc9Δ* haploid mutants were very unstable, and picked up genetic suppressors easily if passaged too many times. Therefore, all *pmt3Δ* and *ubc9Δ* haploid strains used throughout this study were dissected from the diploid parent strain prior to use. Thus, the strain reference for the parent diploid for each haploid is given throughout this study.

3.2.2 Sumoylation in S. pombe Regulates Cell Cycle Progression

As described above, cells lacking Pmt3 and Ubc9, although viable, have growth defects (Figure 3.2). Therefore, we characterised the phenotypes of the mutants to confirm the strains were behaving as previously described, prior to genome wide screening. Firstly, we analysed mid-log growing *pmt3Δ* and *ubc9Δ* mutant cells by microscopy (Figure 3.3 and data not shown). In agreement with previous studies, the *pmt3Δ* and *ubc9Δ* mutants exhibited an array of nuclear defects, including nuclei fragmentation, nuclei misplaced at the cell end, and cells which contained no visible nuclear material (Table 3.1) (Figure 3.3 and data not shown) (al-Khodairy *et al.*, 1995; Tanaka *et al.*, 1999).

DIC DAPI Merge
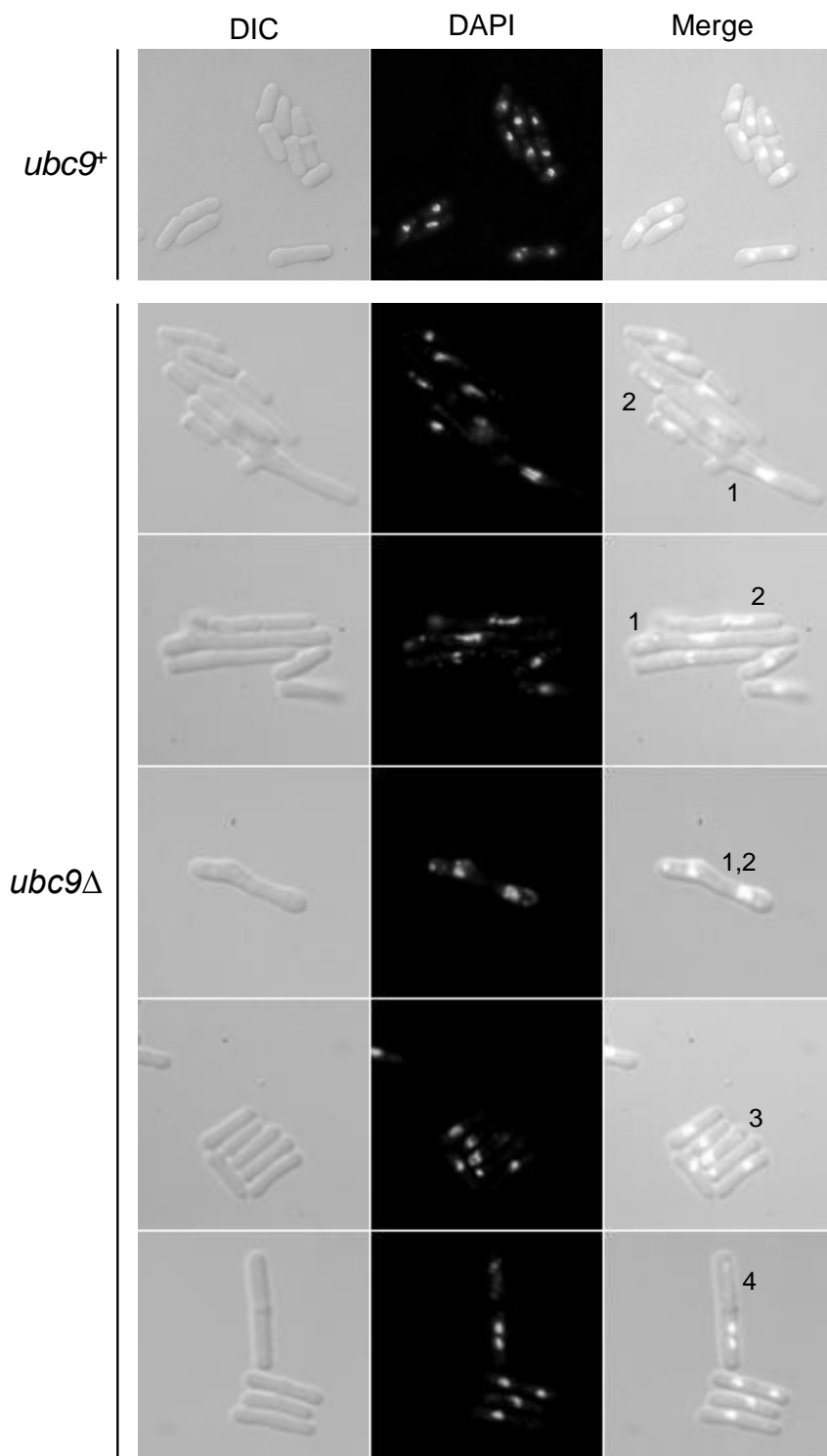
ubc9⁺

ubc9Δ

Figure 3.3: Sumoylation deficient cells have aberrant nuclear and cellular morphologies.
Mid-log phase growing wild type (CL76) and *ubc9*Δ (parent CL53) cells were fixed and stained
with DAPI. Representative images are shown. Cell morphologies were observed as indicated:
1) branched or bent cells 2) cells with fragmented nuclei 3) cells with misplaced nuclei at the
cell end and 4) enucleated cells. White light images (DIC), DAPI stained images, and merged
images are presented. Quantification of nuclear and cellular morphology defects in *ubc9*Δ and
*pmt3*Δ mutants are shown in Table 3.1.

Consistent with the conclusion that *pmt3Δ* and *ubc9Δ* cells have similar defects, the quantification of nuclear and cellular morphology defects associated with *pmt3Δ* and *ubc9Δ* cells were similar (Table 3.1). Furthermore, the *pmt3Δ* and *ubc9Δ* cells also exhibited a previously characterised elongated cell phenotype, which is indicative of cell cycle delay in *S. pombe* (Figure 3.3 and data not shown) (al-Khodairy *et al.*, 1995; Tanaka *et al.*, 1999). Interestingly, as well as an elongated cell morphology, we noted that 7.7% and 7.6% of *pmt3Δ* and *ubc9Δ* mutant cells, respectively, exhibited a bent, branched or misshapen phenotype (Figure 3.3). The particular phenotype has not been previously characterised in sumoylation deficient mutants in *S. pombe*. In conclusion, these data support the hypothesis that *pmt3Δ* and *ubc9Δ* mutants have similar cell defects.

	Number of cells counted (Biological Replicates)	Enucleated cells (%)	Misplaced nuclei (%)	Nuclei fragmentation (%)	Misshapen, bent or branched cells (%)
Wild type (CL76)	432 (n=2)	0.0 ± 0.0	1.1 ± 0.2	0.3 ± 0.3	0.9 ± 0.9
pmt3Δ **(Parent CL49)**	226 (n=3)	4.0 ± 1.1	17.0 ± 5.1	9.3 ± 2.7	7.7 ± 1.3
ubc9Δ **(Parent CL53)**	406 (n=3)	3.9 ± 1.3	15.5 ± 2.9	12.2 ± 6.1	7.6 ± 3.8
fkh2Δ **(Parent RB9)**	72 (n=1)	5.6	11.1	5.6	8.3

Table 3.1: Sumoylation deficient cells have aberrant nuclear and cellular morphologies. Cells displaying the phenotypes illustrated in Figure 3.3 and 3.5 were quantified. For strains with more than one biological replicate, the mean percentage is presented, ± standard deviation.

We next aimed to further characterise the cell cycle defects associated with the loss of sumoylation. Previous cell cycle studies in the lab were investigated using the CHP428 genetic background, hence a *pmt3Δ* strain in the CHP428 genetic background was constructed (for strategy see Figure 2.1). Importantly, it was confirmed that the new *pmt3Δ* strain (parent CL370) displayed similar morphological defects to the *pmt3Δ* strain in the Bioneer background, suggesting the phenotypes associated with the cells are not due to strain background (data not shown). To further characterise the apparent chromosomal segregation defects indicated by the aberrant nuclear morphologies observed in the *pmt3Δ* mutant, we next analysed the sensitivity of *pmt3Δ* cells to the spindle poison TBZ. *pmt3Δ* cells showed reduced growth on TBZ (Figure 3.4 A). For example, 87.6% of CHP428 cells were able to form colonies on 10

µg/ml TBZ compared to only 17.5% of *pmt3Δ* cells (Figure 3.4 B). These data confirm that that the *pmt3Δ* mutant behaves like previously described (Tanaka *et al.*, 1999).

After characterisation of the *pmt3Δ* mutant strain, we next aimed use this mutant for high throughput genetic screening to identify biological processes in which sumoylation regulates. For analysis by SGA, the *pmt3Δ* mutant must be able to successfully cross with a library of deletion mutants and proceed through meiosis to produce double deletion haploid mutants. However, *pmt3Δ* mutant cells were unable mate with strains of the opposite mating type. It was observed that in the nitrogen limiting conditions used to induce mating in *S. pombe*, the *pmt3Δ* mutant cells exhibited a long, branched morphology, and did not arrest like wild type (Figure 3.5). Therefore, the mutant appeared unsuitable for SGA analysis. However, we aimed to further characterise cell cycle defects of the *pmt3Δ* mutant.

3.2.3   Defects in Sumoylation Similar to Forkhead Transcription Factor Mutants

As described in section 3.2.2, *pmt3Δ* and *ubc9Δ* mutant cells have several cell and nuclear morphology defects, and also display increased sensitivity to TBZ.   Intriguingly, these phenotypes are similar to those described in previous studies of genes which regulate M-phase cell cycle gene expression, required for cell cycle progression (Ribar *et al.*, 1999; Buck *et al.*, 2004; Bulmer 2004; Bulmer, 2005). Indeed, cells lacking in the cell cycle -regulated forkhead transcription factor Fkh2 exhibited cells with bent and branched morphologies and nuclear morphology defects, which are also sensitive to TBZ (Bulmer *et al.*, 2004). Similarly, the loss of another cell cycle-regulated forkhead transcription factor, Sep1, also causes a branching phenotype (Ribar *et al.*, 1999; Bulmer, 2005). While previous work in the lab had characterised the *fkh2Δ* mutant (Bulmer *et al.*, 2004), the quantifications were repeated using the same parameters used to characterise the *pmt3Δ* and *ubc9Δ* strains. As expected, the *fkh2Δ* mutant also displayed aberrant nuclear and cell morphologies that were described previously (Bulmer *et al.*, 2004) (Figure 3.6). Strikingly, quantification of the *fkh2Δ*, *pmt3Δ* and *ubc9Δ* revealed that the 3 strains exhibited very similar cell and morphology defects (Table 3.1). Thus, we hypothesised that the mitotic defects of the sumoylation deficient mutants could be due to aberrant regulation of M-phase gene expression. Interestingly, as discussed in the introduction to this thesis (see section 1.2.1), the human homolog of Fkh2, FoxM1, is also sumoylated, however there are contradictions whether sumoylation has a positive or negative effect on the transcriptional activity of FoxM1. Therefore, we hypothesised that the cell cycle defects of the *pmt3Δ* and *ubc9Δ* mutant cells might be due to aberrant cell cycle-regulated gene expression.
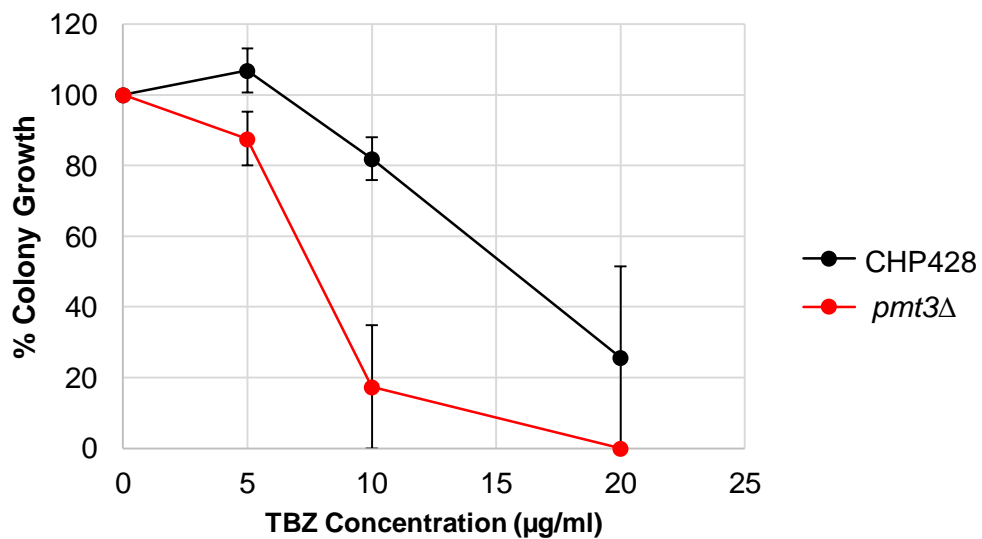
Figure 3.4: *pmt3Δ* cells are sensitive to spindle destabilisation by the drug TBZ. A) 5 fold serial dilutions of mid-log phase growing wild type (CHP428) and *pmt3Δ* (parent CL370) cells were diluted and plated onto YE5S containing the indicated concentrations of TBZ, and incubated for 5 days at 30°C. B) Equal numbers of wild type (CHP428) and *pmt3Δ* (parent CL370) cells were plated onto YE5S containing 0 µg/ml, 5 µg/ml, 10 µg/ml and 20 µg/ml TBZ. After 10 days the number of colonies were counted per plate, and % colony growth calculated from the YE5S only control. Error bars represent the standard deviation from two biological replicates.

	EMM	EMM½G
Wild type		
pmt3Δ		
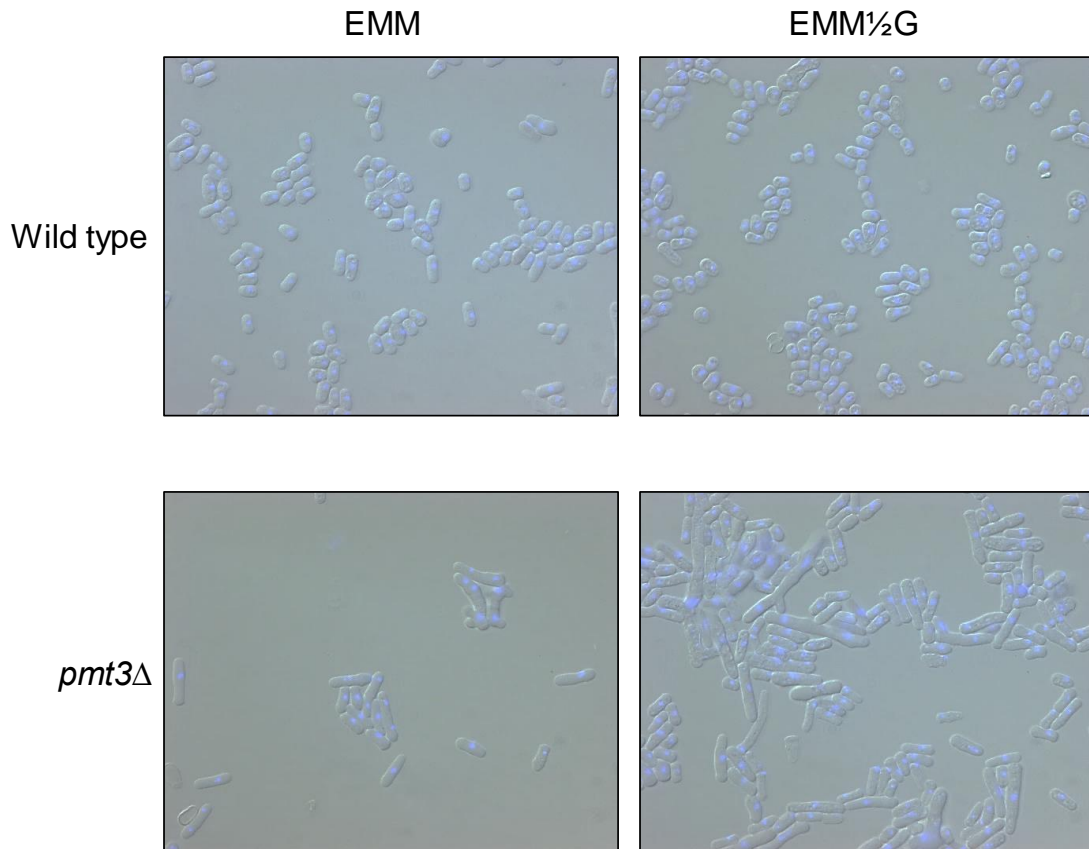
Figure 3.5: Cells lacking Pmt3 do not arrest growth on mating media. Wild type (CHP428) and *pmt3*Δ (parent CL49) cells were grown on EMM or EMM½G agar plates for 3 days at 25°C, to replicate mating conditions. Cells were mounted onto slides and nuclei stained with DAPI, and cells imaged using fluorescence microscopy.

3.2.4 Cells Deficient in Sumoylation Have Increased Levels of fkh2+ Transcripts

Next, to investigate whether sumoylation influences M-phase gene expression, we needed to analyse transcripts of genes regulated by the forkhead transcription factors Fkh2 and Sep1 (Buck *et al.*, 2004; Bulmer *et al.,* 2004; Rustici *et al.*, 2004). The proteins governing the cell cycle-regulated waves of transcription in *S. pombe* are shown in Figure 3.7. The two forkhead transcription factors Sep1 and Fkh2 regulate the transcription of genes containing PCB elements and forkhead consensus motifs in the promoter, such as the cytoskeletal organising gene *cdc15+*, and the polo kinase *plo1+* (Garg *et al.*, 2015; Buck *et al.*, 2004; Bulmer *et al.*, 2004; Rustici *et al.*, 2004; Anderson *et al.*, 2002) (Figure 3.7). The MADS box-like protein Mbx1, also binds to PCB elements, but is not required for periodic gene expression (Buck *et al.*, 2004). Fkh2 and Sep1 transcription factors also regulate the transcription of *fkh2+* itself (Bulmer, 2005), as well as the transcription factor responsible for the next transcription wave *ace2+* (Bulmer *et al.*, 2004; Buck *et al.*, 2004) (Figure 3.4). Sep1 in *S. pombe* appears to have a positive role in M-phase gene expression, as deletion of *sep1+* lowers the transcription of many late cell cycle genes such as *cdc15+*, *plo1+* and *ace2+* (Rustici *et al.*, 2004; Bulmer, 2005). Conversely, deletion of *fkh2+* leads to an increase in levels of *cdc15+* and *spo12+* transcripts (Bulmer *et al.*, 2004). Thus, mRNA levels of *ace2+*, *cdc15+*, *fkh2+*, and *plo1+* were analysed by qRT-PCR, to analyse Fkh2 and Sep1 regulated gene expression in mid-log phase cells and regulated by the forkhead transcription factors (Figure 3.8). In agreement with previous data, loss of *fkh2+* increases the transcript levels of *cdc15+* 2.7-fold, and *plo1+* 3.0-fold in mid-log cultures, indicative of the repressive role of *fkh2+* (Buck *et al.*, 2004; Bulmer *et al.*, 2004) (Figure 3.8). Previous studies have shown *ace2+* transcripts are increased in mid-log phase cells lacking *fkh2+* (Suarez *et al.*, 2015). However, *ace2+* transcripts appear to be unaffected in the *fkh2Δ* mutant in these data (Figure 3.8). The reason for this is unclear.
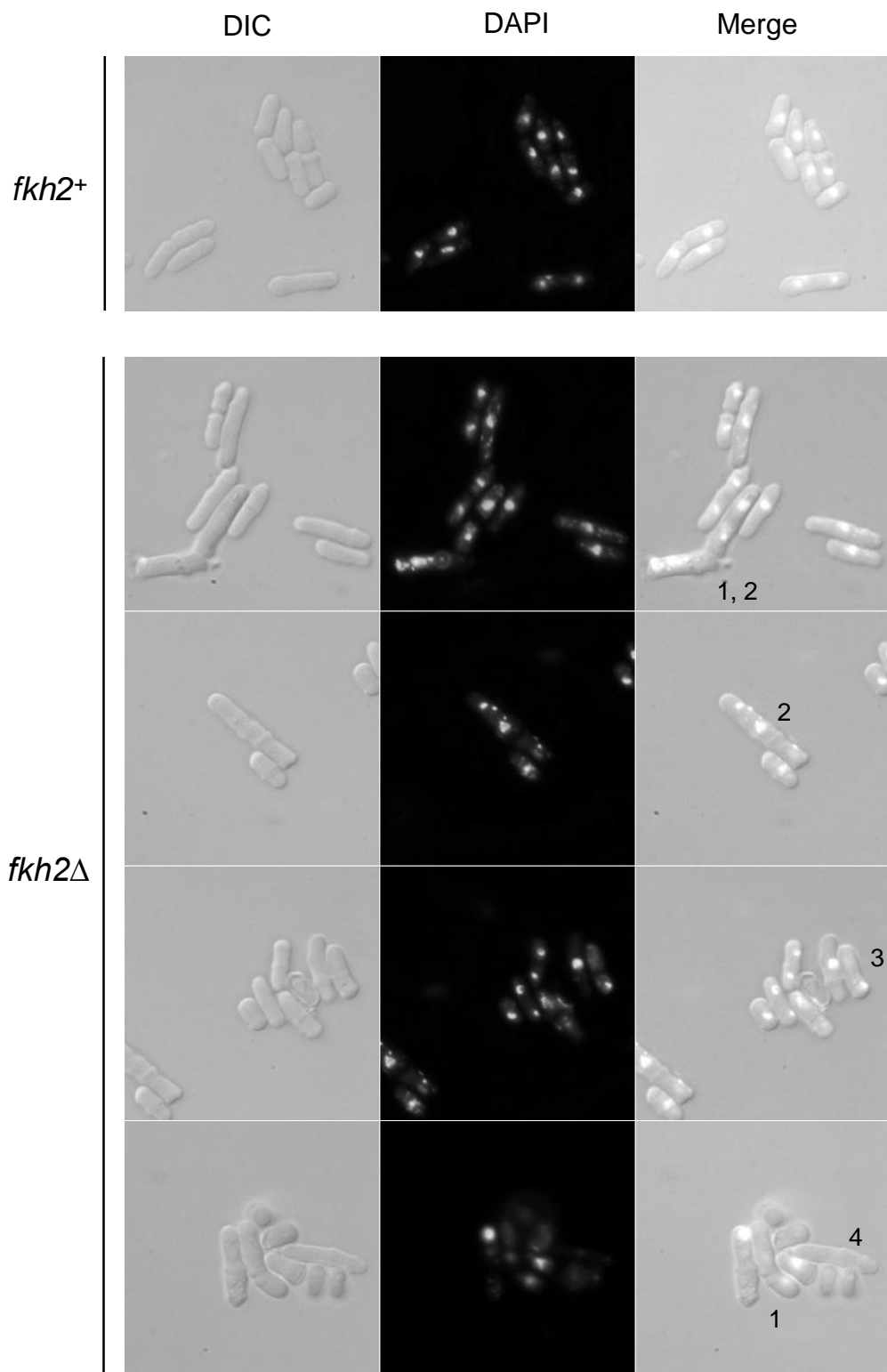
Figure 3.6: Cells lacking Fkh2 have aberrant nuclear and cellular morphologies. Mid-log phase growing wild type (CL76) and *fkh2Δ* (parent RB9) cells were fixed and stained with DAPI. Representative images are shown. Cell morphologies were observed as indicated: 1) branched or bent cells 2) cells with fragmented nuclei 3) cells with misplaced nuclei at the cell end and 4) enucleated cells. White light images (DIC), DAPI stained images, and merged images are presented. Quantification of nuclear and cellular morphology defects in *ubc9Δ* and *pmt3Δ* mutants are shown in Table 3.1.
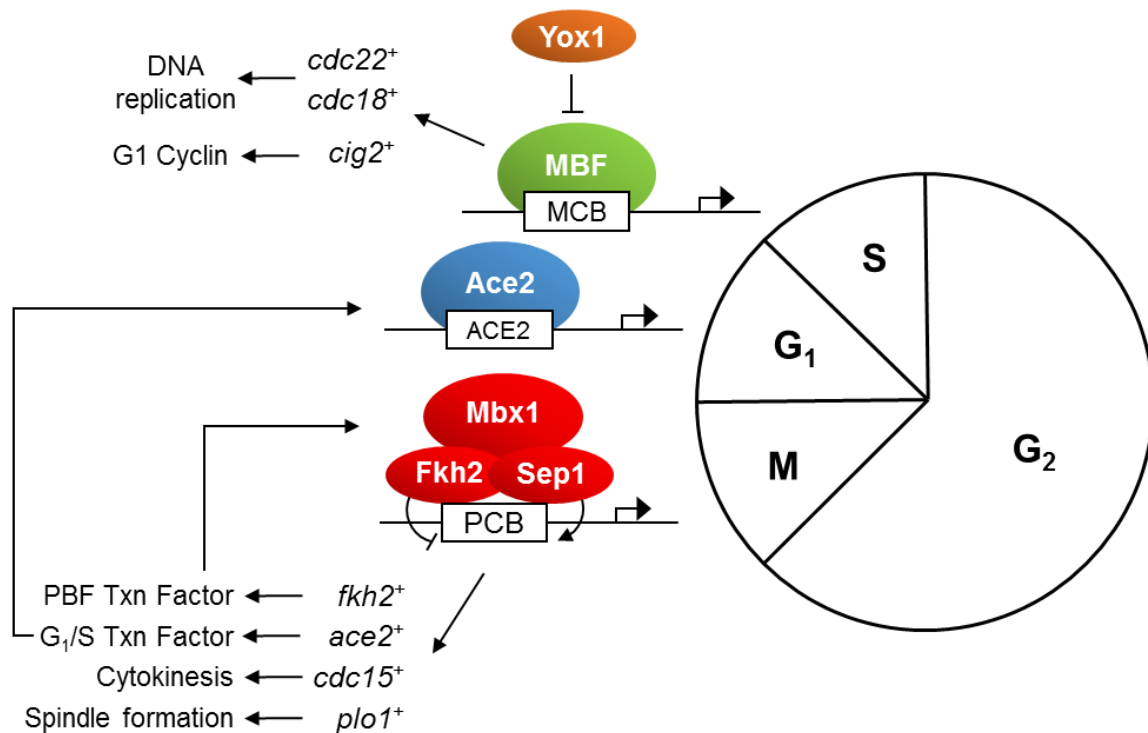
Figure 3.7: Periodic transcription during the late cell cycle in *S. pombe*. The first wave which is composed of Fkh2, Sep1 and Mbx1. Fkh2 appears to have a negative effect on PBF transcribed genes, while Sep1 appears to have a positive regulatory effect. Ace2 and MBF waves occur during G_1/S, in very close succession. MBF is inhibited by Yox1. Representative genes whose expression are regulated by the PBF and MBF transcription factors are shown. Figure adapted from (McInerny, 2004)
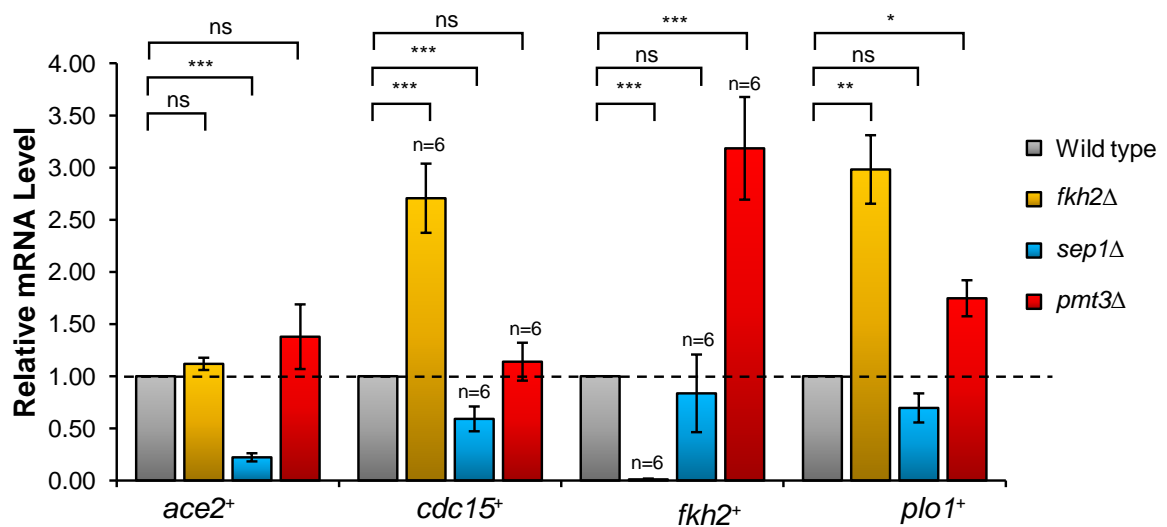
Figure 3.8: Pmt3 influences expression of late cell cycle-regulated genes. qRT-PCR showing mRNA levels of M-phase specific gene expression in mid-log growing wild type (CHP428), *fkh2Δ* (parent RB6), *sep1Δ* (JB355), and *pmt3Δ* (parent CL370) cells. mRNA levels were normalised to *act1*+ transcript levels, and fold changes calculated relative to wild type. Error bars indicate the standard deviation from 3 biological replicates, or 6 biological replicates (indicated above the respective bar). Significance was determined by unpaired 2 tailed student t test. One asterisk (*) indicates p<0.05, double asterisk (**) p<0.01, and triple asterisk (***) p<0.001. No statistical significance is indicated by ns.

However, as predicted, the *sep1Δ* mutant transcript results are consistent with the activating role of Sep1 in late cell cycle dependant gene expression (Figure 3.8). Accordingly, the *sep1Δ* mutant had significantly decreased *ace2+* and *cdc15+* transcripts (0.22 and 0.59-fold relative to wild type respectively). Furthermore, *plo1+* transcripts were reduced 0.70-fold in the *sep1Δ* mutant relative to wild type, although this was outside the boundaries of significance. Strikingly, *fkh2+* transcript levels were increased 3.2-fold in the *pmt3Δ* strain compared to wild type (Figure 3.8). Furthermore, in the *pmt3Δ* mutant, *plo1+* levels were increased 1.75-fold compared to wild type (Figure 3.8). Although *ace2+* transcript levels were marginally increased compared to wild type (1.38-fold relative to wild type), this was not statistically significant. Transcript levels of *cdc15+* in the *pmt3Δ* mutant were also very close to wild type (1.14-fold relative to wild type). Therefore, these data do not initially suggest a general derepression of all M-phase-specific gene expression. However, *pmt3Δ* and *ubc9Δ* cells have cell cycle defects, such as elongated cell morphology and sensitivity to TBZ (see section 3.2.1 and 3.2.2) (al-Khodairy *et al.*, 1995; Tanaka *et al.*, 1999), which could suggest delays in late mitosis. It was possible that the increase in cell cycle-regulated transcripts detected reflected the fact that mid-log cells were simply stalled in the cell cycle phase where these genes were induced.

To test this, we analysed another cell cycle related gene transcript *cdc18+*, which encodes the DNA clamp loader required for DNA replication. The Mlu1 box binding factor (MBF) transcription factor does not regulate the periodicity of *fkh2+* transcripts, however peak *fkh2+* expression coincides closely with peak expression of *cdc18+* which is regulated by the MBF (Bulmer *et al.*, 2004; Purtill *et al.*, 2011), due to these transcriptional waves occuring in close succession (Figure 3.7) (Rustici *et al.*, 2004). Therefore, the prediction would be that if *pmt3Δ* was stalling at a specific cell cycle point while *fkh2+* transcripts were higher, then it would be expected that *cdc18+* would also be increased. As expected, loss of an inhibitor of the MBF, Yox1, raised *cdc18+* transcript levels as expected (Figure 3.9) (Purtill *et al.*, 2011). However, loss of *pmt3Δ* did not increase *cdc18+* transcript levels (Figure 3.9). This was also observed in the *fkh2Δ* and *sep1Δ* mutants, which have aberrant Fkh2 and Sep1 regulated gene expression, but normal *cdc18+* transcript levels (Figure 3.9). Thus, taken together these data suggest that Pmt3 negatively regulates M-phase-specific gene expression. Based on the previous roles of Fkh2 as a repressor and Sep1 as an activator, two models seem plausible. One is that sumoylation represses the positive regulator of the wave, Sep1, and the loss of sumoylation consequently causes hyper activation of Sep1 and increased transcription of M-phase-specific genes. Consistent with this model, *fkh2+* expression is Sep1 dependant, and is induced in *pmt3Δ* cells. However, the role of Fkh2 in the expression of *fkh2+* has not been
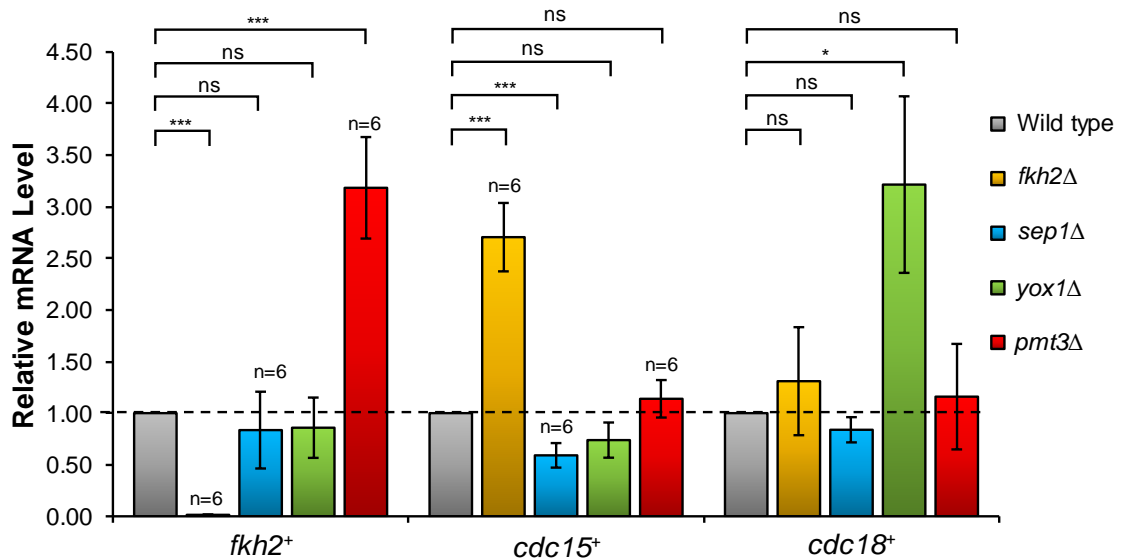
Figure 3.9: Pmt3 influences Sep1 and Fkh2 but not MBF regulated gene expression.
qRT-PCR showing mRNA levels of late M-phase specific and G_1/S-phase specific gene expression in mid-log growing wild type (CHP428), *fkh2Δ* (parent RB6), *sep1Δ* (JB355) *yox1Δ* (FP66), and *pmt3Δ* (parent CL370) cells. mRNA levels were normalised to *act1+* transcript levels, and fold changes calculated relative to wild type. Error bars indicate the standard deviation from 3 biological replicates, or 6 biological replicates (indicated above the respective bar). Significance was determined by unpaired 2 tailed student t test. One asterisk (*) indicates $p < 0.05$, double asterisk (**) $p < 0.01$, and triple asterisk (***) $p < 0.001$. No statistical significance is indicated by ns.

investigated. Hence it is possible that Fkh2 auto-regulates its own expression. Therefore, an alternative hypothesis could be that sumoylation is required for the repressor function of Fkh2, and thus in the absence of Pmt3, Fkh2 is prevented from acting as a repressor, mimicking the *fkh2Δ* phenotypes. More insight could be gained by investigation of cell cycle regulated transcripts in synchronised populations. However, it would be inappropriate to employ HU mediated S-phase block and release experiments on *pmt3Δ* mutants, which are sensitive to the drug (al-Khodairy *et al.*, 1995; Tanaka *et al.*, 1999). Another method of cell cycle synchronisation is by use of a ts allele encoding the phosphatase required for mitotic exit, *cdc25*[+]. Cells expressing the *cdc25-22* mutant block at G_2/M at the non-permissive temperature until release at 25°C (Fantes, 1979). However, attempts to create a *cdc25-22 pmt3Δ* mutant to complete transient temperature block and release experiments were unsuccessful, suggesting synthetic lethality between these genes (data not shown). Thus, we aimed to employ other genetic and biochemical methods to distinguish if either Sep1 over activation, or Fkh2 repression is the basis for aberrant M-phase-specific gene transcription in sumoylation deficient cells.

3.2.5 *pmt3Δ* Cells Retain Nuclear Localisation of Fkh2

Sumoylation can regulate expression by a variety of mechanisms. For example, sumoylation can influence the stability, localisation, or DNA binding abilities of transcription factors (Desterro *et al.*, 1998, Hamard *et al.*, 2007; Myatt *et al.*, 2014; Schimmel *et al.*, 2014). In the case of FoxM1, one study revealed that FoxM1 was shuttled into the cytoplasm and subsequently degraded upon sumoylation (Myatt *et al.*, 2014). Another study showed that the sumoylation of FoxM1 prevented inhibitory dimerization, and thus increased transcriptional activity (Schimmel *et al.*, 2014). Previous studies have shown that although *fkh2*[+] gene expression is regulated in M-phase, Fkh2 is localised to the nucleus during the entire cell cycle and is itself transcriptionally regulated (Bulmer *et al.*, 2004; Bulmer, 2005). In contrast, *sep1*[+] gene expression remains constant during the cell cycle (Rustici *et al.*, 2004). Interestingly, Sep1 appears regulated at the post translational levels (Bulmer, 2005). In particular, previous work has shown that Sep1 shuttles from the cytoplasm to the nucleus during mitosis (Bulmer, 2005). These data pose the possibility that sumoylation could be regulating the nuclear localisation of Fkh2 or Sep1. To investigate these possibilities, we attempted to construct *pmt3Δ* mutants expressing either PK tagged epitope tagged Fkh2 or Sep1 from their normal gene loci. Thus, a heterozygote *pmt3Δ* deletion strain was constructed by transformation of a *pmt3Δ* deletion cassette into a diploid strain heterozygous for *fkh2-PK* expressed from the normal chromosomal loci (see section 2.2.6.1). The *pmt3Δ/pmt3*[+] *fkh2-PK/fkh2*[+] parental strain (CL363) was sporulated, and haploid strains expressing Fkh2-PK lacking *pmt3*[+] and those expressing wild type *pmt3*[+] were selected by the appropriate markers. Fkh2-PK *pmt3Δ* cells and Fkh2 *pmt3*^{+} haploid cells were then grown to mid-log growing phase, fixed, then

analysed by fluorescence microscopy (Figure 3.8). Importantly, in cells expressing Pmt3, Fkh2-PK is localised in the nucleus throughout the cell cycle, as shown by previous data for cells containing Pmt3 (Bulmer, 2005) (Figure 3.10). In cells lacking Pmt3, Fkh2-PK is still visible in the nucleus during the duration of the cell cycle, suggesting that there is no change in Fkh2-PK nuclear accumulation when sumoylation is prevented (Figure 3.8). Interestingly, preliminary data appears to show *pmt3Δ* cells with aberrant branched cellular morphology had dense Fkh2-PK staining over a large nuclear area, suggesting an increased amount of Fkh2-PK in the cell compared to wild type (Figure 3.10), consistent with the gene expression data shown earlier (Figure 3.8 and 3.9). However, this is not conclusive without further experiments. Unfortunately, despite much effort, we were unsuccessful at detecting Sep1-PK by immunofluorescence (data not shown). Previous studies suggest that the signal from Sep1 is indeed weaker than Fkh2 (Bulmer, 2005), thus optimisation of the protocol for Sep1 localisation will be required. This experiment will be critical in the investigation of the role of sumoylation in regulating forkhead transcription factors. However, these data show that Fkh2 localisation does not depend upon sumoylation, in contrast to studies of FoxM1 in human cells (Myatt *et al.*, 2014). However, this information is not sufficient to distinguish between the two hypothesis regarding the potential role of Pmt3 in the regulation of either Sep1 or Fkh2.

3.2.6 Sumoylation Deficient Cells Are Sensitive to Further Alterations of Fkh2

Hence, we next utilised a genetic approach in an attempt to obtain data which supports either the hypothesis that Fkh2 is less functional, or Sep1 is overactive. If the case is that Fkh2 is less functional, we may expect that complete loss of Fkh2 in a mutant lacking sumoylation would have a non-additive effect, as the sumoylation mutant already has lowered Fkh2 activity. On the other hand, an altered phenotype could suggest Sep1 is the target for regulation. Therefore, a heterozygote diploid delete strain *ubc9Δ::KanMX4/ubc9$^+$ fkh2Δ::ura4$^+$/fkh2$^+$* (CL109) was constructed by transforming a *ubc9Δ* deletion cassette into the RB6 *fkh2$^+$/fkh2Δ* diploid (see section 2.2.6.1). These diploids were sporulated, and the spores dissected and the viability and genotype of resulting spores assessed (Figure 3.11 A). However, no spores were viable that were both G418 resistant and *ura$^+$*, suggesting that the *fkh2Δ ubc9Δ* mutant is lethal (Figure 3.11 A). This is consistent with the model that lack of sumoylation is therefore not leading to Fkh2 loss of function, and supports the Sep1 gain of function hypothesis. However, the interpretation of this could be complicated by the many other possible roles of sumoylation,
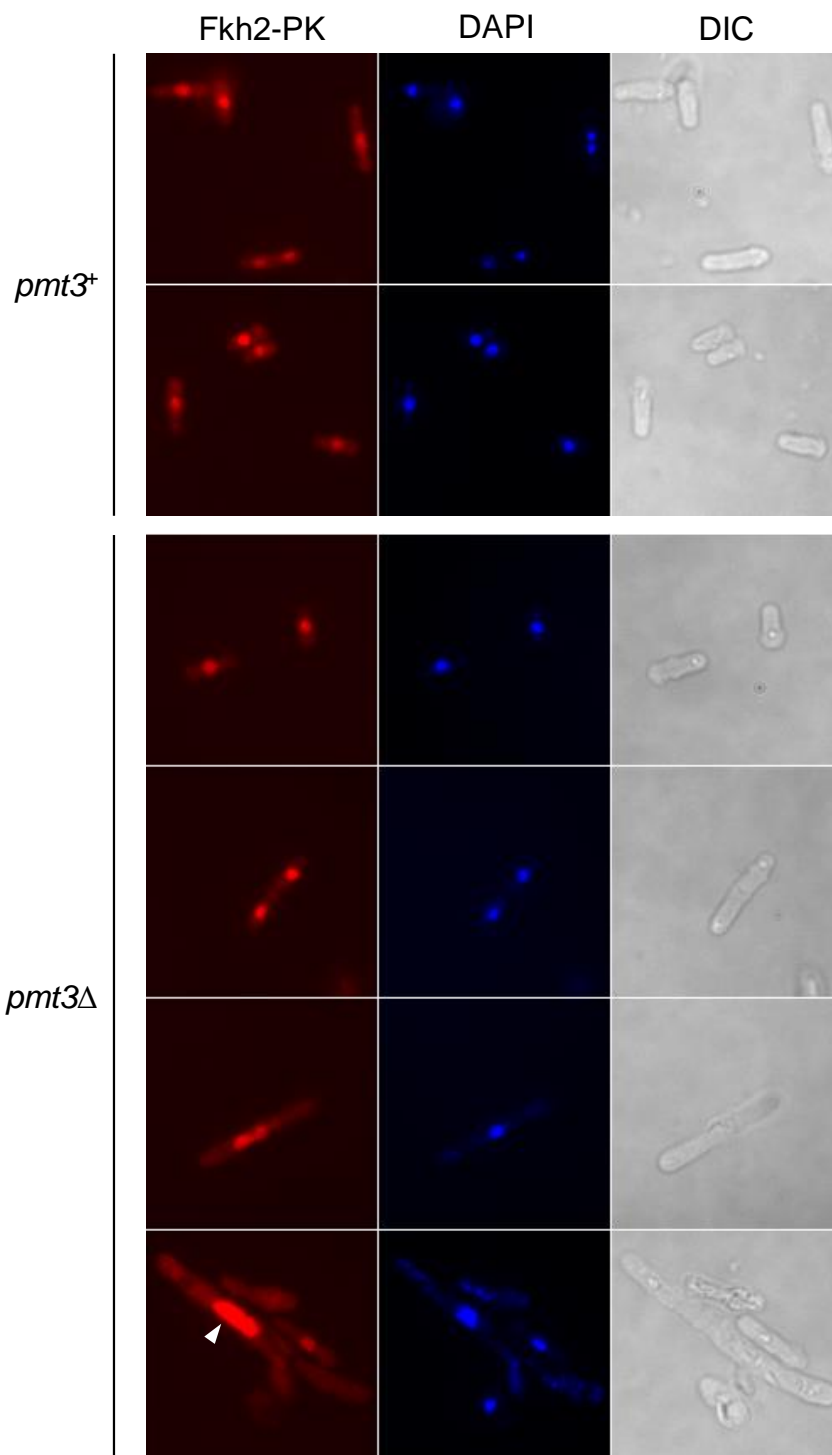
Figure 3.10: The nuclear localisation of Fkh2 is maintained in *pmt3*Δ cells. Wild type and *pmt3*Δ (both from parent CL363) cells expressing Fkh2-PK were grown to mid-log phase, fixed, and immunostained with anti-PK antibody (red), and nuclei stained with DAPI (blue). Images of PK epitope, DAPI, and white light (DIC) image shown. Images are representative of one experiment.

A
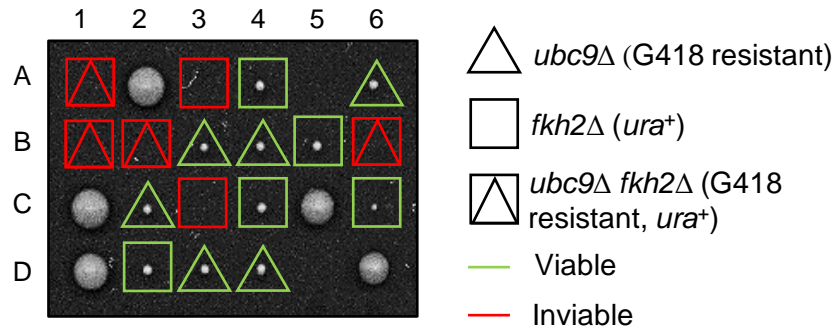
B
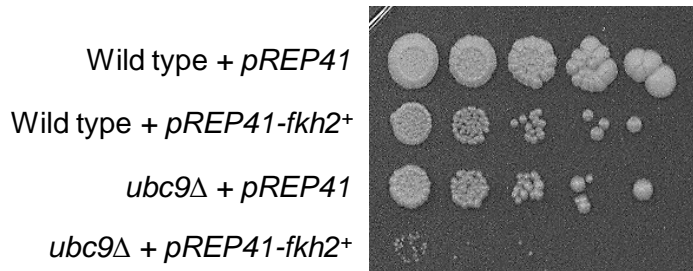
Figure 3.11: Ubc9 acts in an Fkh2 independent pathway. A) Tetrad dissection of *ubc9Δ::KanMX4/ubc9⁺ fkh2Δ::ura4⁺/fkh2⁺* (CL109) diploids. The diploid cells were sporulated, the resulting asci dissected, and spores incubated for 5 days at 30°C. 1-6 represent individual asci dissections, and A-D are haploid spores from each ascus. G418 resistance is indicated by triangles, *ura⁺* auxotrophy is indicated by squares. Viable G418 resistant or *ura⁺* genotypes are shown in green, and inferred genotypes of inviable spores are shown in red. B) Wild type (CHP428) and *ubc9Δ* (parent CL53) strains harbouring pREP41-*fkh2⁺* plasmid expressing *fkh2⁺* under control of a *nmt41⁺* (no message in thiamine) promoter, and pREP41 vector control, were grown to mid-log phase in EMM media containing thiamine to inhibit expression from the *nmt41⁺* promoter. 5 fold serial dilutions of cells were spotted onto EMM media lacking thiamine to induce *nmt41⁺* promoter expression, and incubated at 30°C for 7 days.

and that the summation of the poor growth of the two strains is causing lethality. Therefore, we aimed to investigate this by another method. We attempted to overexpress Fkh2 in the *ubc9Δ* strain. Previous studies have shown that the overexpression of Fkh2 in wild type cells slows the growth of wild type cells, but strains lacking Sep1 are resistant to Fkh2 overexpression (Bulmer *et al.*, 2004; Buck *et al.*, 2004). Hence, if strains lacking sumoylation have repressed Fkh2, then you might predict that mild over expression of Fkh2 could possibly improve the growth of the strain, or at least have less of a detrimental effect on growth compared to wild type. Conversely, as the detrimental effects of Fkh2 overexpression are dependent on Sep1, overexpression of Fkh2 could be predicted to confer extremely slow growth in sumoylation mutants, if Sep1 is indeed overactive. Thus, Fkh2 was overexpressed from a multicopy plasmid pREP41*fkh2*$^+$ from the medium-strength *nmt41*$^+$ (no message in thiamine) promoter, in both wild type and *ubc9Δ* cells (Figure 3.9 B). Indeed, in *ubc9Δ* mutant cells, overexpression of Fkh2 lead to a small amount of colony growth before it was completely inhibited, while *ubc9Δ* cells harbouring the empty pREP41 vector were still able to form colonies. (Figure 3.9 B). We assume that the small amount of growth is due to the lag period before full *nmt41*$^+$ promoter activation before the cells halted growth. Thus, as the *ubc9Δ* mutant cells were sensitive to mild Fkh2 overexpression, it appears that sumoylation deficient cells do not behave like *sep1Δ* cells. While it is again possible that these genetic events are unlinked and the poor growth of the *ubc9Δ* mutant is simply exacerbated by deletion or over expression of Fkh2, the current data is consistent with the model that sumoylation deficient cells have over active Sep1, leading to increased sensitivity to Fkh2 overexpression. Further experimentation will be completed to further explore this relationship.

3.3 Discussion

Here we attempted to resolve published conflicts in sumoylation viability data to ascertain the viability of both the SUMO encoding gene, *pmt3*$^+$, and the SUMO E2 enzyme encoding gene, *ubc9*$^+$, prior to the use of *pmt3Δ* or *ubc9Δ* strains for high throuput genetic screening. Sumoylation is a conserved protein modification across eukaryotes, and is required for viability in many model organisms (Li and Hochstrasser, 1999; Jones *et al.*, 2002; Nacerddine *et al.*, 2005; Talamillo *et al.*, 2008). Interestingly, data suggested that while *S. pombe* lacking Pmt3 grow poorly, sumoylation is not essential for viability (Tanaka *et al.*, 1999). However, data from large scale deletions have suggested that the gene encoding the SUMO conjugating enzyme, *ubc9*$^+$, is required for growth (Kim *et al.*, 2010; Hayles *et al.*, 2013). The viability of both these genes has not previously been directly compared. In this chapter, we have confirmed that the ORF of the *pmt3*$^+$ and *ubc9*$^+$ strains from the diploid deletion collection are completely replaced with a KanMX cassette in the diploids (Figure 3.1), validating that the deletions are correct. Furthermore, our data revealed that although the *pmt3Δ* and *ubc9Δ* strains had differing spore

germination frequencies, both lead to viable colonies which grew similarly under normal growth conditions (Figure 3.2). However, *pmt3Δ* cells were unable to mate and sporulate, meaning these strains were unsuitable for high throughput SGA analysis (Figure 3.5).

Interestingly, we have highlighted a previously unreported cold sensitivity phenotype of the sumoylation mutants in *S. pombe*. Interestingly *siz1Δ siz2Δ* double mutant in *S. cerevisiae* also has cold defects, but the molecular aspect of this is unknown (Johnson and Gupta, 2001). This suggests that this is conserved between the two distantly related yeast. Furthermore, hypothermic and hypoxic conditions have been shown to induce global sumoylation in a protective mechanism (Lee *et al.*, 2007). As the targets of sumoylation during hypothermia have not yet been characterised, it would be interesting to study further the role of sumoylation in the cold stress response.

The roles of sumoylation in cell cycle regulation are indicated in yeast by the G_2/M arrest in *S. cerevisiae* upon depletion of the SUMO encoding gene *SMT3* and the E2 enzyme *UBC9* (Dieckhoff *et al.*, 2004), and the cell cycle defects observed in *pmt3Δ* and *ubc9Δ* mutants in *S. pombe* (al-Khodairy *et al.*, 1995; Tanaka *et al.*, 1999). However, how SUMO regulates cell cycle progression is poorly understood. Here we have identified a previously uncharacterised role of sumoylation in late cell cycle-regulated gene expression in *S. pombe*. We have shown that loss of sumoylation in *S. pombe* increases the expression of some late cell cycle genes under regulation of the forkhead transcription factors Fkh2 and Sep1 (Figure 3.6). Indeed, this effect on periodic gene transcription appears to be specific to genes regulated by Fkh2 and Sep1 (Figure 3.7). The forkhead transcription factors, can both positively and negatively regulate gene transcription (Voth *et al.*, 2007), and accordingly Fkh2 has been shown to be a transcriptional repressor of cell cycle-dependant gene expression, whereas Sep1 has been shown to have an activating role in cell cycle-dependant gene expression. Thus, the observation that loss of sumoylation increases the transcripts regulated by these genes could be attributed to sumoylation positively regulating Fkh2, or negatively regulating Sep1. We find that the *fkh2Δ ubc9Δ* double deletion strain is inviable, suggesting that over active Fkh2 is not the sole cause of mitotic defects of the *ubc9Δ* mutant. Furthermore, overexpression of Fkh2 in the *ubc9Δ* strain leads to cell death, suggestive that Sep1 is over active in the *ubc9Δ* mutant. This leads us to the model that Sep1 is overactive in sumoylation deficient strains.

Relevant to the findings of this study, micro array data sets from unsynchronised *S. pombe* populations have been completed previously (Rustici *et al.*, 2004). Interestingly gene expression of both *sep1Δ* and Sep1 over expression strains were analysed (Rustici *et al.*, 2004). If the model was that Pmt3 was regulating Sep1, we could hypothesis that Sep1 over expression would have a similar effect on gene expression to the loss of *pmt3⁺*. The microarray

data from non-synchronised cultures revealed that *cdc15+* and *plo1+* transcript levels were increased in cells overexpressing Sep1 compared to wild type (1.730-fold change and 1.329-fold change compared to wild type respectively) (Rustici *et al.*, 2004). Sep1 over expression did not greatly affect the transcript levels of the MBF complex targeted gene *cdc18+*, levels of which were similar to wild type (0.937-fold change compared to wild type). However, *fkh2+* levels were relatively close to wild type, if not slightly reduced in cells overexpressing Sep1 (0.913-fold change compared to wild type). This does not agree with our hypothesis that Sep1 hyper activation is leading to increased *fkh2+* levels in the *pmt3Δ* mutant. However, it would be naïve to simply assume Sep1 over expression would have the same gene profile as loss of *pmt3+*. One likely difference between gene expression changes upon Sep1 overexpression compared to the loss of *pmt3Δ* is that in the case of the Sep1 overexpression, regulatory mechanisms are still present. This is of importance as the regulation of Sep1 appears to be from post translational modification (Bulmer, 2005). Perhaps in the event of Sep1 over expression, post translational modifications occur which allow the regulation of the excess Sep1, but these only regulate a certain subset of the genes. Indeed, Sep1 appears to be phosphorylated in a cell cycle-dependant manner, hypothesised to be by Plo1 (Bulmer, 2005). This phosphorylation event appears to coincide with Sep1 accumulation in the nucleus during M-phase (Bulmer, 2004). Thus, the most critical experiments to elucidate this mechanism are to investigate the localisation and protein levels of Sep1 in a *pmt3Δ* mutant. Secondly, detection of Pmt3 modified Sep1 (or Fkh2) would directly link sumoylation to the process, and solidify the data thus far. This was attempted during the project, and the results were inconclusive (data not shown). Sumoylation consensus site searching has identified potential high confidence sumoylation sites in both Fkh2 and Sep1 (Figure 3.12), however, this does not guarantee sumoylation occurs. However, an N-terminally FLAG epitope tagged version of Pmt3 was constructed nearer the end of the project, which will be a useful reagent for detection of sumoylated substrates.

There was contradiction in the literature if sumoylation of the human cell-cycle-regulated forkhead transcription factor FoxM1 had a positive or negative impact on transcription of FoxM1 target genes (Myatt *et al.*, 2014; Schimmel *et al.*, 2014). One study suggested that the sumoylation of FoxM1 prevented the inhibitory dimerization of the transcription factor, thereby increasing the transcriptional activity and promoting mitosis (Schimmel *et al.*, 2014). In contrast, another study concluded that sumoylation promoted FoxM1 cytoplasmic localisation and degradation, and therefore inhibited cell cycle progression (Myatt *et al.*, 2014). Recent

Fkh2

```
  1 MTVRRLESKS EHISDDEERK EQLDYKKQMD VDTDRNIVLN GRLESQIAKL

 51 SVPPHEMRVV DDYSNSKNAE RHSGEIQAYA KFAGSTWTYY VKKIRIILGR

101 EPANPSPKGK NEDLEVIDMN FGPSKVVSRK HAVVEYDLDD QTWNCSVYGR

151 NGIKVDGKLF KNGETVKLTS GSILEVAGLQ MMFVLPNAAE QKQTDESTIK

201 EDAIKSEISA AVNDAAEYGD NKKPPYSYSV MIAQAILSSS ECMMTLSNIY

251 SWISTHYPYY RTTKSGWQNS IRHNLSLNKA FRKVPRKSGE QGKGMKWSIV

301 PEFREEFIAK TRKTPRKRSP SSPVPLLAKK REGSPSLPIP ILPKMKDTSI

351 PAAEPASSTT SARDQTPSTP KDVGSPSTAE TSAEEKQMET YKTPTHAALS

401 DIISTHDYAL DANSASQTKK AAFGSPIGSS TYPTSSPAPF WKYVAVPNPH

451 DWPQVGSYDT ISPYRNPVNS HLIYSQIQQS SPKKIDEQLH DLQGVDLVNG

501 FEGISSWRES MVNKLRSSVS DSPTMNLANS NSKSSPVAVQ RVSTLPQASA

551 NKQAKEMESK MSNSPTQKSK TEENNQAVRA ILDASATMEK QYDLHRLPTP

601 TSQTESASVP QIANPPNSQN LVKEKSPQQY IQVPQSNVKS SA
```

Sep1

```
  1 MNFNSTNPYY FTHEKNLNNA SKYSELPIAY QEIPLQSLPP YPKVASKLKG

 51 VVAGGKENNI ASFQKPSSKA TRPYIPSYTR LTYSVPPLPI PPPSEQSLDT

101 IIYRNPSVSS SQSQEPEEFF LPLDDGKKPP YSYAMLIGMS IIRSPDRRLT

151 LSAIYDWISN TFSFYNKSNN GWQNSIRHNL SLNKAFMKIE RPRNLPGKGH

201 FWSIRPGHEE QFLKLKLRKP GVNSRPAPPV QDVTSSTKYG SSTGSSGFNT

251 FNTSPHIFNQ RHQYLQNYYT ASLTNIPTIS NVNATNFHPL HSQQPYVDTP

301 GIDAPSDLEA KFSDLGVSSV VSVTSPLQSC TNSPSPPLSS PASSASPSES

351 LRNESLGIKS AKSLGLNKDD APVEGPPVSH LEKDVETPSV HDSVLGFNDT

401 VTNLGKKGLK DGTTNTLQIP AVRLPSLPSS PTIKNPSGLL LKRSNSIDFP

451 TPPKALCPKL FCFRDDIVAD DYTKFSLLSP IRSDMSGISA SPNTNLKEHR

501 TRILQMLATP DAKQLSSLTS SDAEFWSVTP LKSSILRNGD ASKQVTLSES

551 PKGDSLLDGG SLSYFTNNIS SVAGLETPSK LPMSKSFDTF EDDFLDPMDM

601 LSFENHFSDF NSNRKVSPVK REVRRKYISS ATTIHSSAAQ DDTYLPSPTK

651 RKMPLLRQTS TLF
```

Figure 3.12: Sumoylation consensus motif searches reveal high confidence sumoylation sites on both Fkh2 and Sep1. Using GPS-SUMO site prediction tool (Zhao et al., 2014), possible Pmt3 mortification sites are shown in red. Significant sumoylation sites are shown (p<0.05). Phosphorylation sites identified by proteomic analysis are shown in green, and those which have been verified in low through put analysis are underlined (Shimada *et al.*, 2008; Koch *et al.*, 2011; Szilagyi *et al.*, 2012; Carpy *et al.*, 2014).

studies in mammalian cells have also added more data for the role of sumoylation in regulating FoxM1. Firstly, SENP-6 has been shown to remove SUMO from FoxM1, leading to stabilisation of FoxM1 (Song *et al.*, 2015). This data supports the hypothesis of the study by Myatt and colleagues (2014), suggesting that sumoylation negatively inhibits the transcriptional activity of FoxM1. This would support our model that sumoylation is negatively regulating Sep1, however this is speculative. Interestingly, as a final observation, studies have shown that Polo-1 Kinase, homolog to *plo1+*, phosphorylates FoxM1, which increases transcriptional activity, by promoting its nuclear accumulation and preventing degradation (Zhang *et al.*, 2015). This strikes interesting similarities with data from other transcription factors, such as the transcription factor Elk-1, whereby phosphorylation via MAPK promoted the desumoylation of the target by SENP interaction, allowing cross talk between phosphorylation and sumoylation (Yang and Sharrocks, 2005). Thus, it is tempting to speculate therefore that the phosphorylation via Polo kinase 1 is recruiting SENP-6 and promoting desumoylation of FoxM1. Interestingly, in sumoylation site searches of Sep1, a non-consensus motif was identified that was surrounded by serine residues which have been found to be phosphorylated in high throughput studies (Koch *et al.*, 2011; Carpy *et al.*, 2014).

Recently published data identified an RFX-transcription factor, Sak1, involved in the regulation of mitosis in *S. pombe* (Garg *et al.*, 2015). Interestingly, it was shown that Sak1, like Sep1, appears to have a positive effect on gene transcription (Garg *et al.*, 2015). Furthermore, ChIP-seq data indicated that while Sep1 bound to a subset of Fkh2 target sequences, Sak1 was able to bind to the whole of Fkh2 regulated genes (Garg *et al.*, 2015). Nonetheless, these data could suggest that although Sep1 and Fkh2 appear to have opposing roles in M-phase gene transcription, Sep1 only regulates a subset of the Fkh2 regulated pool. This adds another layer of complexity to the system, and would be interesting to explore the Sak1 and sumoylation connections to cell cycle-regulated expression.

In this chapter we have established the viability of both *pmt3Δ* and *ubc9Δ* in *S. pombe*. With the data in this chapter and data in the discussion, we propose a preliminary model for how sumoylation could be regulating cell cycle gene transcription. We had aimed to use genetic screening to assess the biological roles of sumoylation. However, during this study we found that the sumoylation deficient strains were unable to cross under our laboratory conditions. Thus, we aimed to investigate the biological roles of sumoylation by SGA analysis using the model organism *S. cerevisiae*. As the SUMO encoding gene, *SMT3*, is essential in *S. cerevisiae*, we used a hypomorphic allele which has not previously been used to study the biological processes of sumoylation.

Chapter Four: Genetic Analysis of *SMT3* in *S. cerevisiae*

4.1 Introduction

The budding yeast *S. cerevisiae* expresses one SUMO homolog, Smt3, which is conjugated to its target proteins via the heterodimeric E1 Aos1/Uba2, the E2 enzyme Ubc9, and one of four E3 ligases Siz1, Siz2/Nfi1, Mms21 and Zip1 (Zhao and Blobel, 2005). As sumoylation is a dynamic modification, Smt3 is then removed from its target by one of two deconjugases, Ulp1 or Ulp2. Unlike *S. pombe* and *C. albicans*, the process of sumoylation is essential in *S. cerevisiae*, and as such most genes involved in the SUMO pathway are essential for cell viability (Dieckhoff *et al.*, 2004). Although several studies have characterised roles for SUMO in DNA metabolic processes and cell cycle regulation, SUMO modifies many other proteins in diverse cellular processes, of which the roles are not understood (Makhnevych *et al.*, 2009; Eifler and Vertegaal, 2015a; Zhao *et al.*, 2004; Leach *et al.*, 2011, Blomster *et al.*, 2009). A recent global interactome screen aimed to reveal the range of processes where SUMO plays a role in *S. cerevisiae* (Makhnevych *et al.*, 2009). A large data set was obtained of Smt3 physical interactions using yeast two hybrid and mass spectrometry data, and was combined with genetic interaction data to produce a broad network of sumoylation interactions. Interestingly, although this revealed biological processes where sumoylation is linked, the relationships with SUMO are not well understood. These processes include cytoskeleton organisation, vesicle mediated transport, and mitochondrion organisation (Makhnevych *et al.*, 2009). Although extensive, the dataset from Makhnevych *et al.* (2009) does not provide quantitative measures of genetic interaction, which is useful to gain further insight into the detected interactions. Identification of suppressing genetic interactions has previously proved very useful in understanding biological processes such as cell cycle regulation, thus isolation of the interactions is likely to be informative to identifying Smt3 functions. Significantly, the dataset did not present any suppressing interactions, which would have aided in dissecting the role of Smt3. However, the only other genetic screen to include a loss of function allele of *SMT3* was within a genome wide screen which aimed to provide a global genetic interaction network in *S. cerevisiae*, and as such provided much less coverage of *SMT3* interactions (Costanzo *et al.*, 2010). Our analysis of the published large scale screens also highlighted that they have not been completely saturating, particularly with the respect of essential gene coverage. Therefore, we aimed to expand these previous studies by performing quantitative analysis of genetic enhancers and suppressors of dysregulated sumoylation in *S. cerevisiae* on a genome wide scale. We decided to take advantage of available yeast mutation collections of essential and non-essential genes, allowing us to screen 4999 genes of the yeast genome, many of which have been previously analysed in other screens.

4.2 Results

4.2.1 Analysis of DAmP Alleles of the Sumoylation Pathway

Many of the sumoylation pathway enzymes are essential in *S. cerevisiae*, which hampers genetic studies of SUMO in this organism. However, to circumvent the problems associated with the study of essential genes in budding yeast, Breslow *et al.* (2008) constructed a decreased abundance by mRNA perturbation (DAmP) library, where a KanMX cassette has been inserted at the 3' end of most the essential genes to destabilizes mRNA transcripts (Figure 4.1). Thus, a viable hypomorphic DAmP allele mutant exists for ~82% of the 1033 essential genes in *S. cerevisiae* (Breslow *et al.*, 2008). Important to this study, many of the essential sumoylation pathway enzymes are included in this library, including *SMT3, AOS1, UBA2, ULP1* and *ULP2.* However, a notable exception is the E2 enzyme, *UBC9.*

A first step in our analysis was identify the phenotypes associated with each of these sumoylation pathway DAmP alleles. Indeed, many of the DAmP allele containing strains from the sumoylation pathway have not been previously characterised. Significantly, the *smt3-DAmP* mutant strain has not been previously characterised. Indeed, this strain was not used in the Makhnevych *et al.* (2009) screen, and although this strain was used in the Costanzo *et al.* (2010) screen, the strain was not comprehensively screened for phenotypes. Hence, cells encoding the DAmP alleles of *SMT3*, *AOS1*, *UBA2*, *ULP1* and *ULP2* were exposed to a range of stresses and growth conditions (Figure 4.2). The sumoylation pathway has been implicated in a wide array of stress responses (Tanaka *et al.*, 1999; al-Khodairy *et al.*, 1995; Hoege *et al.*, 2002; Bossis and Melchior, 2006; Pinto *et al.*, 2012; Sydorskyy *et al.*, 2010), hence a range of stress conditions were tested. The E1 heterodimer of the sumoylation pathway consists of Aos1 and Uba2, which are both essential for viability (Johnson *et al.*, 1997). Surprisingly, however, the cells containing the *aos1-DAmP* allele and *uba2-DAmP* allele display widely differing stress sensitives to the conditions tested. Whereas cells containing the *aos1-DAmP* allele behaved very similarly to wild type control cells, cells containing the *uba2-DAmP* allele were much more sensitive to H_2O_2, HU, TBZ, and caffeine (Figure 4.2). However, cells containing the *smt3-DAmP* allele were acutely sensitive to temperatures below optimum growth conditions, particularly 15°C, and did not display any of the sensitivities that were observed in the *uba2-DAmP* mutant cells (Figure 4.2). The *ulp1-DAmP* allele and *ulp2-DAmP* allele containing strains showed distinct sensitivities. While the *ulp1-DAmP* mutant had a similar phenotype displayed in the *smt3-DAmP* allele containing strain of particularly slow growth at suboptimal temperatures, the presence of the *ulp2-DAmP* allele presented acute
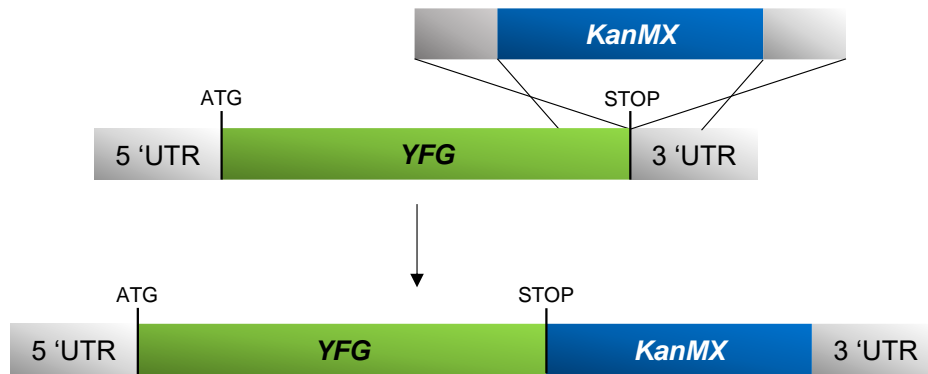
Figure 4.1: Schematic diagram of decreased abundance by mRNA perturbation (DAmP) allele construction. Gene of interest is denoted by *YFG* (Your Favourite Gene). An antibiotic resistance cassette (KanMX) is inserted into the 3' end of *YFG*, directly following the stop codon. The *S. cerevisiae* DAmP allele hypomorphic strain library was constructed previously (Breslow *et al.*, 2008).
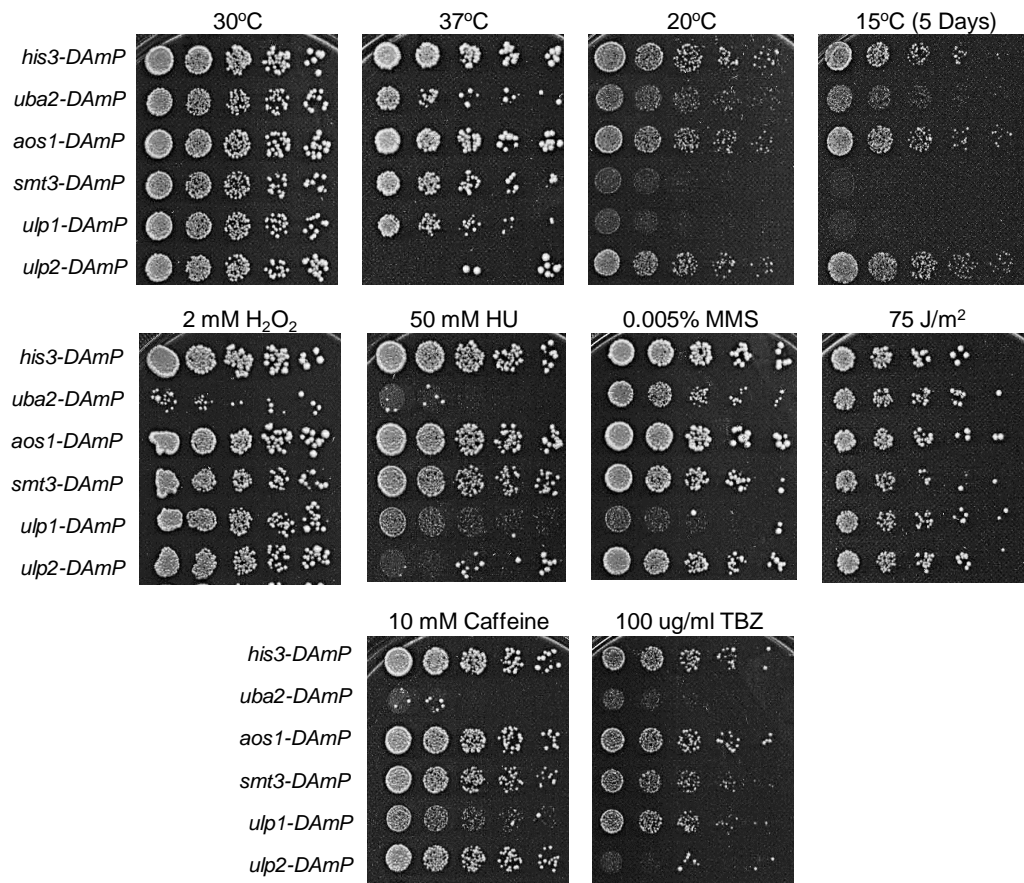
Figure 4.2: Sensitivity analysis of *S. cerevisiae* sumoylation pathway DAmP strains to various growth conditions and stresses. 5 fold serial dilutions of mid-log phase growing *his3-DAmP* (CL90), *uba2-DAmP* (CL91), *aos1-DAmP* (CL93), *smt3-DAmP* (CL92), *ulp1-DAmP* (CL94) and *ulp2-DAmP* (CL95) were spotted onto YPD agar plates with the indicated stresses and growth conditions, and plates incubated at 30ºC for 3 days unless otherwise stated.

temperature sensitivity at 37°C, as well as sensitivity to HU and TBZ (Figure 4.2). These observations are consistent with the previous deletion strains, such as the *ulp2Δ* mutant exhibiting benomyl, HU and temperature sensitivity (Li and Hochstrasser, 2000). The *ulp1-DAmP* allele was the only sumoylation pathway DAmP allele that conferred sensitivity to the DNA alkylating agent MMS (Figure 4.2).

Construction of a hypomorphic DAmP allele gene variant was reported to typically reduce corresponding mRNA transcripts in the order of 2-10 fold (Breslow *et al.*, 2008). It therefore was possible that some of observed differences between the sumoylation pathway DAmP alleles, for example the differing phenotypes of *aos1-DAmP* and *uba2-DAmP* allele containing strains, could be due to the KanMX cassette insertion having a varying effect on mRNA transcripts between the sumoylation pathway genes. To test this possibility, RNA was extracted from the *smt3-DAmP*, *aos1-DAmP, uba2-DAmP*, *ulp1-DAmP* and *ulp2-DAmP* allele containing strains, and mRNA transcript levels of the respective gene compared to a control strain (*his3-DAmP*) (Figure 4.3). As expected, the effect of DAmP allele construction on target gene transcripts varied across all the sumoylation pathway genes. Levels of *SMT3* transcripts dropped 10 fold, while *AOS1* and *ULP1* levels dropped 2 fold (Figure 4.3). However, levels of *ULP2* transcript appeared to be unaffected by the *ulp2-DAmP* allele (Figure 4.3). In contrast to the other strains, *UBA2* transcript levels actually appeared to increase 1.29 fold with the *uba2-DAmP* allele, although this was not statistically significant (Figure 4.3). In conclusion, our analysis described above concludes that the cells containing the *smt3-DAmP* allele displayed the largest drop in gene expression. Furthermore, we have identified slow growth conditions (cold temperature growth), which could be used to screen for suppressors and enhancers in subsequent genetic screening.

4.2.2 Construction of an smt3-DAmP::NatMX Strain for Synthetic Genetic Array (SGA) Analysis

The strain library used for synthetic genetic array (SGA) analysis contains 4291 single deletion mutants for non-essential genes, and 842 DAmP allele strains of essential genes (non-essential genes (Synthetic Deletion Library Version 4 (SDLV4); Tong and Boone, 2006). In this library all the mutants are marked with KanMX conferring G418 resistance. Therefore, to utilise the *smt3-DAmP* strain as a query for SGA analysis, the KanMX antibiotic resistance marker of the *smt3-DAmP* strain must be replaced with another marker, thus allowing selection of double mutants during the SGA process (see 2.2.7.2 for SGA process). Consequently, the KanMX marker was switched for another marker NatMX, conferring resistance to the antibiotic nourseothricin, commercially named clonNAT (strategy shown in Figure 2.2). Correct
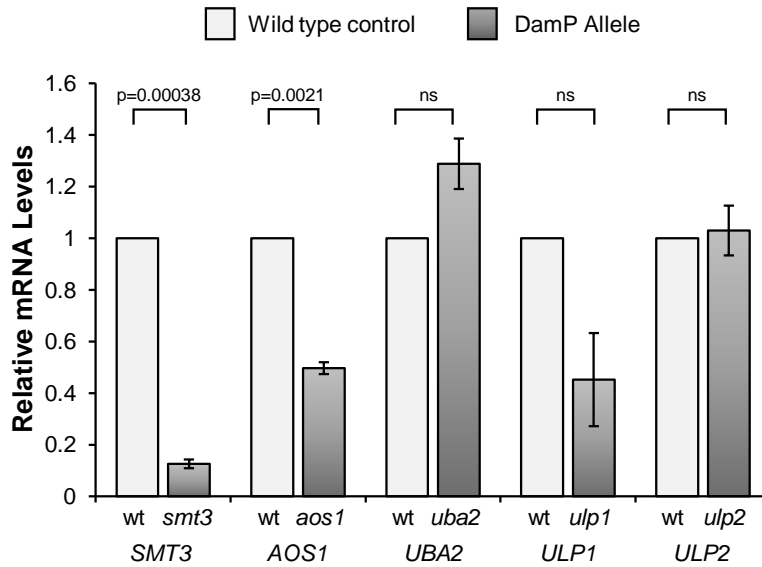
Figure 4.3: RNA analysis of sumoylation pathway DAmP mutants. The relative level of *SMT3*, *UBA2*, *AOS1*, *ULP1* and *ULP2* transcripts expressed from the corresponding mutant DAmP allele for each gene were analysed. mRNA was extracted from *uba2-DAmP* (CL91), *aos1-DAmP* (CL93), *smt3-DAmP* (CL92), *ulp1-DAmP* (CL94) and *ulp2-DAmP* (CL95), transcript levels analysed by qRT-PCR and normalised to a *ACT1* levels, then compared to a wild type *his3-DAmP* (CL90) control. Error bars illustrate the standard deviation of 3 biological replicates. Genes with a statistically significant change in expression compared to wild type control using a two tailed t-test are annotated with p value, those which were not statistically significant (p>0.05) are labelled ns.

integration of the *NatMX* cassette was confirmed by check PCR (Figure 4.4 A). Furthermore, loss of the KanMX cassette was confirmed by sensitivity to G418 (Figure 4.4 B).

Following the RNA analysis of the *smt3-DAmP::KanMX* strain (see Figure 4.3), it was important to confirm the effect of both the *smt3-DAmP::KanMX* and *smt3-DAmP::NatMX* alleles on free Smt3 levels and Smt3 conjugates. Hence, protein extracts from *smt3-DAmP::NatMX* and wild type *S. cerevisiae* were collected and analysed by western blotting with anti-Smt3 antibodies (Figure 4.5). These data revealed that there was a reduced pool of free Smt3 in the *smt3-DAmP:NatMX* strain. Furthermore, it suggests that high molecular weight Smt3 conjugates are reduced in the *smt3-DAmP::NatMX* strain (Figure 4.5).

Next, the phenotypes of the *smt3-DAmP::NatMX* strain were examined to identify any effects associated with the KanMX to NatMX marker switch (Figure 4.6). These analyses revealed that replacement of the KanMX cassette with a NatMX cassette caused decreased fitness at 30°C (Figure 4.6). Furthermore, the switch of NatMX cassette for a KanMX cassette in the *smt3-DAmP* allele appeared to further reduce growth at cold temperatures, observed by further reduced growth at 20°C (Figure 4.6) The basis of these enhanced phenotypes associated with the NatMX cassette are unclear. However, it is interesting to note the NatMX cassette has a high GC content (Goldstein and McCusker, 1999), and it is possible that this interferes with transcription of *SMT3* transcripts to a greater extent than the KanMX cassette, causing a further lowering of *SMT3* transcripts. However, we have not directly compared either *SMT3* transcripts or Smt3 protein levels in the *smt3-DAmP:KanMX* and *smt3-DAmP::NatMX* strains, so without further experiments this is purely speculation. All studies from this point onward use the *smt3-DAmP:NatMX* (CL100) strain, so for simplicity the *smt3-DAmP::NatMX* strain will be named *smt3* for the remainder of this thesis.

Having constructed the *smt3* mutant strain we next investigated the phenotypes of the *smt3* cells before performing the SGA analysis. These data would provide a useful baseline for the characterisation of any identified suppressors or enhancers of the growth of the *smt3* mutant. Microscopic analysis of the *smt3* mutant cells revealed that reduced levels of Smt3 led to an increase in the number of large budded cells, indicative of cell cycle delay (Figure 4.7 A) (Table 4.1).
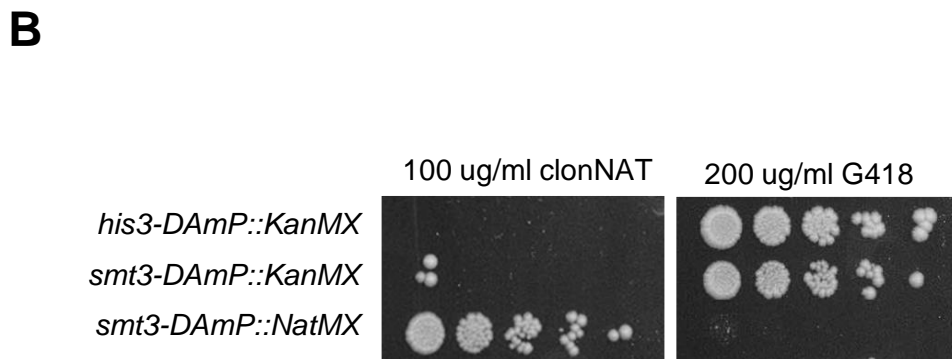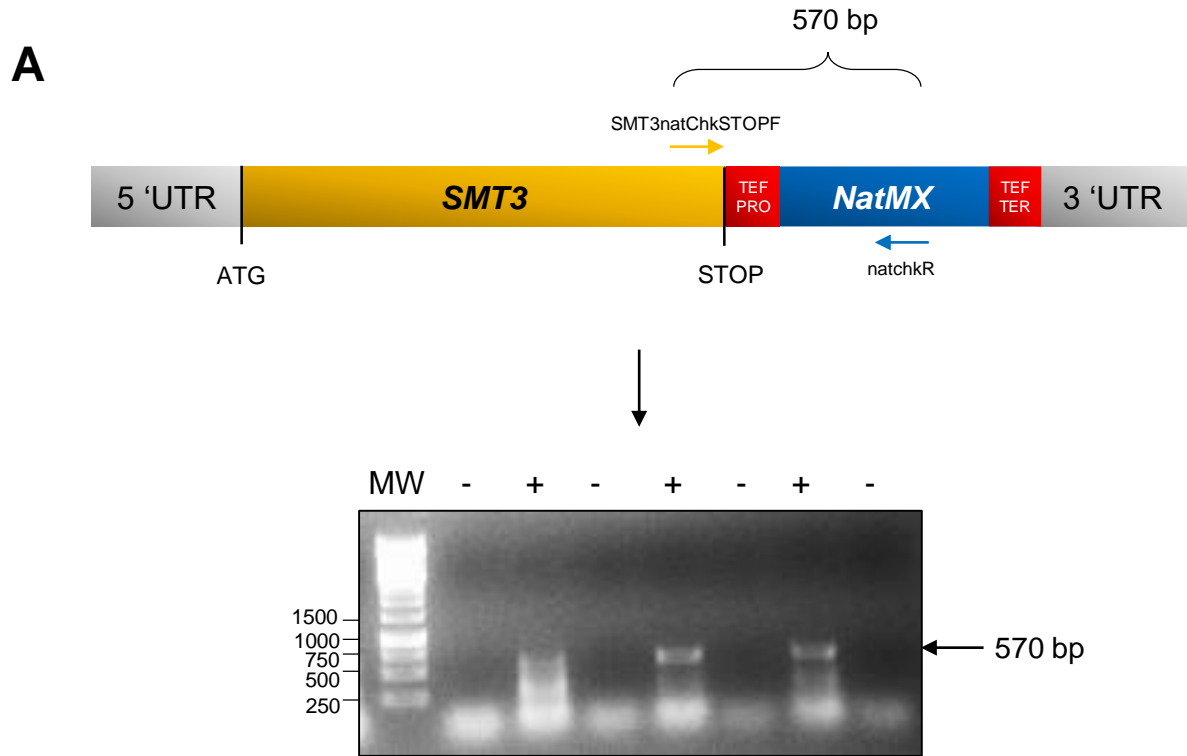
Figure 4.4: KanMX cassette is successfully switched to NatMX in *smt3-DAmP::NatMX* strain. A) PCR was performed using gDNA from clonNAT resistant *smt3-DAmP* transformants as a template, and one primer specific to *SMT3* and another specific to the NatMX cassette. PCR products were analysed by agarose gel electrophoresis. Negative PCR products are indicated by -, positive PCR products are indicated by +. B) *smt3-DAmP::NatMX* strain positive for NatMX cassette integration by PCR was grown on YPD containing the indicated concentration of clonNAT and G418.
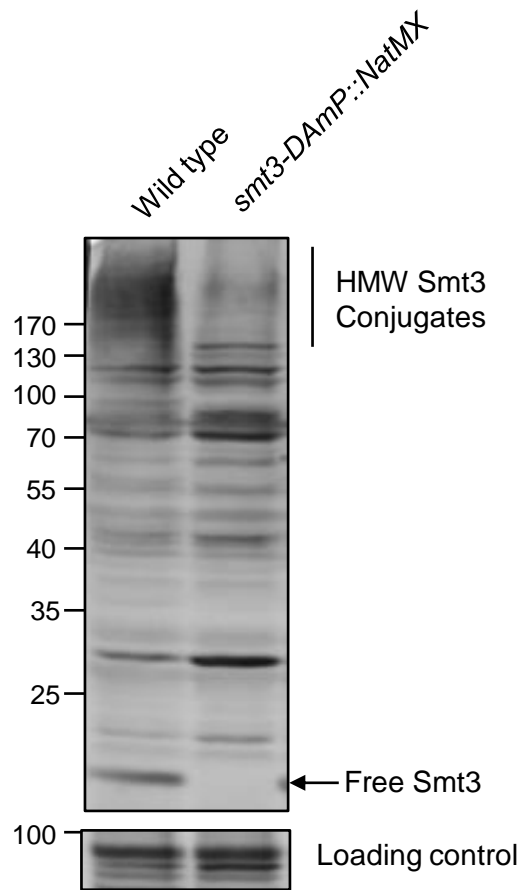
Figure 4.5: *smt3-DAmP::NatMX* **allele reduces free Smt3 levels and affects HMW Smt3 conjugates.** Protein was extracted from mid-log growing phase wild type (BY4741) and *smt3-DAmP::NatMX* (CL100) cells and analysed by western blotting. Proteins were probed with anti-Smt3, and anti-Skn7 antibody used as loading control

	30°C	20°C	15°C (7 Days)
his3-DAmP::KanMX			
smt3-DAmP::KanMX			
smt3-DAmP::NatMX			
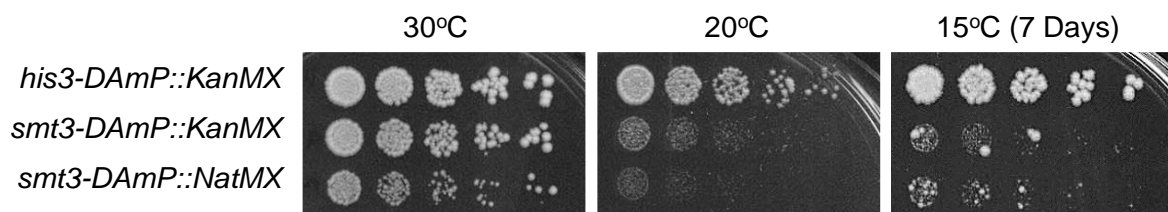
Figure 4.6: Sensitivity to suboptimal temperature in *smt3-DAmP::KanMX* mutant is conserved in the *smt3-DAmP::NatMX* mutant. 5 Fold serial dilutions of mid-log phase growing *his3-DAmP::KanMX* (CL90), *smt3-DAmP::KanMX* (CL92) and *smt3-DAmP::NatMX* (CL100) cells were spotted onto YPD agar plates, and plates incubated the indicated temperature for 3 days unless otherwise stated.
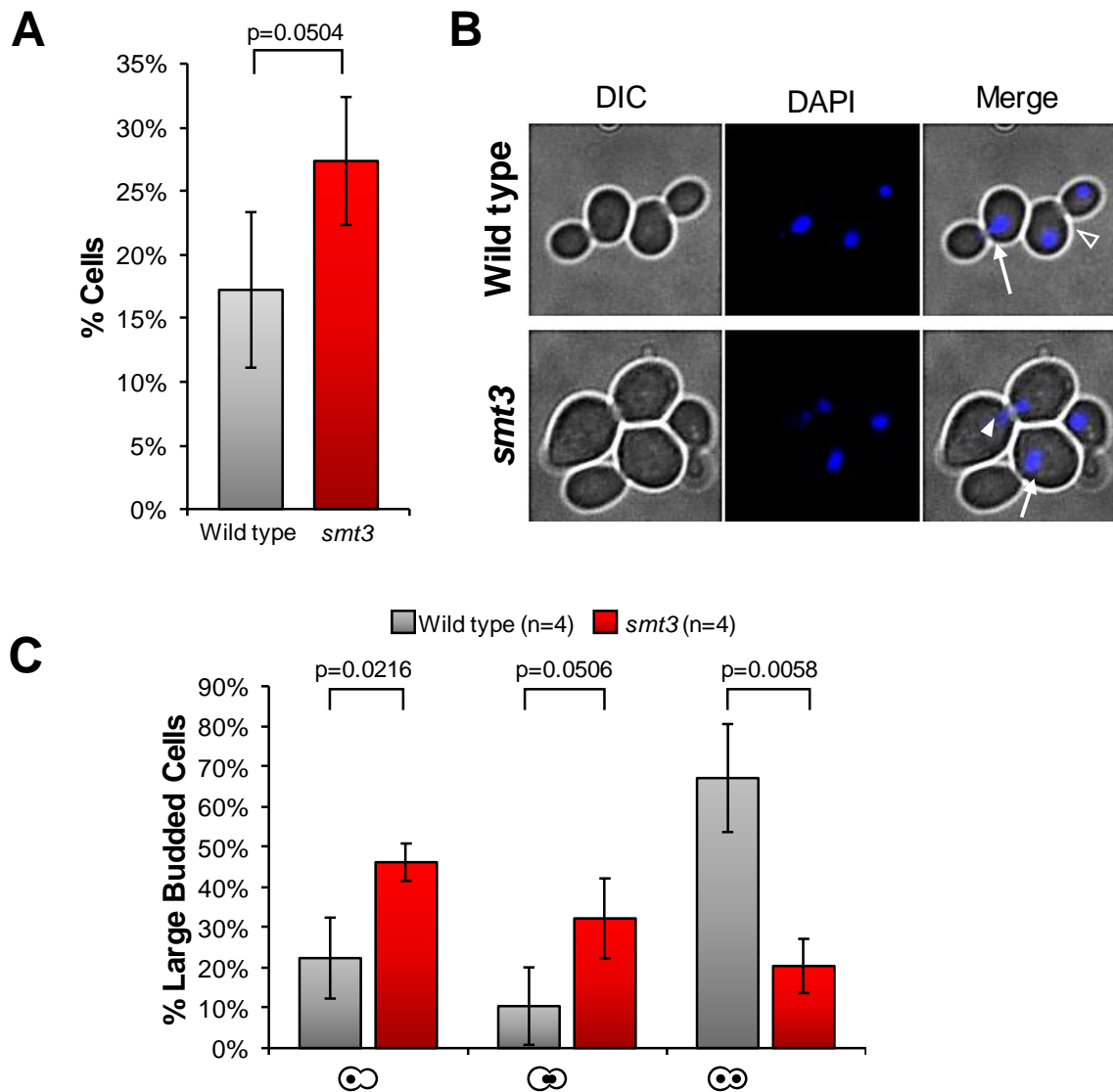
Figure 4.7: *smt3* cells have cell cycle and nuclear morphology defects. Mid-log phase growing wild type (BY4741) and *smt3* (CL100) cells were fixed and stained with DAPI to visualise DNA. Cells were classed as large budded when the bud to mother cell diameter ratio is at least 0.75, as described previously (Huffaker *et al.*, 1988). A) The number of large budded cells were counted from a total of 389 and 340 wild type and *smt3* cells respectively from 4 independent biological replicates. Approximately 100 cells were counted per replicate, and the standard deviation between replicates indicated as error bars. The p value is derived from a 2 tailed unpaired student t test. B) Examples of the 3 nuclear morphologies observed in large budded cells: fully divided nuclei (open arrow head), nuclei in the mother cell (arrow), or nuclei across the bud neck (closed arrow head). C) The 3 nuclear morphologies described in B) were quantified in wild type and *smt3* large budded cells. Percentages of large budded cells displaying the described morphologies are shown. Data obtained from 4 independent replicates of 67 wild type and 93 *smt3* large budded cells. Error bars indicate the standard deviation of the 4 biological replicates. The p values are derived from 2 tailed unpaired student t tests.

Strain	Number large budded cells	Total number of cells	%	Biological Replicates
Wild type (BY4741)	67	389	17.2 ± 5.1	4
***smt3* (CL100)**	93	340	27.4 ± 6.0	4

Table 4.1: Percentages of large budded wild type and *smt3* cells counted for analysis in Figure 4.7. Large budded cells classed as bud to mother ratio >0.75. Standard deviation between 4 biological replicates is indicated as ±%.

Furthermore, some of the large budded *smt3* cells also grew a lot larger than wild type strains (Figure 4.7 B). Hence, to further characterise this cell cycle delay, the nuclear morphologies of these cells were examined using DAPI staining (Figure 4.7 B and C). Cells containing fully divided nuclei (Figure 4.7 B, open arrow head), nuclei in the mother cell (Figure 4.7 B, arrow), or nuclei across the bud neck (Figure 4.7 B, closed arrow head) were counted. These analyses indicated that 46.6% of large budded *smt3* cells had 1 undivided nucleus visible in the mother bud, compared to 22.4% of wildtype cells (Figure 4.7 C). Moreover, in contrast to wild type where 76.5% large budded cells had fully divided nuclei, only 22.7% of large budded *smt3* cells had completed mitosis (Figure 4.7 C), which was highly significant (p=0.0058).

To further investigate the DNA morphology of these strains, DNA content of the *smt3* cells were analysed by FACs analysis (Figure 4.8 A). Interestingly, gating analysis revealed that a significantly increased population of *smt3* mutant cells had >2N DNA content compared to wild type, (3.65±0.05% vs 0.35±0.025%, p=0.000459) indicative of aneuploidy (Figure 4.8 B). Hence, taken together these results suggest that the *smt3* strain has significant mitosis defects.

Having successfully created the *smt3* strain and assessed its phenotypes, the next step to introduce markers and switch the mating type of the *smt3* strain for SGA analysis was necessary. Hence, the *MATa smt3* strain (CL100) was crossed with an appropriate *MATα* strain (AR3) to obtain a *MATα smt3* strain (CL107) containing markers required for SGA (*can1Δ*::*STE2pr-Sp_his5* and *lyp1Δ::HphMX::LEU2)*. The *smt3* (CL100) strain was successfully able to undergo mating and sporulation, and all markers segregated appropriately (2:2). 6/30 of the spores analysed were found to contain the *can1Δ*::*STE2pr-Sp_his5* and *lyp1Δ::HphMX::LEU2* markers, and were *MATα*. The resulting strain (CL107) was verified for the presence of the NatMX cassette at the 3' end of *SMT3* using PCR, and was confirmed to behave similarly to the parent *smt3* CL100 strain in respect to growth.
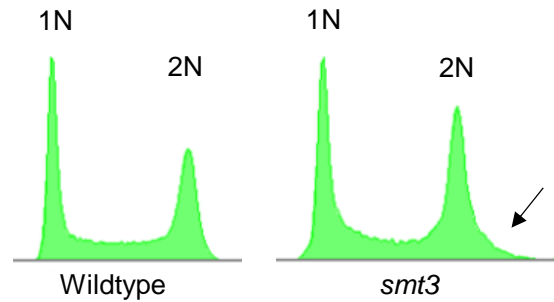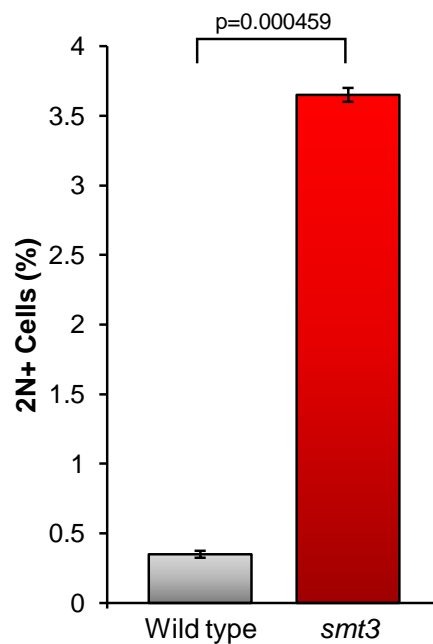
Figure 4.8: *smt3* **cells have chromosomal segregation defects.** Mid-log growing phase wild type (BY4741) and *smt3* (CL100) cells were fixed in 70% ethanol, DNA stained with SYTOX green and DNA content analysed by flow cytometry. A) DNA content histogram from wild type and *smt3* cells. Arrow indicates cells with DNA content above 2N, suggestive of aneuploidy. B) Gating analysis of cells containing above 2N DNA content in wild type and *smt3* mutant cells. Error bars indicate the standard deviation from two replicates. The p value is derived from a 2 tailed unpaired student t test.

4.2.3 SGA analysis of smt3-DAmP Revealed Novel Genetic Interactions

The protocol showing the conditions used for high throughput SGA is shown in Figure 4.9 A. The *smt3* SGA query strain (CL107) was crossed with an array of 4291 deletion mutants of non-essential genes (Giaever *et al.*, 2002), and 878 DAmP allele mutants of essential genes (Breslow *et al.*, 2008). The SGA procedure was conducted at 30°C, due to the slower growth of the smt3 strain at temperatures below this. While the library contains both deletions and the hypomorphic DAmP mutants, the array mutants are termed *yfgΔ* (your favourite gene) for simplicity. The final haploid *smt3 yfgΔ* double mutant strains were selected using the SGA procedure. Photographs of the SGA array growing colonies were analysed using software called Colonyzer, which measures the growth rate of microorganisms on agar (Lawless *et al.*, 2010). These analyses gave each double mutant strain a quantitative fitness measure. To reduce the risk of erroneous results, each cross is repeated 4 times, as illustrated by the 4 spots for each gene (Figure 4.9 B). The final dataset of genes was trimmed by removal of 134 *yfgΔ* library mutants which are either sterile and therefore unable to cross with the *smt3* SGA query strain (CL107), or are auxotrophic for supplements used in the SGA process, for example *LEU* gene mutants.

A

Mating	**24hr Rich Media**
Diploid Selection	**36hr G418 + cloNAT**
Sporulation	**5 days Sporulation Media**
MATa Selection	**Minimal Drop Out Histidine + Canavadine**
Meiotic Progeny Selection	**Minimal + G418**
	Minimal + G418 + cloNAT

MATα smt3::NatMX ✕ MATa yfg::KanMX

MATα/a smt3::NatMX yfg::KanMX

α   a
α   a

MATa yfg::KanMX   MATa smt3::NatMX yfg::KanMX   MATa smt3::NatMX   MATa

MATa smt3::NatMX yfg::KanMX   MATa smt3::NatMX

MATa smt3::NatMX yfg::KanMX

Final double mutant strain

B

Suppressors Enhancers

Figure 4.9: The synthetic genetic array (SGA) process in *S. cerevisiae*. A) Schematic diagram illustrating the synthetic genetic array (SGA) process. The *MAT*α haploid strain containing the query *smt3-DAmP*::*NatMX* (CL107) allele is crossed with a library of 4291 non-essential gene deletions, and 878 essential genes containing DAmP alleles. All library strains, illustrated as *yfg*::*KanMX* (*Your Favourite Gene*) in the diagram, have the gene of interest interrupted with a gentamicin resistance marker (KanMX). Diploids containing both *smt3*::*NatMX* and *yfg*::*KanMX* are selected by repinning crosses onto nourseothricin (cloNAT) and kanamycin (G418) containing plates. Resulting diploids were sporulated on sporulation media for 5 days. *MAT*a haploids were selected using the SGA allele *can1Δ*::*STE2pr-Sp_his5*. Deletion of *CAN1* confers resistance to L-canavanine. The *S. pombe his5*⁺ gene (which complements *S. cerevisiae HIS3*) is regulated by the *STE2* promoter, which is only induced in *MAT*a cells, allowing selection of histidine prototrophic *MAT*a cells which can grow on minimal media lacking histidine. Final double deletion mutants were selected during rounds of G418 and cloNAT selection, with 48 hour regrowth between each re-pin. B) 18 final SGA plates were obtained, and an example plate shown. Genetic enhancers shown in red, and genetic suppressors shown in green. 4 replicates of each double mutant were pinned onto the final plate, and the mean fitness calculated.

The quantitative fitness measures of the *smt3 yfg*Δ strains returned by Colonyzer were plotted against the fitness measures of a control cross giving a fitness plot (Figure 4.10). The dashed grey line indicates the line of equal fitness, i.e. the position where an *smt3 yfg*Δ mutant would lie if it grew at an equivalent rate to the *yfg*Δ mutant alone. However, as the fitness of the *smt3* strain and some *yfg*Δ mutant strains will clearly alter from wild type, it would be more likely that even in the absence of genetic interaction between *smt3* and *yfg*Δ, the resulting *smt3 yfg*Δ strain would have a fitness equivalent to the product of the individual *smt3* fitness and the *yfg*Δ fitness. This assumption is termed the multiplicative model of fitness (Mani *et al.*, 2008). Thus, a fitness prediction of the *smt3 yfg*Δ strain was made based on the fitness of the *smt3* strain, and the fitness of each individual *yfg*Δ strain. A linear predictor of the fitness of the population is shown by the solid grey line (Figure 4.10). The Genetic Interaction Score (GIS) is calculated by comparing the expected fitness to the experimentally determined fitness, and the larger the deviation the more severe the genetic interaction (Addinall *et al.*, 2011). Enhancing interactions, where the fitness of the *smt3 yfg*Δ strain is much lower than would be expected by the multiplicative fitness model show a negative GIS score. Genes which were significant enhancers are represented as red circles on the plot (Figure 4.10). Suppressing interactions, where fitness of the *smt3 yfg*Δ strain is increased more than predicted have a positive GIS score, and those which were significant are shown in green on the plot (Figure 4.10). Thus, a GIS score around zero suggests there is no genetic interaction which are shown as grey open circles (Figure 4.10). As the *smt3* query strain alone already has a low fitness, combining the *smt3* with any non-interacting gene will cause a reduction in fitness in the *smt3 yfg*Δ mutant. Thus, the estimated population fitness line (Figure 4.10, solid grey line) is lower than equal fitness line (Figure 4.10, dashed grey line). It is also important to note that due to the effect of neighbouring colonies on the crowded SGA plates, there will be some variability of fitness due to the arrangement of strains on the SGA plates. Therefore, as the *smt3* single mutant strain has a lower fitness than the wild type strain, strains containing suppressor deletions were predicted to form larger colonies on the *smt3 yfg*Δ experimental SGA plate than on the control single *yfg*Δ SGA plate.
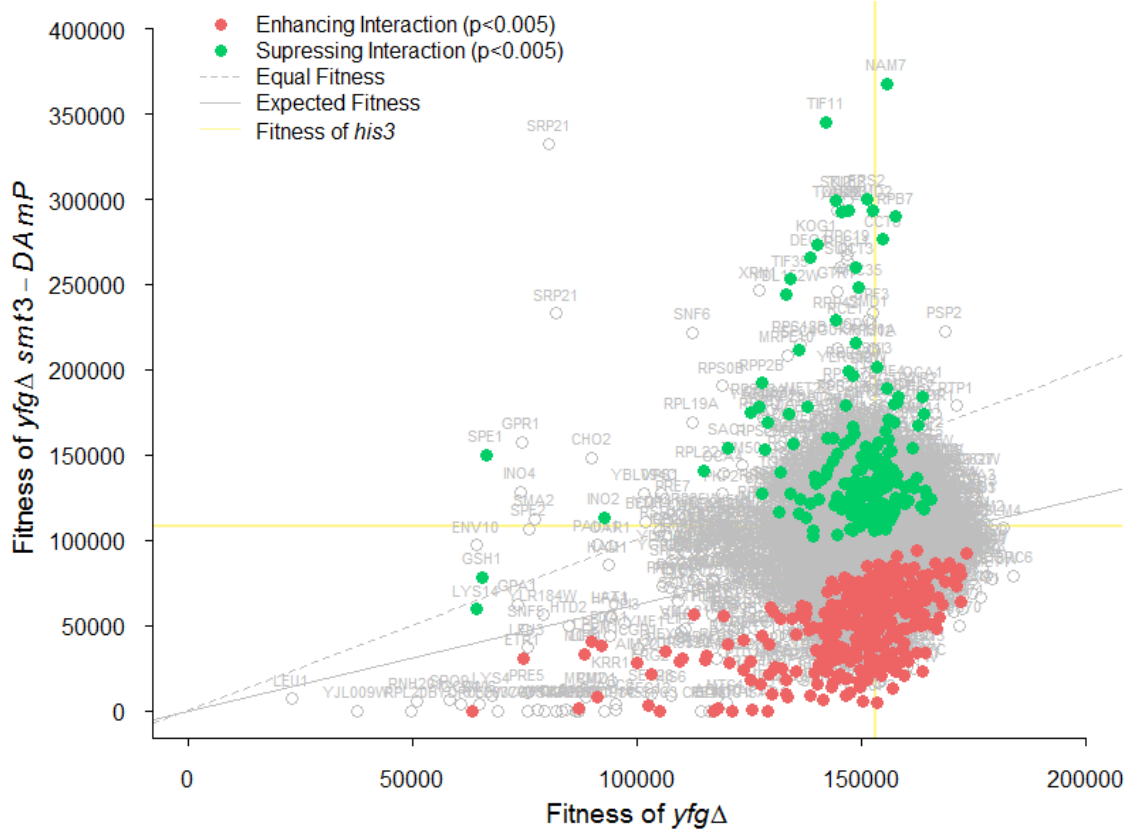
Figure 4.10: Fitness of library strains (*yfgΔ*) plotted against the fitness of *smt3-DAmP::NatMX yfgΔ* double mutant strains. The yeast deletion collection was crossed with the *smt3-DAmP::NatMX* query strain (CL107) in at least 4 replicate crosses per query strain, and the fitness of the resulting strains were measured. All gene pairs from library array are illustrated on the fitness plot as open grey circles, and significant suppressors and enhancers (p≤0.005) are indicated by closed green and red circles respectively, and labelled with gene name. The line of equal growth is indicated by a dashed line. The average fitness of the *his3-DAmP::KanMX* (x axis) and *smt3-DAmP::NatMX his3-DAmP::KanMX* strain (y axis) are indicated by solid yellow lines. The line of expected fitness is shown by a solid grey line.

Having obtained the initial data, the interacting genes were sorted by ascending GIS scores, with the top 1% (49 genes), 2% (99 genes) and 5% (249 genes) of genes classed as high, medium and low suppressing genetic interactions. The same numbers of genes in the lowest 1%, 2% and 5% GIS scores were classed as high, medium and low negative enhancing genetic interactions. P values of the hits were disregarded in this preliminary analysis, as the p values are calculated by assessing the standard error between the 4 replicate colonies, and consequently 1 out of 4 mis-pinned colonies may skew the statistical analysis. Furthermore, due to the structure of the array plates, many genes are actually repeated more than 4 times in the screen, which increases the n number causing higher p values. For gene lists of top 5% enhancers and top 5% of suppressors from the SGA analysis, see Appendix A and Appendix B, respectively.

Having identified enhancers and suppressors of the *smt3* strain, we next used gene ontologies (GO) to identify the biological processes which sumoylation was involved in, particularly in the pool of suppressing interactions which have not previously been uncovered. Gene ontology (GO) terms are used to describe the biological process, molecular function or cellular component of a gene product in a way which is comparable across species. GO terms form a hierarchy, where less specific parent terms, such as 'DNA metabolic process', then have child terms 'DNA repair' and 'DNA recombination' and such forth. GO terms are useful for finding enrichment of processes within large data sets, such as the analysis of SGA data. (Ashburner *et al.*, 2000). Thus, we analysed the top 5% of each interaction type to assess which biological processes are associated with both the enhancers and suppressors.

The top 5% enhancers and 5% suppressors were categorised into wide biological processes using the GO Slim Mapper analysis tool on the Saccharomyces Genome Database (SGD). Hypergeometric analysis was used to identify processes which are significantly enriched in the gene list, relative to the frequency that genes are of that process within the genome (Figure 4.11). Where appropriate, the parent terms for processes were shown, to avoid repeating similar processes. These analyses revealed that many of the enhancing genes were involved in DNA replication, DNA recombination, DNA repair, and mitotic and meiotic cell cycle including chromosome segregation (Figure 4.11). This is perhaps unsurprising considering the phenotypes outlined previously. Furthermore, chromatin organisation and histone modification were also highlighted as significant biological processes, as well as telomere organisation (Figure 4.11). These biological processes have been already highlighted as enhancing genes previously, which validates the screen in comparison to the previous data (Makhnevych *et al.*, 2009).
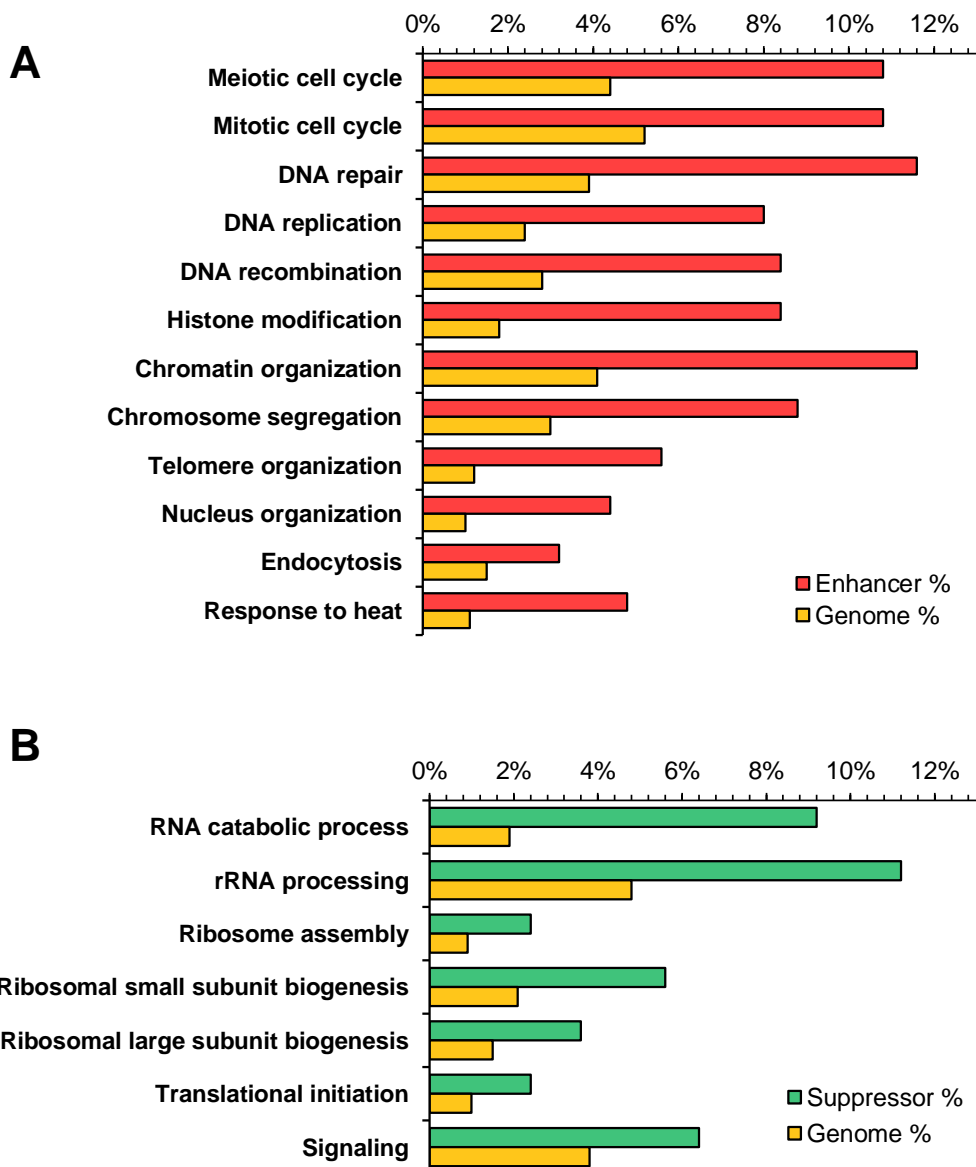
Figure 4.11: GO Biological Process terms of top 5% enhancers and suppressors of the *smt3* query allele reveals different GO terms between enhancers and suppressors. GO Slim Mapping analysis was completed on the top 5% enhancers (A, red bars) and top 5% suppressors (B, green bars). GO analysis consigns the genes into wide categories of biological processes, showing the frequency of potential hits in the genome. Significance of hits are calculated using hypergeometric analysis, by comparing sample to genome frequency. Significant hits (p≤0.05) are shown. Bars show the % hits from the population of enhancers or suppressors (249 genes) or the genome (6338 genes). Enhancers are illustrated as red bars, suppressors as green bars, and the genome frequency is represented in yellow.

In contrast, the suppressors of loss of Smt3 function are less well characterised, so this is the first large scale analysis of suppressors of loss of *SMT3* function. Interestingly, although the GO analysis returned fewer significant hits for the suppressors, there was highly significant enrichment for genes involved in RNA catabolism, and translational processes such as the biogenesis and assembly of ribosomes, and rRNA processing (Figure 4.11).

Positive and negative interaction data can be used to provide insight into which protein complexes may be regulated by Smt3. In *S. cerevisiae*, many gene products have been consigned into functioning protein complexes, thus allowing identification of specific complexes within lists of genes (GO consortium). Therefore, to gain further insight into how the *smt3* allele is affecting specific biological processes in more detail in *S. cerevisiae*, we grouped enhancing and suppressing genes into known protein complexes. Thus, the top 5% enhancers and suppressors were analysed using the GO Macromolecular Complex Slim Map analysis tool on SGD. Protein complexes were deemed significant by hypergeometric distribution, and statistically significant complexes returned from the analysis are shown in Figure 4.12. Complexes containing strong enhancers of *smt3* have roles in DNA replication and repair such as the Mre11 complex, the Slx1-Slx4 complex, RecQ helicase Topo III complex, and the Holliday Junction resolvase complex (Figure 4.12). Other significant hits including mostly enhancing genes were within the nuclear pore complex, histone deacetylase complex, and within the proteasome core and regulatory particle (Figure 4.12). Similar analysis of the suppressor genes revealed that 3 complexes in RNA catabolism were significantly enriched. These were the Ski complex, the exosome, and the cytoplasmic mRNA processing body (Figure 4.12). Furthermore, many biological complexes involved in protein translation were also enriched within the suppressors, such as translation initiation (multi-eIF complex). Furthermore, suppressors and enhancers (30 and 10 respectively) were identified within the ribosome subunits (Figure 4.12). With regard to the mRNA catabolism and protein translation, it is possible that the basis of suppression is due to increased Smt3 expression levels, rather than a direct involvement with these processes.

Interestingly, one of the complexes which was significant in our Macromolecular Complex analysis was the Arp2/3 complex (Figure 4.12), a seven subunit essential complex involved in the formation of branched filamentous actin (F actin) (Rouiller *et al.*, 2008). In *S. cerevisiae*, this complex functions in the movement of cortical actin patches (Winter *et al.*, 1997), which form the membrane invaginations required for endocytosis (Warren *et al.*, 2002), which was enriched in my Biological Process analysis (Figure 4.12). Significantly, DAmP allele mutants of the two main components of this complex, Arp2 and Arp3, were very significant suppressors
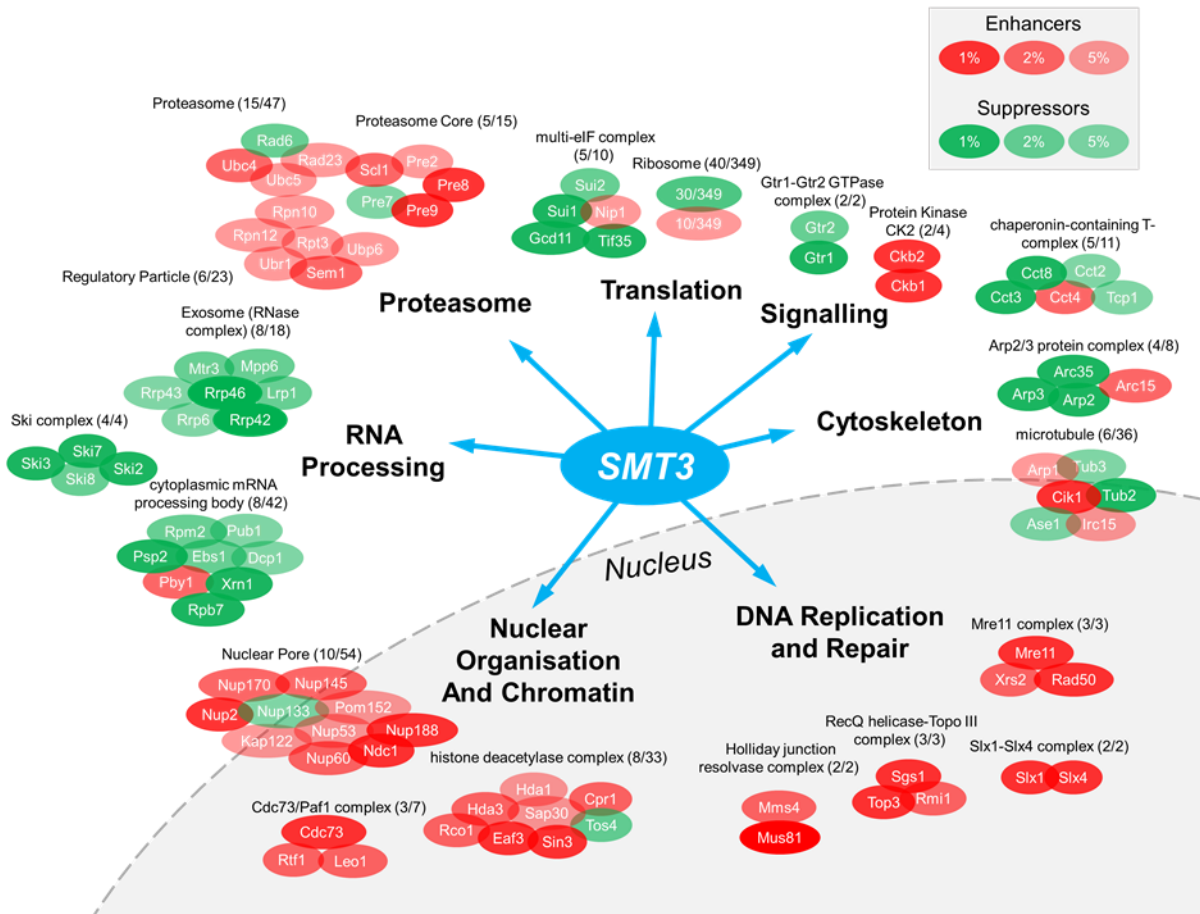
Figure 4.12: *SMT3* **genetic interactors within complexes in** *S. cerevisiae.* **Top 5% of** enhancing and top 5% of supressing genes from our SGA were analysed using GO Macromolecular Complex Slim Map. This analysis places the genes listed into functioning complexes within *S. cerevisiae*. Significance is calculated by comparing the number of successes in the gene list to the number present on the genome. All complexes shown here are significant (p≤0.05). Red circles represent enhancing interactors, while green circles represent supressing interactions. Interactors are coloured indicating low (top 5%), medium (top 2%) and high (1%) strength, as indicated on the key. The number of hits/number of genes within the complex are indicated, and complexes are grouped according to cellular process and by nuclear or cytoplasmic function.

in my screen. *arp2-DAmP* and *arp3-DAmP* had the top 6th and 7th GIS scores respectively, and *arc35-DAmP*, encoding another Arp2/3 complex component Arc35, was the 24th top hit.

Interestingly, *arc15-DAmP*, encoding another the Arc15 subunit of the complex Arc15, was actually an enhancer in my screen. In addition to the Arp2/3 complex, other cytoskeleton associated genes were found to be significant suppressors in the screen. In particular, *tub2-DAmP* was one of the most significant suppressors in our screen (4th top hit). Furthermore, the mammalian homologs of Arp2, Arp3 and Arc35 have been identified sumoylation targets in high throughput screens, which suggests that the regulation of the cytoskeleton by SUMO is conserved in higher eukaryotes (Table 4.2).

S. cerevisiae	Smt3 Conjugate?	*H. sapiens*	SUMO Conjugate?
Arp2	Not detected	ACTR2	SUMO-2 (Vigodner *et al.*, 2013) (Wen *et al.*, 2014) SUMO-3 (Lamoliatte *et al.*, 2014)
Arp3	Not detected	ACTR3	SUMO-2 and SUMO-3 (Wen *et al.*, 2014)
		ACTR3B	-
Arc35	Yes (Makhnevych *et al.*, 2009) (Wohlschlegel *et al.*, 2004)	ARPC2	SUMO-1 (Kristensen *et al.*, 2012) SUMO-2 (Wen *et al.*, 2014)

Table 4.1: Suppressors of the *smt3* strain are sumoylated in *S. cerevisiae* and *H. sapiens*. Evidence of genetic interaction with *SMT3* and physical interaction with Smt3 for *S. cerevisiae* is shown, and any evidence of physical SUMO interactions with mammalian Arp2/3 complex counterparts shown.

A surprisingly high number of suppressors from our SGA analysis are from within complexes involved in the cytoskeleton (Figure 4.12). Taken with other high throughput proteomic data linking these proteins with the sumoylation system, and the number of positive interaction within our screen, we hypothesised a major role of Smt3 in *S. cerevisiae*, and perhaps in higher eukaryotes, could be the regulation of the actin and tubulin cytoskeleton. Other than the published physical interaction data (Table 4.2), there is no other data published on the role of sumoylation and the cytoskeleton. Thus, these data have revealed a novel link between SUMO and conserved processes.

4.3 Discussion

Many studies have implicated Smt3 in diverse roles such as DNA replication and repair and cell cycle regulation. However large scale screens have shown Smt3 modifies many other cellular targets but the cellular implications of these are unknown, and genetic interaction screens have also shown many pathways that require Smt3 function for viable growth. However, very little is known about which pathways are supressed by loss of Smt3 function. Therefore, in the body of work we aimed to identify which pathways are aberrantly regulated when Smt3 function is lost.

4.3.1 Analysis of the Costanzo et al. (2010) Dataset

Having identified both suppressors and enhancers of the growth of the *smt3-DAmP* strain at 30°C, we wanted to compare and validate the hits from the SGA against data from a genome wide screen by Costanzo and colleagues (2010) that also used the *smt3-DAmP* allele (Costanzo *et al.*, 2010). 1712 different query strains, including the *smt3-DAmP*, were screened against 4293 non-essential deletion strains, giving rise to ~5.4 million gene pairs (Costanzo *et al.*, 2010). Most likely due to the high number of genetic interactions produced in this screen, no quantitative fitness measures were provided. Therefore, 31 enhancing genetic interactions and 4 suppressing genetic interactions for the *smt3-DAmP* allele were reported on the interaction database BIOGRID (Chatr-Aryamontri *et al.*, 2015). These genes were compared against the top 1% and 5% of enhancers (Figure 4.13 A) and top 1% and 5% of suppressors (Figure 4.13 B) from our dataset. Interestingly, although the two screens were performed using an *smt3-DAmP* hypomorphic allele, a surprisingly small overlap between the two groups of genes were detected (Figure 4.13). When comparing the top 5% of enhancers from our screen with the Costanzo *et al.* (2010) dataset, 11 genes appeared unique to the Costanzo *et al.* (2010) dataset. These 11 genes are shown in Table 4.3.

One of these genes, *TIR3,* can be seen to have an enhancing interaction on the final plate images; however, the GIS score for *TIR3* is missing from our fitness data, even before the data was trimmed for sterile genes. We can only hypothesise that the gene is missing from the programing used to analyse the GIS scores. Two other genes, *MRN1* and *RTT109*, were actually significant enhancers in our screen with a p value ≤0.05, but these genes were outside the cut off of the top 5% enhancers used in our analysis. However, *BPT1*, *FSP1*, *HSP12*, *SOK2*, *UPS1*, *YJL147C* and *YJR120W* had GIS scores placing them as non-interactors, while E*CM25* was actually close to being a significant suppressor (Table 4.3).
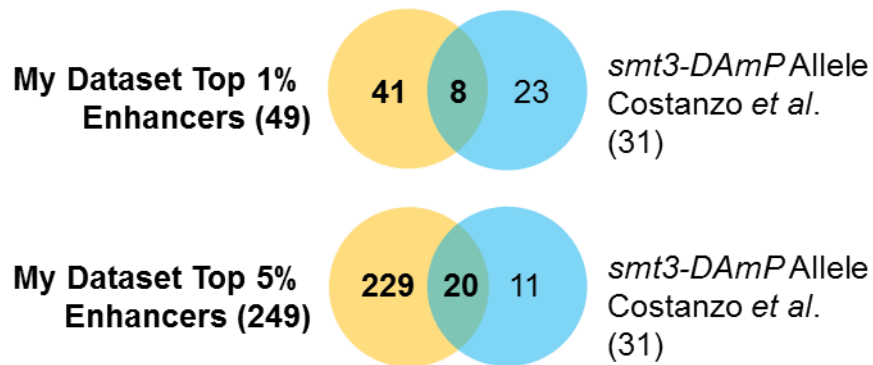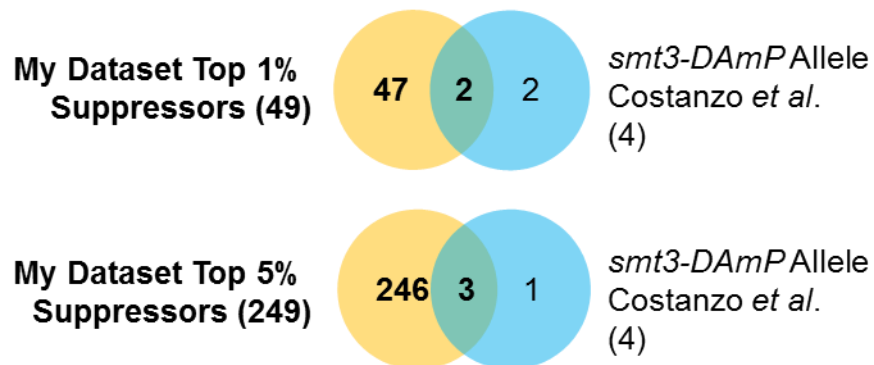
Figure 4.13: Venn diagrams illustrating the overlap between enhancing and supressing interactions of *smt3* **from my SGA dataset and the SGA dataset from Costanzo** *et al.* **(2010).** A) The top 1% and 5% (49 and 249 genes respectively) of enhancing interactions from my dataset (shown in yellow) were compared with the 31 genetic enhancers from the Costanzo *et al.* (2010) dataset (shown in blue). B) The top 1% and 5% (49 and 249 genes respectively) of suppressing interactions from my dataset (shown in yellow) were compared with the 4 genetic suppressors from the Costanzo *et al.* (2010) dataset (shown in blue).

Unique Costanzo *et al.* (2009) Enhancing Genes	Rank within my 4998 genes from GIS score	Within lowest % of GIS scores	Enhancer or Suppressor	P value
BPT1	1699	34.0	N/A	0.404
ECM25	4561	91.3	Very Weak Suppressor	0.055
FPS1	3056	61.1	N/A	0.541
HPS12	1941	38.8	N/A	0.526
MRN1	366	7.3	Weak Enhancer	0.00234
RTT109	278	5.6	Enhancer	1.45E-07
SOK2	1190	23.8	N/A	0.168
TIR3	-		-	-
UPS1	4249	86.9	N/A	0.202
YJL147C	3893	77.9	N/A	0.333
YJR120W	3958	79.2	N/A	0.0966

Table 4.2: Enhancing genetic interactions from my dataset and Costanzo *et al.* (2010) were compared for shared genes. The genes shown in the table are the 11 genes that were unique to the Costanzo *et al.* (2010) dataset. The GIS scores from my dataset were ranked in ascending order with the lowest GIS scores and therefore most enhancing genes first, and then ranking of the 11 enhancing genes in my data shown. The position of the gene within the lowest % of interaction scores is also shown, to illustrate where the gene lies in comparison to my 5% cut off. If the gene is significant or narrowly significant, I have labelled as enhancer or suppressor (shown in green or yellow respectively), and provided the p value for the gene.

As previously mentioned, our screen and the Costanzo *et al.* (2010) screen used the same DAmP hypomorphic allele of *smt3*, and the same non-essential deletion array in the S288C strain background. Furthermore, the same multiplicative model of genetic interaction was used to identify hits. We were therefore surprised by the number of non-overlapping genes, shown in Table 4.3. There are a few differences between the two screens, which may help elucidate the differences between these screens. For example, the Costanzo *et al.* (2010) screen used more stringent noise removal that what was used in our screen, such as compensating for the layout of the array. However, no such noise removal has been completed on my dataset. However, another important difference is the lack of essential genes in the Costanzo *et al.* (2010) deletion array. Within our top 5% of enhancing genes, 44 out of 249 (18.5%) are essential DAmP alleles. Indeed, this is similar to the ratio of essential alleles in the array, where 878 out of the 4999 genes screened are essential DAmP alleles (17.6%). Furthermore, there is an enrichment for essential genes when the top 1% of enhancing genes are considered, where 25 out of 49 (51.0%) are essential DAmP alleles. This could suggest that the presence of DAmP alleles within our enhancers and suppressors could mean that although the non-overlapping genes outlined in Table 4.3 appear not be genetic interactors in our study, they have just now fell below detection in our 1% and 5% cut offs. Thus, we further investigated the non-overlapping genes (Table 4.3). Costanzo *et al.* (2010) reported 4 genes, *AIR2*, *XRN1*, *MSN4* and *DEG1* as suppressors for the *smt3*. Within our top 1% of suppressors, two hits from Costanzo *et al.* (2010), *XRN1* and *DEG1,* were shared, and within our top 5% of suppressors, the 3 genes *AIR2*, *XRN1* and *DEG1* were shared (Figure 4.12 B). Curiously, the

transcription factor *MSN4* was actually an enhancer within our SGA, again highlighting the variations between the two independent experiments. It is interesting to note that *AIR2*, *DEG1* and *XRN1* are involved in RNA catabolism consistent with the model that these mutants could be recusing the *smt3-DAmP* phenotype by increasing *SMT3* mRNA transcripts.

4.3.2 Analysis of the Makhnevych et al. (2009) Dataset

Another global screen was performed for *SMT3* genetic interaction by Makhnevych *et al.* (2009). This screen used a strain carrying a temperature sensitive (ts) allele of *SMT3*, *smt3-331*, which blocks growth above the non-permissive temperature. The *smt3-311* strain was constructed in a paper to find cells which arrested with unseparated sister chromosomes at the restrictive temperature (37°C) (Biggins *et al.*, 2001), which is likely to change any identified genetic interactions. The *smt3-331* strain was used as a query against the *S. cerevisiae* deletion collection of non-essential genes, and 787 ts allele variants of essential genes. There are 500 unique genes within the array, as some essential genes have multiple ts mutants within the array (Li *et al.*, 2011). This is rationalised that the inclusion of multiple mutants of the same gene in the array increases the likelihood that all aspects of the genes biological function are being screened effectively, as individual ts mutations of the same gene can affect distinct and separable biological functions (Schaerer-Brodbeck and Riezman, 2003). Thus, this study gained more genome coverage compared to the Costanzo *et al.* (2010) screen, as essential as well as non-essential genes were analysed. However, during the SGA process, only synthetic lethal or severely enhancing genetic interactions were considered and analysed (Makhnevych *et al.*, 2009). It appears that even if positive genetic interactions were present within this SGA, these were simply discounted during the analysis. Further to this, the data does not provide quantitative genetic interactions. Thus, our dataset provides the novel aspect of both suppressing genetic interactions, as well as quantitative analysis of genetic interaction.

The overlap between the enhancers from the Costanzo *et al.* (2010) dataset, the Makhnevych *et al.* (2009) dataset and our top 1% and 5% enhancer datasets are illustrated in Figure 4.14 and in Table 4.4. In a manner similar to the analysis of the Costanzo *et al.* (2010) dataset, there was a degree of overlap between the Makhnevych *et al.* (2009) data and our dataset, but less of an overlap between the Makhnevych *et al.* (2009) dataset and the Costanzo *et al.* (2010) dataset (Figure 4.14). Furthermore, there is a large pool of genetic enhancers which appear to be unique to each dataset (Figure 4.14). However, between the 3 different screens, 13 genes were shared (Figure 4.14). A high proportion of those genes (7 of the 13, 53.8%) were within my top 1% of enhancers, (Table 4.4). This suggests there is a good correlation

Costanzo *et al.* (2010) and My Data (7)		All 3 Screens (13)		Makhnevych *et al.* (2009) and My Data (40)	
ARP1	Actin-Related Protein	ASF1	Anti-Silencing Function	ARF1	ADP-Ribosylation Factor
CSM3	Chromosome Segregation in Meiosis	CAC2	Chromatin Assembly Complex	BRE1	BREfeldin A sensitivity
FKS1	FK506 Sensitivity	CKB1	Casein Kinase Beta subunit	BRE2	BREfeldin A sensitivity
HIR3	HIstone Regulation	CTF4	Chromosome Transmission Fidelity	CDC73	Cell Division Cycle
MOG1	Multicopy suppressor Of ts Gsp1	NUP2	NUclear Pore	CKB2	Casein Kinase Beta' subunit
NEM1	Nuclear Envelope Morphology	RAD51	RADiation sensitive	CRG1	Cantharidin Resistance Gene
NUP188	NUclear Pore	RCO1	-	EAF3	Esa1p-Associated Factor
		RRM3	rDNA Recombination Mutation	ELG1	Enhanced Level of Genomic instability
		SGS1	Slow Growth Suppressor	ENP1	Essential Nuclear Protein
		SLX1	Synthetic Lethal of unknown (X) function	ESC2	Establishment of Silent Chromatin
		SLX4	Synthetic Lethal of unknown (X) function	HDA1	Histone DeAcetylase
		SRS2	Suppressor of Rad Six	HDA3	Histone DeAcetylase
		VID22	Vacuolar Import and Degradation	KAP122	KAryoPherin
				MMS4	Methyl MethaneSulfonate sensitivity
				MUS81	MMS and UV Sensitive
				NFI2 (SIZ2)	Neck Filament Interacting
				NHP10	Non-Histone Protein
				NUP170	NUclear Pore
				RCY1	ReCYcling
				RMI1	RecQ Mediated genome Instability
				RPN12	Regulatory Particle Non-ATPase
				RSM28	Ribosomal Small subunit of Mitochondria
				RTF1	Restores TBP Function
				RTT106	Regulator of Ty1 Transposition
				SDC1	Set1c, homologue of Dpy30 from C.elegans
				SET2	SET domain-containing
				SIN3	Switch Independent
				SLX8	Synthetic Lethal of unknown (X) function
				SPT21	SuPpressor of Ty
				SRO7	Suppressor of rho3
				SWD3	Set1c, WD40 repeat protein
				THR1	THReonine requiring
				TOP3	TOPoisomerase
				UBC4	UBiquitin-Conjugating
				UBP6	UBiquitin-specific Protease
				ULS1	Ubiquitin Ligase for SUMO conjugates
				VPS71	Vacuolar Protein Sorting
				Dubious	Overlaps with CAC2
				Dubious	Overlaps with TOP3
				Dubious	Overlaps with MMS4

Table 4.3: Lists of enhancing genes which are shared between three *SMT3* interaction screens; my dataset, Costanzo *et al.* (2010) and Makhnevych *et al.* (2009). Genes within my top 1% of enhancers are labelled blue, genes within my top 2% of enhancers are labelled green, and genes within my top 5% of enhancers are labelled yellow.
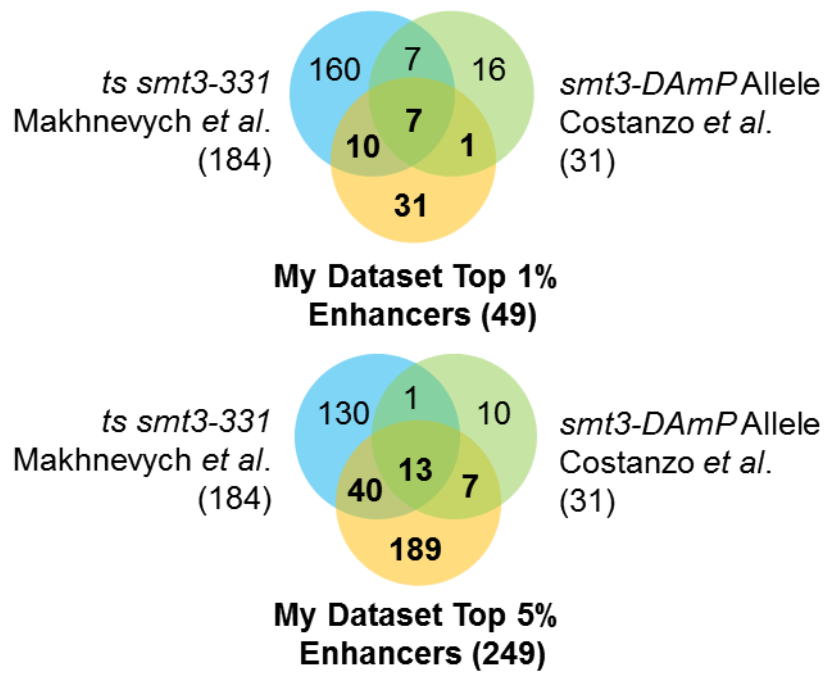
Figure 4.14: Venn diagrams illustrating the overlap between genes showing enhancing genetic interaction with _SMT3_ from our dataset, the Costanzo _et al._ (2010) dataset, and the Makhnevych _et al._ (2009) dataset. The top 1% and 5% (49 and 249 genes respectively) of enhancing interactions from my dataset (shown in yellow) were compared with the 31 genetic enhancers from the Costanzo _et al._ (2010) dataset (shown in green) and the 184 genetic enhancers from the Makhnevych _et al._ (2009) dataset (shown in blue).

between shared interactions between the screens, and the severity of the GIS score in my interaction data. Thus, it provides some confidence in the quantitative GIS scores provided in our dataset. Furthermore, it suggests that the strongest genetic interactions uncovered in our dataset are more likely to be the interactions which are able to be replicated, as shown by the enhancing interactions.

4.3.3 The Relevance of Loss of Function Allele in SGA

Similar to our SGA analysis, the Makhnevych *et al.* (2009) array also included essential genes in the dataset. It was postulated that the lack of shared genes between the three datasets was at least partly due the lack of essential genes in Costanzo *et al.* (2010) study. Indeed, in the Makhnevych *et al.* (2009) dataset, 27 out of 184 enhancers were ts alleles, and of our top 5% of enhancers, 46 of 249 genes were essential DAmP alleles. However, within the 40 genes shared between our top 5% of enhancers and those identified by Makhnevych *et al.* (2009) only one gene, *ENP1*, was essential (Fig 4.14, Table 4.5).

This result was surprising, as we had perhaps expected a higher proportion of the shared enhancing interactions to be essential genes. The basis for this is not clear but could be due to a number of reasons. Perhaps the *smt3-DAmP* allele and the *smt3-331* allele strains are dysfunctional in distinct biological processes, thus the two SGAs are probing these differing biological roles of Smt3. Furthermore, perhaps the use of either the ts allele or DAmP allele library also effects the biological process highlighted in the SGA. Interestingly, neither the ts allele nor DAmP allele library is complete, suggesting a lack of overlap of available genes. Indeed, of the 1156 essential genes in the *S. cerevisiae* genome (Giaever *et al.*, 2002), 500 unique genes are available in the collection of 787 ts allele mutants (Li *et al.*, 2011), and 878 of the essential genes are available as DAmP alleles (Breslow *et al.*, 2008). 98 of the 500 ts genes are unavailable as DAmP strains, while 476 of the essential genes are only available as DAmP strains (Figure 4.15).
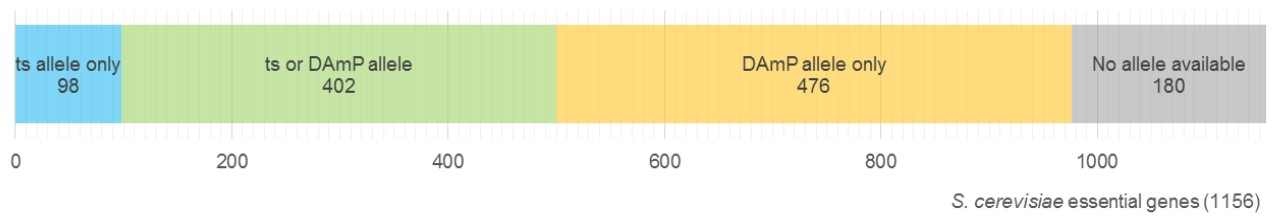
Figure 4.15: Illustration of loss of function alleles available for the 1156 essential *S. cerevisiae* genes.

Makhnevych *et al.* (2009). essential Genes (27)		My dataset essential Genes (46)	
ts only	**ts and DAmP**	**DAmP only**	**ts and DAmP**
ACT1	DBF4	ATM1	APC2
COG3	POL3	AVO1	ARC15
CRM1	CDC48	CAB1	CCT4
CTF8	CDC36	ESF2	CMD1
DBF2	CDC7	GPI15	COF1
MMS21	ABD1	HCA4	**ENP1**
STU2	CDC19	IQG1	GCD10
SWC4	BRN1	LCD1	GPI13
UBC9	**ENP1**	NIP1	NDC1
	DAN2	NOC4	NUP145
	CDC6	OST2	PHS1
	CDC8	PRE8	PRE2
	ULP1	RIB3	PRP4
	CDC11	RPB8	RET3
	CDC20	RPC31	RPN12
	BET2	RPL33A	RPT3
	ARP4	RPS31	SAD1
	CDC37	SAR1	SEC12
		SCL1	SLN1
		YJL032W	SPC3
		YLR198C	TAF10
		YLR317W	TAF13
		YPL238C	TFB3

Table 4.4: Essential enhancers of the Makhnevych *et al*,. (2009) *smt3-331* ts allele from the ts allele array (27 genes) (Tong and Boone, 2006), and my *smt3-DAmP* allele dataset from the DAmP allele array (46 genes). Genes are shown as ts only, DAmP only or available as both alleles.

Thus, 402 essential genes were in both libraries as ts and DAmP alleles. Hence, it was hypothesised that the lack of overlap of essential genes between our dataset and the Makhnevych *et al.* dataset could be attributed to the differential representation of essential genes between the screens. Indeed, this appeared to be partially true when the essential enhancing genes from the two screens were analysed (Table 4.5). 9/27 of the essential genes in the Makhnevych *et al.* (2009) enhancers were only available as ts alleles, and 23/46 of the enhancers from my dataset were only available as DAmP alleles (Table 4.5). Thus, taken together these data demonstrate that the choice of hypomorphic allele used as a query in genetic screens may have a large impact upon the genetic interactions that are produced. During this process we identified that although sumoylation has been implicated in a wide range of biological processes, the information becomes surprisingly difficult to then pinpoint specific protein complexes to choose for further analysis. Through this screening process and data analysis, we have potentially highlighted some key strategies in the handling of SGA data to gain the most informative insight into a complicated system, such as sumoylation. Firstly, the use of positive and negative interaction data provided a powerful technique in pinpointing important protein complexes within large biological process terms. Secondly, the second analysis has highlighted the importance of screening multiple loss of function alleles in both queries and libraries. Thus, in the case of complex genetic networks, it would be suggested that both the DAmP and ts allele libraries are combined to create an even more comprehensive and powerful screening library, which will make the best use of the current resources available. Lastly, again for complex genetic networks such as sumoylation, these analyses also highlight the importance of quantitative measurements of genetic interaction, as this aids in the identification of the most crucial protein complexes, and even protein components within that complex, within what would otherwise be a mass of data. In one final point, SGA can be utilised to answer more specific questions by the use of point mutants. This was used recently for sumoylation, where the biological role of Smt3 chain formation was investigated using a mutant form of SMT3 lacking all lysine's (*smt3-allR*) (Srikumar *et al.*, 2013).

In this chapter, we have characterised a loss of function allele of *SMT3*, which has reduced Smt3 protein levels. We have characterised that the loss of Smt3 leads to slow growth and extremely slow growth in cold temperatures, as well as mitotic defects. This strain was then used as a query in SGA analysis to identify novel biological functions of sumoylation in the model organism *S. cerevisiae*. Excitingly, we have uncovered that the slow growth associated with the loss of Smt3 function can be rescued by alleles which would dysregulate both the actin and tubulin cytoskeleton. Therefore, in the next chapter we confirmed that these hits are positive, and characterise this novel process.

Chapter Five: SUMO Regulates the Actin and Tubulin Cytoskeleton in *S. cerevisiae*

5.1 Introduction

Sumoylation has roles in many cellular processes, and sumoylated targets in many diverse cellular pathways have been identified (Makhnevych *et al.*, 2009). Interestingly, sumoylation is essential in *S. cerevisiae*, but the underlying basis of this essentiality is unknown. As described in the previous chapter, a high throughput screen revealed that the slow growth phenotype of a hypomorphic *smt3* mutant can be rescued by disruption of the actin and tubulin cytoskeleton, namely components of the Arp2/3 complex, and β-tubulin.

The Arp2/3 complex binds within existing actin filaments, and the actin related subunits Arp2 and Arp3 promote the nucleation of another F actin filament from the mother filament, creating an actin branch (Kim *et al.*, 2006), while Arc35 is thought to provide a structural role within the Arp2/3 complex (Winter *et al.,* 1999). In *S. cerevisiae*, the Arp2/3-dependant branched actin forms motile actin patches which are important for endocytosis and cell division (Kim *et al.*, 2006). Another cytoskeletal component tubulin forms polymers containing an alpha (α) (encoded by *TUB1, TUB3* in *S. cerevisiae*) and beta (β) (encoded by *TUB2* in *S. cerevisiae*) tubulin monomer (Schatz *et al.*, 1988; Huffaker *et al.*, 1988). Due to the fundamental cellular roles of microtubules and actin branching, both tubulin and the Arp2/3 complex are conserved in eukaryotes. Interestingly, however, there are very little data linking tubulin and the Arp2/3 complex. In *S. cerevisiae*, strains encoding a ts variant of Arc35 (*arc35-1*) have a cell cycle arrest phenotype where at the non-permissive temperature the cells block as large budded cells and short mitotic spindles, and well as displaying defects in endocytosis and F actin dynamics (Schaerer-Brodbeck and Riezman, 2000). Interestingly, over expression of the gamma (λ) tubulin monomer Tub4, found at microtubule organising centres to nucleate microtubules (Gombos *et al.*, 2013), in the *arc35-1* mutant suppressed the cell cycle arrest phenotype, but did not rescue the defects in endocytosis (Schaerer-Brodbeck and Riezman, 2003). Furthermore, overexpression of the casein kinase II subunit Ckb2 also rescued the tubulin defects of *arc35-1*, but not the F actin and endocytosis defects (Schaerer-Brodbeck and Riezman, 2003), and this gene was a very strong enhancer in our screen (ranked 3/4999, see Appendix A). These results suggest there is a cell cycle-specific role for Arc35. In addition to yeast studies, work in *A. thalania* revealed that the homolog of Arc35, ARPC2, contained a microtubule binding site, suggesting a connection to microtubule function (Havelkova *et al.*, 2015). Interestingly, high throughput proteomic data revealed that the Arp2/3 complex components Arc35, Arc40, and the tubulin monomers Tub1 and Tub2 are each sumoylated (Makhnevych *et al.*, 2009). However, despite these links, the role of sumoylation in the regulation of both the actin and tubulin cytoskeleton has not been explored at great depth in

the literature. Our genetic interaction data thus provide an exciting hypothesis that Arp2/3 and tubulin could operate within the same pathway to rescue the growth defects associated with the *smt3* mutant. Furthermore, both tubulin and the Arp2/3 complex are essential in *S. cerevisiae*, suggesting that defects in the functions of these conserved proteins could underpin the essential role of SUMO in budding yeast. Therefore, the aims of this chapter are to investigate whether F actin or tubulin dynamics are aberrant in the *smt3* mutant, and to study the relationships between these vital cellular processes, and suppression of the *smt3* mutant phenotypes.

5.2 Results

5.2.1 Mutations in Arp2/3 Complex Components and Tubulin Suppress the Slow Growth Phenotype in smt3 *Mutant Cells*

In our genetic screen we identified mutants encoding 3 Arp2/3 complex components, *ARP2*, *ARP3* and *ARC35,* as genetic suppressors of the *smt3* slow growth phenotype (Chapter 4, Figure 4.12). We also found that mutation of the β-tubulin encoding gene, *TUB2*, acts as a genetic suppressor of the *smt3* allele. As genes encoding the Arp2/3 complex components and β-tubulin are essential, these genes were present in the DAmP collection in the library array. Hypomorphic DAmP alleles of the *ARP2*, *ARP3, ARC35,* and *TUB2* genes, will be referred to as *arp2, arp3, arc35,* and *tub2* respectively for the remainder of this study.

Before further analysis, we first checked that suppression of the *smt3* growth defect by the DAmP alleles of *ARP2*, *ARP3*, *ARC35* and *TUB2* genes were not artefacts of the SGA process by assessing the growth of the *arp2 smt3*, *arp3 smt3, arc35 smt3* and *tub2 smt3* double mutants compared to the *smt3* single *mutant* (Figure 5.1). This data confirmed that the *arp2*, *arp3*, *arc35* and *tub2* mutant alleles all rescued the growth of the *smt3* strain at steady state conditions (Figure 5.1). Furthermore, the slow growth at 15°C was also rescued in all the double mutants (Figure 5.1). Thus, we were confident that the *arp2*, *arp3*, *arc35* and *tub2* alleles were suppressing the growth defects associated with the *smt3* mutant.

5.2.2 F actin Morphology is Aberrant in the smt3 *Mutant, and is Rescued by Both* arp3 *and* tub2 *Alleles*

Data from our high throughput genetic screen highlighted the possibility that Smt3 normally regulates the actin cytoskeleton in *S. cerevisiae*. Therefore, to gain insight into the relationships between the Arp2/3 and Tub2 genetic suppression of the *smt3* mutant, it was important to first test if loss of function of Smt3 led to aberrant F actin function.

Figure 5.1: Hypomorphic alleles of genes encoding Arp2/3 complex components and β-tubulin rescue the slow growth defect associated with the *smt3* mutant. 5 fold serial dilutions of mid-log phase growing cells were spotted onto YPD agar plates and incubated at the indicated temperatures for 2 days unless otherwise stated. The strains used were wild type (BY4741), *smt3* (CL100), *arp2* (CL340), *arp2 smt3* (CL237), *arp3* (CL341), *arp3 smt3* (CL238), *arc35* (CL628), *arc35 smt3* (CL239) and *tub2* (CL480), and *tub2 smt3* (CL486) strains shown.
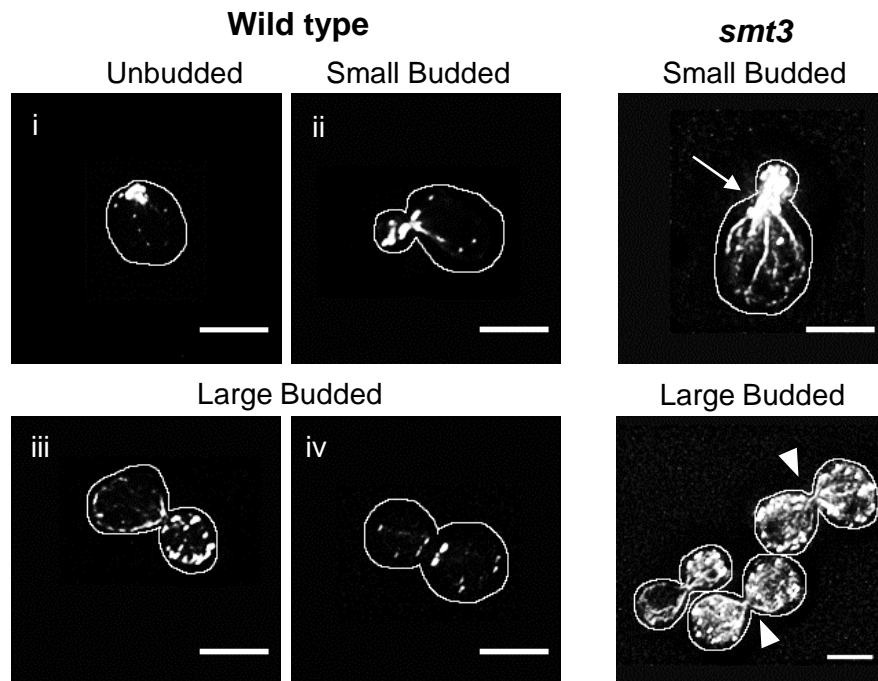
Figure 5.2: *smt3* **mutant cells display increased F actin staining, and actin morphology defects.** Mid-log phase growing wild type (BY4741) and *smt3* CL100) cells were fixed, and F actin stained using Alexa-488® phalloidin. Images were deconvoluted by iterative algorithm. Representative images of unbudded, small budded and large budded wild type cells, and aberrant small budded and large budded *smt3* cells are shown. Panels indicate actin morphology as follows: i) actin patches at nascent bud site, ii) actin patches localised in daughter bud, with actin cables present at the bud neck oriented along mother and daughter cell axis, iii) same as ii) but in large budded cell, and iv) actin mislocalised across mother and daughter cell, with actin staining at the bud neck. Aberrant actin morphology in *smt3* mutant cells are indicated as follows: arrows indicate brightly stained actin structures; arrow heads indicate large budded cells with actin patches mislocalised across mother and daughter cells, but bud neck staining is absent. All images are from the same experiment, i.e. all strains collected and stained together, and exposure time equal between all images. Scale bar represents 50 pixels in the raw image.

Hence, wild type and *smt3* cells were fixed, and actin patches and cables stained with fluorescent phalloidin, a toxin which specifically binds to F actin and not actin monomers (Figure 5.2) (Cooper, 1987). The actin cytoskeleton is regulated in a cell cycle-dependant manner in *S. cerevisiae* (described in (Amberg, 1998)). Briefly, in wild type *S. cerevisiae* cells, actin patches become localised at the emerging bud site (Figure 5.2 i), then are asymmetrically localised in the daughter cell (Figure 5.2 ii and iii). Following mitosis, the patches lose polarity, and spread across both mother and daughter cells, followed rapidly by staining of the actin-myosin ring at the bud neck (Figure 5.2 iv). Cables are generally less visible than patches and require longer exposure times, but are observed to form along the cell cortex oriented along the mother to daughter cell axis, particularly near the region of the bud neck (Figure 5.2 ii and iii). Upon microscopic study, it was immediately apparent that the fluorescent staining of all actin structures, both patches and cables, appeared to be significantly increased in *smt3* mutant cells relative to wild type, irrespective of cell cycle stage (Figure 5.2). Indeed, quantification of fluorescence in unbudded cells from images collected with the same exposure revealed that the *smt3* mutant cells had a statistically significant 1.7-fold increase in signal compared to wild type cells (Figure 5.3 A). Furthermore, a particularly striking phenotype of the stained *smt3* cells that was observed was a significant increase in large budded cells with mislocalised patches and absent bud neck staining (Figure 5.3 B). This particular F actin morphology in large budded cells was uncommon in wild type cells (Figure 5.4 B), suggesting a specific cell cycle defect associated with loss of Smt3 activity. Hence taken together these results indicate that Smt3 normally regulated F actin dynamics.

Having established that F actin levels were generally increased in *smt3* mutant cells, and identified specific F actin defects in large budded *smt3* mutant cells, we next investigated the effects on F actin of the various DAmP alleles that suppress the *smt3* growth defect (Figure 5.4, Figure 5.5). Phalloidin staining of F actin in *arp3* cells revealed decreased F actin staining, and in particular less actin patch staining, relative to wild type (Figure 5.4). Importantly, F actin staining in *arp3 smt3* mutant cells was reduced compared to the *smt3* mutant (Figure 5.4). Interestingly, it was also observed that *tub2 smt3* mutant cells had reduced staining of F actin compared to the *smt3* single mutant (Figure 5.5). Actin morphology in large budded cells was quantified from *arp3* and *tub2* mutant cells, and the respective *smt3* double mutants, which revealed that the proportion of large budded cells with mislocalised actin patch staining and absent bud neck staining was significantly decreased in both *arp3 smt3* and *tub2 smt3* double mutant cells compared to *smt3* single mutant cells (Figure 5.6, p values shown). Taken together these results are consistent with a model were the presence of either *arp3* or *tub2* allele reduce F actin staining in cells with reduced levels of Smt3.
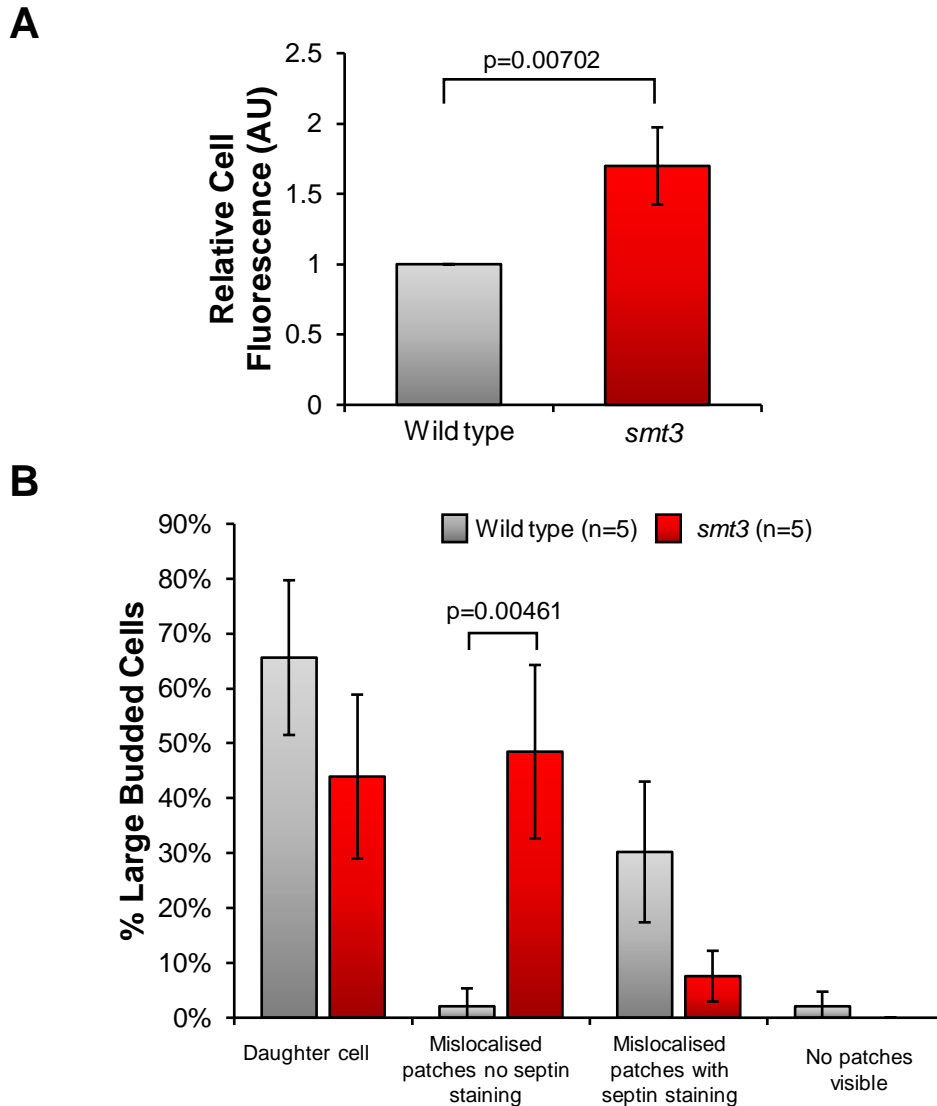
Figure 5.3: F actin staining of *smt3* mutant cells reveals increased F actin staining, and actin morphology defects. Mid-log phase growing wild type (BY4741) and *smt3* (CL100) cells were fixed, and F actin stained using Alexa-488® phalloidin. A) Total corrected cell fluorescence of Alexa-488® phalloidin stained wild type and *smt3* mutant unbudded cells was quantified, and the fold change fluorescence compared to wild type calculated. The mean fold change of fluorescence of 5 biological repeats is shown. Error bars indicate the standard deviation of the mean fold change from 5 biological replicates. The p value is derived from a 2 tailed unpaired student t test. Total number of unbudded cells quantified for wild type and *smt3* was 230 and 167 respectively. B) Quantification of F actin morphology of large budded wild type and *smt3* mutant cells. Cells were classed as large budded when the daughter to mother diameter ratio exceeded 0.75, as described previously (Huffaker *et al.*, 1988). Percentages were calculated from 96 and 132 large budded wild type and *smt3* cells respectively, from 5 biological replicates. Error bars indicate the standard deviation of the 5 biological replicates. The p value is derived from a 2 tailed unpaired student t test.
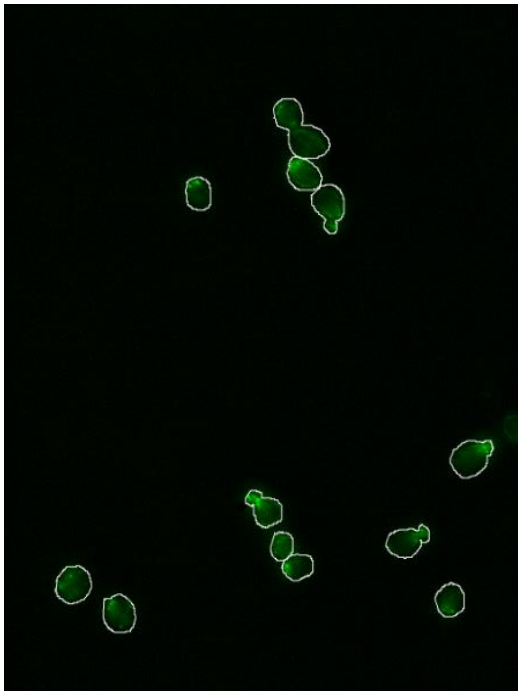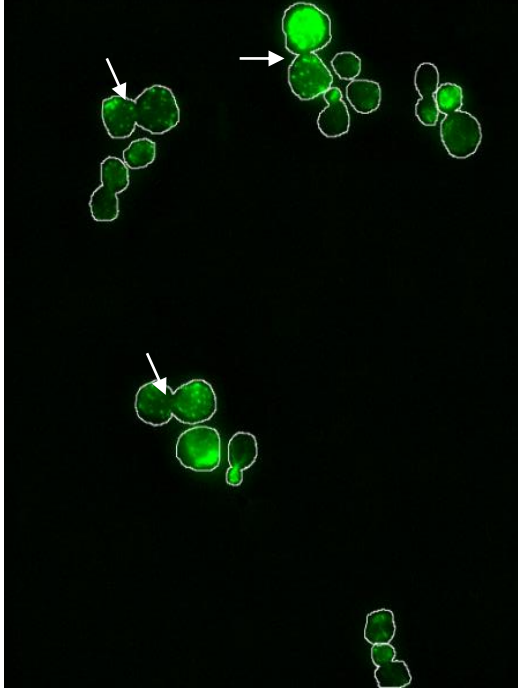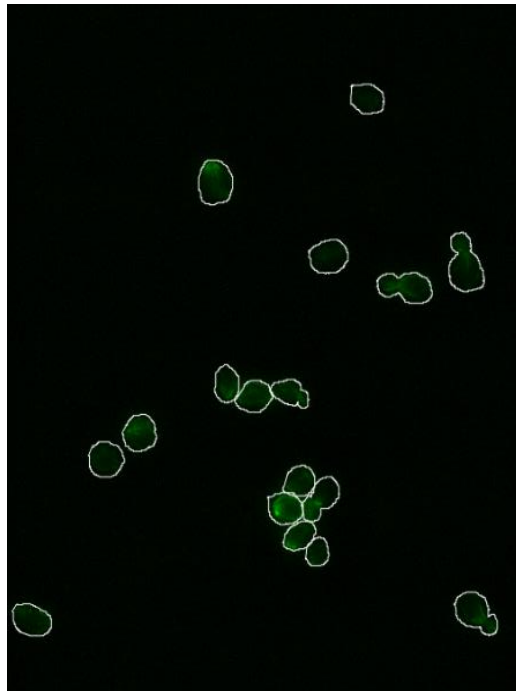
smt3

arp3 smt3
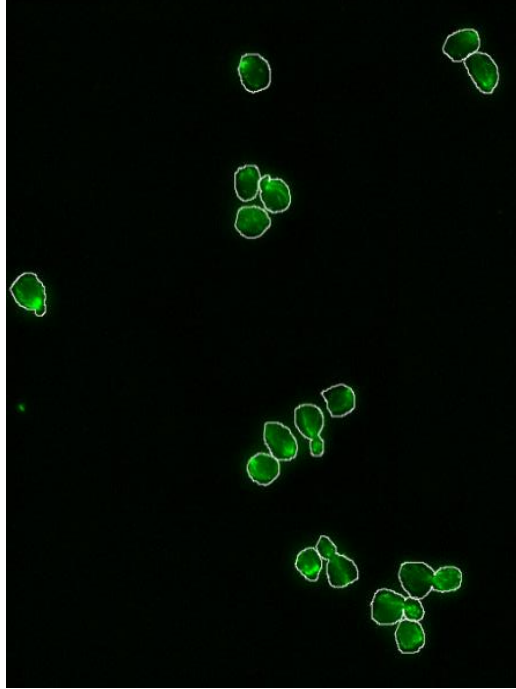
Wild type

arp3

Figure 5.4: Aberrant F actin morphology in *smt3* mutant cells is rescued by the *arp3-DAmP* allele. Mid-log phase growing wild type (BY4741), *smt3* (CL100), *arp3* (CL341) and *arp3 smt3* (CL238) cells were fixed and F actin stained using Alexa-488® phalloidin. Images are representative of 3 experiments. Arrows indicate cells where cortical actin patches are mislocalised and neck staining is absent. All images are from the same experiment, i.e. all strains collected and stained together, and exposure time equal between all images.
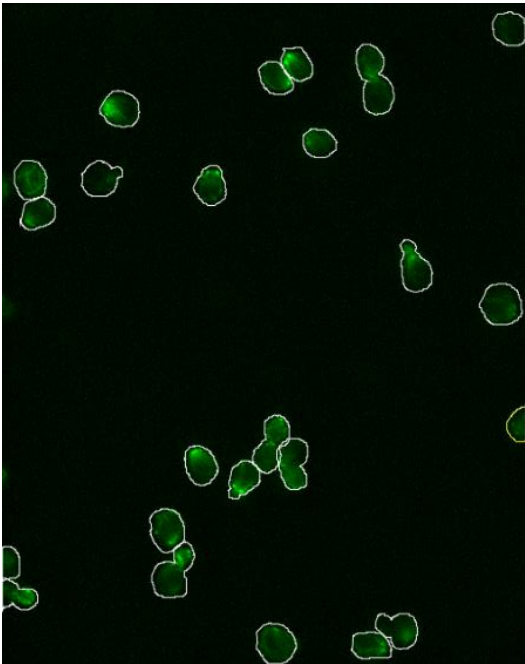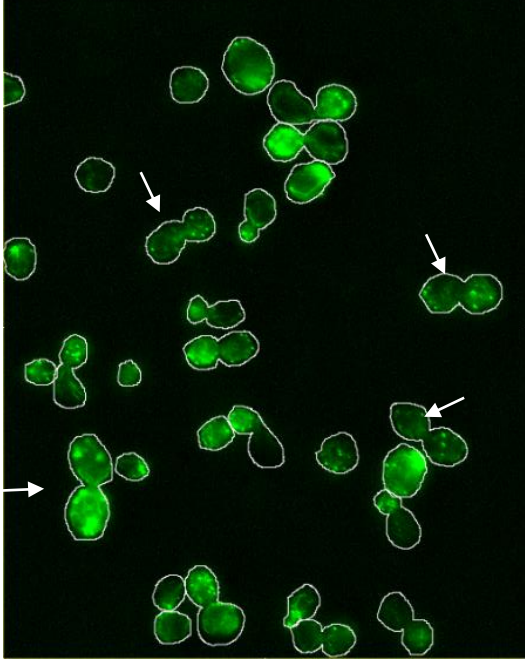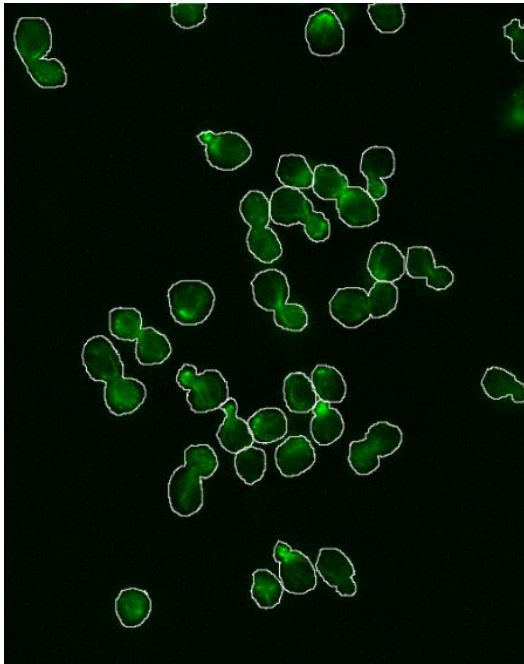
smt3

tub2 smt3
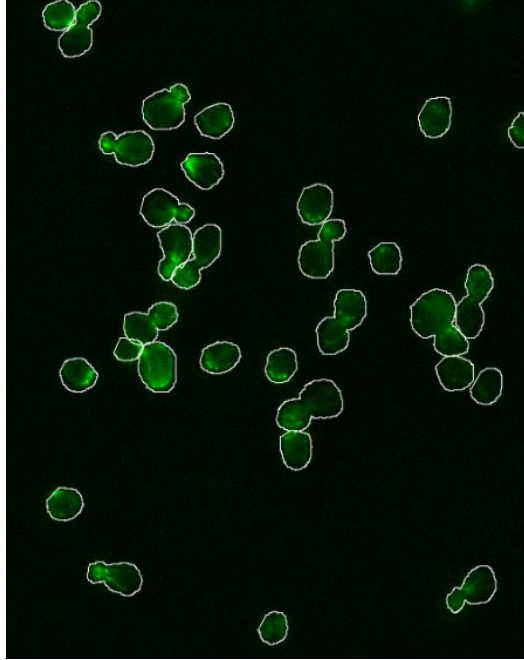
Wild type

tub2

Figure 5.5: Aberrant F actin morphology in *smt3* mutant cells is rescued by the *tub2-DAmP* allele. A) Mid-log phase growing wild type (BY4741), *smt3* (CL100), *tub2* (CL480), and *tub2 smt3* (CL486) cells were fixed and F actin stained using Alexa-488® phalloidin. Images are representative of 2 experiments. Arrows indicate cells where cortical actin patches are mislocalised and neck staining is absent. All images are from the same experiment, i.e. all strains collected and stained together, and exposure time equal between all images.

A
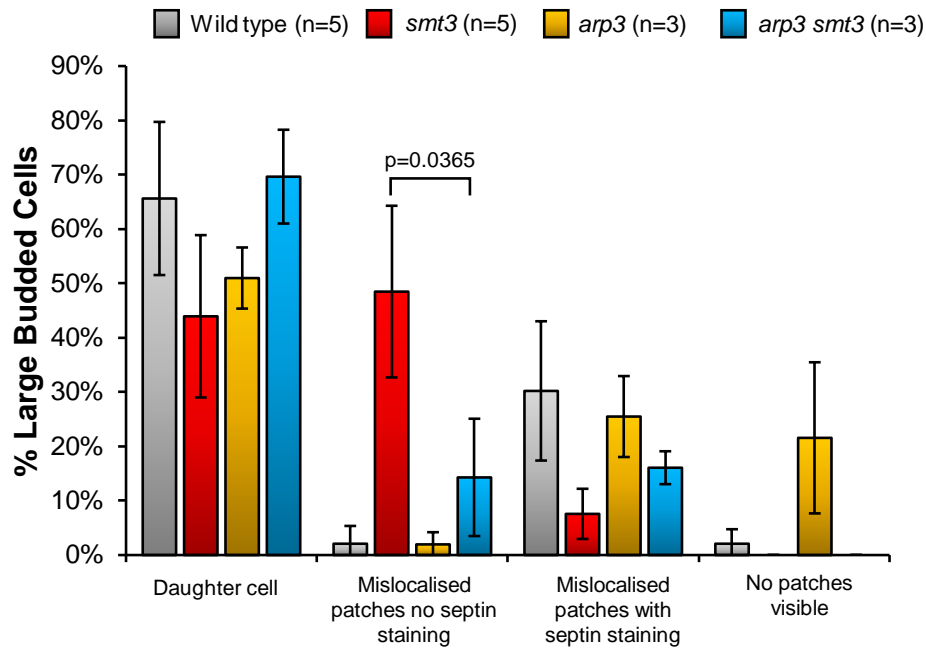
B
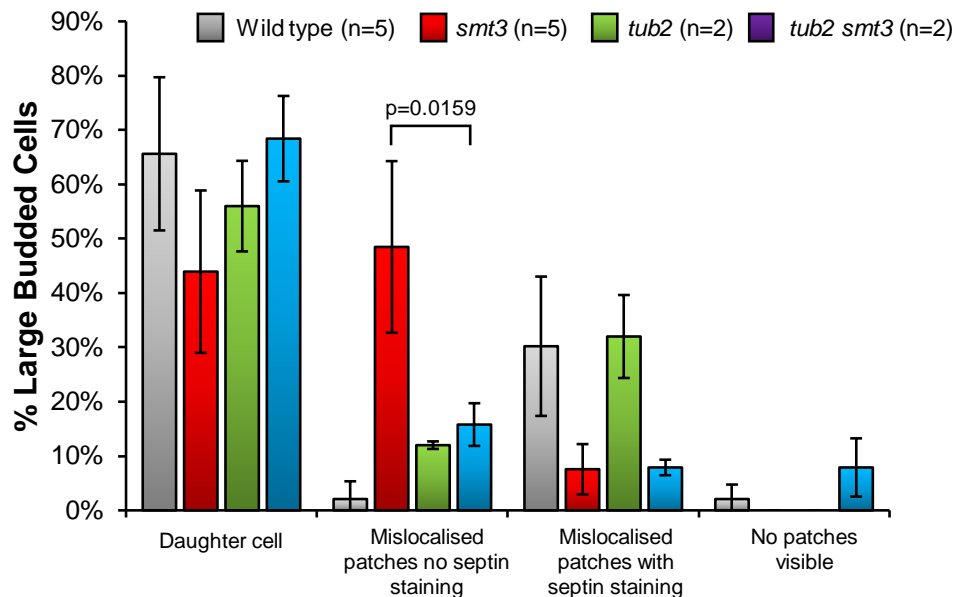
Figure 5.6: Quantification of the effects of *arp3* and *tub2* mutant alleles on the actin morphology defects associated with *smt3* mutant cells. A) Mid-log phase growing wild type (BY4741), *smt3* (CL100), *arp3* (CL341) and *arp3 smt3* (CL238) cells were fixed and F actin stained using Alexa-488® phalloidin. Cells were classed as large budded when the ratio of daughter to mother diameter exceeded 0.75, as described previously (Huffaker *et al.*, 1988). Error bars indicate standard deviation from at least 2 biological replicates. P values are derived from 2 tailed unpaired student t test. A) Percentages shown are from 96, 132, 30 and 40 large budded wild type, *smt3*, *arp3* and *arp3 smt3* cells respectively. B) Same as A), but strains shown are wild type (BY4741), *smt3* (CL100), *tub2* (CL480), and *tub2 smt3* (CL486). Percentages are shown from 96, 132, 25 and 38 large budded wild type, *smt3*, *tub2* and *tub2 smt3* cells respectively.

5.2.3 Spindle Microtubule Morphology is Aberrant in the smt3 Mutant

Having established roles for Smt3 in F actin dynamics the next step was to investigate the relationships between Smt3 and tubulin. Therefore, microtubules were visualised in wild type and *smt3* mutant cells using anti-α-Tubulin antibodies (anti-TAT1) (Figure 5.7 A). In wild type cells, nuclear division is achieved by the microtubule spindle elongating over the mother and daughter cells, separating the nuclei (Figure 5.7 A) (Page and Snyder, 1993). Observing only large budded cells, the *smt3* strain appeared to have two particularly striking tubulin defects. One tubulin defect in the *smt3* mutant cells is an increased proportion of short, densely stained microtubules, near the bud neck (Figure 5.7 A i). Indeed, 16.2% of large budded wild type cells had microtubules solely in the mother cell, compared to 38.6% of *smt3* mutant cells (quantified from 37 wild type and 70 *smt3* large budded mutant cells, 3 biological replicates). Secondly, in contrast to wild type cells, the spindles of some *smt3* mutant cells seem unable to elongate fully to the opposite poles of each cell as in wild type cells, and, moreover, this often coincides with the detection of the nuclei 'stalled' in the bud neck (Figure 5.7 A ii). Indeed, measurement of the tubulin length of in both wild type and *smt3* mutant cells whose nuclei was either spanning the bud neck, or separated into the mother and daughter, revealed that the average length of microtubules in *smt3* mutant cells were reduced (Figure 5.7 B). This is before taking to account the larger size of the *smt3* cells, which would be expected to cause an increase in the average spindle length. Interestingly, similar to the effect of *smt3* on F actin staining, tubulin staining appeared to be increased in *smt3* mutant cells (Figure 5.6 and 5.7). In conclusion, these data suggest that Smt3 is required for normal tubulin dynamics in mitosis.

Having revealed tubulin defects associated with the *smt3* mutant allele, we then examined whether the supressing *arp3* and *tub2* mutant alleles affected tubulin morphology (Figure 5.8 and 5.9). Immunostaining appeared to show less microtubule staining in *tub2* mutant cells compared to wild type cells (Figure 5.8). Furthermore, *tub2 smt3* double mutant cells appear to display reduced tubulin immunostaining compared to *smt3* single mutant cells (Figure 5.8). To investigate the possibility that the Arp2/3 complex might affect tubulin morphology, the same analysis was repeated using single *arp3* mutant cells and *arp3 smt3* double mutant cells (Figure 5.9). Interestingly, *arp3 smt3* double mutant cells appeared to display reduced tubulin immunostaining compared to the *smt3* single mutant cells (Figure 5.9). As described above, *smt3* cells contain shorter microtubules in cells with dividing nuclei, hence microtubule lengths were measured in *arp3, tub2* single mutant cells, and in *arp3 smt3* and *tub2 smt3* double mutant cells with DNA in the bud neck or across the mother and daughter (Figure 5.10). Interestingly, neither the *arp3 smt3* or *tub2 smt3* double mutant rescues the shorter tubulin length defect of the *smt3* mutant (Figure 5.10). Furthermore, these data reveal the *arp3* single mutant anaphase cells have reduced microtubule length compared to equivalent wild type

A
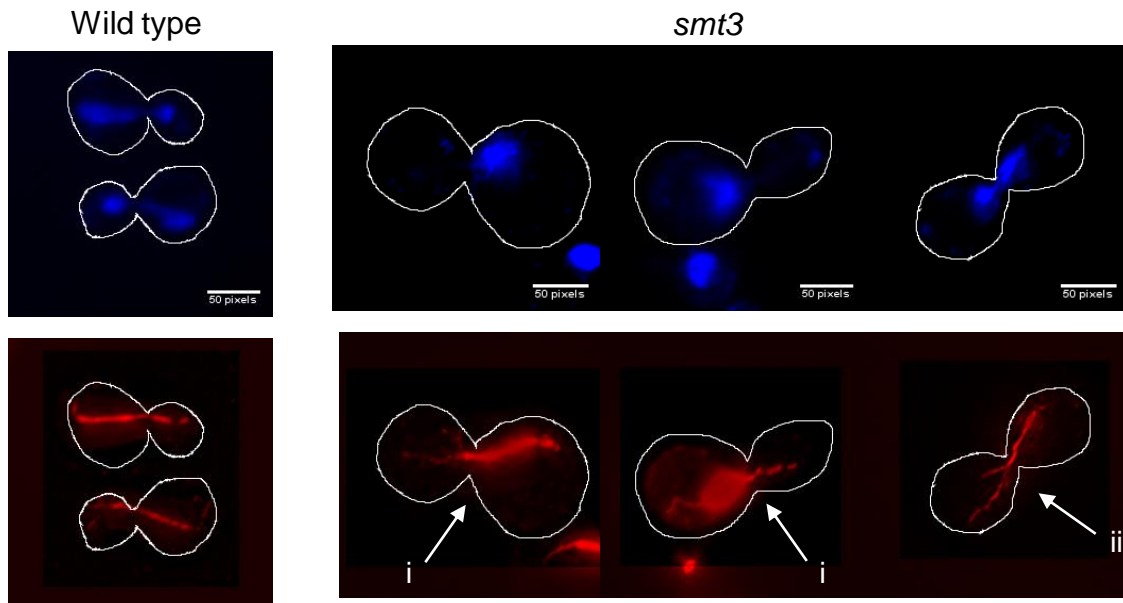
B
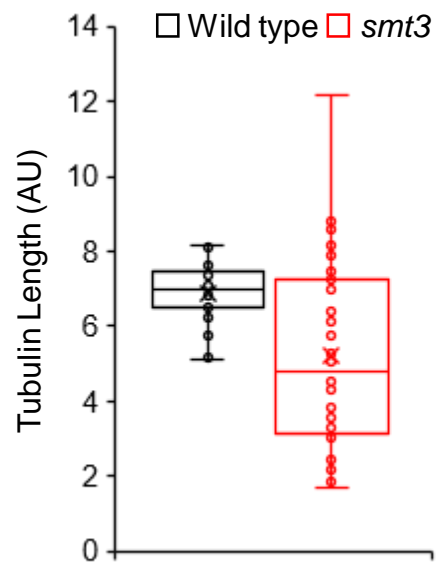
Figure 5.7: *smt3* mutant cells have microtubule spindle morphology defects. Mid-log phase growing wild type (BY4741) and *smt3* (CL100) cells were fixed, and tubulin stained with anti-TAT1 antibody. Cells were classed as large budded when the daughter to mother diameter ratio exceeded 0.75, as described previously (Huffaker *et al.*, 1988). A) Representative large budded cells shown of wild type and *smt3* cells. Images were deconvoluted by iterative algorithm. Arrows indicate aberrant microtubules as follows: i) densely stained microtubules in mother cell, and ii) tubulin across bud neck but not completely elongating to the cell ends. All images are from the same experiment, i.e. all strains fixed and immunostained together, and exposure time equal between all images. Scale bar represents 50 pixels in the raw image. B) Spindle length was measured in large budded wild type and *smt3* cells which have a DNA mass either in the bud neck or with separated nuclei using ImageJ software. Lengths from 26 wild type and 38 *smt3* cells were measured from 3 biological replicates. AU is arbitrary units of length.
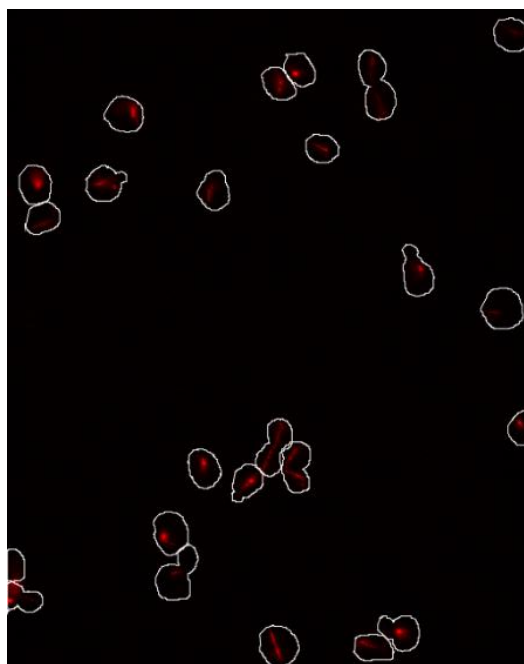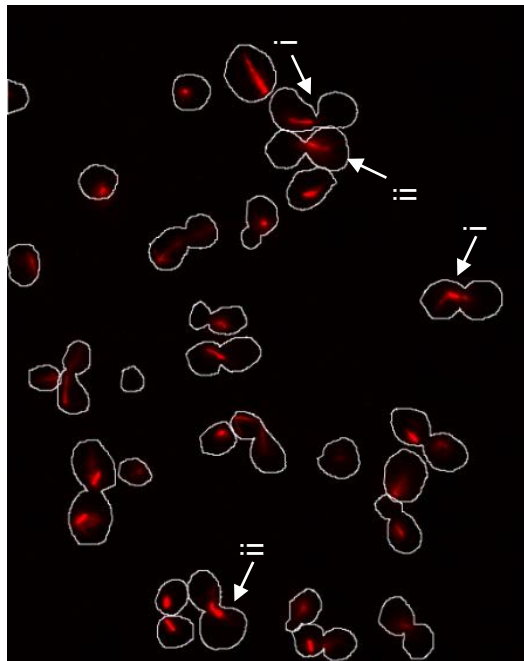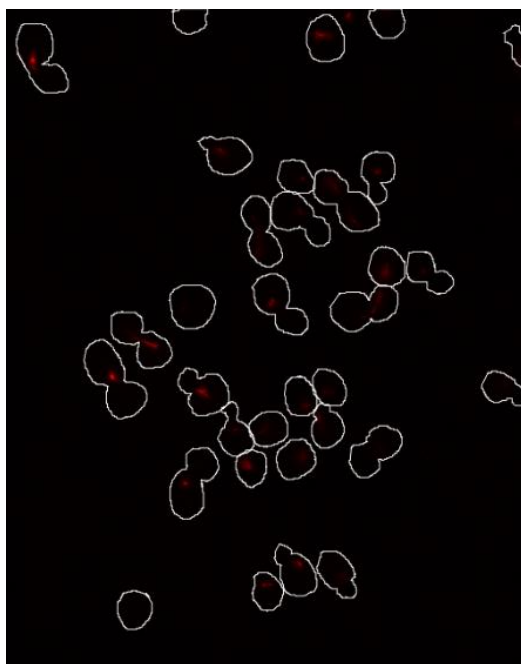
smt3

tub2 smt3
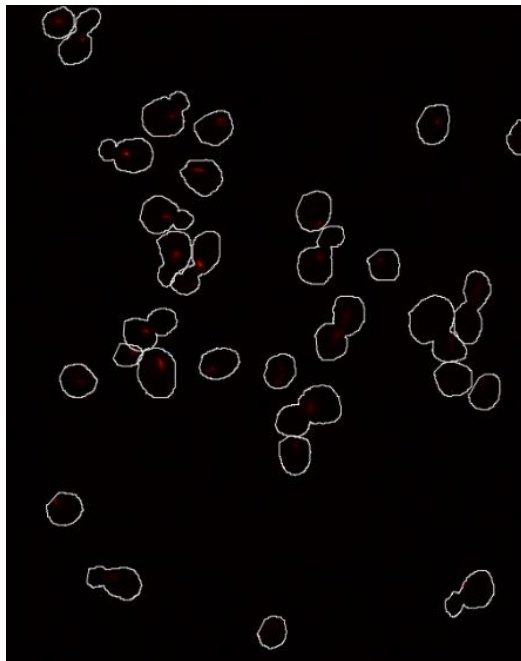
Wild type

tub2

Figure 5.8: Aberrant tubulin morphology in *smt3* mutant cells is altered by the *tub2-DAmP* allele. Mid-log phase growing wild type (BY4741), *smt3* (CL100), *tub2* (CL480), and *tub2 smt3* (CL486) cells were fixed, and tubulin stained with anti-TAT1 antibody. Arrows indicate aberrant microtubules as follows: i) densely stained microtubules in mother cell, and ii) tubulin across bud neck but not completely elongating to the cell ends. Images are representative of two experiments. All images are from the same experiment, i.e. all strains collected and immunostained together, and exposure time equal between all images.
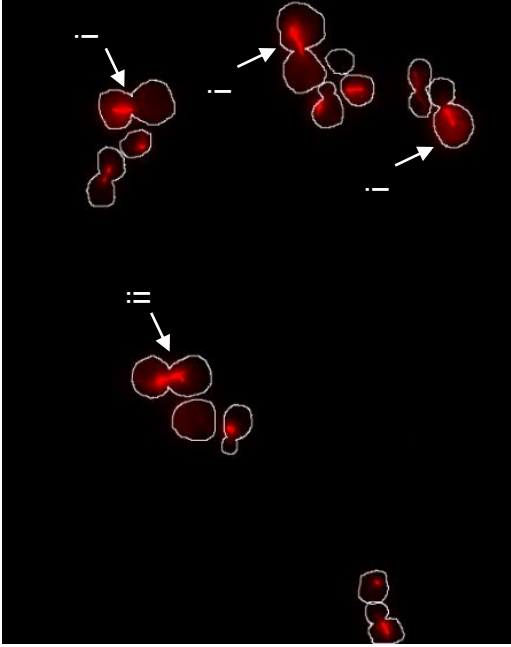
smt3

arp3 smt3

Wild type
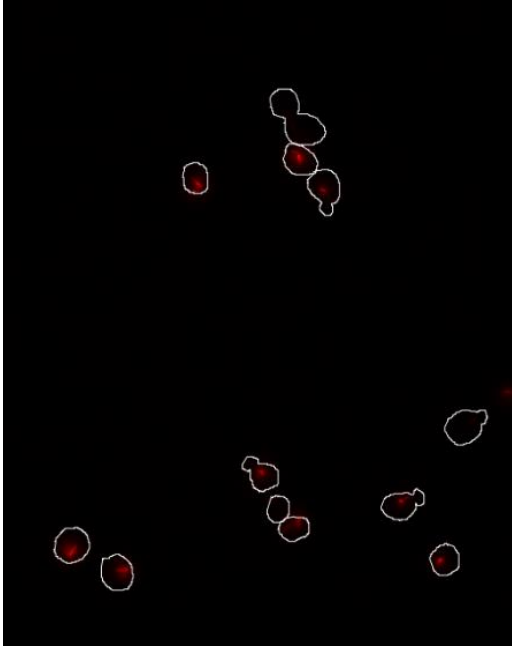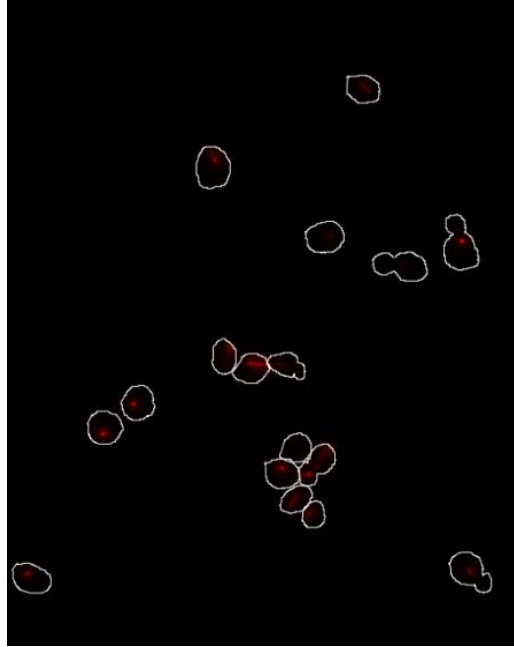
arp3

Figure 5.9: Aberrant tubulin morphology in *smt3* mutant cells is altered by the *arp3-DAmP* allele. Mid-log phase growing wild type (BY4741), *smt3* (CL100), *arp3* (CL341) and *arp3 smt3* (CL238) cells were fixed, and tubulin stained with anti-TAT1 antibody. Arrows indicate aberrant microtubules as follows: i) densely stained microtubules in mother cell. ii) tubulin across bud neck but not completely elongating to the cell ends. Images are representative of two experiments. All images are from the same experiment, i.e. all strains collected and immunostained together, and exposure time equal between all images.
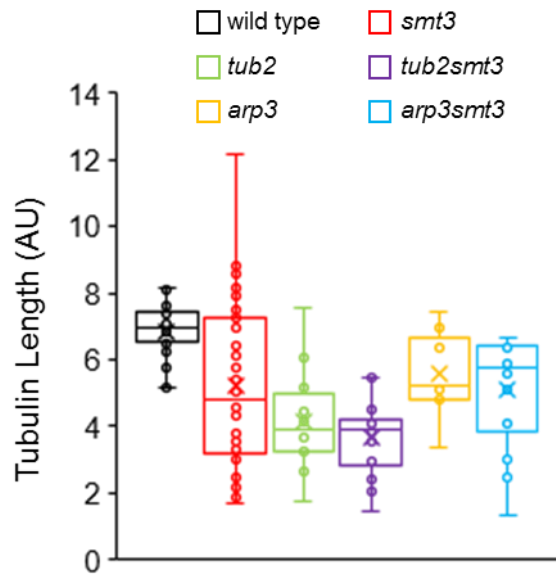
Figure 5.10: Short tubulin spindle length in *smt3* mutant cells is not rescued by *arp3* or *tub2* DAmP alleles. Mid-log phase growing wild type (BY4741), *smt3* (CL100), *arp3* (CL341) and *arp3 smt3* (CL238), *tub2* (CL480), and *tub2 smt3* (CL486) cells were fixed, and tubulin stained with anti-TAT1 antibody. Cells were classed as large budded when the daughter to mother diameter ratio exceeded 0.75, as described previously (Huffaker *et al.*, 1988). Spindle length was measured in large budded wild type and *smt3* cells which have a DNA mass either in the bud neck or with separated nuclei using ImageJ software. Microtubules were measured from 36 wild type, 70 *smt3*, 13 *arp3*, 17 *arp3 smt3*, 25 *tub2*, and 37 *tub2 smt3* large budded cells from at least 2 biological replicates. AU is arbitrary units of length.

cells, consistent with the proposal that the *arp3* mutant allele influences microtubule function (Figure 5.8). Nevertheless, this data does not appear to provide evidence to support a correlation between suppression of the *smt3* slow growth phenotype and tubulin length. However, the fact that the *arp3*, *tub2*, and *smt3* mutant alleles all influence tubulin morphologies further supports the hypothesis that the actin and tubulin cytoskeleton and sumoylation are working together in a tripartite relationship. It appears that if either tubulin, actin, or sumoylation is perturbed, the regulation of the other two processes are also affected. These data together could suggest that sumoylation of cytoskeletal proteins regulates their function.

5.2.4   Arc35 Sumoylation Could Not Be Detected

To further investigate the relationships between SUMO and F actin and microtubule dynamics, we next attempted to identify relevant sumoylated targets. As a first step to test the ability of such targets, we attempted to investigate the sumoylation of Arc35, a component of the Arp2/3 complex which has been previously shown to be sumoylated (Wohlschlegel *et al.*, 2004; Sung *et al.*, 2013). Furthermore, the *arc35* mutant was identified as a suppressor in our screen, suggesting a genetic linkage to Smt3 function. Therefore, Arc35 seemed a good candidate to identify sumoylation of cytoskeleton components. A strain expressing a 3HA epitope tagged version of Arc35 from the normal gene locus was constructed (CL268) (Chapter 2, section 2.2.6.3), and importantly the epitope tag did not appear to affect cell growth (Figure 5.11 A). Next, an *smt3* mutant strain expressing Arc35-3HA was also constructed, to allow any changes in sumoylation status of Arc35 to be detected. Smt3 modified Arc35-3HA would be expected to have a molecular weight of ~52 kDa, although poly sumoylation could occur leading to larger increases in molecular weight. Analysis of protein extracts from wild type *SMT3* cells expressing Arc35-3HA revealed two bands specific to the HA tagged lanes, which could be consistent with unsumoylated and sumoylated forms of Arc35-3HA (Figure 5.11 B, lane 1, arrow and asterisk). However, the relative intensities of these bands were unaffected by the *smt3* allele (Figure 5.11 B, compare lane 1 and lane 2, arrow and asterisk). To confirm the identity of the potential sumoylated Arc35-3HA band, Smt3 conjugates were immunoprecipitated by an anti-Smt3 antibody in wild type untagged and Arc35-3HA expressing protein extracts, and analysed by western blotting for presence of sumoylated Arc35-3HA by probing with anti-HA antibody (Figure 5.11 C). While a band of the expected height of sumoylated Arc35-3HA was detected in the tagged lane immunoprecipitates, a similarly sized band in the non-tagged wild type strain was also detected, although at lower levels than in the Arc35-3HA tagged lane (Figure 5.11 C, lanes 3 and lanes 6). This could be detection of the heavy chain of the anti-Smt3 antibody used in the immunoprecipitation (Figure 5.11 B). Therefore, it is difficult to ascertain if this is sumoylated Arc35-3HA.
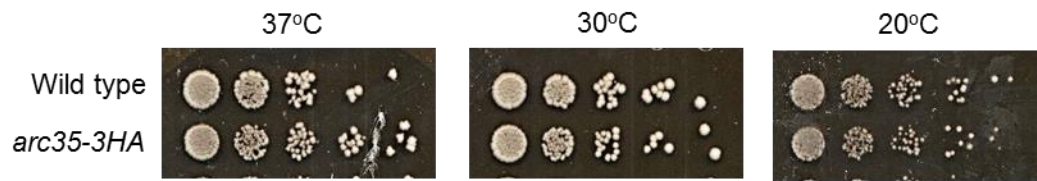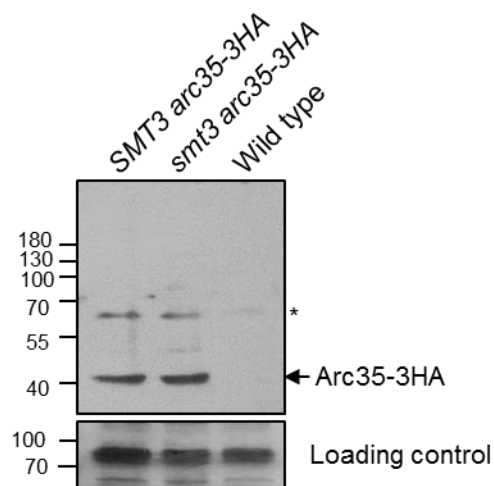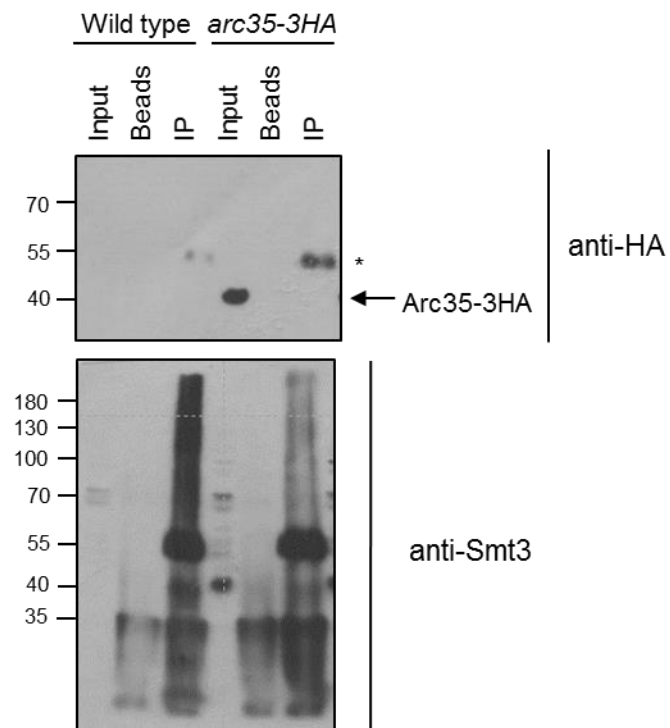
Figure 5.11: Arc35 sumoylation cannot be detected in wild type or *smt3* mutant cells. A) 5 fold serial dilutions of wild type (BY4741) and *arc35-3HA* (CL268) strains were plated onto YPD and incubated at the indicated temperatures for 3 days. B) TCA protein samples were collected from mid-log phase growing cells expressing Arc35-3HA with wild type *SMT3* (CL268) or the *smt3* allele (CL474), and analysed by western blotting. Blots were probed with anti-HA antibody, and stripped and reprobed with anti-Skn7 for loading. Asterisk (*) indicates bands above the size of Arc35-3HA (~40 kDa) that are specific to the HA tagged lanes. C) Soluble protein extracts from mid-log phase growing cells wild type (BY4741) and Arc35-3HA expressing (CL268) cells were immunoprecipitated with anti-Smt3 antibody, and analysed by western blotting. Immunoprecipitated proteins were probed with anti-HA, and stripped and reprobed with anti-Smt3 antibody. Asterisk (*) indicates HA reactive band consistent with Arc35~Smt3. Input is 1% of protein extract which was immunoprecipitated. Beads is protein-A/G beads only, without the addition of anti-Smt3 antibody.

Improvements to the detection methods will be required to ascertain the sumoylation status of Arc35, for example optimisation of primary and secondary antibodies in detection to minimise none specific binding. It is possible that Arc35 is not a Smt3 target in our system, thus our methods will require validating with a well characterised Smt3 substrate. Alternatively, another approach, such as mass spectrometry, could be used to compare the sumoylation status of cytoskeletal components in wild type and *smt3* mutant cells. Identifying substrates would be key to understanding the molecular mechanism underpinning the growth defects of *smt3* mutant cells, and role of Smt3 modification in cytoskeletal regulation.

5.2.5 Sumoylation and the Cytoskeleton in Cold Stress Response

While we have elucidated that misregulated sumoylation causes increased levels of F actin and tubulin, and defects in microtubule and actin dynamics, it is not clear what the cellular consequence of these defects are. Hence to gain further insight into the relationships between Smt3, F actin and microtubules, we investigated other phenotypes associated with the *smt3* allele. As described in Chapter 4, our studies revealed that *smt3* mutant cells are cold sensitive (Figure 4.6). Interestingly, previous studies have shown that cells lacking both the E3 ligases Siz1 and Siz2 are also cold sensitive (Chen *et al.*, 2005; Johnson and Gupta, 2001). As shown above we have confirmed that the cold sensitive phenotype associated with the *smt3* allele was reversed in the *arp2 smt3*, *arp3 smt3*, *arc35 smt3* and *tub2 smt3* double mutants (Figure 5.1). Interestingly, many *S. cerevisiae* tubulin mutants are cold sensitive (Schatz *et al.*, 1988; Huffaker *et al.*, 1988), and, furthermore, F actin levels have been shown to increase upon cold treatment of *S. cerevisiae* cells (Yeh and Haarer, 1996). We therefore hypothesised that the cold sensitivity of the *smt3* mutant was due to misregulation of F actin and microtubules.

To test this hypothesis, cold temperature shock was induced in wild type and *smt3* mutant cells by rapidly cooling cultures from $30^{\circ}C$ to $20^{\circ}C$. F actin and tubulin were then analysed in these cells 10 and 60 minutes after the temperature shift (Figure 5.12). F actin staining increased in wild type cells after 10 minutes, which agrees with previously shown experiments (Figure 5.12) (Yeh and Haarer, 1996). Interestingly, however, the F actin staining appeared to return to near wild type levels after 60 minutes of incubation at $20^{\circ}C$ (Figure 5.12). Similarly, tubulin immunostaining increased upon cold incubation in wild type cells, and decreased after 60 minutes of incubation (Figure 5.12). Strikingly, the transient increase of both F actin staining and tubulin immunostaining did not appear to occur in the *smt3* mutant strain (Figure 5.13). Indeed, quantification of fluorescence from F actin staining and tubulin immunostaining in unbudded cells revealed that after 10 minutes of cold shock, wild type cells show 1.91-fold increase and 1.60-fold increase in actin relative to the levels observed at $30^{\circ}C$ (Figure 5.14).

DIC | Merge | Tubulin | F actin

30°C

10 min

60 min

20°C

151
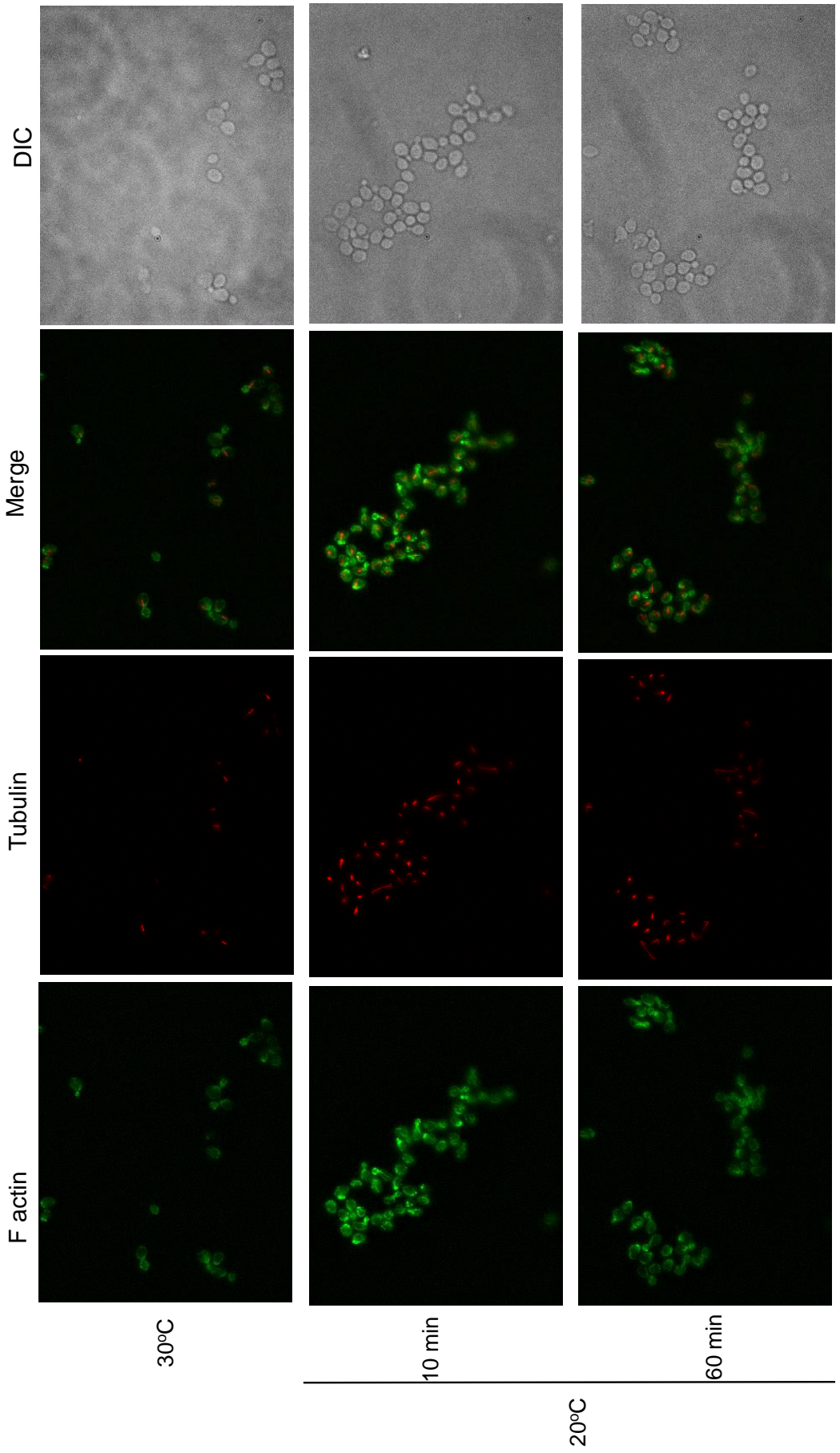
Figure 5.12: Cold stress induces a rapid yet transient polymerisation of F actin and tubulin in wild type cells. Mid-log phase growing wild type (BY4741) cells were cooled rapidly from 30°C to 20°C, and cells were fixed after 10 and 60 minutes. F actin was stained using Alexa-488® phalloidin, and tubulin immunostained with anti-TAT1 antibody. Presented images show F actin staining (green), tubulin staining (red), the two stains merged, and DIC. All images are from the same experiment, i.e. all strains collected and stained together, and exposure time equal between all images. Images are representative of two experiments.

DIC

Merge

Tubulin

F actin

30°C

10 min

60 min

20°C

153
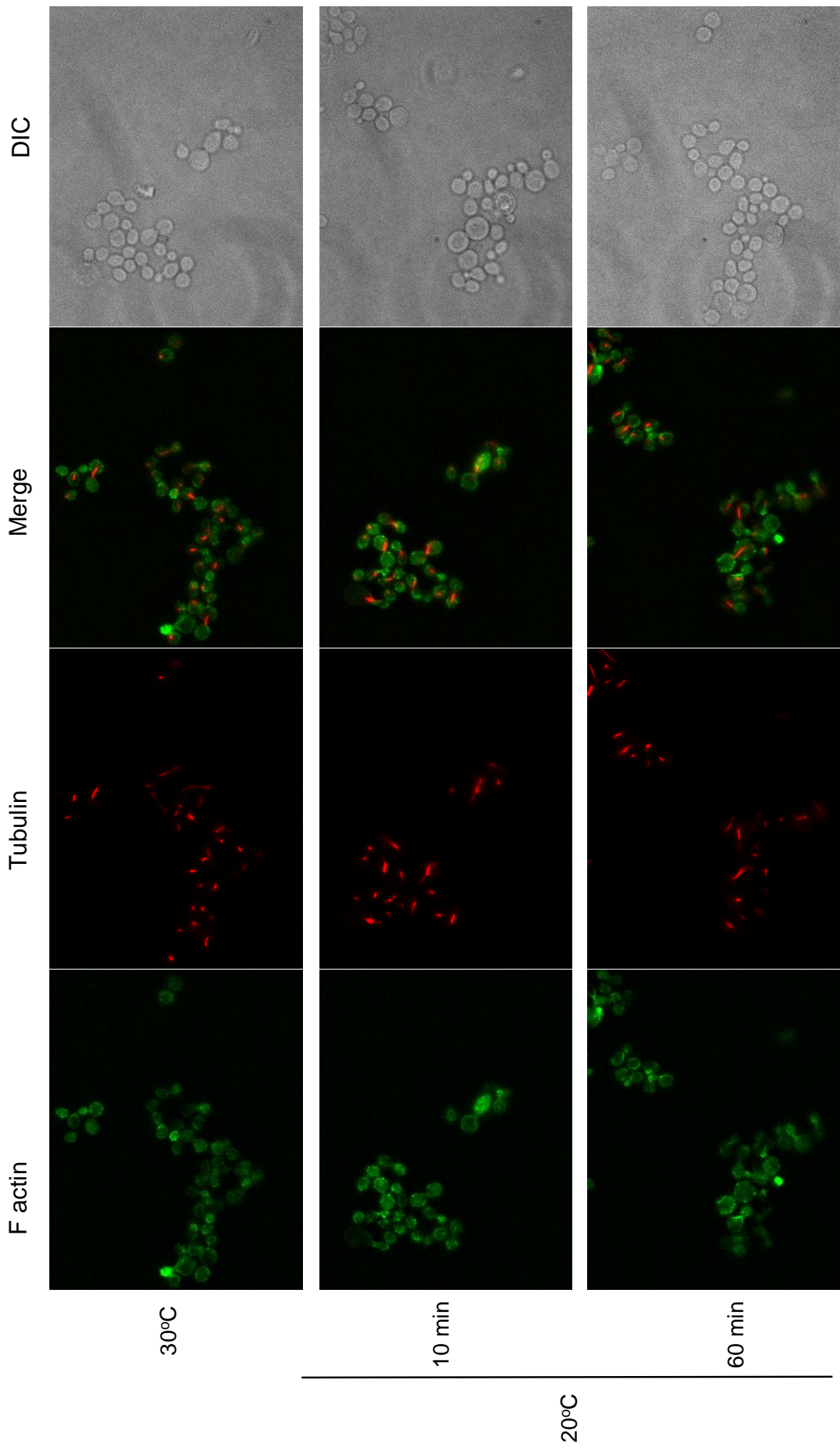
Figure 5.13: The rapid polymerisation of F actin and tubulin in response to cold stress is lost in *smt3* mutant cells. Mid-log phase growing *smt3* (CL100) cells were cooled rapidly from 30°C to 20°C, and cells were fixed after 10 and 60 minutes. F actin was stained using Alexa-488® phalloidin, and tubulin immunostained with anti-TAT1 antibody. Presented images show F actin staining (green), tubulin staining (red), and the two stains merged. All images are from the same experiment, i.e. all strains collected and stained together, and exposure time equal between all images. Images are representative of two experiments.

Consistent with previous data, *smt3* cells had an increase in F actin and tubulin levels at 30°C (Figure 5.14). However, in *smt3* mutant cells, F actin staining and tubulin immunostaining levels did not show a reproducible transient increase in fluorescence levels after shift to 20°C (Figure 5.14). It is, however, interesting to note that the fold increase of F actin staining and tubulin immunostaining levels after 10 minutes of incubation at 20°C, was a similar fold increase to the fluorescence from the *smt3* mutant at 30°C (Figure 5.14). These data together suggest that loss of sumoylation prevents the proper cytoskeleton response to cold shock. One hypothesis for this is that Smt3 provides the response to the cold temperature by altering F actin and tubulin dynamics to cope with the cold stress, potentially by altering Smt3 modification of cytoskeletal proteins. Perhaps the increased F actin and tubulin polymerisation in steady state in *smt3* mutant cells, prevents the dynamic alteration of the cytoskeleton that is required for the cold shock response.

It has been previously shown that global sumoylation changes are induced by stress, such as the sumoylation responses to oxidative stress, heat shock and ethanol stress (Bossis and Melchior, 2006; Pinto *et al.*, 2012; Sydorskyy *et al.*, 2010). Interestingly, previous work has shown that sumoylation is induced by hypothermic conditions in mammalian cells (Lee *et al.*, 2007). Hence, a prediction could be that a change in global sumoylation in response to cold stress is targeting the cytoskeletal proteins, eliciting a change in cytoskeleton dynamics. Thus, to test this hypothesis, wild type cells were exposed to cold stress at 20°C as described above, and protein extracts were analysed by western blot using an anti-Smt3 antibody (Figure 5.15). Interestingly, an induction of high molecular weight anti-Smt3 antibody reactive bands after 10 minutes of cold exposure was observed, consistent with an accumulation of Smt3 conjugates. (Figure 5.15 A and B). Furthermore, the levels of Smt3 conjugates appeared to return to pre cold temperature stress levels after 240 minutes of incubation at 20°C (Figure 5.15 A and B). The dynamics of Smt3 conjugation, and the F actin and tubulin response, suggests that these pathways are linked in the cold response. However, further experiments are required to determine if these processes are linked. For example, identification of substrates which are sumoylated during cold stress would provide evidence that Smt3 is regulating cytoskeleton dynamics in response to cold.

5.2.6 Genetic Analysis of Sumoylation Pathway Enzymes in the Cold Response

Previous studies have shown that changes in global sumoylation by heat stress or oxidative stress can be induced by inhibiting the SUMO deconjugation enzymes (Bossis and Melchior, 2006; Pinto *et al.*, 2012; Sydorskyy *et al.*, 2010). Alternatively, sumoylation changes can also be induced by the E3 ligases, observed in DNA damage induced sumoylation events (Branzei *et al.*, 2006; Parker *et al.*, 2008). As described above, we and others have identified that
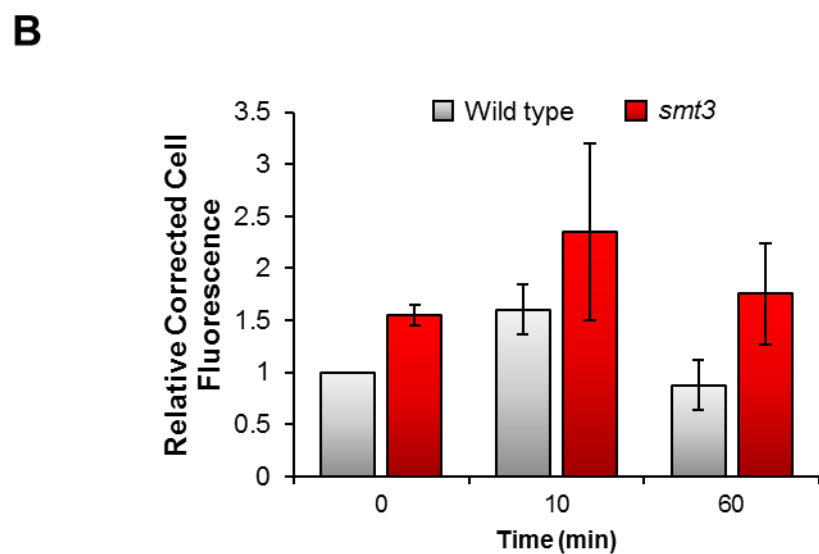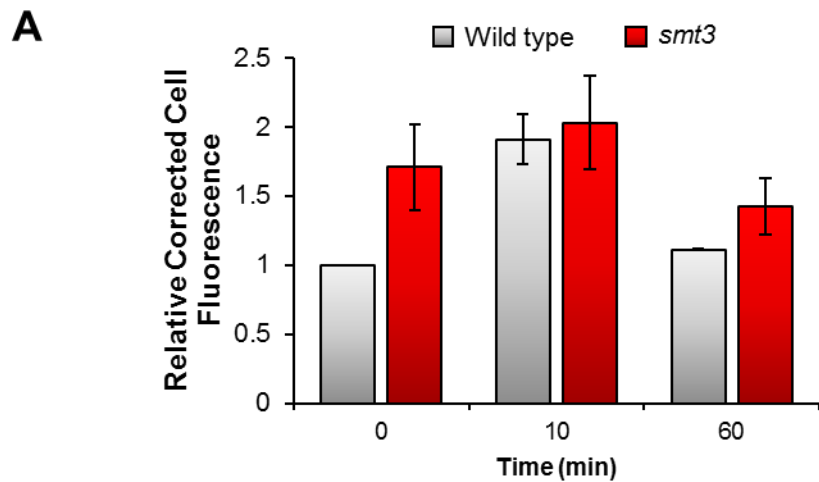
Figure 5.14: Quantification of F actin and tubulin staining in response to cold temperature stress in wild type and *smt3* mutant cells. Mid-log phase growing wild type (BY4741) and *smt3* (CL100) cells were cooled rapidly from 30°C to 20°C, and cells were fixed after 10 and 60 minutes. F actin was stained using Alexa-488® phalloidin, and tubulin stained with anti-TAT1 antibody. Total cell fluorescence was quantified for A) F actin and B) tubulin for unbudded cells, and the fold change from wild type time=0 calculated. Error bars represent standard deviation from two biological replicates.
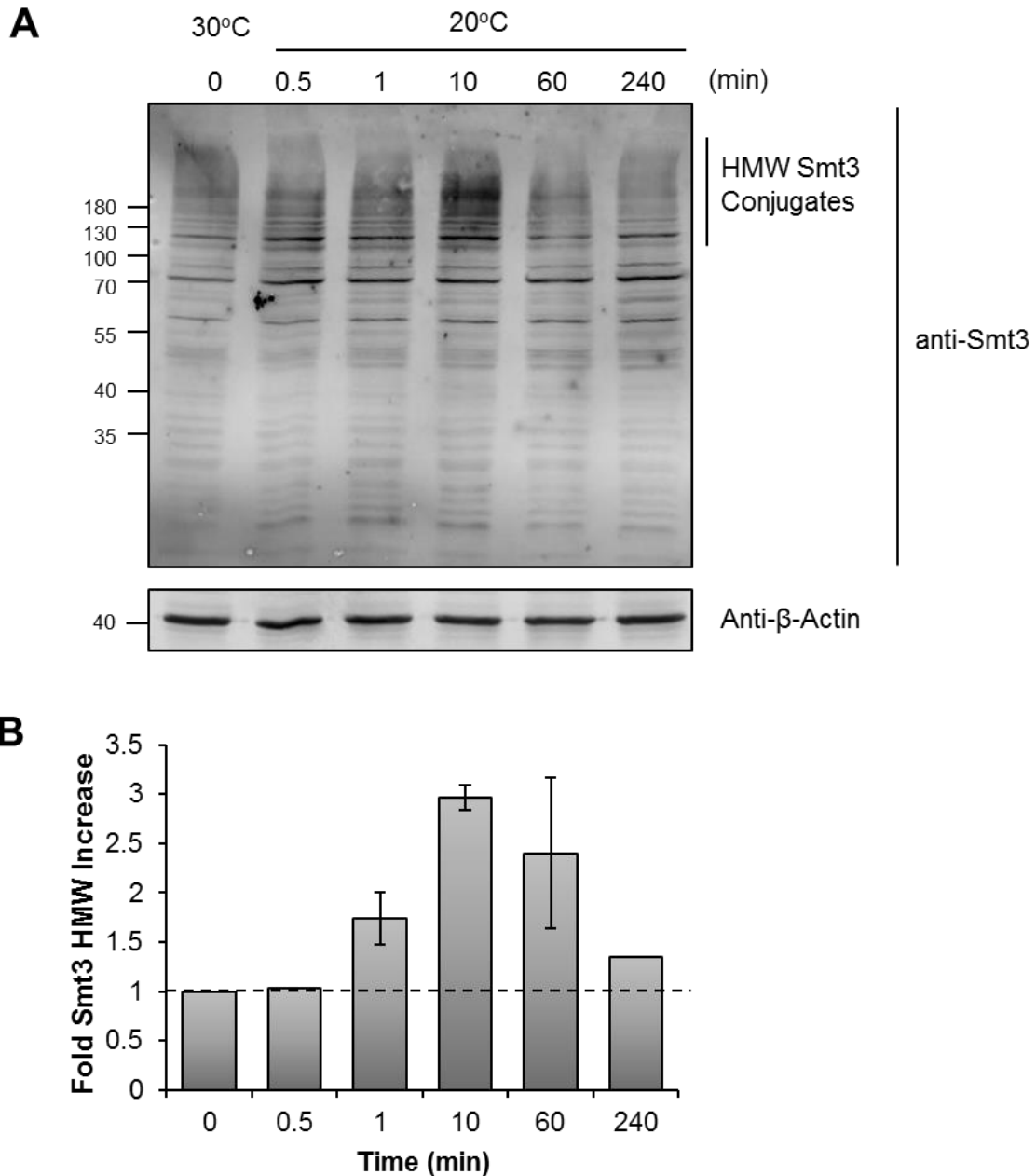
Figure 5.15: The levels of Smt3 high molecular weight (HMW) conjugates are induced by cold temperatures stress. A) Mid-log phase growing wild type cells (BY4741) were cooled rapidly from 30°C to 20°C, and TCA protein samples collected at the indicated time points. Protein was extracted, separated by SDS-PAGE, and analysed by western blotting using anti-Smt3 antibodies. Blots were stripped, and re-probed with anti-β-Actin. HMW Smt3 conjugates are indicated. B) The HMW bands indicated were quantified, and the fold change from 30°C calculated. Standard deviation from two biological replicates the of 1, 10 and 60-minute time points is shown as error bars. Other time points (0.5 and 240 minute) were repeated once.

changes in global sumoylation are triggered by cold stress (Figure 5.15) (Lee *et al.*, 2007). Thus we investigated the potential role of the SUMO E3 ligases and deconjugases in the response to cold temperature stress. *S. cerevisiae* contains two major SUMO E3 ligases Siz1 and Siz2 (Strunnikov *et al.*, 2001; Johnson and Blobel 1999), and two deconjugases Ulp1 and Ulp2 (Li and Hochstrasser, 1999; Schwienhorst *et al.*, 2000). To explore the roles of these proteins in the response to cold stress, the sensitivity of *smt3*, *siz1Δ*, *siz2Δ*, *ulp1-DAmP*, and *ulp2-DAmP* single mutants and the respective *smt3* double mutants to cold temperature stress was examined (Figure 5.16). Of the single mutants, only *smt3* and *ulp1-DAmP* mutant cells were unable to grow at 15°C, which was consistent with previous analyses of these mutants (Figure 4.2, Figure 5.16). The basis of the cold sensitivity of the *ulp1-DAmP* mutant is not clear, as the enzyme also plays a role in the activation of the Smt3 precursor in addition to roles in protein desumoylation (Li and Hochstrasser, 2000). Interestingly, analyses of the double mutants revealed that only *siz2Δ* was able to rescue the cold temperature growth defect associated with the *smt3* allele (Figure 5.16). The nature of this suppression is unclear, but suggests there is an underlying specificity within the sumoylation conjugation pathway in the cold response.

Given the relationships between *siz2Δ* and the suppression of the cold sensitive phenotype of the *smt3* mutant, allele, we were therefore interested to investigate the effects of these sumoylation conjugation and deconjugation enzymes on F actin. Thus, *siz1Δ*, *siz2Δ*, *ulp1-DAmP*, and *ulp2-DAmP* single mutant cells and the respective *smt3* double mutant cells were fixed, and F actin stained using phalloidin. (Figure 5.17 and 5.18). Initial analysis of the single mutants indicated that the *siz1Δ*, *siz2Δ*, *ulp1-DAmP* and *ulp2-DAmP* single mutants appeared to have a negligible effect on F actin (Figure 5.17 and 5.18). It could be that *ulp1-DAmP* allele containing cells have increased intensity of F actin staining compared to wild type, however this would need to be repeated and quantified to confirm this result. Interestingly, *siz1Δ smt3* double mutant cells appear to have increased F actin staining over even larger cell sizes (Figure 5.17). However, while *siz2Δ smt3* cells are very large sized, the intensity of F actin staining in large budded cells appears reduced compared to *smt3* mutant cells, or *siz1Δ smt3* mutant cells (Figure 5.17). This effect is difficult to quantify however, due to the larger cell size and the low number of unbudded cells which were previously used to quantify F actin levels. Thus, to gain insight into the F actin in these mutants, we quantified the F actin morphology of these mutants as completed above (Table 5.1). Upon quantification, we could not see a clear correlation between an F actin morphology and the cold sensitivity (Table 5.1). Most of the mutants which were cold sensitive also contained the *smt3* allele, and as such they displayed the characteristic mislocalised patch and absent bud neck F actin staining of the *smt3* mutation. However, *ulp1-DAmP* single mutant cells which were cold sensitive, but
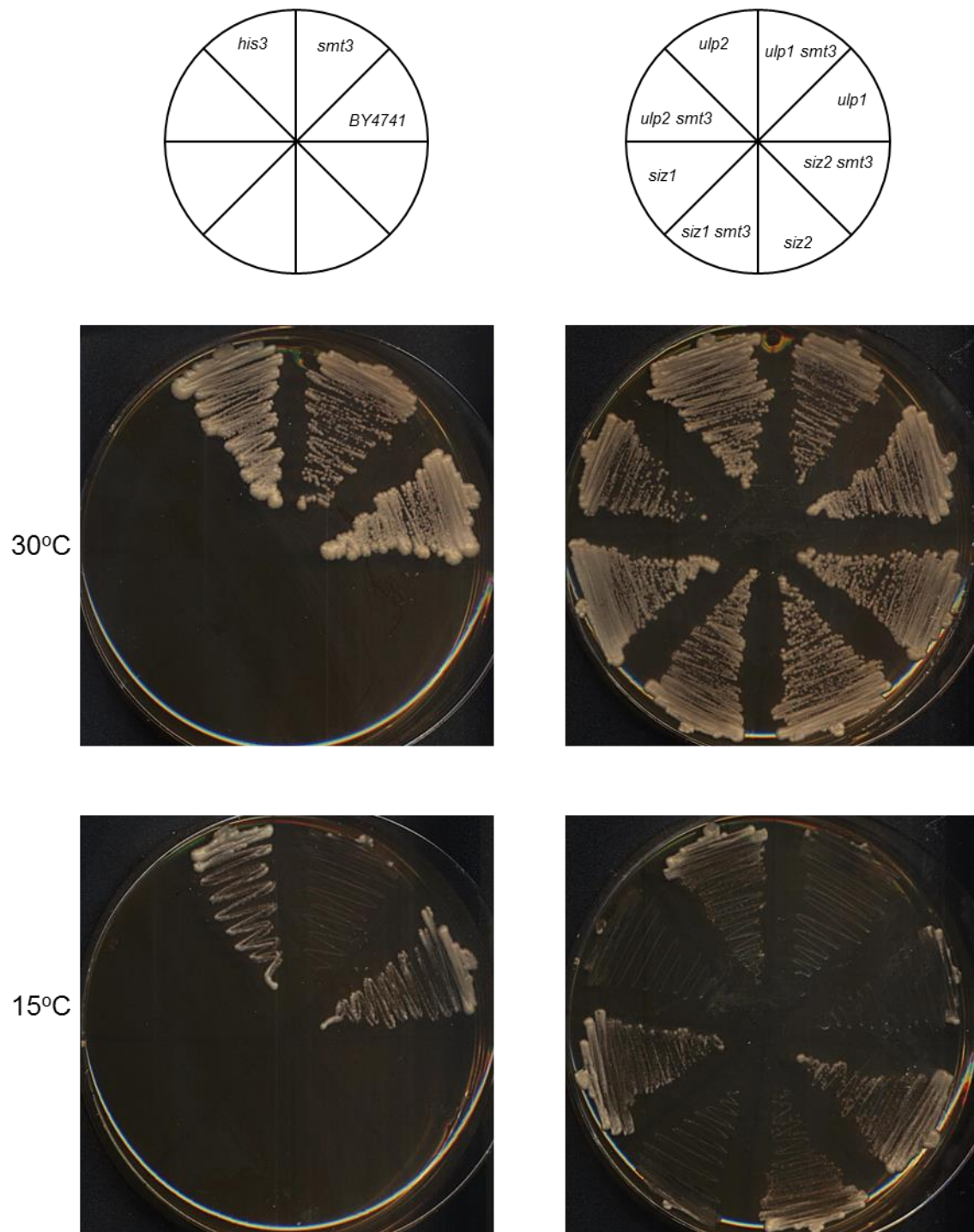
Figure 5.16: Specific sumoylation pathway enzymes are important for the cellular response to cold temperature stress. Wild type (BY4741), *smt3* (CL100), *his3-DAmP* (CL90), *ulp1-DAmP* (CL94), *ulp2-DAmP* (CL95), *ulp1-DAmP smt3* (CL280), *ulp2-DAmP smt3* (CL284), *siz1Δ* (CL253), *siz2Δ* (CL260), *siz1Δ smt3* (CL227), *siz2Δ smt3* (CL163) strains were streaked onto YPD media, and incubated at 3 days at the indicated temperatures.

159
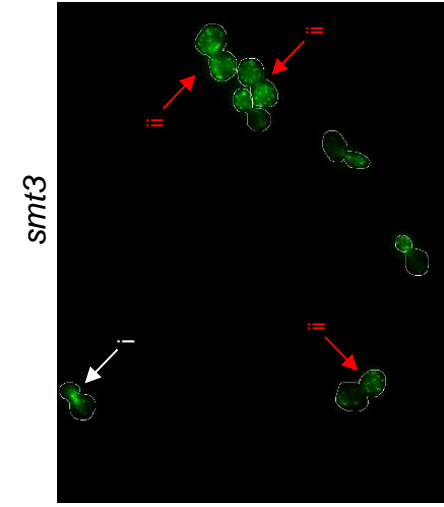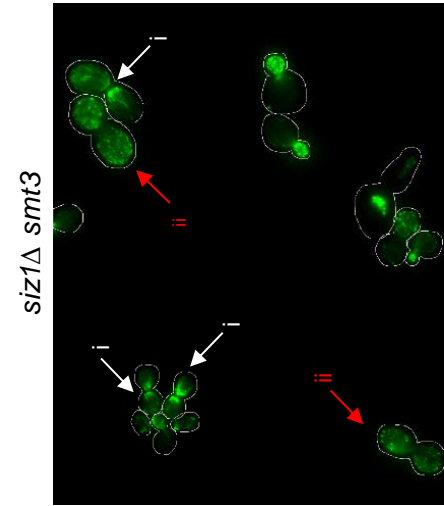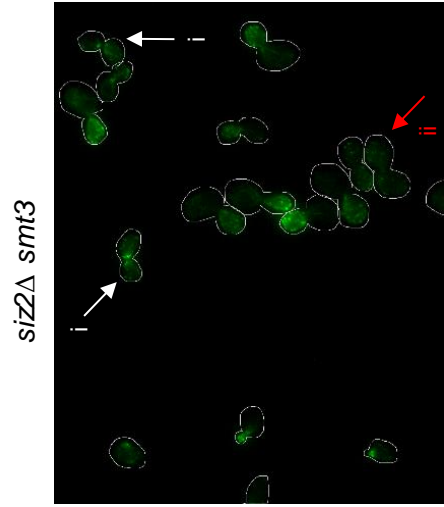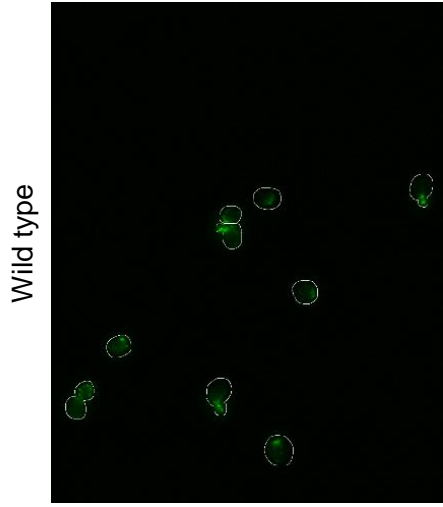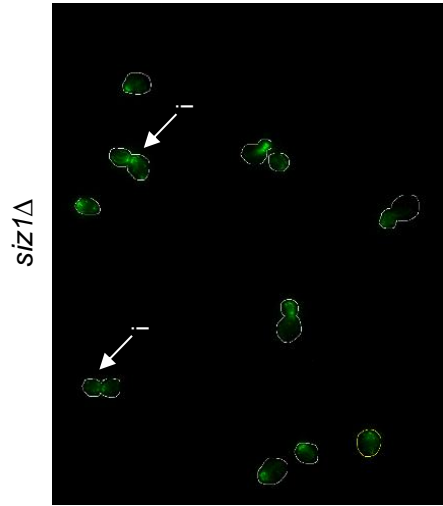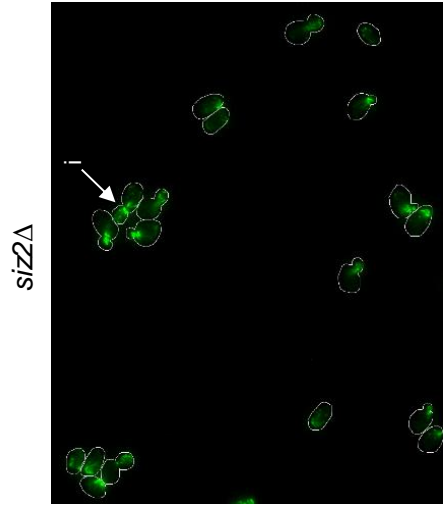
Figure 5.17: F actin morphology is affected by loss of E3 SUMO ligases Siz1 and Siz2 in *smt3* **mutant cells.** Wild type (BY4741), *smt3* (CL100), *siz1Δ* (CL253), *siz2Δ* (CL260), *siz1Δ smt3* (CL227), *siz2Δ smt3* (CL163) mid-log phase growing cells were fixed, and F actin stained using Alexa-488® phalloidin. Arrows indicate actin morphology in large budded cells as follows: i) actin patches mislocalised with actin staining present at the bud neck (white arrows) and ii) actin patches mislocalised, but absent actin staining at bud neck (red arrows). All images are from the same experiment, i.e. all strains collected and stained together, and exposure time equal between all images. Images representative of 2 experiments.

ulp2-DAmP

ulp2-DAmP smt3

ulp1-DAmP

ulp1-DAmP smt3
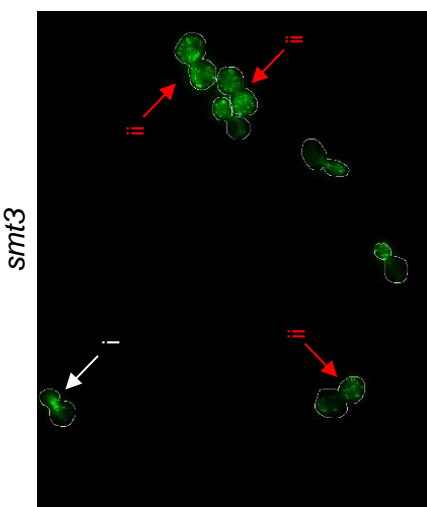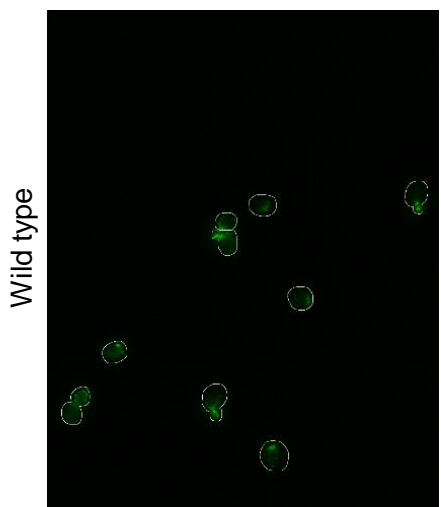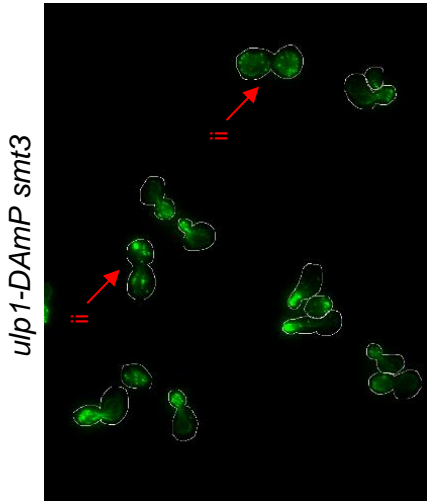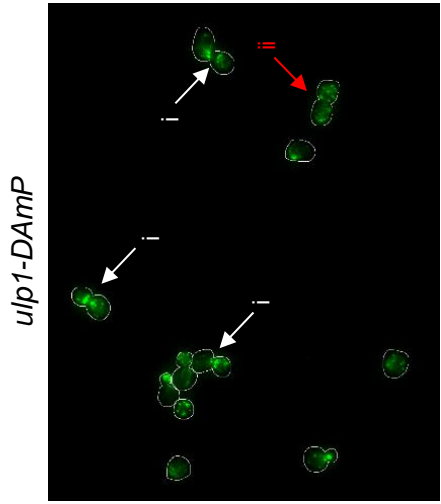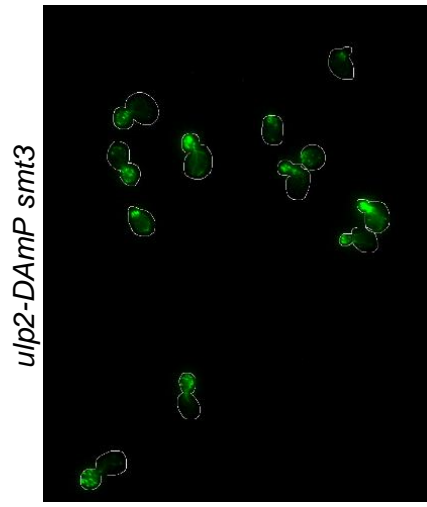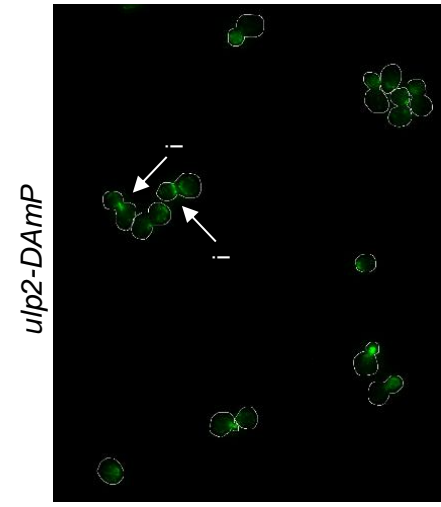
Wild type

smt3

Figure 5.18: F actin morphology is affected by SUMO deconjugases *ulp1* and *ulp2* DAmP mutant alleles in *smt3* mutant cells. Wild type (BY4741), *smt3* (CL100), *ulp1-DAmP* (CL94), *ulp2-DAmP* (CL95), *ulp1-DAmP smt3* (CL280), and *ulp2-DAmP smt3* (CL284) mid-log phase growing cells were fixed, and F actin stained using Alexa-488® phalloidin. Arrows indicate actin morphology in large budded cells as follows: i) actin patches mislocalised with actin staining present at the bud neck (white arrows) and ii) actin patches mislocalised, but absent actin staining at bud neck (red arrows). All images from the same experiment, i.e. all strains collected and stained together, and exposure equal between all images. Images representative of 2 experiments for wild type (BY4741), *smt3* (CL100), *ulp1-DAmP smt3* (CL280), and *ulp2-DAmP smt3* (CL284). Images representative of 1 experiment of *ulp1-DAmP* (CL94), *ulp2-DAmP* (CL95).

Strain	Actin patches in daughter cell (%)	Mislocalised patches, bud neck staining absent (%)	Mislocalised patches, bud neck staining (%)	Total cells	% cells large budded
Wild type (BY4741)	51±8	9±2	40±9	241	24%
smt3 **(CL100)**	35±1	45±2	20±1	242	39%
siz1Δ **(CL253)**	45±9	2±2	53±7	196	24%
siz1Δ smt3 **(CL227)**	30±19	40±3	30±17	60	50%
siz2Δ **(CL260)**	39±13	15±7	45±7	108	31%
siz2Δ smt3 **(CL163)**	68±12	12±10	20±3	134	49%
ulp1-DAmP **(CL94)**	35	19	46	100	26%
ulp1-DAmP smt3 **(CL280)**	50±0	44±2	6±2	87	39%
ulp2-DAmP **(CL95)**	29	6	65	54	31%
ulp2-DAmP smt3 **(CL284)**	46±8	26±14	28±6	92	50%

Table 5.1: Analysis of F actin morphology in Smt3 conjugation and deconjugation pathway mutants. Wild type (BY4741), *smt3* (CL100), *siz1Δ* (CL253), *siz1Δ smt3* (CL227), *siz2Δ* (CL260), *siz2Δ smt3* (CL163), *ulp1-DAmP* (CL94), *ulp1-DAmP smt3* (CL280), *ulp2-DAmP* (CL95) and *ulp2-DAmP smt3* (CL284) mid-log phase growing cells were fixed, and F actin stained using Alexa-488® phalloidin. Cells were classed as large budded when the daughter to mother diameter ratio exceeded 0.75, as described previously (Huffaker *et al.*, 1988). F actin morphology was quantified in large budded cells as follows: i) actin patches in daughter bud, ii) actin patches mislocalised with actin staining present at the bud neck, iii) actin patches mislocalised, but absent actin staining at bud neck. Data are presented as percentage cells counted for each morphology ± the standard deviation of 2 biological replicates, if 2 replicates have been completed. The total number of cells in each experiment and the % large budded cells are also presented. The strains which exhibit cold sensitivity are shaded grey.

did not contain the *smt3* allele, did not have a significant increase of cells displaying this phenotype in the data (Table 5.1). However, more cells with the *ulp1-DAmP* mutation will need to be quantified before the relevance of the specific F actin morphology defect in *smt3* mutant cells in cold sensitivity can be ascertained. It is however interesting to note that in the *siz2Δ smt3* mutant cells, which are not cold sensitive, this specific defect appears reduced (Table 5.1). Thus, it can be concluded that the sumoylation conjugation and deconjugation enzymes appear to have different effects on F actin morphology, and thus suggests that perhaps differential regulation of F actin by SUMO is provided by the specificity of these enzymes. More study will be required to identify the substrates of these enzymes, and how these enzymes are regulated in cold and steady state conditions to influence F actin dynamics. It would also be of interest to further study microtubule dynamics in these strains. However, through this study we have highlighted a previously uncharacterised role of sumoylation in the regulation of the yeast cytoskeleton components F actin and tubulin.

5.3 Discussion

Although sumoylation is essential in *S. cerevisiae*, the underlying link to viability is unknown. Furthermore, many proteomic screens have identified sumoylation targets within a wide array of biological processes, but the relative importance of these modifications for cell survival is unknown. Through genetic screening in the previous chapter, we had shown that hypomorphic alleles of Arp2/3 complex genes *ARP2*, *ARP3* and *ARC35*, and the β-tubulin encoding gene *TUB2*, can suppress the slow growth defects of *smt3* mutant cells. This suppression could have been indirect, but in this chapter we have shown that indeed *smt3* mutant cells have aberrant F actin and microtubule morphology, indicating that SUMO plays an important role in these aspects of the cytoskeleton (Figure 5.2 and 5.7). Interestingly, although there is some previous data suggesting a functional link between the Arp2/3 complex and tubulin, remarkably little is known about these relationships (Schaerer-Brodbeck and Riezman, 2003; Havelkova *et al.*, 2015). In this study we have strengthened these connections and, moreover, shown that sumoylation is intimately linked to both of these processes (Figure 5.4, 5.5, 5.8 and 5.9). However, it is still unclear how sumoylation is effecting F actin dynamics and tubulin.

The mitotic delay does not appear to be due to activation of the spindle assembly checkpoint, as deletion of genes required for the spindle assembly checkpoint, such as Mad2 and Bub3, were not genetic interactors in our screen. Deletion of these genes also did not rescue the short spindle arrest phenotype also observed in strains expressing the *smt3-331* allele (Biggins *et al.*, 2001). Interestingly, in the *smt3* mutant we saw an increased staining of tubulin (Figure 5.7, 5.8 and 5.9). Interestingly, data of stress sensitivity testing of *tub2* and *tub2 smt3* double mutant cells reveals that presence of the *smt3* allele rescues the sensitivity of the *tub2* strain

to benomyl and TBZ (Figure 5.19). These data suggest that the *smt3* allele is acting to stabilise microtubules in the *tub2* strain. However, it unknown how this is taking place. It could be that in the *smt3* mutant microtubule levels are increased, which is below detection by immunofluorescence, or it could be that *smt3* provides a polymerising role of tubulin in the cell. Attempts to quantify protein levels of β-tubulin were attempted during the study, but an antibody used did not detect *S. cerevisiae* β-tubulin. Although it appears that the *smt3* strain is growing more slowly on 100 ug/ml TBZ compared to wild type, this could be due to the slower growth of the strain (Figure 5.15). It would therefore be interesting to complete survival analysis of the *smt3* mutant to lethal dosages of microtubule depolymerising drugs, to assess if the *smt3* strain is more resistant to microtubule destabilisation than wild type. This will give insight into how the *smt3* allele could rescue microtubule depolymerising *tub2* mutant cells.

During the course of this study, we identified a F actin morphological defect in cells with reduced Smt3, where an increased proportion of large budded cells had mislocalised actin patches across mother and daughter cells, but with absent bud neck staining consistent with the actin myosin ring (Figure 5.3 and 5.4). As described in the introduction (see section 1.2.2), the cell cycle-regulated sumoylation of the yeast septins at the bud neck has been well characterised (Johnson and Blobel, 1999; Takahashi *et al.*, 1999; Johnson and Gupta, 2001). However, studies did not find any link between septin sumoylation and septin function, but F actin was not studied in these strains (Johnson and Blobel, 1999). Surprisingly, little is known about the interaction of septins and F actin, but current research is now undergoing to elucidate how these cytoskeleton proteins may regulate each other, and data suggests that the septins promote the curving of F actin filaments to form actin rings (Mavrakis *et al.*, 2014; Huber *et al.*, 2015). Until sumoylation substrates are identified this is purely speculative, but it would be interesting to test if any identified cytoskeletal substrates are regulated in a cell cycle-dependant manner, as it is tempting to speculate that perhaps the modification of septins is not required for septin function per se, but septin sumoylation occurs within a 'SUMO cloud' localised at the bud neck where F actin dynamics are required for mitosis and cytokinesis, for example the formation of the actin-myosin ring, and the sumoylation of other endocytic vesicles required for cell wall formation at the bud neck during cytokinesis (Hurley and Hanson, 2010).

In this study we identified that cells with reduced levels of Smt3 grew extremely slowly at temperatures below optimum growth conditions (Figure 4.2), which has also been observed in cells lacking the two E3 ligases Siz1 and Siz2 (Chen *et al.*, 2005; Johnson and Gupta, 2001). We have provided evidence in this study for a cold stress global sumoylation response in *S. cerevisiae* (Figure 5.15). Furthermore, initial data suggest there is a specificity to cold stress sumoylation conjugation through the E3 ligases Siz1 and Siz2, as the excessively reduced growth in cold conferred by the *smt3* allele is rescued in *siz2Δ smt3* mutant cells, but not in

siz1Δ smt3 double mutants (Figure 5.16). One of the studies reported that the slow growth phenotype of the *siz1Δ siz2Δ* double mutant strain at 30ºC was due to increased copy numbers of the endogenous 2µm plasmid (Chen *et al.*, 2005). However, the study reported that while there were no changes in plasmid copy number between cells grown at 30ºC and 20ºC, the growth rate was further decreased (Chen *et al.*, 2005). It was therefore hypothesized that the cold sensitive defect at 20ºC was not due to 2µm plasmid copy number, and as such another unknown pathway was causing the slow growth in cold conditions in the *siz1Δ siz2Δ* double mutant cells (Chen *et al.*, 2005). This is very relevant to our data, and is consistent with our finding that aberrant cytoskeleton regulation could be causal in the extremely slow growth in cold conditions observed in the *smt3* mutant. In this study, we have only investigated the cold stress response in *smt3* mutant cells. However, many other stresses in *S. cerevisiae* cause mass changes in cytoplasmic F actin morphology, such as treatment with HU (Enserink *et al.*, 2006), and heat shock (Yeh and Haarer, 1996). As described in the introduction, global sumoylation is also influenced by many stresses (see section 1.2.3). This data could provide a functional link between sumoylation and the cytoskeleton, for many different stress responses. Thus, it would be of great interest to identify the sumoylated substrates of the cytoskeleton, and identify if the sumoylation status of these components changes during various stress conditions, and then correlate these with a possible response in F actin and tubulin dynamics.

Both the actin cytoskeleton and the sumoylation pathway regulate and interact with many cellular components. Further research into other genetic interactions uncovered in our SGA identified many other pathway components which were linked to cytoskeleton regulation. Of these other potential hits, the chaperonin containing TCP1 (CCT) complex was of particular interest to our study (Figure 4.16). This essential complex is a specialised chaperonin for the folding of actin and tubulin, and is conserved from prokaryotes to eukaryotes. The CCT complex co-ordinates the folding of actin and tubulin, and interestingly, *tcp1-DAmP*, *cct3-DAmP* and *cct8-DAmP* alleles of the Tcp1, Cct3 and Cct8 subunits were genetic suppressors of the slow growth *smt3* defect in our screen (ranked 146/4999, 19/4999 and 14/4999 respectively, see Appendix B). Furthermore, the *cct4-DAmP* allele of the Cct4 subunit was a genetic enhancer in our screen (ranked 39/4999, see Appendix A). Indeed, the Cct3 and Cct8 subunits have been identified as sumoylation targets in both *S. cerevisiae* and human cells in high throughput studies (Table 5.2). Most interestingly, mRNA and protein levels of Tcp1 and Cct2 are regulated by cold temperatures in *S. cerevisiae* (Somer *et al.*, 2002). Investigations of how sumoylation may be regulating this complex in the folding of actin and tubulin in cells, at both 30ºC and cold temperatures, would be of interest to study.

In this chapter we have confirmed that perturbation of the Arp2/3 complex, and of the β-tubulin monomer, suppresses the slow growth phenotype associated with the *smt3* mutant. Thus, we have revealed a previously undiscovered role of sumoylation in the regulation of the cytoskeleton. Furthermore, we have identified a cold sumoylation stress response in *S. cerevisiae*, and therefore perhaps elucidated the molecular basis of cold sensitivity of *smt3* mutant cells.

.,
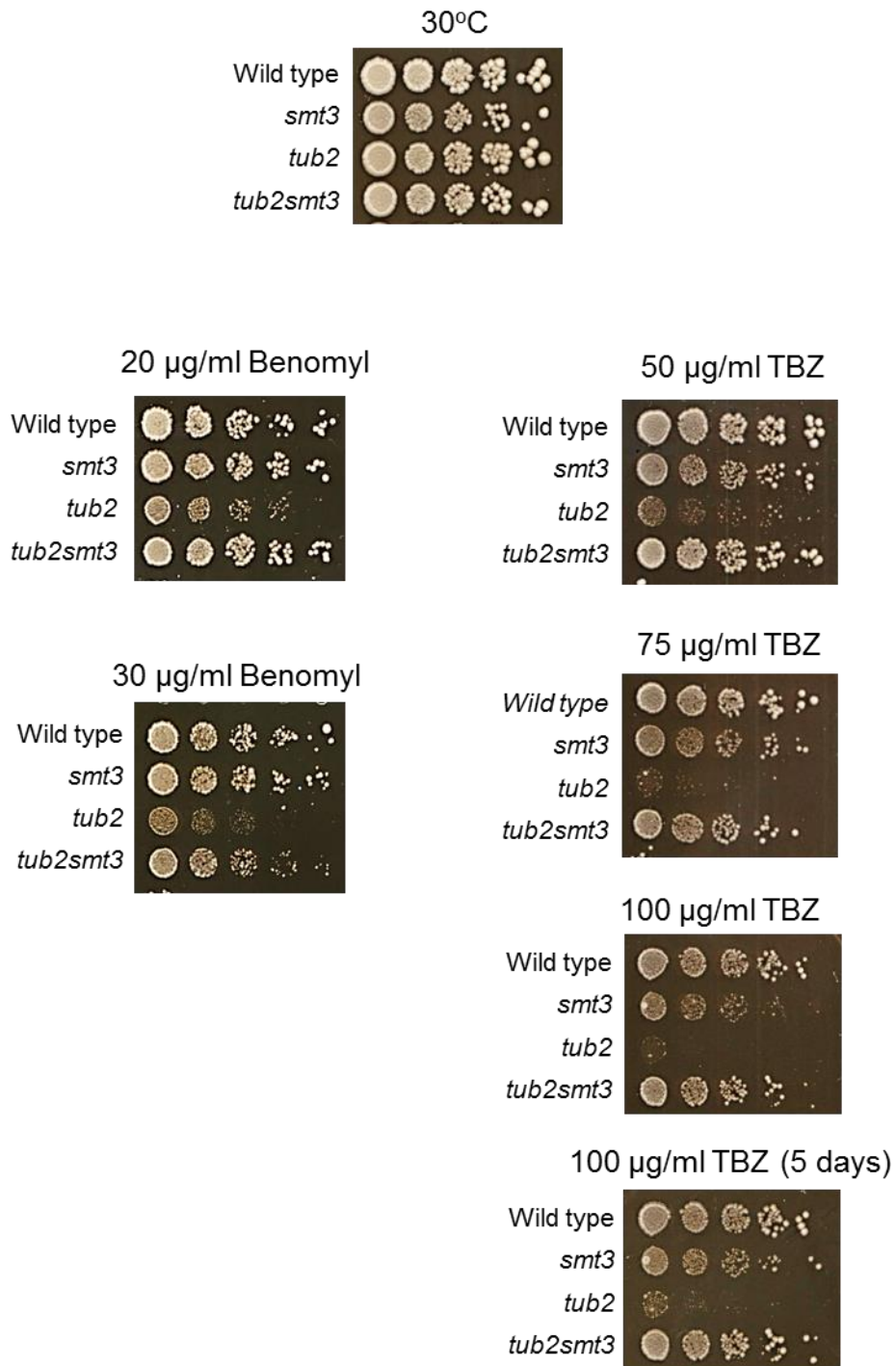
Figure 5.19: *smt3* allele suppresses the sensitivity of *tub2* mutant to spindle depolymerising drugs. 5 fold serial dilutions of mid-log phase growing cells were spotted onto YPD agar plates with the indicated stresses and incubated at 30°C for 3 days.

Chapter Six: Final discussion

Sumoylation is a highly conserved protein modification in eukaryotes, which modifies proteins within many diverse cellular pathways. The process of sumoylation is essential in many model organisms such as *S. cerevisiae*, but is not essential in the fission yeast *S. pombe*. Sumoylation can activate or inhibit the activity of a substrate protein, by changing the subcellular localisation, stability, or binding properties of a sumoylated target. Many proteomic screens have identified sumoylated proteins within many cellular processes, many of which have not been further characterised in the literature. However, it is difficult to identify which modifications of what processes are the most critical for growth. Thus the aim of this project was use high throughput genetic screening to gain insight into the biological functions of sumoylation.

6.1 Summarising Key Findings from this Study

The E2 Ubc9 is the sole conjugating enzyme for identified for the process of sumoylation. However, published data in *S. pombe* has shown that *pmt3Δ* mutants lacking the only SUMO encoding gene in *S. pombe* are viable, while *ubc9Δ* mutants are non-viable (al-Khodairy *et al.*, 1995; Tanaka *et al.*, 1999; Kim *et al.*, 2010; Hayles *et al.*, 2013). This could suggest further roles for Ubc9 outside of sumoylation. In this study we confirmed that both haploid *pmt3Δ* and *ubc9Δ* mutants from the *S. pombe* deletion collection are viable. We attempted to use these strains for SGA analysis but these strains were unable to undergo meiosis, and therefore were not suitable for SGA analysis. However, we have identified a novel role for sumoylation in late cell cycle-regulated gene expression in *S. pombe*. Specifically, we have identified that loss of sumoylation appears to cause an increase in transcription of genes *fkh2+* and *plo1+*. These genes are regulated by two forkhead transcription factors in the cell cycle, Sep1, a positive regulator, and Fkh2, a negative regulator. We found that lack of sumoylation does not affect the subcellular localisation of Fkh2. Furthermore, we have revealed that cells lacking sumoylation are extremely sensitive to over expression of Fkh2, which has previously been shown to be viable in cells lacking Sep1 (Buck *et al.*, 2004). These data taken together suggests that cells lacking sumoylation are exhibiting phenotypes which would be expected from Sep1 hyper activation. The Fkh2 homolog in mammalian cells, FoxM1, was shown to be sumoylated. However, these studies were contradictory in the proposed function of sumoylation, as publications had identified that sumoylation of FoxM1 had both a positive and negative role on FoxM1 function (Myatt *et al.*, 2014; Schimmel *et al.*, 2014). Here, we have provided evidence that sumoylation appears to be negatively regulating late M-phase gene transcription in *S. pombe*.

Due to the complications with the *S. pombe* mutants, we aimed to employ high throughput screening on the yeast *S. cerevisiae*. Thus, we characterised a *smt3* mutant with reduced *SMT3* transcripts and protein levels. We identified that the *smt3* strain was slow growing, and showed extremely slow growth in cold temperatures, as shown previously with the *siz1Δ siz2Δ* double mutant (Johnson and Gupta, 2001; Chen *et al.*, 2005). This strain was used as a query for SGA analysis. Strikingly, by analysing the protein complex components of the resulting positive and negative genetic interactions, we found enrichment for genes involved in the yeast actin and tubulin cytoskeleton (Figure 4.12). In particular, protein complex study highlighted Arp2/3 complex members, which regulate actin branching in yeast, and microtubule proteins, namely the β-tubulin monomer, as suppressors of the slow growth phenotype associated with the *smt3* allele. Previous screens had shown various components of these complexes were sumoylation substrates in both *S. cerevisiae* and mammalian cells, but no study had directly investigated the role of sumoylation in the regulation of the cytoskeleton. Previous studies had indicated that the Arp2/3 complex component, Arc35, interacted with microtubule spindles (Schaerer-Brodbeck and Riezman, 2003), thus we hypothesised that these two pathways were functioning together to rescue the slow growth of the *smt3* mutant.

Therefore, we aimed to firstly determine if the *smt3* mutant had any F actin or tubulin defects. Indeed, we identified that in the *smt3* mutant strain, there appeared to be an increased amount of staining of both F actin, and of tubulin. Furthermore, the *smt3* mutant strain had shorter microtubule spindles, a defect which was observed in an *smt3-331* temperature sensitive mutant (Biggins *et al.*, 2001). Interestingly, misregulation of the actin cytoskeleton by an *arp3* hypomorphic mutant rescued the F actin staining of the *smt3* mutant, but also rescued the increased tubulin staining of *smt3* cells. Furthermore, a *tub2* hypomorphic allele also reduced the staining of tubulin in *smt3* mutant cells, but also the increased F actin staining of *smt3* cells. Interestingly, we identified that misregulation of the Arp2/3 complex, namely by reduction of actin patches, reduced the formation of the microtubule spindle. Therefore, our data suggest that actin, tubulin and sumoylation regulate each other in a tripartite relationship.

As stated above, *smt3* cells grow extremely slowly in conditions below optimum temperature. As microtubules and F actin depolymerise upon cold stress, we hypothesized that these two pathways were connected. Indeed, we identified that upon cold stress in wild type cells, F actin and tubulin undergo a transient polymerisation event. Interestingly, this effect is not observed in *smt3* mutant cells, suggesting a connection between sumoylation and cold induced cytoskeleton dynamics. Indeed, we then identified a novel cold stress induced global sumoylation event in *S. cerevisiae*. The relative timing of F actin and tubulin polymerisation appears to coincide with the induction of global sumoylation, which suggests that these processes might be linked. Therefore, we have identified a novel role for sumoylation in the

regulation of F actin and tubulin dynamics. While these dynamics are also important for growth in optimal conditions, these dynamics could be critical for cell growth during cold conditions.

In conclusion, during the course of this study, we have provided evidence that sumoylation appears to negatively regulate M-phase gene transcription in *S. pombe*. Furthermore, we have identified a novel role for sumoylation in the regulation of both the actin and tubulin cytoskeleton. Furthermore, we have identified a global sumoylation response upon cold stress, and provided possible links for the stress response and regulation of the actin and tubulin cytoskeleton. This data could provide a springboard for much future investigation.

In retrospect with the data collected in the subsequent chapters in *S. cerevisiae*, it is interesting to note that many of the late M-phase genes induced by the PCB wave in *S. pombe* and the equivalent wave in *S. cerevisiae*, encode actin remodelling components. It is interesting to consider in light of the data in the subsequent chapters, that the PCB wave governs the transcription of many genes required for cytokinesis, such as *cdc15*[+] which is essential for actin morphology changes during cytokinesis (Roberts-Galbraith *et al.*, 2009; McDonald *et al.*, 2015). An interesting follow up to this would be to analysis F actin and microtubules in the *S. pombe* mutant. Furthermore, the *pmt3Δ* and *ubc9Δ* haploid mutants were cold sensitive, which could suggest conservation of these mechanisms in these evolutionary divergent yeast, which suggests that these processes are well conserved.

6.2 A Role for Arp2/3 and SUMO in the Nucleus

Previous to this study, the roles of the Arp2/3 complex have mostly been based solely in the cytoplasm, with few studies suggesting otherwise. The presence of Arp2/3 in the nucleus, and even the formation of actin, was controversial. Hence, when we detected changes in the cytoplasmic actin changes reported in this study, we mainly focused on the roles of cytoplasmic actin and tubulin. However, Arp2/3 has been shown to aid transcription from RNA polII promoters (Yoo *et al.*, 2007). Another study implicated Arp3, as well as Tub2, at chromatin. The study investigated proteins which increased chromatin localisation after treatment with the acylating agent MMS in *S. cerevisiae* and fascinatingly, Arp3 and Tub2 were 2 of 33 proteins found to localise to the chromatin after MMS treatment (Kim *et al.*, 2011). Only a subset of these hits were analysed further on the basis of MMS sensitivity. The paper tested the *arp3-DAmP* mutant that was used in this study, and was then disregarded as the *arp3-DAmP* strain did not have MMS sensitivity. Independently, other labs investigating the role of nuclear actin and gene expression have separately connected the Arp2/3 complex, Smt3, and with the nuclear actin remodelling complex, Ino80. Ino80 is a chromatin remodelling complex which uses other actin related proteins Arp4, Arp5 and Arp8 to remodel global nucleosome architecture, with roles in DNA repair and replication, chromosome segregation, transcription

(Conaway and Conaway, 2009). Excitingly, pull down experiments of Ino80 in *S. cerevisiae* recovered Arp3 in these extracts, and many components of this complex are sumoylated (Papamichos-Chronakis M., personal communications). Ino80 mutants have defective transcriptional elongation, and an experiment will be completed in the near future, where the *smt3*, *arp3* and *arp3 smt3* mutants will be assayed using 6-azaracil. Strains which are defective in transcriptional elongation, such as *ino80* mutants, are sensitive to this drug, so this assay will quickly ascertain if the *smt3* mutant has defects in transcription elongation, and if these are elevated in the *arp3 smt3* double mutant.

Along this thread of nuclear actin, some data suggest that the branching of the Arp2/3 complex within the nucleus provides a matrix framework for the nuclear bodies within the nucleus (Feric *et al.*, 2015), which is very interesting considering that sumoylation has such a well characterised role in the regulation of PML nuclear bodies, for example in viral infection (see 1.4.4.1). However, even considering the data discussed above, the existence of nuclear actin is still controversial within the actin field, due to difficulty in the detection of actin within the nucleus. So while this is a very interesting topic for future study, the roles of sumoylation in the regulation of cytosolic actin may need to be elucidated first.

6.3 Implications in Infectious Diseases

There is a growing body of evidence that host sumoylation systems are often targeted upon infection by a wide range of infectious organisms, from pathogenic bacteria to virus infection (see 1.4.4). Many of these modifications have been observed but the molecular mechanism behind them are poorly understood. The bacterial *L. monocytogenes* toxin LLO, which specifically targets Ubc9 for degradation causes a massive decrease in sumoylation (Ribet *et al.*, 2010). The global changes in sumoylation modification status upon LLO has recently been analysed in a large scale proteomics screen (Impens *et al.*, 2014). Interestingly, most sumoylated substrates saw a large decline in sumoylation, but many cytoskeletal proteins were unaffected by the degradation of Ubc9 (Impens *et al.*, 2014). The cells were treated with LLO for a relatively short period of time of 20 minutes, which suggests that the sumoylation of cytoskeletal factors could be fairly stable and are not removed quickly and reconjugated, as must be for those factors which were quickly desumoylated upon Ubc9 degradation (Impens *et al.*, 2014).

Interestingly, localisation of the Arp2/3 complex to the nucleus is observed in times of pathogenic infection, and is thought to aid viral replication (Goley *et al.*, 2006). Another family of proteins, the WASp proteins, which bind and activate the Arp2/3 complex, are involved in this nuclear localisation. Excitingly, WASp has been identified as a sumoylated substrate in helper T cells, which allows the changes in gene transcription required for immune and

inflammatory responses (Sarkar *et al.*, 2015). Independently, another lab has shown evidence that the activation of T lymphocytes promotes a Arp2/3 dependant upregulation of nuclear actin polymerisation, leading to gene transcription changes required for T cell activation (Tsopoulidis., N, personal communications). Again, the role of Arp2/3 in the nucleus and gene transcription is still controversial. However, it is very tempting to speculate that our data are perhaps highlighting an evolutionary conserved link of sumoylation and gene transcription, conserved in T cells in the regulation of immune responses.

The fungal pathogen *C. albicans* is one of the few model organisms studied that does not require sumoylation for growth. However, *smt3Δ* mutants are unable to undergo the morphogeneic switch from the yeast form to the hyphal form. Furthermore, many cytoskeletal proteins were also identified as sumoylated in *C. albicans*, such as Tub1, Cct7 and Mlc1. It is interesting, on reflection of the results in this study that while the Arp2/3 complex is still essential for *C. albicans* hyphal formation (which is unsurprising due to the role of actin in cell morphology), that the Arp2/3 complex is also non-essential for growth. Furthermore, *C. albicans* can even perform endocytosis in the absence of *arp2* or *arp3* (Epp *et al.*, 2010). This could suggest that the essential role of Arp2/3 that is required in other organisms must have an alternate pathway in *C. albicans*. This could provide a hypothesis that the essential function of sumoylation in *S. cerevisiae* is in regulating the Arp2/3 complex, as both sumoylation and the Arp2/3 complex are non-essential in *C. albicans,* while both are essential in *S. cerevisiae.* However, this hypothesis is conflicted with the genetic data in *S. pombe*, as the Arp2/3 pathway is still essential for viability, while sumoylation is dispensible (Hayles *et al.*, 2013).

6.4 Sumoylation and Cold Shock – Protecting Tissues

Recent published data has linked sumoylation to cold stress. It has been shown in ground squirrels that an increase in global sumoylation occurs during hibernation and induced hypothermia (Lee *et al.*, 2014). However, the crucial targets of sumoylation which are allowing survival during cold in these squirrels was not known. We have found evidence that aberrant actin dynamics is correlated with cold sensitivity in the *smt3*, *siz1Δ smt3*, and *siz2Δ smt3* mutants. However, the *ulp1-DAmP* mutant appeared to have normal actin dynamics, which could suggest that desumoylation is required at a different point of the cell cycle, or that these are unlinked. These data could be relevant to the clinical process of therapeutic hypothermia, which has long been used as a neuroprotective measure preventing damage to brain tissue, without the mechanism of action yet understood (during stroke). Our data could provide insight into the functional targets of these processes, as we have shown that tubulin and actin polymerisation is effected by cold, in dynamics which appear to be similar to the conjugation of sumoylation. Interestingly, microtubule depolymerisation is essential for cold resistance, as

shown in plants and *S. cerevisiae* (Bartolo and Carter, 1991). Could it be that the depolymerisation of microtubules and actin provides the signal to the sumoylation machinery to induce the protective cold sumoylation? Many cold sensitive mutants of *S. cerevisiae* and *C. elegans* loose viability after long cold incubations, due to aberrant microtubule structures, leading to lethal cell cycle events (Chan *et al.*, 2010). Fascinatingly, prior incubation of the cold sensitive mutants of *S. cerevisiae* and *C. elegans* in hypoxic conditions rescued the subsequent cold lethality. Could sumoylation could be preventing this occurrence? No data thus far has tied together the hypothermic and hypoxic global sumoylation to a mechanism, and it is tempting to speculate that the link could be through microtubule depolymerisation. During the course of this study, a paper of hypothermia in mammalian cells has shown that the cooling induced sumoylation of ribosome assembly factor EXOSC10, disrupts ribosome biogenesis during cold induction (Knight *et al.*, 2016). Interestingly, many ribosome-related genes were also highlighted in this screen, and of importance, the EXOSC10 homolog in *S. cerevisiae*, Rrp6, was a suppressor in our screen, ranked 121/4999 genes (p=0.02). Unfortunately, due to limited time and resources, and the pool of data already implicating SUMO in ribosome biogenesis, the ribosomal hits were not analysed at length throughout the study, as we selected the cytoskeletal story to follow up from the screen. However, this does provide some validation that our screen appears to be identifying sumoylation events that are conserved in higher eukaryotes, and indeed within the context of cold stress.

6.5 Outstanding Questions

Due to the nature of this project, many more new questions can be proposed. In the short term, mutants with knock outs of candidate lysines within the Arp2/3 and CCT complex will need to be constructed to identify how sumoylation is effecting the tubulin and actin cytoskeleton. These mutants could then be used to identify if phenotypes associated with the *smt3* strain can be recreated with these unsumoylatable mutants, such as the increased actin and tubulin staining or cold sensitivity. Unfortunately, due to the essentiality of these genes, and the number of components that are sumoylated, this could be time consuming. Therefore, perhaps a directed approach to identify which targets are differentially sumoylated in wild type compared to the *smt3* mutant cells could help give an overview of the altered SUMO landscape in the *smt3* mutant, and indicate suitable targets for further analysis. Further to identifying the sumoylated substrates would be identifying when and where this sumoylation event takes place. Therefore, the modification status of these proteins could be studied throughout the cell cycle, or during cold shock. It would be interesting to then assess how the subcellular localisation and stability of these proteins were affected by the modification.

Secondly to this would be investigating what is causing this apparent increase in staining of F actin and tubulin. Proteins which are known to be involved in the assembly and disassembly

of actin and tubulin filaments, and factors which promote the bundling of filaments which could be leading to the appearance of increased staining due to thicker, denser filaments should be investigated in the *smt3* mutant. Genes which govern actin crosslinking, the formins and myosins, are either not present in the screen or are functionally redundant, so would require the knockouts of both genes two properly investigate. *In vitro* Arp2/3 actin polymerisation assays have been used on yeast whole cell extracts by the polymerisation of actin on WASp coated beads. This could be very interesting to study in extracts from *S. cerevisiae* expressing varying levels of Smt3 (Michelot *et al.*, 2010). Furthermore, use of characterised actin tubulin mutants with known assembly or disassembly defects could be used to properly identify how *smt3* is regulating these processes. Finally, all the data collected thus far has been using fixed cells. As the processes of both sumoylation and cytoskeleton regulation are dynamic, it would be extremely interesting to use live staining to visualise how these structures are regulated *in vivo*. How tubulin and actin behave in wild type *S. cerevisiae* cells is well characterised, by use of Tub2 fused to green fluorescent protein (GFP), or a 17-amino acid GFP peptide actin stain, Lifeact. These experiments are critical in our understanding of the role of sumoylation in these complexes. Finally, it would be interesting to identify if either the essentiality of *SMT3* could be rescued by the *arp3-DAmP* mutant, or the loss of Arp2/3 function could by rescued by the *smt3-DAmP*. This was attempted during the project but due to time constraints this was not completed. Future studies would involve identifying if regulation of the cytoskeleton by sumoylation is indeed conserved in higher eukaryotes. siRNA knockdowns of Ubc9 in mammalian cell lines has been used previously to lower global conjugation levels, allowing the study of both SUMO-1 and SUMO-2/3 conjugation simultaneously for initial experiments.

6.6 Concluding Remarks

Although sumoylated cytoskeletal proteins have been identified in large proteomic screens repeatedly, there have been no studies thus far to examine the role of Smt3 in regulating these processes. In this study we have presented that indeed, there is a genetic link between the actin and tubulin cytoskeleton, which appears to be negatively regulated by sumoylation. As described above, due to the wide range of cellular processes that both sumoylation and the cytoskeleton play roles in, there is a wide array of potential avenues for future work to tease out how these two very complex processes are functioning. With the surprisingly low amount of information regarding actin dynamics *in vivo*, it is crucial that we identify how sumoylation is regulating actin, as this has implications in many disease states.

Appendix A

Top 5% of enhancers of *smt3* SGA. Systematic name provided, and standard gene name on SGD of the gene at time of print are shown. Genes were ranked by descending GIS, and top 249/4999 (5%) genes shown. Query Fitness is average fitness measure from the experimental *smt3 yfgΔ* crosses, and Control Fitness is the average fitness measures of the *yfgΔ* single mutant from background control crosses. Query SE and Control SE are the standard error of the fitness measurements from all replicate crosses. The number of times the gene appears in the array, and therefore the number of replicate crosses completed, is shown in No. Array. P value calculated from the control and query finesses, and the query and control fitness SE.

Rank (/4999)	Systematic Name	Standard Name	GIS	Query Fitness	Control Fitness	Query SE	Control SE	No. Array	P Value
1	YLR335W	*NUP2*	-91051.1	4393.56	153661	3073.41	1223.15	4	3.82E-05
2	YPR023C	*EAF3*	-87865.6	5713.99	150658	5636.53	1115.23	4	0.000497
3	YOR039W	*CKB2*	-84588.9	13074.5	157233	131.497	1115.58	4	5.56E-07
4	YNL038W	*GPI15*	-82799.5	8434.1	146881	1485	1873.85	4	2.09E-08
5	YMR179W	*SPT21*	-81228.9	6417.44	141106	3382.94	541.932	4	0.00014
6	YDR146C	*SWI5*	-80681.9	10973.8	147561	5339.89	1016.53	4	0.000552
7	YFR005C	*SAD1*	-80277	0	129242	0	6726.02	4	0.000308
8	YKL216W	*URA1*	-79568	16156.3	154111	14243.7	2360.49	4	0.010871
9	YLR317W	*YLR317W*	-79258.6	20323.6	160322	7333.31	2154.42	4	0.001329
10	YLR015W	*BRE2*	-79211.9	13883.4	149879	2901.29	1573.66	4	2.73E-05
11	YBR228W	*SLX1*	-78504.1	23558.9	164316	865.699	1024.1	4	1.93E-09
12	YML098W	*TAF13*	-77599	799.733	126218	612.328	12153.9	4	0.001873
13	YMR198W	*CIK1*	-77244.3	8705.89	138375	610.451	1072.6	4	1.99E-10
14	YJL168C	*SET2*	-76560.9	17518.3	151463	1634.27	1869.62	4	8.56E-08
15	YPL143W	*RPL33A*	-75798.1	13546.1	143840	6291.7	4261.66	4	0.000359
16	YML031W	*NDC1*	-75750	15.4991	121979	15.4991	15511	4	0.004286
17	YDR467C	*YDR467C*	-75647.2	24797.8	161711	12180.9	1591.99	4	0.008172

18	YLR373C	VID22	-75628.7	17151.5	149371	342.015	1005.15	4	4.69E-09
19	YDL190C	UFD2	-75349.2	20582.1	154444	3324.96	1692.37	4	6.19E-05
20	YLR234W	TOP3	-75091	7864.9	133555	552.646	1023.64	4	1.93E-10
21	YOR144C	ELG1	-75075.1	22993.9	157886	1650.41	1001.79	4	2.83E-06
22	YGL019W	CKB1	-74658.7	21557.5	154903	11706.3	2116.5	4	0.00737
23	YDR249C	YDR249C	-73890.9	19655.4	150605	5185.37	239.307	4	0.000743
24	YLR283W	YLR283W	-73750.8	25693.2	160100	9905.51	697.506	4	0.004964
25	YGR135W	PRE9	-73287.4	16511.5	144572	1540.35	1109.16	4	1.11E-06
26	YLR167W	RPS31	-73167.2	21750.7	152813	2510.03	1761.58	4	9.35E-06
27	YIL147C	SLN1	-73133.7	47.7955	117818	47.7955	10628	4	0.001575
28	YLR418C	CDC73	-73056.5	9515.71	132937	2742.62	1095.62	4	5.42E-05
29	YNL171C	YNL171C	-72909.4	18459	147098	1256.38	2138.52	4	1.74E-08
30	YPR144C	NOC4	-72731.8	18279.9	146524	4119.17	1704.2	4	0.000206
31	YPL010W	RET3	-72369.4	-7.24122	116499	16.8029	25875.7	4	0.020457
32	YGR097W	ASK10	-71934.8	1677.47	118512	1677.47	8618.96	4	0.000402
33	YLR135W	SLX4	-71759	25398.9	156419	2139.97	2635.13	4	3.98E-07
34	YML092C	PRE8	-71458.8	24794.4	154963	9282.61	2568.49	4	0.003879
35	YDR477W	SNF1	-71310.1	28605.9	160860	734.929	1589.31	4	6.26E-09
36	YLR320W	MMS22	-71300.1	9596.66	130240	1766.6	741.821	4	1.22E-05
37	YMR190C	SGS1	-71149.6	15732.5	139876	2917.47	1338	4	5.85E-05
38	YGL035C	MIG1	-71115.5	27862.1	159349	2706.26	2467.66	4	4.88E-06
39	YDL143W	CCT4	-71089.4	-0.37781	114450	0.377812	19275.1	4	0.009549
40	YJL123C	MTC1	-70387	4304.21	120249	4227.47	40092	4	0.064371
41	YOL004W	SIN3	-70255.2	19661.1	144761	1377.73	1071.03	4	5.53E-07
42	YDR386W	MUS81	-70137.4	26296.4	155253	723.57	759.246	4	3.24E-09
43	YML113W	DAT1	-69941.5	27687.7	157178	3723.31	841.367	4	0.000267

44	YMR165C	PAH1	-69634.9	20627.2	145317	914.65	5938.54	4	0.000172
45	YDR476C	YDR476C	-69596.9	27104.6	155684	9468.02	1249.78	4	0.005021
46	YHR031C	RRM3	-69180.1	33107.1	164677	4434.23	2729.31	4	0.000162
47	YML103C	NUP188	-69131	27395.7	155403	6208.89	1102.69	4	0.001416
48	YDL203C	ACK1	-69031.7	24081.9	149908	6354.84	901.688	4	0.001575
49	YBR100W	YBR100W	-68810.4	21687.5	145697	683.109	8224.36	4	0.000758
50	YDR155C	CPR1	-67704.6	26739.4	152050	5958.12	1456.1	4	0.001226
51	YIL062C	ARC15	-67672.3	27907.4	153878	4663.38	1802.87	8	7.83E-07
52	YMR075W	RCO1	-67460.2	29077.5	155421	2873.68	1525.83	4	4.97E-05
53	YNL218W	MGS1	-67204.1	33720.8	162484	5113.18	1732.1	4	0.000658
54	YER095W	RAD51	-67015.6	27381.5	151974	3024.7	655.073	4	0.000163
55	YOR191W	RIS1	-66841.8	32512.7	159956	3150.95	2181.36	4	3.56E-05
56	YBR247C	ENP1	-66271.5	29178.7	153670	14392.9	580.593	4	0.019226
57	YDR161W	YDR161W	-65993.3	29956.8	154475	6708.12	2446.11	4	0.001587
58	YKL046C	DCW1	-65761.8	32456.4	158126	10673.3	647.485	4	0.008551
59	YLR066W	SPC3	-65689.2	0	105756	0	7944.66	4	0.000916
60	YJR074W	MOG1	-65462.2	22892.8	142247	5619.21	1555.84	4	0.001081
61	YPR032W	SRO7	-64956.2	32427.8	156783	6841.42	3257.21	4	0.001436
62	YBR094W	PBY1	-64893.1	29939.4	152675	17221.01	1273.09	4	2.58E-06
63	YJL115W	ASF1	-64876	17948.8	133344	13114.31	447.835	4	8.88E-06
64	YDR289C	RTT103	-64834.9	23787.7	142678	6826.66	1297.55	4	0.002255
65	YNL250W	RAD50	-64555	22020.5	139382	2341.41	2354	24	2.18E-24
66	YNL140C	YNL140C	-64510.1	30420.3	152833	7661.07	3910.64	4	0.00202
67	YOR156C	NFI1	-63788.4	33876.1	157235	2162.86	1555.92	4	8.09E-06
68	YMR224C	MRE11	-63609.4	15457.2	127293	654.464	1334.49	28	3.11E-49
69	YBR082C	UBC4	-62812.3	29111.8	147993	1174.56	1075.9	8	4.48E-14
70	YMR067C	UBX4	-62629.3	39015.8	163643	9576.04	1107.57	4	0.007092

71	YBL079W	NUP170	-62541.1	32043.8	152277	892.723	1846.59	4	2.44E-08
72	YBR098W	MMS4	-62423.9	32088.9	152161	357.325	1403.86	4	3.31E-07
73	YDR494W	RSM28	-62417.5	36487.4	159232	5625.87	1528.62	4	0.001268
74	YAR002W	NUP60	-62286.7	32113.8	151980	803.202	1306.09	4	2.55E-09
75	YNL291C	MID1	-62182.4	27839.6	144931	11871.9	765.493	4	0.013467
76	YNL151C	RPC31	-61771.8	34888.9	155619	12030.6	822.577	4	0.014219
77	YLR235C	YLR235C	-61615.4	22663.3	135684	1356.46	995.029	4	1.23E-06
78	YNR026C	SEC12	-61073.8	2680.46	102641	2679.35	9920.74	4	0.000728
79	YML102W	CAC2	-61035.9	31403.6	148823	3640.98	575.984	4	0.00042
80	YDR499W	LCD1	-60897.8	29513.9	145558	22206	2438.04	4	0.070845
81	YGL263W	COS12	-60673.4	37804.9	158545	12840.3	923.526	4	0.017846
82	YCL061C	MRC1	-60282	29140.9	143966	4404.94	1259.9	4	0.000642
83	YJL084C	ALY2	-60039	34153	151644	14890.6	996.334	4	0.027315
84	YGL244W	RTF1	-59944.7	18219.7	125841	184.846	11601.6	4	0.003626
85	YMR301C	ATM1	-59938.9	34298.8	151718	11751.1	2320.19	4	0.013841
86	YPR179C	HDA3	-59880	34435.1	151842	19961.8	5109.04	4	0.055875
87	YGL011C	SCL1	-59859.1	28215.7	141796	3071.16	2724.43	4	2.19E-05
88	YHR146W	CRP1	-59230.9	40600.1	160723	8274.31	2041.81	4	0.004982
89	YNL123W	NMA111	-59195.2	40003.9	159706	4922.5	521.89	4	0.001195
90	YDR320C	SWA2	-59175.9	33579.5	149331	11150	1036.14	4	0.012902
91	YBR146W	MRPS9	-59152.5	28278.1	140759	1057.08	4587.47	4	5.90E-05
92	YOR123C	LEO1	-59142.6	29235	142283	982.308	1269.52	4	1.24E-08
93	YGL092W	NUP145	-59136.5	130.166	95416.2	125.851	19929.1	4	0.017426
94	YJL092W	SRS2	-59128.2	33167	148591	1219.57	7000.77	4	0.000447
95	YMR063W	RIM9	-59116.4	36877	154544	3184.77	1664.35	4	0.00012
96	YDR363W-A	SEM1	-58729.5	31424.6	145143	1960.62	1374.86	4	8.39E-06
97	YNL206C	RTT106	-58511.6	33814.9	148641	4005.82	1187.16	4	0.000513

98	YMR075C-A	YMR075C-A	-58355.9	32931.1	146967	1314.61	1500.27	4	1.16E-07
99	YDR049W	VMS1	-58287	22155.7	129509	4328.55	474.094	4	0.000851
100	YLR198C	YLR198C	-57905.3	0	93224.6	0	22732.9	4	0.026236
101	YPL242C	IQG1	-57792	33249.9	146573	9228.06	1367.87	4	0.007911
102	YDR531W	CAB1	-57478.1	44057.5	163467	7686.52	1040.94	4	0.004767
103	YNL254C	RTC4	-57420.9	37528.6	152864	6969.52	704.69	4	0.003657
104	YDL074C	BRE1	-57175.5	25296.3	132775	712.308	2190.02	8	1.48E-12
105	YKR055W	RHO4	-57118.5	38060.9	153234	6547.27	2252.14	4	0.002408
106	YPR103W	PRE2	-57090	37147.9	151718	3932.19	2154.64	8	3.78E-07
107	YBR175W	SWD3	-56877.1	32976	144659	502.037	2341.39	4	6.79E-06
108	YFR010W	UBP6	-56713.3	24393.5	130578	3747.66	310.948	4	0.000611
109	YHR134W	WSS1	-56534.8	34511	146579	5625.15	1711.69	4	0.001641
110	YJR126C	VPS70	-56229.4	50526.1	171871	10590	986.214	4	0.012885
111	YBR174C	YBR174C	-56143.9	31964.1	141849	1088.76	1971.37	4	4.93E-08
112	YGL045W	RIM8	-55997.2	42500	158575	9741.86	1328.43	4	0.01016
113	YAL024C	LTE1	-55929.3	36938.4	149512	2737.57	336.606	4	0.00024
114	YPR135W	CTF4	-55917.4	25536.9	131137	1583.13	2271.11	4	2.29E-07
115	YHR200W	RPN10	-55876.8	34326.8	145223	3245.67	3931.96	4	1.63E-05
116	YHR030C	SLT2	-55418.3	37903	150242	23232.3	2292.26	4	0.09689
117	YGL250W	RMR1	-55393.1	37536.6	149612	9508.08	1039.77	4	0.009883
118	YBR099C	YBR099C	-55344.4	38636.7	151305	1145.21	397.767	4	9.26E-06
119	YMR048W	CSM3	-55311.2	41274.1	155497	5350.93	2749.82	4	0.000984
120	YDR183W	PLP1	-55285.1	39018	151823	2593.47	1179.3	4	9.45E-05
121	YLR127C	APC2	-55274.2	4124.21	95628.3	4124.21	19262	4	0.014203
122	YDR492W	IZH1	-55227.6	48323.9	166713	2234.42	1165.54	4	4.30E-05
123	YPL144W	POC4	-55173.4	33286.2	142415	12252.8	558.345	4	0.020407
124	YOR124C	UBP2	-55110.4	43122.5	158150	5156.47	1215.81	4	0.001497

125	YPL024W	RMI1	-54880.6	34554.2	143985	3008.29	1289.59	4	0.000176
126	YNL021W	HDA1	-54793.3	33586.4	142287	4967.34	1503.2	4	0.001229
127	YIL076W	SEC28	-54392.5	9819.89	103379	1090.2	14500.8	4	0.008556
128	YIL086C	YIL086C	-54222.6	37961.5	148412	17090.6	1156.47	4	0.050242
129	YPL238C	YPL238C	-54187.9	81.8229	87371.4	81.8229	21433	4	0.026754
130	YNL288W	CAF40	-53970.3	49100.8	165939	8555.88	2285.32	4	0.007131
131	YOR224C	RPB8	-53761.1	1.08122	86554.4	4.92353	33711	4	0.082673
132	YML102C-A	YML102C-A	-53627.4	36669.2	145373	1249.96	3006.55	4	1.51E-06
133	YDL002C	NHP10	-53594.5	37574.7	146778	2328.79	6193.37	4	7.94E-05
134	YFR052W	RPN12	-53521.2	49452.9	165783	4360.42	1055.14	8	4.13E-06
135	YKR094C	RPL40B	-53512.6	39740.5	150133	14968.2	1576.45	4	0.037106
136	YOL147C	PEX11	-53119.8	39685	149411	11616.4	1358.28	4	0.019319
137	YJL204C	RCY1	-52927.9	36327.1	143696	13043.8	1328.84	4	0.026712
138	YDL006W	PTC1	-52858.2	24199.2	124058	10701.95	7304.81	4	0.00089
139	YDR059C	UBC5	-52775.7	42499	153387	5093.93	700.422	4	0.00182
140	YPL218W	SAR1	-52763.9	1488.79	87344	1506.86	2877.43	4	6.70E-07
141	YDL226C	GCS1	-52713.8	40053.5	149351	1667.51	827.466	4	2.00E-05
142	YBR170C	NPL4	-52502.9	35385.6	141496	7111.81	1063.24	4	0.004908
143	YIL137C	TMA108	-52428.2	47296.1	160551	6436.31	1045.49	4	0.003645
144	YLL042C	ATG10	-52406.6	45062.7	156921	6798.34	4144.4	4	0.002285
145	YPL057C	SUR1	-52338.7	39043.3	147120	8026.65	968.276	4	0.007138
146	YDR496C	PUF6	-52043	40720.4	149344	2925.32	790.375	28	8.07E-17
147	YFR035C	YFR035C	-51839.2	51917.5	167043	8210.58	4371.52	4	0.005201
148	YJL032W	YJL032W	-51769.1	897.07	84789.8	897.07	28704.4	4	0.062126
149	YML027W	YOX1	-51757	49400	162857	6355.46	2980.88	4	0.002444
150	YHR004C	NEM1	-51625.7	47170.8	159057	9487.22	2283.43	4	0.011219
151	YDR167W	TAF10	-51608.5	75.4364	83208.5	73.551	28643.8	4	0.062465

152	YNR054C	ESF2	-51554.9	46907.4	158519	8034.33	2418.05	4	0.006564
153	YLL031C	GPI13	-51522.2	46820.1	158326	9576.12	1530.94	4	0.012124
154	YDR369C	XRS2	-51503.6	35574.7	140192	1835.04	1648.05	4	3.83E-06
155	YLR021W	IRC25	-51487.1	35505.5	140054	1561.73	882.912	4	1.21E-05
156	YLR381W	CTF3	-51450	46735	158073	10724	1838.6	4	0.016625
157	YGR040W	KSS1	-51275.8	48745	161028	12831.6	1013.53	4	0.027919
158	YMR232W	FUS2	-51155.2	42425.6	150660	14993.6	1090.59	4	0.041942
159	YMR309C	NIP1	-51045.7	22.6482	82217.4	24.5285	32669.4	4	0.086516
160	YML052W	SUR7	-50989.1	41328.2	148626	15773.4	365.026	4	0.048105
161	YML062C	MFT1	-50837.2	38536.7	143887	3346.11	1504.47	4	0.000308
162	YHR025W	THR1	-50825.5	52950.2	167073	20513	2745.33	4	0.088971
163	YNR006W	VPS27	-50639.6	50107	162197	8200.7	975.255	4	0.008347
164	YKL214C	YRA2	-50602.3	38809.3	143948	3493.89	4297.01	4	4.09E-05
165	YJL033W	HCA4	-50467.2	49268.2	160569	8402.66	857.125	4	0.009089
166	YNL307C	MCK1	-50448.8	41967.3	148785	3129.76	453.673	4	0.00048
167	YDR318W	MCM21	-50411.2	50225.4	162020	3282.2	992.367	4	0.000432
168	YHL027W	RIM101	-50401.4	47731.7	157989	9180.88	2604.75	4	0.010601
169	YJL097W	PHS1	-50308.3	50609.2	162472	11032.4	1732.93	4	0.019228
170	YHR129C	ARP1	-50288.5	31571.9	131791	9214.23	1185.75	4	0.011797
171	YDR487C	RIB3	-50266.4	53821.8	167577	4089.45	2718.47	4	0.000345
172	YPR173C	VPS4	-50245.3	38411.1	142732	1782.68	1223.37	4	1.17E-05
173	YER056C	FCY2	-50184.8	45393.4	153876	13457.6	1505.23	4	0.033255
174	YDR186C	YDR186C	-50179.7	44106.7	151796	5372.85	962.056	4	0.002396
175	YGR025W	YGR025W	-49944	53373.2	166335	21964.4	1512.14	4	0.107426
176	YMR153W	NUP53	-49835	46475.4	155055	9956.93	743.171	4	0.015238
177	YDR338C	YDR338C	-49668	49321.9	159369	5573.59	2160.62	4	0.002096
178	YDR460W	TFB3	-49646.7	53337.9	165800	7459.14	1045.68	4	0.006666

179	YML033W	YML033W	-49477.8	45406	152758	6652.44	1808.74	4	0.00433
180	YDR147W	EKI1	-49430.3	45446.9	152747	4203.9	1374.27	4	0.000962
181	YOR103C	OST2	-49406.1	22.3787	79577.3	22.3787	28535.5	4	0.068564
182	YLR449W	FPR4	-49051.2	45107.1	151590	12223.5	1549.82	4	0.027364
183	YNL062C	GCD10	-49042.5	54247.6	166292	13745.8	1003.59	4	0.03746
184	YER116C	SLX8	-48978	28768.5	125168	549.44	1178.78	4	9.19E-09
185	YNR062C	YNR062C	-48871.3	43096.8	148064	13081.5	1481.03	4	0.033091
186	YML076C	WAR1	-48854.2	48212.2	156272	5493.25	1154.56	4	0.002693
187	YGL221C	NIF3	-48727.1	49197.6	157654	12771.5	1040.48	4	0.031496
188	YNR005C	YNR005C	-48685.5	46914.7	153911	3383.24	1816.29	4	0.000285
189	YDL213C	NOP6	-48489.7	44852.3	150276	7057.6	1550.91	4	0.005764
190	YBR109C	CMD1	-48489	8210.26	91282.8	8212.32	7358.1	4	0.004293
191	YLL005C	SPO75	-48420	46447.1	152731	10809.4	1115.94	4	0.02055
192	YDR154C	YDR154C	-48405.1	45655.4	151432	4553.16	1046.45	4	0.001533
193	YOR275C	RIM20	-48342.7	49409.5	157376	6740.25	1059.49	4	0.005315
194	YMR274C	RCE1	-48205.5	57818	170692	20271.1	1547.75	4	0.097639
195	YDL192W	ARF1	-48003.4	46668.4	152417	3778.56	1916.57	4	0.000486
196	YDL034W	YDL034W	-47872.9	53161.4	162660	4926.88	2577.85	4	0.001196
197	YMR247C	RKR1	-47676.5	46928.1	152308	3218.02	2288.69	4	0.000141
198	YOL078W	AVO1	-47616.7	816.799	77975.5	818.046	26092.3	4	0.060409
199	YML041C	VPS71	-47541.7	59347.5	172086	16557	565.067	4	0.063942
200	YMR129W	POM152	-47519.9	52472.4	160982	17860.8	3150.13	4	0.075437
201	YGR184C	UBR1	-47480.6	49451.3	156055	11931.2	2992.31	4	0.026855
202	YGL136C	MRM2	-47428.3	7959.02	89170.7	5039.74	25476	4	0.052182
203	YLL050C	COF1	-47260.3	0	76086.7	0	26298.1	4	0.062847
204	YGL046W	YGL046W	-47249.7	47791.9	153012	9669.6	1425.16	4	0.01595
205	YKR091W	SRL3	-47124.7	49569.2	155672	39268.5	1164.38	4	0.316256

206	YPL055C	LGE1	-47101.8	41812.4	143147	2332.79	2213.3	4	1.45E-05
207	YIL146C	ATG32	-47034.8	47929.6	152888	10618.4	1158.25	4	0.021101
208	YDL206W	YDL206W	-46984.4	51170.7	158025	8344.27	1203.38	4	0.010735
209	YJR094C	IME1	-46812.7	42344.9	143539	12140.8	4782.85	4	0.027324
210	YML070W	DAK1	-46779.1	47257.8	151394	2452.66	1004.32	4	0.000161
211	YML007W	YAP1	-46730.2	48402	153158	12048.4	967.053	4	0.030182
212	YGL124C	MON1	-46327.8	48773.2	153108	11993.2	6603	4	0.024889
213	YPR178W	PRP4	-46324.3	45707.9	148167	14054.7	1112.71	8	0.013175
214	YIL025C	YIL025C	-46240.9	49664.4	154403	4040.59	2819.33	4	0.000415
215	YPL017C	IRC15	-45872	49850.8	154109	5946.43	3021.3	4	0.002739
216	YDR284C	DPP1	-45860.4	47375	150104	3410.79	1486.26	4	0.000485
217	YJR137C	ECM17	-45727.2	54606.8	161532	8327.48	2274.12	4	0.01068
218	YKR064W	OAF3	-45719.9	54742.3	161739	20322.8	1541.02	4	0.109832
219	YML034W	SRC1	-45312.5	48833	151569	4741.39	720.714	4	0.002289
220	YDL210W	UGA4	-45211.9	48927.8	151560	2911.47	1137.58	4	0.000337
221	YNL297C	MON2	-45206.8	50536.2	154141	10495.8	1402.73	4	0.022614
222	YMR263W	SAP30	-45062.1	50653.6	154097	5539.86	3313.19	4	0.001923
223	YHR209W	CRG1	-45053.9	51888.9	156073	11295.4	1336.01	4	0.027857
224	YMR060C	SAM37	-45000.9	51480.6	155330	8886.13	1294.52	4	0.014452
225	YDR394W	RPT3	-44993.6	48765.7	150948	4122.58	1523.57	8	6.88E-06
226	YNL336W	COS1	-44964.5	56310.6	163048	16965.5	4317.38	4	0.07526
227	YEL037C	RAD23	-44960.5	49369.6	151866	4585.08	926.943	4	0.002023
228	YER111C	SWI4	-44874.7	56871.7	163806	6025.91	979.074	4	0.004746
229	YGL016W	KAP122	-44846.9	45233.7	145025	5141.36	829.572	4	0.00298
230	YLR342W	FKS1	-44618	48412.8	149775	3595.73	3869.38	4	0.000112
231	YNL294C	RIM21	-44596.2	49266.1	151113	7562.86	4790.64	4	0.005751
232	YDR497C	ITR1	-44446.3	50877.3	153466	2671.26	770.794	4	0.000345

233	YNR074C	AIF1	-44396.1	49875.8	151773	7856.1	676.277	4	0.010844
234	YGR263C	SAY1	-44320.5	65720.3	177160	10736.7	3089.72	4	0.023879
235	YDR469W	SDC1	-44305.2	44892.7	143604	7136.38	1080.73	4	0.008098
236	YFR030W	MET10	-44287.7	54596.1	159198	26073.8	383.616	4	0.187966
237	YDR363W	ESC2	-44132	44747.1	143091	4352.09	790.925	4	0.001868
238	YGR052W	FMP48	-44025.2	56341.1	161585	19758.5	1322.36	4	0.112081
239	YCL010C	SGF29	-43923.8	50968.8	152772	2396.77	2271.32	4	2.32E-05
240	YBR275C	RIF1	-43877.1	53728.4	157140	4060.07	4778.69	4	0.000201
241	YDL201W	TRM8	-43772.7	52833.7	155531	16649.2	2515.93	4	0.077748
242	YPL100W	ATG21	-43709.5	49533.2	150116	4677.28	1025.54	4	0.002297
243	YJL049W	YJL049W	-43426.5	52238.2	154015	3521.77	1216	4	0.000796
244	YER181C	YER181C	-43329.1	55262.9	158728	7005.63	1019.88	4	0.008211
245	YJR140C	HIR3	-43318.3	48511.9	147842	7815.68	1628.06	4	0.010863
246	YDR525W-A	SNA2	-43316.1	53596.7	156025	4365.16	1742.53	4	0.001447
247	YMR139W	RIM11	-43292.1	52264.7	153842	14073.1	1404.76	4	0.054002
248	YMR216C	SKY1	-43195.8	49157	148683	4371.09	1353.96	4	0.001715
249	YDR165W	TRM82	-43102.4	50506.5	150705	1495.23	1301.26	4	3.91E-06

Appendix B

Top 5% of suppressors of *smt3* allele from SGA analysis. Systematic name provided, and standard gene name on SGD of the gene at time of print are shown. Genes were ranked by ascending GIS, and top 249/4999 (5%) genes shown. Query Fitness is average fitness measure from the experimental *smt3 yfgΔ* crosses, and Control Fitness is the average fitness measures of the *yfgΔ* single mutant from background control crosses. Query SE and Control SE are the standard error of the fitness measurements from all replicate crosses. The number of times the gene appears in the array, and therefore the number of replicate crosses completed, is shown in No. Array. P value calculated from the control and query finesses, and the query and control fitness SE.

Rank (/4999)	Systematic Name	Standard Name	GIS	Query Fitness	Control Fitness	Query SE	Control SE	No. Array	P Value
1	YMR080C	*NAM7*	267324	363945	155555	10787.6	2184.93	4	0.000119
2	YMR260C	*TIF11*	244789	333340	142562	26861.1	1040.99	4	0.002782
3	YLR398C	*SKI2*	207980	297649	144363	13764.9	861.607	4	0.00062
4	YFL037W	*TUB2*	203871	295119	146904	34706.1	1846.1	4	0.009797
5	YFL022C	*FRS2*	201692	295689	151329	10816.1	2981.26	4	0.000248
6	YDL029W	*ARP2*	194469	285131	145960	19100.1	3943.89	8	1.61E-05
7	YJR065C	*ARP3*	194441	286228	147772	13923.3	2590.94	8	1.89E-06
8	YNL131W	*TOM22*	193254	283384	145104	30209.2	592.942	4	0.007731
9	YHR077C	*NMD2*	192720	287518	152621	9747.13	1182.1	28	1.11E-17
10	YDR404C	*RPB7*	184803	282915	157955	20364.1	1890	8	3.92E-05
11	YHR186C	*KOG1*	182388	269924	140928	21753.5	849.745	4	0.003546
12	YFL001W	*DEG1*	179202	265649	139174	17151.6	1564.09	4	0.001828
13	YKL122C	*SRP21*	178711	229953	82495.5	92336.2	30410.7	4	0.14708
14	YJL008C	*CCT8*	175994	272687	155671	14522.6	1823	4	0.001151
15	YDR045C	*RPC11*	169247	260567	147021	28156.7	2130.68	4	0.009138
16	YNL113W	*RPC19*	167082	258461	147115	30578	1364.8	4	0.012012

17	YDR429C	TIF35	165954	249442	134412	819 3.18	365 2.52	4	0.000 116
18	YGL173C	XRN1	164140	243599	127924	374 77.8	170 0.67	4	0.021 986
19	YJL014W	CCT3	163740	256635	149556	143 53.9	752. 502	4	0.001 434
20	YNL244C	SUI1	160835	251321	145677	436 67.9	227 1.02	4	0.034 607
21	YDL152W	YDL152 W	157810	240701	133450	106 49.6	340 1.38	4	0.000 467
22	YML121W	GTR1	153928	243525	144246	219 94	115 5.88	4	0.005 957
23	YHL025W	SNF6	149586	219604	112724	846 09.5	294 3.1	4	0.175 213
24	YNR035C	ARC35	146570	239510	149628	306 28.4	163 2.55	8	0.001 994
25	YGR072 W	UPF3	135895	231111	153292	434 53.2	131 9.05	4	0.052 144
26	YDL111C	RRP42	135868	225555	144391	829 1.71	652 1.28	4	7.03E -05
27	YGR074 W	SMD1	131375	226096	152496	187 31.7	153 3.71	4	0.005 876
28	YML026C	RPS18B	127793	212278	136016	366 04.6	797. 244	4	0.039 72
29	YOL010W	RCL1	126342	217579	146887	423 32	339 7.11	4	0.058 193
30	YNL284C	MRPL10	125211	208525	134130	107 844	434 4.28	4	0.329 646
31	YFL005W	SEC4	123929	208522	136190	112 31.6	433 7.38	4	0.001 05
32	YER025W	GCD11	120591	213000	148774	125 12.6	152 3.67	4	0.002 281
33	YDR454C	GUK1	119582	209594	144915	177 77	367 5.49	4	0.006 197
34	YDR382 W	RPP2B	115968	195536	128100	894 7.18	840. 028	4	0.000 963
35	YLR048W	RPS0B	115651	189585	119030	240 61.6	372 7.04	4	0.016 649
36	YML017W	PSP2	115627	220185	168334	197 33.7	394. 137	4	0.009 906
37	YGR214 W	RPS0A	115477	210479	152948	263 19.2	109 2.66	4	0.021 888
38	YDL035C	GPR1	114897	161265	74650.4	837 83.7	301 17.6	4	0.265 555
39	YBR091C	TIM12	113600	208604	152952	531 89.5	131 1.77	4	0.122 33
40	YKL184W	SPE1	110108	151386	66455.5	772 6.3	624. 375	4	0.000 732
41	YPR189W	SKI3	106226	201874	153988	626 0.26	961. 958	4	0.000 407
42	YGR095C	RRP46	104367	196313	148029	137 91.3	752. 556	4	0.004 756
43	YLR402W	YLR402 W	103850	195810	148051	138 28.9	259 8.86	4	0.004 546

44	YBR084C-A	RPL19A	103358	173369	112714	23605.6	13501	4	0.016633
45	YOR076C	SKI7	102536	196538	151339	19229.1	3276.74	4	0.012374
46	YNL064C	YDJ1	99101	193583	152112	27225.6	697.417	4	0.035723
47	YMR143W	RPS16A	97184.6	175978	126853	4196.34	1214.17	4	0.000121
48	YPL239W	YAR1	96146.9	174130	125549	10318	465.959	4	0.002603
49	YLR185W	RPL37A	94375.2	175260	130220	17761.7	1312.44	4	0.012918
50	YOL064C	MET22	93009.4	178904	138286	11672.5	1819.15	4	0.003908
51	YHR021C	RPS27B	92898	184923	148156	19423.8	1455.42	4	0.017259
52	YOR035C	SHE4	92729.4	189626	155998	5760.66	2663.54	4	0.000243
53	YGR157W	CHO2	90613.7	146788	90437.1	16447.3	1106.63	4	0.011695
54	YMR116C	ASC1	89934.5	169315	127799	16322.5	3590.5	4	0.01097
55	YLR388W	RPS29A	89914.5	173130	133972	6360.7	467.011	4	0.000753
56	YHR081W	LRP1	89865	171851	131994	14351.3	1301.55	4	0.008104
57	YLR435W	TSR2	89037.2	178476	143992	13584.8	2860.51	4	0.006669
58	YOR182C	RPS30B	88824.8	180089	146930	8526.94	2031.06	4	0.001614
59	YOR293W	RPS10A	88082.4	168420	129339	10929	2484.51	4	0.003559
60	YDL175C	AIR2	86469.7	188443	164172	2120.79	1918.67	4	6.41E-07
61	YNL099C	OCA1	85954.8	187946	164200	24452.6	1578.74	4	0.038934
62	YDR206W	EBS1	85503.1	183367	157556	4279.41	2241.57	4	9.16E-05
63	YGR163W	GTR2	83710.1	182350	158805	9677.29	2379.96	4	0.002818
64	YOL108C	INO4	82497.4	128607	74233.7	99613	31007.6	4	0.471887
65	YLR448W	RPL6B	82366.2	169714	140625	13688	1083.14	4	0.009102
66	YKL032C	IXR1	82230.5	173355	146705	39197.3	7073.4	4	0.126183
67	YLR363C	NMD4	81766.8	180009	158164	9613.11	2561.06	4	0.002897
68	YGL058W	RAD6	81196.4	162184	130386	33993.3	17788.5	4	0.092432
69	YPL178W	CBC2	81172.2	166599	137533	13995.2	509.288	4	0.010178
70	YKL212W	SAC1	80879.6	155740	120522	9746.3	6003.67	4	0.001725

71	YOR265W	RBL2	80809	177278	155310	20684.5	3770.81	4	0.028936
72	YGR158C	MTR3	79918.7	175302	153561	15430.4	961.958	4	0.013897
73	YGR046W	TAM41	79842.4	170784	146411	14210.5	722.43	4	0.011103
74	YNL068C	FKH2	79710.8	177243	157023	29847.7	2559.66	4	0.075441
75	YNL056W	OCA2	79300.5	180060	162218	14251.8	2177.76	4	0.011061
76	YLR087C	CSF1	77761.2	167828	145003	24066.4	2570.13	4	0.047842
77	YDL061C	RPS29B	76969.2	157106	129017	5232.83	2413.79	4	0.000332
78	YNL103W	MET4	76250	169865	150715	18853.3	1741.34	4	0.026992
79	YDR083W	RRP8	74192	162721	142528	4561.68	2759.23	4	0.000144
80	YPR095C	SYT1	73854.1	171138	156622	6333.51	1613.74	4	0.001115
81	YOR078W	BUD21	73525.2	157423	135071	9827.82	4484.78	4	0.00331
82	YDR067C	OCA6	73113.9	162360	143682	4498.57	3051.73	4	0.00011
83	YML091C	RPM2	73002.9	162600	144247	39721	2650.5	4	0.163322
84	YNR024W	MPP6	72889.7	174893	164219	8487.71	7128.8	4	0.000963
85	YIL057C	RGI2	72770.3	164873	148280	15392.7	1057.82	4	0.017832
86	YOR183W	FYV12	72398.8	156294	135066	22771.6	651.447	4	0.050095
87	YLR200W	YKE2	72209.2	154312	132182	11313.3	1506.78	4	0.007547
88	YOR256C	TRE2	71027.6	156003	136806	115965	9752.3	4	0.583781
89	YOR179C	SYC1	70704.7	168688	157748	7762.15	976.265	4	0.002687
90	YIL161W	YIL161W	70038.1	165962	154433	12672.9	1341.67	4	0.011478
91	YLR037C	DAN2	69247.6	163865	152329	85487.1	4439.54	4	0.477306
92	YPL266W	DIM1	68803.8	160979	148397	8542.62	1341.27	4	0.003783
93	YJL136C	RPS21B	68631.8	161071	148822	6552.5	6739.31	4	0.00028
94	YLR061W	RPL22A	68459.8	139882	114987	9141.33	919.073	4	0.004828
95	YDR128W	MTC5	68377.9	159215	146243	3594.74	580.087	4	0.000285
96	YGR100W	MDR1	68260.5	172208	167350	77135.7	5285.86	4	0.44152
97	YDR431W	YDR431W	68178.9	159856	147596	3218.38	832.217	4	0.000172

98	YDL081C	RPP1A	67960.8	159057	146661	14205.4	1536.32	4	0.017117
99	YPL232W	SSO1	67842.2	163120	153393	19095.8	2643.43	4	0.037483
100	YMR230W	RPS10B	67794.1	154844	140146	12813.8	1038.88	4	0.013052
101	YBL094C	YBL094C	67738	131049	101928	62240.2	33994.8	4	0.365598
102	YGR187C	HGH1	67565	161827	151756	13483.3	2534.48	4	0.014618
103	YCR095C	OCA4	67531.7	141792	119555	8689.22	39978.9	4	0.066704
104	YDR201W	SPC19	67047.7	156340	143756	10633.3	3483.24	4	0.006737
105	YLR024C	UBR2	66775.7	159728	149648	17554.7	5579.17	4	0.029476
106	YKR087C	OMA1	66586.5	168117	163459	17620.2	2062.02	4	0.032098
107	YJR007W	SUI2	66443.2	150843	135879	20714.6	3321.04	4	0.048308
108	YMR185W	RTP1	66131	172776	171692	65160.3	989.991	4	0.384895
109	YHR049W	FSH1	66060.4	158289	148484	11700.4	1720.32	4	0.01064
110	YLR242C	ARV1	65712.8	152841	140271	15498.3	2419.14	4	0.023437
111	YGR130C	YGR130C	65416.3	162374	156097	4754.12	1262.08	4	0.000655
112	YDR066C	RTR2	64650.6	161694	156235	5355.48	1442.33	4	0.000979
113	YMR036C	MIH1	64507.4	165315	162295	7635.56	3906.8	4	0.001993
114	YDL062W	YDL062W	64434.2	154497	144997	4706.67	878.499	4	0.00075
115	YNL032W	SIW14	64075.9	152240	141940	11751.1	1994.97	4	0.01162
116	YKR001C	VPS1	63405.5	128855	105370	10376.6	3382.46	4	0.007423
117	YML066C	SMA2	63379.8	111307	77160.1	19472.8	44717.8	4	0.116593
118	YKR063C	LAS1	62825.7	156596	150965	10010.8	3101.72	4	0.006958
119	YGL144C	ROG1	62081.3	145650	134542	12733.7	3094.59	4	0.015342
120	YPL063W	TIM50	61852.3	138780	123850	123235	6630.45	4	0.65036
121	YOR001W	RRP6	61624.9	156656	152995	13761	864.024	4	0.020668
122	YPL089C	RLM1	61450.9	154190	149305	17527.2	3402.98	4	0.038276
123	YDR409W	SIZ1	61207.2	156968	154171	9165.15	860.388	4	0.006735
124	YLR371W	ROM2	61191.3	156714	153787	5582.48	1625.49	4	0.001277

125	YNL153C	GIM3	60611.1	156155	153821	8604.58	2672.82	4	0.004895
126	YLR280C	YLR280C	60146.5	153965	151043	1974.34	237.536	4	7.20E-05
127	YOL052C	SPE2	59912.8	107141	76034.5	2488.59	25363	4	0.030307
128	YEL003W	GIM4	59559.3	148310	142884	10519.1	10410.07	4	0.010747
129	YGR213C	RTA1	58739.3	157312	158697	46795.9	2097.96	4	0.298304
130	YOL138C	RTC1	58232.3	148349	145083	9394.27	727.447	4	0.008372
131	YGL259W	YPS5	58221.7	156056	157509	34347.2	1789.14	4	0.188608
132	YGL213C	SKI8	57936.3	147265	143815	42318.6	2124.11	4	0.264499
133	YOR014W	RTS1	57908.1	140090	132309	5260.05	1984.42	4	0.001077
134	YCR076C	FUB1	57883	152952	153056	1861.65	816.224	4	2.75E-05
135	YDR123C	INO2	57741.2	115405	92835.1	5545.57	1795.55	4	0.001422
136	YDL083C	RPS16B	57698.5	150613	149587	10666.3	1901.04	4	0.011836
137	YHL029C	OCA5	57628.8	149778	148356	38027.8	4980.73	4	0.226936
138	YPL026C	SKS1	57234.1	153970	155739	19210.5	7594.67	4	0.054798
139	YFR032C-A	RPL29	57162.2	152312	153186	39497	2708.62	4	0.243655
140	YPR016C	TIF6	57007.9	146735	144456	29949.3	2239.82	4	0.15302
141	YDR368W	YPR1	56949.1	150979	151384	4751.93	1246.02	4	0.001013
142	YDR294C	DPL1	56740.2	151587	152699	5203.31	497.6	4	0.001607
143	YHR106W	TRR2	56719.7	143133	139121	17394.4	4001.42	4	0.045635
144	YGR073C	YGR073C	56698.6	147777	146631	11688.7	4607.19	4	0.013991
145	YGL079W	KXD1	56679.8	154680	157775	14818.8	5625.92	4	0.028162
146	YDR212W	TCP1	56654.8	150128	150488	14462.4	3832.27	4	0.027858
147	YFL034C-A	RPL22B	56580.8	149754	150004	3806.8	2169.85	4	0.000228
148	YLR065C	ENV10	56572.1	96555.7	64371.5	55847.8	37554.7	4	0.402659
149	YPL101W	ELP4	56310.2	145769	144024	2960.97	2772.13	4	2.03E-05
150	YML124C	TUB3	55801.6	150176	151938	8036.71	513.005	4	0.006079
151	YIL157C	COA1	55408.7	149501	151484	20253.9	3464.89	4	0.070769

152	YDR414C	*ERD1*	55394.7	150919	153789	6674.43	1252.29	4	0.003381
153	YNL136W	*EAF7*	55133.4	141906	139699	10954.5	1454.98	4	0.014772
154	YNL228W	*YNL228W*	55122.8	144554	143980	21833.8	8490.91	4	0.082477
155	YDR370C	*DXO1*	54790.9	148549	150946	5246.48	972.123	4	0.001703
156	YPL165C	*SET6*	54648.7	152078	156855	4100.09	1862.77	4	0.000475
157	YGL174W	*BUD13*	54525	143771	143682	16436.5	3601.05	4	0.043812
158	YMR035W	*IMP2*	54467.7	156718	164618	10058.7	1496.97	4	0.011964
159	YNL013C	*YNL013C*	54438.8	151474	156222	7359.09	2011.33	4	0.004394
160	YFL002C	*SPB4*	54027.1	141157	140274	13829.5	2216.3	4	0.029126
161	YBL087C	*RPL23A*	53932.9	140865	139956	6953.98	1304.34	4	0.004134
162	YGL094C	*PAN2*	53890.7	154393	161803	4436.21	3902.42	4	0.000193
163	YGR118W	*RPS23A*	53767.1	144854	146644	29704.6	1286.75	4	0.167958
164	YDR526C	*YDR526C*	53342.9	138324	136814	26072	7065.71	4	0.132059
165	YKL023W	*YKL023W*	53014.5	148156	153173	35546	3208.08	4	0.232669
166	YPL157W	*TGS1*	52771.8	134607	131750	12610.5	1698.47	4	0.024427
167	YDR329C	*PEX3*	52484.1	144781	148594	7486.9	2787.1	4	0.00461
168	YAL042W	*ERV46*	52330	147966	153968	3416.82	2112.97	4	0.000172
169	YKR016W	*MIC60*	51969.1	136140	135510	9068.21	822.739	4	0.010412
170	YBL041W	*PRE7*	51894.9	119175	108317	27712.7	8674.66	4	0.15684
171	YDR392W	*SPT3*	51679.1	148199	155392	5391.64	483.558	4	0.002359
172	YML038C	*YMD8*	51568.3	139772	142003	6520.22	6172.99	4	0.001164
173	YCR085W	*YCR085W*	51541.9	145661	151526	8888.14	1262.72	4	0.009885
174	YBR041W	*FAT1*	51395.5	144863	150478	2979.11	2052.39	4	8.30E-05
175	YGL059W	*PKP2*	51192.5	125592	119780	12615.2	16687.6	4	0.021206
176	YOR058C	*ASE1*	51034.3	144901	151121	62764	2539.23	4	0.475746
177	YCR087W	*YCR087W*	50990.6	143975	149700	5292.1	1358.33	4	0.002002
178	YDR031W	*MIX14*	50579.4	143427	149479	51835.4	5951.43	4	0.401536

179	YBR200W	BEM1	50444.9	113841	102064	50613	34086.6	4	0.409654
180	YGR242W	YGR242W	50292.2	141520	146872	13043.8	5493.6	4	0.026926
181	YGL242C	YGL242C	50147	142139	148102	18303.2	4450.31	4	0.069713
182	YNL278W	CAF120	49957.4	138736	142929	46971.5	23273.3	4	0.373356
183	YGR028W	MSP1	49948.2	135640	137960	31140.5	3770.8	4	0.207016
184	YOL044W	PEX15	49727.6	142141	148781	9442.99	2604.99	4	0.011961
185	YJL211C	YJL211C	49447.4	142918	150483	8722.92	558.433	4	0.010805
186	YOL149W	DCP1	49357.7	150486	162811	27967.4	1858.06	4	0.175733
187	YBL104C	SEA4	49293.1	145074	154202	3531.67	2224.84	4	0.000236
188	YKR082W	NUP133	49226.7	135588	139037	8663.33	1469.7	4	0.010337
189	YKL146W	AVT3	49037	139418	145508	22991.2	3589.59	4	0.122171
190	YGL159W	YGL159W	48997.3	145124	154760	11894.2	492.332	4	0.025882
191	YPL198W	RPL7B	48676.3	142118	150436	8376.91	4102.98	4	0.007234
192	YJL212C	OPT1	48615.6	143292	152424	6439.31	1809.94	4	0.004096
193	YOL159C	YOL159C	48421.4	148707	161455	10813.1	601.605	4	0.02069
194	YML064C	TEM1	48348	143687	153492	31959.7	1864.42	4	0.227542
195	YKL176C	LST4	48118.2	133198	136973	11176	1699.4	4	0.022516
196	YDR339C	FCF1	48009.5	136352	142227	4964.02	6542.22	4	0.000352
197	YPR134W	MSS18	47965.9	133646	137941	61731.9	1316.67	4	0.493814
198	YER129W	SAK1	47818.9	144199	155167	996.141	1735.88	4	6.03E-08
199	YNL016W	PUB1	47768.4	137932	145159	16004.3	3710.83	4	0.056872
200	YNL080C	EOS1	47597.7	128856	130822	64676.8	343.365	4	0.515093
201	YDL045C	FAD1	47506	144205	155680	10980	1453.81	4	0.022349
202	YDR415C	YDR415C	47319.3	113655	106797	4612.78	40832.3	4	0.158022
203	YHR207C	SET5	47155.4	139900	149315	22561.7	202.896	4	0.127767
204	YFR031C-A	RPL2A	47051.8	140394	150276	15256.9	1396.25	4	0.05372
205	YHR198C	AIM18	46933	138031	146663	7801.82	546.511	4	0.00913

206	YDR152W	GIR2	46862.1	141904	153013	17051.2	930.177	4	0.070754
207	YHR017W	YSC83	46601.9	134879	142121	27592	3353.7	4	0.189709
208	YGL227W	VID30	46601.1	136939	145440	12670.6	2287.98	4	0.033934
209	YPR088C	SRP54	46544.1	140534	151320	30478.3	3242.13	4	0.22418
210	YDR265W	PEX10	46370.5	137977	147482	31938.2	1444.71	4	0.242465
211	YGR058W	PEF1	46350.2	134428	141800	4812.48	1811.27	4	0.001677
212	YCR005C	CIT2	46332.7	138406	148233	7918.53	7583.04	4	0.004269
213	YMR161W	HLJ1	46308	140968	152398	17332.1	1240.85	4	0.075426
214	YHR047C	AAP1	46208.8	143112	156009	10303.4	2061.08	4	0.019793
215	YLR378C	SEC61	46164.7	127819	131459	9650.72	7028.31	4	0.010963
216	YIL142W	CCT2	46099.9	148688	165162	50900.5	2943.07	4	0.431975
217	YCR035C	RRP43	46091.9	125493	127832	60900.4	3135.97	4	0.002889
218	YOL130W	ALR1	46048.3	145574	160232	19134.5	3677.92	4	0.094382
219	YMR031C	EIS1	45828.3	137336	147322	10621.7	1110.27	4	0.022671
220	YHR094C	HXT1	45812.8	143774	157713	9355.35	1860.01	4	0.015511
221	YIL135C	VHS2	45806.3	140928	153142	10911.4	1366.76	4	0.024279
222	YBL024W	NCL1	45597.3	136535	146405	5875.65	4692.63	4	0.00158
223	YMR223W	UBP8	45581.2	146446	162387	19825.9	1306.62	4	0.104969
224	YGR189C	CRH1	45180.9	141435	154965	14321.9	1032.33	4	0.050927
225	YAL061W	BDH2	45171.2	137410	148499	25824.84	2358.1	4	3.30E-05
226	YBR283C	SSH1	45100.8	136184	146639	11518.3	2182.82	4	0.028698
227	YIR007W	YIR007W	44875.4	146651	163853	12323.8	1365.01	4	0.035368
228	YJR084W	CSN12	44830.9	136476	147543	34760.8	2242.07	4	0.287638
229	YOL055C	THI20	44670.4	142422	157375	2871.2	948.34	4	0.00039
230	YHR057C	CPR2	44593.9	133593	143284	9214.5	2073.61	4	0.015821
231	YDL056W	MBP1	44584.2	136245	147569	4392.33	1239.96	4	0.001645
232	YOL041C	NOP12	44549.6	131285	139640	9644.09	905.699	4	0.018899

233	YMR119 W-A	*YMR119 W-A*	44393.5	139997	153917	6610.81	602.181	4	0.006636
234	YMR001C	*CDC5*	44294.6	131579	140523	4359.19	10577.3	4	0.002163
235	YLR183C	*TOS4*	44185.5	140502	155064	24188.9	905.727	4	0.165197
236	YJL134W	*LCB3*	44048.5	138367	151849	8330.8	823.155	4	0.013016
237	YNR029C	*YNR029 C*	44032.8	129532	137649	7240.73	2400.33	4	0.00749
238	YHR152 W	*SPO12*	43966.7	124566	129761	22810.3	22074.5	4	0.160421
239	YCL064C	*CHA1*	43906	141168	156587	4519.1	1840.24	4	0.001527
240	YPR143W	*RRP15*	43902.6	135921	148144	18590.9	412.618	4	0.099251
241	YHR066 W	*SSF1*	43681.6	142715	159439	27326	2062.65	4	0.2082
242	YML100W	*TSL1*	43610.9	138863	153351	10501.1	831.319	4	0.02522
243	YBL107C	*MIX23*	43372.6	140031	155614	2172.47	1926.98	4	1.96E-05
244	YLR257W	*YLR257 W*	43318.6	141310	157761	12547.9	1411.42	4	0.040509
245	YMR307 W	*GAS1*	43219.1	130718	140868	11380.8	1907.2	4	0.031318
246	YOL134C	*YOL134 C*	43169.6	128646	137613	15224.2	2249.62	4	0.065254
247	YKR011C	*YKR011 C*	43073.1	138113	153009	11707.3	1598.3	4	0.03427
248	YBR223C	*TDP1*	43008.8	137665	152391	6593.98	2277.26	4	0.005959
249	YGR265 W	YGR265 W	42962.1	112184	111444	5405.19	22474.3	4	0.047147

Bibliography

Addinall, S.G., Holstein, E.M., Lawless, C., Yu, M., Chapman, K., Banks, A.P., Ngo, H.P., Maringele, L., Taschuk, M., Young, A., Ciesiolka, A., Lister, A.L., Wipat, A., Wilkinson, D.J., Lydall, D. (2011) 'Quantitative fitness analysis shows that NMD proteins and many other protein complexes suppress or enhance distinct telomere cap defects', *PLOS Genetics*, 7(4) p. e1001362

Albuquerque, C.P., Wang, G., Lee, N.S., Kolodner, R.D., Putnam, C.D. and Zhou, H. (2013) 'Distinct SUMO ligases cooperate with Esc2 and Slx5 to suppress duplication-mediated genome rearrangements', *PLoS Genet*, 9(8), p. e1003670.

al-Khodairy, F., Enoch, T., Hagan, I.M. and Carr, A.M. (1995) 'The Schizosaccharomyces pombe hus5 gene encodes a ubiquitin conjugating enzyme required for normal mitosis', *J Cell Sci*, 108 (Pt 2), pp. 475-86.

Altmannova, V., Eckert-Boulet, N., Arneric, M., Kolesar, P., Chaloupkova, R., Damborsky, J., Sung, P., Zhao, X., Lisby, M. and Krejci, L. (2010) 'Rad52 SUMOylation affects the efficiency of the DNA repair', *Nucleic Acids Res*, 38(14), pp. 4708-21.

Amberg, D.C. (1998) 'Three-dimensional imaging of the yeast actin cytoskeleton through the budding cell cycle', *Mol Biol Cell*, 9(12), pp. 3259-62.

Anderson, M., Ng, S.S., Marchesi, V., MacIver, F.H., Stevens, F.E., Riddell, T., Glover, D.M., Hagan, I.M., McInerny, C.J. (2002) 'plo1+ regulates gene transcription at the M–G1 interval during the fission yeast mitotic cell cycle', *EMBO J*, 21(21), pp. 5745-55.

Andrews, E.A., Palecek, J., Sergeant, J., Taylor, E., Lehmann, A.R. and Watts, F.Z. (2005) 'Nse2, a component of the Smc5-6 complex, is a SUMO ligase required for the response to DNA damage', *Mol Cell Biol*, 25(1), pp. 185-96.

Armstrong, A.A., Mohideen, F. and Lima, C.D. (2012) 'Recognition of SUMO-modified PCNA requires tandem receptor motifs in Srs2', *Nature*, 483(7387), pp. 59-63.

Armstrong, R.A. (2013) 'What causes alzheimer's disease?', *Folia Neuropathol*, 51(3), pp. 169-88.

Ashburner, M., Ball, C.A., Blake, J.A., Botstein, D., Butler, H., Cherry, J.M., Davis, A.P., Dolinski, K., Dwight, S.S., Eppig, J.T., Harris, M.A., Hill, D.P., Issel-Tarver, L., Kasarskis, A., Lewis, S., Matese, J.C., Richardson, J.E., Ringwald, M., Rubin, G.M. and Sherlock, G. (2000) 'Gene ontology: tool for the unification of biology. The Gene Ontology Consortium', *Nat Genet*, 25(1), pp. 25-9.

Barral, Y. and Kinoshita, M. (2008) 'Structural insights shed light onto septin assemblies and function', *Curr Opin Cell Biol*, 20(1), pp. 12-8.

Bartolo, M.E. and Carter, J.V. (1991) 'Effect of microtubule stabilization on the freezing tolerance of mesophyll cells of spinach', *Plant Physiol*, 97(1), pp. 182-7.

Bayer, P., Arndt, A., Metzger, S., Mahajan, R., Melchior, F., Jaenicke, R. and Becker, J. (1998) 'Structure determination of the small ubiquitin-related modifier SUMO-1', *J Mol Biol*, 280(2), pp. 275-86.

Becker, J., Barysch, S.V., Karaca, S., Dittner, C., Hsiao, H.H., Berriel Diaz, M., Herzig, S., Urlaub, H. and Melchior, F. (2013) 'Detecting endogenous SUMO targets in mammalian cells and tissues', *Nat Struct Mol Biol*, 20(4), pp. 525-31.

Bencsath, K.P., Podgorski, M.S., Pagala, V.R., Slaughter, C.A. and Schulman, B.A. (2002) 'Identification of a multifunctional binding site on Ubc9p required for Smt3p conjugation', *J Biol Chem*, 277(49), pp. 47938-45.

Bergink, S., Ammon, T., Kern, M., Schermelleh, L., Leonhardt, H. and Jentsch, S. (2013) 'Role of Cdc48/p97 as a SUMO-targeted segregase curbing Rad51-Rad52 interaction', *Nat Cell Biol*, 15(5), pp. 526-32.

Bermudez-Lopez, M., Pocino-Merino, I., Sanchez, H., Bueno, A., Guasch, C., Almedawar, S., Bru-Virgili, S., Gari, E., Wyman, C., Reverter, D., Colomina, N. and Torres-Rosell, J. (2015) 'ATPase-dependent control of the Mms21 SUMO ligase during DNA repair', *PLoS Biol*, 13(3), p. e1002089.

Bernier-Villamor, V., Sampson, D.A., Matunis, M.J. and Lima, C.D. (2002) 'Structural basis for E2-mediated SUMO conjugation revealed by a complex between ubiquitin-conjugating enzyme Ubc9 and RanGAP1', *Cell*, 108(3), pp. 345-56.

Beroukhim, R., Mermel, C.H., Porter, D., Wei, G., Raychaudhuri, S., Donovan, J., Barretina, J., Boehm, J.S., Dobson, J., Urashima, M., Mc Henry, K.T., Pinchback, R.M., Ligon, A.H., Cho, Y.J., Haery, L., Greulich, H., Reich, M., Winckler, W., Lawrence, M.S., Weir, B.A., Tanaka, K.E., Chiang, D.Y., Bass, A.J., Loo, A., Hoffman, C., Prensner, J., Liefeld, T., Gao, Q., Yecies, D., Signoretti, S., Maher, E., Kaye, F.J., Sasaki, H., Tepper, J.E., Fletcher, J.A., Tabernero, J., Baselga, J., Tsao, M.S., Demichelis, F., Rubin, M.A., Janne, P.A., Daly, M.J., Nucera, C., Levine, R.L., Ebert, B.L., Gabriel, S., Rustgi, A.K., Antonescu, C.R., Ladanyi, M., Letai, A., Garraway, L.A., Loda, M., Beer, D.G., True, L.D., Okamoto, A., Pomeroy, S.L., Singer, S., Golub, T.R., Lander, E.S., Getz, G., Sellers, W.R. and Meyerson, M. (2010) 'The landscape of somatic copy-number alteration across human cancers', *Nature*, 463(7283), pp. 899-905.

Biggins, S., Bhalla, N., Chang, A., Smith, D.L. and Murray, A.W. (2001) 'Genes involved in sister chromatid separation and segregation in the budding yeast Saccharomyces cerevisiae', *Genetics*, 159(2), pp. 453-70.

Blomster, H.A., Hietakangas, V., Wu, J., Kouvonen, P., Hautaniemi, S. and Sistonen, L. (2009) 'Novel proteomics strategy brings insight into the prevalence of SUMO-2 target sites', *Mol Cell Proteomics*, 8(6), pp. 1382-90.

Boggio, R., Colombo, R., Hay, R.T., Draetta, G.F. and Chiocca, S. (2004) 'A mechanism for inhibiting the SUMO pathway', *Mol Cell*, 16(4), pp. 549-61.

Boggio, R., Passafaro, A. and Chiocca, S. (2007) 'Targeting SUMO E1 to ubiquitin ligases: a viral strategy to counteract sumoylation', *J Biol Chem*, 282(21), pp. 15376-82.

Bohm, S., Mihalevic, M.J., Casal, M.A. and Bernstein, K.A. (2015) 'Disruption of SUMO-targeted ubiquitin ligases Slx5-Slx8/RNF4 alters RecQ-like helicase Sgs1/BLM localization in yeast and human cells', *DNA Repair (Amst)*, 26, pp. 1-14.

Bonner, J.N., Choi, K., Xue, X., Torres, N.P., Szakal, B., Wei, L., Wan, B., Arter, M., Matos, J., Sung, P., Brown, G.W., Branzei, D. and Zhao, X. (2016) 'Smc5/6 Mediated Sumoylation of the Sgs1-Top3-Rmi1 Complex Promotes Removal of Recombination Intermediates', *Cell Rep*, 16(2), pp. 368-78.

Bossis, G. and Melchior, F. (2006) 'Regulation of SUMOylation by reversible oxidation of SUMO conjugating enzymes', *Mol Cell*, 21(3), pp. 349-57.

Branzei, D., Sollier, J., Liberi, G., Zhao, X., Maeda, D., Seki, M., Enomoto, T., Ohta, K. and Foiani, M. (2006) 'Ubc9- and Mms21-Mediated Sumoylation Counteracts Recombinogenic Events at Damaged Replication Forks', *Cell*, 127(3), pp. 509-522.

Breslow, D.K., Cameron, D.M., Collins, S.R., Schuldiner, M., Stewart-Ornstein, J., Newman, H.W., Braun, S., Madhani, H.D., Krogan, N.J. and Weissman, J.S. (2008) 'A comprehensive strategy enabling high-resolution functional analysis of the yeast genome', *Nat Methods*, 5(8), pp. 711-8.

Brill, S.J. and Stillman, B. (1991) 'Replication factor-A from Saccharomyces cerevisiae is encoded by three essential genes coordinately expressed at S phase', *Genes Dev*, 5(9), pp. 1589-600.

Buck, V., Ng, S.S., Ruiz-Garcia, A.B., Papadopoulou, K., Bhatti, S., Samuel, J.M., Anderson, M., Millar, J.B. and McInerny, C.J. (2004) 'Fkh2p and Sep1p regulate mitotic gene transcription in fission yeast', *J Cell Sci*, 117(Pt 23), pp. 5623-32.

Bulmer, R. (2005) *The Regulation of the Cell Division Cycle by Forkhead Proteins in Schizosaccharomyces pombe*. PhD thesis. University of Newcastle Upon Tyne.

Bulmer, R., Pic-Taylor, A., Whitehall, S.K., Martin, K.A., Millar, J.B., Quinn, J. and Morgan, B.A. (2004) 'The forkhead transcription factor Fkh2 regulates the cell division cycle of Schizosaccharomyces pombe', *Eukaryot Cell*, 3(4), pp. 944-54.

Burgess, R.C., Rahman, S., Lisby, M., Rothstein, R. and Zhao, X. (2007) 'The Slx5-Slx8 complex affects sumoylation of DNA repair proteins and negatively regulates recombination', *Mol Cell Biol*, 27(17), pp. 6153-62.

Bylebyl, G.R., Belichenko, I. and Johnson, E.S. (2003) 'The SUMO isopeptidase Ulp2 prevents accumulation of SUMO chains in yeast', *J Biol Chem*, 278(45), pp. 44113-20.

Carpy, A., Krug, K., Graf, S., Koch, A., Popic, S., Hauf, S., Macek, B. (2014) 'Absolute proteome and phosphoproteome dynamics during the cell cycle of Schizosaccharomyces pombe (Fission Yeast)' *Mol Cell Proteomics* 13(8), pp. 1925-36.

Casamayor, A. and Snyder, M. (2003) 'Molecular dissection of a yeast septin: distinct domains are required for septin interaction, localization, and function', *Mol Cell Biol*, 23(8), pp. 2762-77.

Chan, K., Goldmark, J.P. and Roth, M.B. (2010) 'Suspended animation extends survival limits of Caenorhabditis elegans and Saccharomyces cerevisiae at low temperature', *Mol Biol Cell*, 21(13), pp. 2161-71.

Chatr-Aryamontri, A., Breitkreutz, B.J., Oughtred, R., Boucher, L., Heinicke, S., Chen, D., Stark, C., Breitkreutz, A., Kolas, N., O'Donnell, L., Reguly, T., Nixon, J., Ramage, L., Winter, A., Sellam, A., Chang, C., Hirschman, J., Theesfeld, C., Rust, J., Livstone, M.S., Dolinski, K. and Tyers, M. (2015) 'The BioGRID interaction database: 2015 update', *Nucleic Acids Res*, 43(Database issue), pp. D470-8.

Chen, R.E. and Thorner, J. (2007) 'Function and regulation in MAPK signaling pathways: lessons learned from the yeast Saccharomyces cerevisiae', *Biochim Biophys Acta*, 1773(8), pp. 1311-40.

Chen, X.L., Reindle, A. and Johnson, E.S. (2005) 'Misregulation of 2 microm circle copy number in a SUMO pathway mutant', *Mol Cell Biol*, 25(10), pp. 4311-20.

Chen, Y.J., Chuang, Y.C., Chuang, C.N., Cheng, Y.H., Chang, C.R., Leng, C.H. and Wang, T.F. (2016) '*S. cerevisiae* Mre11 recruits conjugated SUMO moieties to facilitate the assembly and function of the Mre11-Rad50-Xrs2 complex', *Nucleic Acids Res*, 44(5), pp. 2199-213.

Cheng, C.H., Lo, Y.H., Liang, S.S., Ti, S.C., Lin, F.M., Yeh, C.H., Huang, H.Y. and Wang, T.F. (2006) 'SUMO modifications control assembly of synaptonemal complex and polycomplex in meiosis of Saccharomyces cerevisiae', *Genes Dev*, 20(15), pp. 2067-81.

Cheng, J., Kang, X., Zhang, S. and Yeh, E.T. (2007) 'SUMO-specific protease 1 is essential for stabilization of HIF1alpha during hypoxia', *Cell*, 131(3), pp. 584-95.

Cheng, X. and Kao, H.Y. (2012) 'Post-translational modifications of PML: consequences and implications', *Front Oncol*, 2, p. 210.

Choi, K., Szakal, B., Chen, Y.H., Branzei, D. and Zhao, X. (2010) 'The Smc5/6 complex and Esc2 influence multiple replication-associated recombination processes in Saccharomyces cerevisiae', *Mol Biol Cell*, 21(13), pp. 2306-14.

Chung, I. and Zhao, X. (2015) 'DNA break-induced sumoylation is enabled by collaboration between a SUMO ligase and the ssDNA-binding complex RPA', *Genes Dev*, 29(15), pp. 1593-8.

Cipolla, L., Maffia, A., Bertoletti, F. and Sabbioneda, S. (2016) 'The Regulation of DNA Damage Tolerance by Ubiquitin and Ubiquitin-Like Modifiers', *Front Genet*, 7, p. 105.

Comerford, K.M., Leonard, M.O., Karhausen, J., Carey, R., Colgan, S.P. and Taylor, C.T. (2003) 'Small ubiquitin-related modifier-1 modification mediates resolution of CREB-dependent responses to hypoxia', *Proc Natl Acad Sci U S A*, 100(3), pp. 986-91.

Conaway, R.C. and Conaway, J.W. (2009) 'The INO80 chromatin remodeling complex in transcription, replication and repair', *Trends Biochem Sci*, 34(2), pp. 71-7.

Cooper, J.A. (1987) 'Effects of cytochalasin and phalloidin on actin', *The Journal of Cell Biology*, 105(4), p. 1473.

Costanzo, M., Baryshnikova, A., Bellay, J., Kim, Y., Spear, E.D., Sevier, C.S., Ding, H., Koh, J.L., Toufighi, K., Mostafavi, S., Prinz, J., St Onge, R.P., VanderSluis, B., Makhnevych, T., Vizeacoumar, F.J., Alizadeh, S., Bahr, S., Brost, R.L., Chen, Y., Cokol, M., Deshpande, R., Li, Z., Lin, Z.Y., Liang, W., Marback, M., Paw, J., San Luis, B.J., Shuteriqi, E., Tong, A.H., van Dyk, N., Wallace, I.M., Whitney, J.A., Weirauch, M.T., Zhong, G., Zhu, H., Houry, W.A., Brudno, M., Ragibizadeh, S., Papp, B., Pal, C., Roth, F.P., Giaever, G., Nislow, C., Troyanskaya, O.G., Bussey, H., Bader, G.D., Gingras, A.C., Morris, Q.D., Kim, P.M., Kaiser, C.A., Myers, C.L., Andrews, B.J. and Boone, C. (2010) 'The genetic landscape of a cell', *Science*, 327(5964), pp. 425-31.

Cremona, C.A., Sarangi, P., Yang, Y., Hang, L.E., Rahman, S. and Zhao, X. (2012) 'Extensive DNA damage-induced sumoylation contributes to replication and repair and acts in addition to the mec1 checkpoint', *Mol Cell*, 45(3), pp. 422-32.

Dantas Ada, S., Day, A., Ikeh, M., Kos, I., Achan, B. and Quinn, J. (2015) 'Oxidative stress responses in the human fungal pathogen, Candida albicans', *Biomolecules*, 5(1), pp. 142-65.

Datta, S., Snow, C.J. and Paschal, B.M. (2014) 'A pathway linking oxidative stress and the Ran GTPase system in progeria', *Mol Biol Cell*, 25(8), pp. 1202-15.

de Albuquerque, C.P., Liang, J., Gaut, N.J. and Zhou, H. (2016) 'Molecular Circuitry of the SUMO (Small Ubiquitin-like Modifier) Pathway in Controlling Sumoylation Homeostasis and Suppressing Genome Rearrangements', *J Biol Chem*, 291(16), pp. 8825-35.

De Antoni, A., Pearson, C.G., Cimini, D., Canman, J.C., Sala, V., Nezi, L., Mapelli, M., Sironi, L., Faretta, M., Salmon, E.D. and Musacchio, A. (2005) 'The Mad1/Mad2 complex as a template for Mad2 activation in the spindle assembly checkpoint', *Curr Biol*, 15(3), pp. 214-25.

Denison, C., Rudner, A.D., Gerber, S.A., Bakalarski, C.E., Moazed, D. and Gygi, S.P. (2005) 'A proteomic strategy for gaining insights into protein sumoylation in yeast', *Mol Cell Proteomics*, 4(3), pp. 246-54.

Desterro, J.M., Rodriguez, M.S. and Hay, R.T. (1998) 'SUMO-1 modification of IkappaBalpha inhibits NF-kappaB activation', *Mol Cell*, 2(2), pp. 233-9.

Dieckhoff, P., Bolte, M., Sancak, Y., Braus, G.H. and Irniger, S. (2004) 'Smt3/SUMO and Ubc9 are required for efficient APC/C-mediated proteolysis in budding yeast', *Molecular Microbiology*, 51(5), pp. 1375-1387.

Ding, S.L. and Shen, C.Y. (2008) 'Model of human aging: recent findings on Werner's and Hutchinson-Gilford progeria syndromes', *Clin Interv Aging*, 3(3), pp. 431-44.

Dorval, V. and Fraser, P.E. (2006) 'Small ubiquitin-like modifier (SUMO) modification of natively unfolded proteins tau and alpha-synuclein', *J Biol Chem*, 281(15), pp. 9919-24.

Dulic, V.E., M; Elguindi, I; Raths, S; Singer, B; Riezman, H 194 (1991) 'Guide to yeast genetics and molecular biology' 1991/01/01 *Methods Enzymol*. pp. 697-710.

Duval, D., Duval, G., Kedinger, C., Poch, O. and Boeuf, H. (2003) 'The 'PINIT' motif, of a newly identified conserved domain of the PIAS protein family, is essential for nuclear retention of PIAS3L', *FEBS Lett*, 554(1-2), pp. 111-8.

Eckhoff, J. and Dohmen, R.J. (2015) '*In vitro* Studies Reveal a Sequential Mode of Chain Processing by the Yeast SUMO (Small Ubiquitin-related Modifier)-specific Protease Ulp2', *J Biol Chem*, 290(19), pp. 12268-81.

Eifler, K. and Vertegaal, A.C. (2015a) 'Mapping the SUMOylated landscape', *Febs j*, 282(19), pp. 3669-80.

Eifler, K. and Vertegaal, A.C. (2015b) 'SUMOylation-Mediated Regulation of Cell Cycle Progression and Cancer', *Trends Biochem Sci*, 40(12), pp. 779-93.

Enserink, J.M., Smolka, M.B., Zhou, H., Kolodner, R.D. (2006) 'Checkpoint proteins control morphogenetic events during DNA replication stress in Saccharomyces cerevisiae', *J Cell Biol*, 175(5), pp. 729-41

Epp, E., Walther, A., Lepine, G., Leon, Z., Mullick, A., Raymond, M., Wendland, J. and Whiteway, M. (2010) 'Forward genetics in Candida albicans that reveals the Arp2/3 complex is required for hyphal formation, but not endocytosis', *Mol Microbiol*, 75(5), pp. 1182-98.

Everett, R.D. and Chelbi-Alix, M.K. (2007) 'PML and PML nuclear bodies: implications in antiviral defence', *Biochimie*, 89(6-7), pp. 819-30.

Fantes, P. (1979) 'Epistatic gene interactions in the control of division in fission yeast', *Nature*, 279, pp. 428-30.

Feric, M., Broedersz, C.P. and Brangwynne, C.P. (2015) 'Soft viscoelastic properties of nuclear actin age oocytes due to gravitational creep', *Scientific Reports*, 5, p. 16607.

Filosa, G., Barabino, S.M. and Bachi, A. (2013) 'Proteomics strategies to identify SUMO targets and acceptor sites: a survey of RNA-binding proteins SUMOylation', *Neuromolecular Med*, 15(4), pp. 661-76.

Flynn, R.L. and Zou, L. (2011) 'ATR: a master conductor of cellular responses to DNA replication stress', *Trends Biochem Sci*, 36(3), pp. 133-40.

Forsburg, S.L. and Nurse, P. (1991) 'Cell cycle regulation in the yeasts Saccharomyces cerevisiae and Schizosaccharomyces pombe', *Annu Rev Cell Biol*, 7, pp. 227-56.

Frampton, J., Irmisch, A., Green, C.M., Neiss, A., Trickey, M., Ulrich, H.D., Furuya, K., Watts, F.Z., Carr, A.M. and Lehmann, A.R. (2006) 'Postreplication repair and PCNA modification in Schizosaccharomyces pombe', *Mol Biol Cell*, 17(7), pp. 2976-85.

Galanty, Y., Belotserkovskaya, R., Coates, J. and Jackson, S.P. (2012) 'RNF4, a SUMO-targeted ubiquitin E3 ligase, promotes DNA double-strand break repair', *Genes & Development*, 26(11), pp. 1179-1195.

Gali, H., Juhasz, S., Morocz, M., Hajdu, I., Fatyol, K., Szukacsov, V., Burkovics, P. and Haracska, L. (2012) 'Role of SUMO modification of human PCNA at stalled replication fork', *Nucleic Acids Res*, 40(13), pp. 6049-59.

Gao, C., Ho, C.C., Reineke, E., Lam, M., Cheng, X., Stanya, K.J., Liu, Y., Chakraborty, S., Shih, H.M. and Kao, H.Y. (2008) 'Histone deacetylase 7 promotes PML sumoylation and is essential for PML nuclear body formation', *Mol Cell Biol*, 28(18), pp. 5658-67.

Gao, Y.G., Song, A.X., Shi, Y.H., Chang, Y.G., Liu, S.X., Yu, Y.Z., Cao, X.T., Lin, D.H. and Hu, H.Y. (2005) 'Solution structure of the ubiquitin-like domain of human DC-UbP from dendritic cells', *Protein Sci*, 14(8), pp. 2044-50.

García-Rodríguez, N., Wong, R.P. and Ulrich, H.D. (2016) 'Functions of Ubiquitin and SUMO in DNA Replication and Replication Stress', *Frontiers in Genetics*, 7, p. 87.

Garg, A., Futcher, B. and Leatherwood, J. (2015) 'A new transcription factor for mitosis: in Schizosaccharomyces pombe, the RFX transcription factor Sak1 works with forkhead factors to regulate mitotic expression', *Nucleic Acids Res*, 43(14), pp. 6874-88.

Gavet, O. and Pines, J. (2010) 'Progressive activation of CyclinB1-Cdk1 coordinates entry to mitosis', *Dev Cell*, 18(4), pp. 533-43.

Giaever, G., Chu, A.M., Ni, L., Connelly, C., Riles, L., Veronneau, S., Dow, S., Lucau-Danila, A., Anderson, K., Andre, B., Arkin, A.P., Astromoff, A., El Bakkoury, M., Bangham, R., Benito, R., Brachat, S., Campanaro, S., Curtiss, M., Davis, K., Deutschbauer, A., Entian, K.-D., Flaherty, P., Foury, F., Garfinkel, D.J., Gerstein, M., Gotte, D., Guldener, U., Hegemann, J.H., Hempel, S., Herman, Z., Jaramillo, D.F., Kelly, D.E., Kelly, S.L., Kotter, P., LaBonte, D., Lamb,

D.C., Lan, N., Liang, H., Liao, H., Liu, L., Luo, C., Lussier, M., Mao, R., Menard, P., Ooi, S.L., Revuelta, J.L., Roberts, C.J., Rose, M., Ross-Macdonald, P., Scherens, B., Schimmack, G., Shafer, B., Shoemaker, D.D., Sookhai-Mahadeo, S., Storms, R.K., Strathern, J.N., Valle, G., Voet, M., Volckaert, G., Wang, C.-y., Ward, T.R., Wilhelmy, J., Winzeler, E.A., Yang, Y., Yen, G., Youngman, E., Yu, K., Bussey, H., Boeke, J.D., Snyder, M., Philippsen, P., Davis, R.W. and Johnston, M. (2002) 'Functional profiling of the Saccharomyces cerevisiae genome', *Nature*, 418(6896), pp. 387-391.

Goehring, A.S., Rivers, D.M., Sprague G.F. (2003) 'Urmylation: a ubiquitin-like pathway that functions during invasive growth and budding in yeast', *Mol Biol Cell* 14(11), pp. 4329-41.

Goldstein, A.L. and McCusker, J.H. (1999) 'Three new dominant drug resistance cassettes for gene disruption in Saccharomyces cerevisiae', *Yeast*, 15(14), pp. 1541-53.

Goley, E.D., Ohkawa, T., Mancuso, J., Woodruff, J.B., D'Alessio, J.A., Cande, W.Z., Volkman, L.E. and Welch, M.D. (2006) 'Dynamic nuclear actin assembly by Arp2/3 complex and a baculovirus WASP-like protein', *Science*, 314(5798), pp. 464-7.

Gombos, L., Neuner, A., Beynskyy, M., Fava, L.L., Wade, R.C., Sachse, C., Schibel, E. (2013) 'GTP regulates the microtubule nucleation activity of λ-tubulin', Nat Cell Biol, 15(11), pp. 1317-27.

Gonzalez-Prieto, R., Cuijpers, S.A., Kumar, R., Hendriks, I.A. and Vertegaal, A.C. (2015) 'c-Myc is targeted to the proteasome for degradation in a SUMOylation-dependent manner, regulated by PIAS1, SENP7 and RNF4', *Cell Cycle*, 14(12), pp. 1859-72.

Gregoire, S. and Yang, X.J. (2005) 'Association with class IIa histone deacetylases upregulates the sumoylation of MEF2 transcription factors', *Mol Cell Biol*, 25(6), pp. 2273-87.

Griffiths, D.J., Barbet, N.C., McCready, S., Lehmann, A.R. and Carr, A.M. (1995) 'Fission yeast rad17: a homologue of budding yeast RAD24 that shares regions of sequence similarity with DNA polymerase accessory proteins', *Embo j*, 14(23), pp. 5812-23.

Gruenbaum, Y. and Foisner, R. (2015) 'Lamins: nuclear intermediate filament proteins with fundamental functions in nuclear mechanics and genome regulation', *Annu Rev Biochem*, 84, pp. 131-64.

Grunwald, M. and Bono, F. (2011) 'Structure of Importin13-Ubc9 complex: nuclear import and release of a key regulator of sumoylation', *EMBO J*, 30(2), pp. 427-38.

Hagan, I., and K. R. Ayscough (2000) 'Fluorescence microscopy in yeast', in Allan, V.J. (ed.) *Protein localization by fluorescence microscopy*. New York, N.Y: Oxford University Press, pp. 179-206.

Hamard, P.J., Boyer-Guittaut, M., Camuzeaux, B., Dujardin, D., Hauss, C., Oelgeschlager, T., Vigneron, M., Kedinger, C. and Chatton, B. (2007) 'Sumoylation delays the ATF7 transcription factor subcellular localization and inhibits its transcriptional activity', *Nucleic Acids Res*, 35(4), pp. 1134-44.

Hamon, M.A., Ribet, D., Stavru, F. and Cossart, P. (2012) 'Listeriolysin O: the Swiss army knife of Listeria', *Trends Microbiol*, 20(8), pp. 360-8.

Hanawalt, P.C. (2015) 'Historical perspective on the DNA damage response', *DNA Repair (Amst)*, 36, pp. 2-7.

Havelkova, L., Nanda, G., Martinek, J., Bellinvia, E., Sikorova, L., Slajcherova, K., Seifertova, D., Fischer, L., Fiserova, J., Petrasek, J. and Schwarzerova, K. (2015) 'Arp2/3 complex subunit ARPC2 binds to microtubules', *Plant Sci*, 241, pp. 96-108.

Hay, R.T. (2007) 'SUMO-specific proteases: a twist in the tail', *Trends Cell Biol*, 17(8), pp. 370-6.

Hayles, J., Wood, V., Jeffery, L., Hoe, K.L., Kim, D.U., Park, H.O., Salas-Pino, S., Heichinger, C. and Nurse, P. (2013) 'A genome-wide resource of cell cycle and cell shape genes of fission yeast', *Open Biol*, 3(5), p. 130053.

Hecker, C.M., Rabiller, M., Haglund, K., Bayer, P. and Dikic, I. (2006) 'Specification of SUMO1- and SUMO2-interacting motifs', *J Biol Chem*, 281(23), pp. 16117-27.

Hickey, C.M., Wilson, N.R. and Hochstrasser, M. (2012) 'Function and regulation of SUMO proteases', *Nat Rev Mol Cell Biol*, 13(12), pp. 755-66.

Hietakangas, V., Anckar, J., Blomster, H.A., Fujimoto, M., Palvimo, J.J., Nakai, A. and Sistonen, L. (2006) 'PDSM, a motif for phosphorylation-dependent SUMO modification', *Proc Natl Acad Sci U S A*, 103(1), pp. 45-50.

Himmels, S.F. and Sartori, A.A. (2016) 'Controlling DNA-End Resection: An Emerging Task for Ubiquitin and SUMO', *Front Genet*, 7, p. 152.

Ho, C.W., Chen, H.T. and Hwang, J. (2011) 'UBC9 autosumoylation negatively regulates sumoylation of septins in Saccharomyces cerevisiae', *J Biol Chem*, 286(24), pp. 21826-34.

Ho, J.C., Warr, N.J., Shimizu, H. and Watts, F.Z. (2001) 'SUMO modification of Rad22, the Schizosaccharomyces pombe homologue of the recombination protein Rad52', *Nucleic Acids Res*, 29(20), pp. 4179-86.

Hochstrasser, M. (2000) 'Evolution and function of ubiquitin-like protein-conjugation systems', *Nat Cell Biol*, 2(8), pp. E153-7.

Hoege, C., Pfander, B., Moldovan, G.L., Pyrowolakis, G. and Jentsch, S. (2002) 'RAD6-dependent DNA repair is linked to modification of PCNA by ubiquitin and SUMO', *Nature*, 419(6903), pp. 135-41.

Hoyt, M.A., Totis, L. and Roberts, B.T. (1991) '*S. cerevisiae* genes required for cell cycle arrest in response to loss of microtubule function', *Cell*, 66(3), pp. 507-17.

Huber, F., Boire, A., López, A.P., Koenderink, G.H. (2015) 'Cytoskeletal crosstalk: when three different personalities team up', *Curr Opin Cell Biol,* 32, pp. 39-47.

Huffaker, T.C., Thomas, J.H. and Botstein, D. (1988) 'Diverse effects of beta-tubulin mutations on microtubule formation and function', *J Cell Biol*, 106(6), pp. 1997-2010.

Hurley, J.H. and Hanson, P.I. (2010) 'Membrane budding and scission by the ESCRT machinery: it's all in the neck', *Nat Rev Mol Cell Biol*, 11(8), pp. 556-66.

Impens, F., Radoshevich, L., Cossart, P. and Ribet, D. (2014) 'Mapping of SUMO sites and analysis of SUMOylation changes induced by external stimuli', *Proc Natl Acad Sci U S A*, 111(34), pp. 12432-7.

Irqeba, A.A., Yang, L., Panahi, M., Wang, Y. (2014) 'Regulating Global Sumoylation by a MAP Kinase Hog1 and Its Potential Role in Osmo-Tolerance in Yeast', *PLOS one*, 9(2), p. e87306.

Jentsch, S. and Pyrowolakis, G. (2000) 'Ubiquitin and its kin: how close are the family ties?', *Trends Cell Biol*, 10(8), pp. 335-42.

Johnson, A. and Skotheim, J.M. (2013) 'Start and the restriction point', *Curr Opin Cell Biol*, 25(6), pp. 717-23.

Johnson, E.S. and Blobel, G. (1997) 'Ubc9p is the conjugating enzyme for the ubiquitin-like protein Smt3p', *J Biol Chem*, 272(43), pp. 26799-802.

Johnson, E.S. and Blobel, G. (1999) 'Cell cycle-regulated attachment of the ubiquitin-related protein SUMO to the yeast septins', *J Cell Biol*, 147(5), pp. 981-94.

Johnson, E.S. and Gupta, A.A. (2001) 'An E3-like Factor that Promotes SUMO Conjugation to the Yeast Septins', *Cell*, 106(6), pp. 735-744.

Johnson, E.S., Schwienhorst, I., Dohmen, R.J. and Blobel, G. (1997) 'The ubiquitin-like protein Smt3p is activated for conjugation to other proteins by an Aos1p/Uba2p heterodimer', *Embo j*, 16(18), pp. 5509-19.

Jones, D., Crowe, E., Stevens, T.A. and Candido, E.P. (2002) 'Functional and phylogenetic analysis of the ubiquitylation system in Caenorhabditis elegans: ubiquitin-conjugating enzymes, ubiquitin-activating enzymes, and ubiquitin-like proteins', *Genome Biol*, 3(1), p. RESEARCH0002.

Kagey, M.H., Melhuish, T.A. and Wotton, D. (2003) 'The polycomb protein Pc2 is a SUMO E3', *Cell*, 113(1), pp. 127-37.

Kalkat, M., Chan, P.K., Wasylishen, A.R., Srikumar, T., Kim, S.S., Ponzielli, R., Bazett-Jones, D.P., Raught, B. and Penn, L.Z. (2014) 'Identification of c-MYC SUMOylation by mass spectrometry', *PLoS One*, 9(12), p. e115337.

Karpova, T.S., McNally, J.G., Moltz, S.L. and Cooper, J.A. (1998) 'Assembly and function of the actin cytoskeleton of yeast: relationships between cables and patches', *J Cell Biol*, 142(6), pp. 1501-17.

Kelley, J.B., Datta, S., Snow, C.J., Chatterjee, M., Ni, L., Spencer, A., Yang, C.S., Cubenas-Potts, C., Matunis, M.J. and Paschal, B.M. (2011) 'The defective nuclear lamina in Hutchinson-gilford progeria syndrome disrupts the nucleocytoplasmic Ran gradient and inhibits nuclear localization of Ubc9', *Mol Cell Biol*, 31(16), pp. 3378-95.

Kessler, J.D., Kahle, K.T., Sun, T., Meerbrey, K.L., Schlabach, M.R., Schmitt, E.M., Skinner, S.O., Xu, Q., Li, M.Z., Hartman, Z.C., Rao, M., Yu, P., Dominguez-Vidana, R., Liang, A.C., Solimini, N.L., Bernardi, R.J., Yu, B., Hsu, T., Golding, I., Luo, J., Osborne, C.K., Creighton, C.J., Hilsenbeck, S.G., Schiff, R., Shaw, C.A., Elledge, S.J. and Westbrook, T.F. (2012) 'A SUMOylation-dependent transcriptional subprogram is required for Myc-driven tumorigenesis', *Science*, 335(6066), pp. 348-53.

Kilmartin, J.V. and Adams, A.E. (1984) 'Structural rearrangements of tubulin and actin during the cell cycle of the yeast Saccharomyces', *J Cell Biol*, 98(3), pp. 922-33.

Kim, D.R., Gidvani, R.D., Ingalls, B.P., Duncker, B.P. and McConkey, B.J. (2011) 'Differential chromatin proteomics of the MMS-induced DNA damage response in yeast', *Proteome Sci*, 9, p. 62.

Kim, D.-U., Hayles, J., Kim, D., Wood, V., Park, H.-O., Won, M., Yoo, H.-S., Duhig, T., Nam, M., Palmer, G., Han, S., Jeffery, L., Baek, S.-T., Lee, H., Shim, Y.S., Lee, M., Kim, L., Heo, K.-S., Noh, E.J., Lee, A.-R., Jang, Y.-J., Chung, K.-S., Choi, S.-J., Park, J.-Y., Park, Y., Kim, H.M., Park, S.-K., Park, H.-J., Kang, E.-J., Kim, H.B., Kang, H.-S., Park, H.-M., Kim, K., Song, K., Song, K.B., Nurse, P. and Hoe, K.-L. (2010) 'Analysis of a genome-wide set of gene deletions in the fission yeast Schizosaccharomyces pombe', *Nat Biotech*, 28(6), pp. 617-623.

Kim, K., Galletta, B.J., Schmidt, K.O., Chang, F.S., Blumer, K.J. and Cooper, J.A. (2006) 'Actin-based motility during endocytosis in budding yeast', *Mol Biol Cell*, 17(3), pp. 1354-63.

Klug, H., Xaver, M., Chaugule, Viduth K., Koidl, S., Mittler, G., Klein, F. and Pichler, A. (2013) 'Ubc9 Sumoylation Controls SUMO Chain Formation and Meiotic Synapsis in Saccharomyces cerevisiae', *Molecular Cell*, 50(5), pp. 625-636.

Knight, J.R., Bastide, A., Peretti, D., Roobol, A., Roobol, J., Mallucci, G.R., Smales, C.M. and Willis, A.E. (2016) 'Cooling-induced SUMOylation of EXOSC10 down-regulates ribosome biogenesis', *Rna*, 22(4), pp. 623-35.

Knipscheer, P., Flotho, A., Klug, H., Olsen, J.V., van Dijk, W.J., Fish, A., Johnson, E.S., Mann, M., Sixma, T.K. and Pichler, A. (2008) 'Ubc9 Sumoylation Regulates SUMO Target Discrimination', *Molecular Cell*, 31(3), pp. 371-382.

Koch, A., Krug, K., Pengelley, S., Macek, B., Hauf, S. (2011) 'Mitotic substrates of the kinase aurora with roles in chromatin regulation identified through quantitative phosphoproteomics of fission yeast' *Sci Signal,* 4(179):rs6.

Kohler, J.B., Tammsalu, T., Jorgensen, M.M., Steen, N., Hay, R.T. and Thon, G. (2015) 'Targeting of SUMO substrates to a Cdc48-Ufd1-Npl4 segregase and STUbL pathway in fission yeast', *Nat Commun*, 6, p. 8827.

Komander, D. (2009) 'The emerging complexity of protein ubiquitination', *Biochem Soc Trans*, 37(pt 5), pp. 937-53.

Kouranti, I., McLean, J.R., Feoktistova, A., Liang, P., Johnson, A.E., Roberts-Galbraith, R.H. and Gould, K.L. (2010) 'A global census of fission yeast deubiquitinating enzyme localization and interaction networks reveals distinct compartmentalization profiles and overlapping functions in endocytosis and polarity', *PLoS Biol*, 8(9).

Krejci, L., Van Komen, S., Li, Y., Villemain, J., Reddy, M.S., Klein, H., Ellenberger, T. and Sung, P. (2003) 'DNA helicase Srs2 disrupts the Rad51 presynaptic filament', *Nature*, 423(6937), pp. 305-9.

Kristensen, A.R., Gsponer, J. and Foster, L.J. (2012) 'A high-throughput approach for measuring temporal changes in the interactome', *Nat Methods*, 9(9), pp. 907-9.

Kroetz, M.B., Su, D. and Hochstrasser, M. (2009) 'Essential role of nuclear localization for yeast Ulp2 SUMO protease function', *Mol Biol Cell*, 20(8), pp. 2196-206.

Kurepa, J., Walker, J.M., Smalle, J., Gosink, M.M., Davis, S.J., Durham, T.L., Sung, D.Y. and Vierstra, R.D. (2003) 'The small ubiquitin-like modifier (SUMO) protein modification system in

Arabidopsis. Accumulation of SUMO1 and -2 conjugates is increased by stress', *J Biol Chem*, 278(9), pp. 6862-72.

Lamoliatte, F., Caron, D., Durette, C., Mahrouche, L., Maroui, M.A., Caron-Lizotte, O., Bonneil, E., Chelbi-Alix, M.K. and Thibault, P. (2014) 'Large-scale analysis of lysine SUMOylation by SUMO remnant immunoaffinity profiling', *Nat Commun*, 5, p. 5409.

Lawless, C., Wilkinson, D.J., Young, A., Addinall, S.G. and Lydall, D.A. (2010) 'Colonyzer: automated quantification of micro-organism growth characteristics on solid agar', *BMC Bioinformatics*, 11, p. 287.

Leach, M.D., Stead, D.A., Argo, E. and Brown, A.J. (2011) 'Identification of sumoylation targets, combined with inactivation of SMT3, reveals the impact of sumoylation upon growth, morphology, and stress resistance in the pathogen Candida albicans', *Mol Biol Cell*, 22(5), pp. 687-702.

Lee, Y.-j., Miyake, S.-i., Wakita, H., McMullen, D.C., Azuma, Y., Auh, S. and Hallenbeck, J.M. (2007) 'Protein SUMOylation is massively increased in hibernation torpor and is critical for the cytoprotection provided by ischemic preconditioning and hypothermia in SHSY5Y cells', *Journal of cerebral blood flow and metabolism : official journal of the International Society of Cerebral Blood Flow and Metabolism*, 27(5), pp. 950-962.

Lee, Y.J., Mou, Y., Klimanis, D., Bernstock, J.D. and Hallenbeck, J.M. (2014) 'Global SUMOylation is a molecular mechanism underlying hypothermia-induced ischemic tolerance', *Front Cell Neurosci*, 8, p. 416.

Lewicki, M.C., Srikumar, T., Johnson, E. and Raught, B. (2015) 'The *S. cerevisiae* SUMO stress response is a conjugation–deconjugation cycle that targets the transcription machinery', *Journal of Proteomics*, 118, pp. 39-48.

Li, H., Niu, H., Peng, Y., Wang, J. and He, P. (2013) 'Ubc9 promotes invasion and metastasis of lung cancer cells', *Oncol Rep*, 29(4), pp. 1588-94.

Li, R. and Murray, A.W. (1991) 'Feedback control of mitosis in budding yeast', *Cell*, 66(3), pp. 519-31.

Li, S.J. and Hochstrasser, M. (1999) 'A new protease required for cell-cycle progression in yeast', *Nature*, 398(6724), pp. 246-51.

Li, S.J. and Hochstrasser, M. (2000) 'The yeast ULP2 (SMT4) gene encodes a novel protease specific for the ubiquitin-like Smt3 protein', *Mol Cell Biol*, 20(7), pp. 2367-77.

Li, S.J. and Hochstrasser, M. (2003) 'The Ulp1 SUMO isopeptidase: distinct domains required for viability, nuclear envelope localization, and substrate specificity', *J Cell Biol*, 160(7), pp. 1069-81.

Li, Y., Wang, H., Wang, S., Quon, D., Liu, Y.W. and Cordell, B. (2003) 'Positive and negative regulation of APP amyloidogenesis by sumoylation', *Proc Natl Acad Sci U S A*, 100(1), pp. 259-64.

Li, Z., Vizeacoumar, F.J., Bahr, S., Li, J., Warringer, J., Vizeacoumar, F.S., Min, R., VanderSluis, B., Bellay, J., DeVit, M., Fleming, J.A., Stephens, A., Haase, J., Lin, Z.-Y., Baryshnikova, A., Lu, H., Yan, Z., Jin, K., Barker, S., Datti, A., Giaever, G., Nislow, C., Bulawa, C., Myers, C.L., Costanzo, M., Gingras, A.-C., Zhang, Z., Blomberg, A., Bloom, K., Andrews,

B. and Boone, C. (2011) 'Systematic exploration of essential yeast gene function with temperature-sensitive mutants', *Nature Biotechnology*, 29(4), pp. 361-367.

Lin, D., Tatham, M.H., Yu, B., Kim, S., Hay, R.T. and Chen, Y. (2002) 'Identification of a substrate recognition site on Ubc9', *J Biol Chem*, 277(24), pp. 21740-8.

Lois, L.M. and Lima, C.D. (2005) 'Structures of the SUMO E1 provide mechanistic insights into SUMO activation and E2 recruitment to E1', *Embo j*, 24(3), pp. 439-51.

Longtine, M.S., McKenzie, A., 3rd, Demarini, D.J., Shah, N.G., Wach, A., Brachat, A., Philippsen, P. and Pringle, J.R. (1998) 'Additional modules for versatile and economical PCR-based gene deletion and modification in Saccharomyces cerevisiae', *Yeast*, 14(10), pp. 953-61.

Lu, C.Y., Tsai, C.H., Brill, S.J. and Teng, S.C. (2010) 'Sumoylation of the BLM ortholog, Sgs1, promotes telomere-telomere recombination in budding yeast', *Nucleic Acids Res*, 38(2), pp. 488-98.

Makhnevych, T., Ptak, C., Lusk, C.P., Aitchison, J.D. and Wozniak, R.W. (2007) 'The role of karyopherins in the regulated sumoylation of septins', *J Cell Biol*, 177(1), pp. 39-49.

Makhnevych, T., Sydorskyy, Y., Xin, X., Srikumar, T., Vizeacoumar, F.J., Jeram, S.M., Li, Z., Bahr, S., Andrews, B.J., Boone, C. and Raught, B. (2009) 'Global Map of SUMO Function Revealed by Protein-Protein Interaction and Genetic Networks', *Molecular cell*, 33(1), pp. 124-135.

Mani, R., St Onge, R.P., Hartman, J.L.t., Giaever, G. and Roth, F.P. (2008) 'Defining genetic interaction', *Proc Natl Acad Sci U S A*, 105(9), pp. 3461-6.

Maniatis, T.F., E.F.; Sambrook, J. (1983) 'Molecular cloning. A laboratory manual by T Maniatis, E F Fritsch and J Sambrook. pp 545. Cold Spring Harbor Laboratory, New York. 1982. $48 ISBN 0-87969-136-0', *Biochemical Education*, 11(2), pp. 82-82.

Martin, S.W. and Konopka, J.B. (2004) 'SUMO modification of septin-interacting proteins in Candida albicans', *J Biol Chem*, 279(39), pp. 40861-7.

Matic, I., Schimmel, J., Hendriks, I.A., van Santen, M.A., van de Rijke, F., van Dam, H., Gnad, F., Mann, M. and Vertegaal, A.C. (2010) 'Site-specific identification of SUMO-2 targets in cells reveals an inverted SUMOylation motif and a hydrophobic cluster SUMOylation motif', *Mol Cell*, 39(4), pp. 641-52.

Mautsa, N., Prinsloo, E., Bishop, O.T. and Blatch, G.L. (2011) 'The PINIT domain of PIAS3: structure-function analysis of its interaction with STAT3', *J Mol Recognit*, 24(5), pp. 795-803.

Mavarkis, M., Azou-Gros, Y., Tsai, F.C., Alvarado, J., Bertin, A., IV. F., Kress, A., Brasselet, S., Koenderink, G.H., Lecuit, T.(2014) 'Septins promote F-actin ring formation by crosslinking actin filaments into curved bundles', *Nat Cell Biol*, 16(4), pp. 322-34.

McDonald, N.A., Vander Kooi, C.W., Ohi, M.D. and Gould, K.L. (2015) 'Oligomerization but Not Membrane Bending Underlies the Function of Certain F-BAR Proteins in Cell Motility and Cytokinesis', *Dev Cell*, 35(6), pp. 725-36.

McDonald, W.H., Pavlova, Y., Yates, J.R., 3rd and Boddy, M.N. (2003) 'Novel essential DNA repair proteins Nse1 and Nse2 are subunits of the fission yeast Smc5-Smc6 complex', *J Biol Chem*, 278(46), pp. 45460-7.

Meluh, P.B. and Koshland, D. (1995) 'Evidence that the MIF2 gene of Saccharomyces cerevisiae encodes a centromere protein with homology to the mammalian centromere protein CENP-C', *Mol Biol Cell*, 6(7), pp. 793-807.

Mendenhall, M.D. and Hodge, A.E. (1998) 'Regulation of Cdc28 cyclin-dependent protein kinase activity during the cell cycle of the yeast Saccharomyces cerevisiae', *Microbiol Mol Biol Rev*, 62(4), pp. 1191-243.

Metzger, M.B., Hristova, V.A. and Weissman, A.M. (2012) 'HECT and RING finger families of E3 ubiquitin ligases at a glance', *J Cell Sci*, 125(Pt 3), pp. 531-7.

Michelot, A., Costanzo, M., Sarkeshik, A., Boone, C., Yates, J., Drubin, D. (2010) 'Reconstitution and Protein Composition Analysis of Endocytic Actin Patches', *Curr Biol*, 20(21), pp. 1890-9.

Minty, A., Dumont, X., Kaghad, M. and Caput, D. (2000) 'Covalent modification of p73alpha by SUMO-1. Two-hybrid screening with p73 identifies novel SUMO-1-interacting proteins and a SUMO-1 interaction motif', *J Biol Chem*, 275(46), pp. 36316-23.

Moldovan, G.L., Pfander, B. and Jentsch, S. (2006) 'PCNA controls establishment of sister chromatid cohesion during S phase', *Mol Cell*, 23(5), pp. 723-32.

Moreno, S., Klar, A., Nurse, P. (1991) 'Molecular genetic analysis of fission yeast Schizosaccharomyces pombe', *Methods Enzymol*, 194, pp. 795-823.

Morgan, B.A., Banks, G.R., Toone, W.M., Raitt, D., Kuge, S. and Johnston, L.H. (1997) 'The Skn7 response regulator controls gene expression in the oxidative stress response of the budding yeast Saccharomyces cerevisiae', *Embo j*, 16(5), pp. 1035-44.

Moschos, S.J., Jukic, D.M., Athanassiou, C., Bhargava, R., Dacic, S., Wang, X., Kuan, S.F., Fayewicz, S.L., Galambos, C., Acquafondata, M., Dhir, R. and Becker, D. (2010) 'Expression analysis of Ubc9, the single small ubiquitin-like modifier (SUMO) E2 conjugating enzyme, in normal and malignant tissues', *Hum Pathol*, 41(9), pp. 1286-98.

Moschos, S.J., Smith, A.P., Mandic, M., Athanassiou, C., Watson-Hurst, K., Jukic, D.M., Edington, H.D., Kirkwood, J.M. and Becker, D. (2007) 'SAGE and antibody array analysis of melanoma-infiltrated lymph nodes: identification of Ubc9 as an important molecule in advanced-stage melanomas', *Oncogene*, 26(29), pp. 4216-25.

Muller, S. and Dejean, A. (1999) 'Viral immediate-early proteins abrogate the modification by SUMO-1 of PML and Sp100 proteins, correlating with nuclear body disruption', *J Virol*, 73(6), pp. 5137-43.

Murata, T., Hotta, N., Toyama, S., Nakayama, S., Chiba, S., Isomura, H., Ohshima, T., Kanda, T. and Tsurumi, T. (2010) 'Transcriptional repression by sumoylation of Epstein-Barr virus BZLF1 protein correlates with association of histone deacetylase', *J Biol Chem*, 285(31), pp. 23925-35.

Murray, J.M. and Carr, A.M. (2008) 'Smc5/6: a link between DNA repair and unidirectional replication?', *Nat Rev Mol Cell Biol*, 9(2), pp. 177-82.

Myatt, S.S., Kongsema, M., Man, C.W., Kelly, D.J., Gomes, A.R., Khongkow, P., Karunarathna, U., Zona, S., Langer, J.K., Dunsby, C.W., Coombes, R.C., French, P.M., Brosens, J.J. and Lam, E.W. (2014) 'SUMOylation inhibits FOXM1 activity and delays mitotic transition', *Oncogene*, 33(34), pp. 4316-29.

Nacerddine, K., Lehembre, F., Bhaumik, M., Artus, J., Cohen-Tannoudji, M., Babinet, C., Pandolfi, P.P. and Dejean, A. (2005) 'The SUMO pathway is essential for nuclear integrity and chromosome segregation in mice', *Dev Cell*, 9(6), pp. 769-79.

Nagai, S., Dubrana, K., Tsai-Pflugfelder, M., Davidson, M.B., Roberts, T.M., Brown, G.W., Varela, E., Hediger, F., Gasser, S.M. and Krogan, N.J. (2008) 'Functional targeting of DNA damage to a nuclear pore-associated SUMO-dependent ubiquitin ligase', *Science*, 322(5901), pp. 597-602.

Nakahira, M., Macedo, J.N., Seraphim, T.V., Cavalcante, N., Souza, T.A., Damalio, J.C., Reyes, L.F., Assmann, E.M., Alborghetti, M.R., Garratt, R.C., Araujo, A.P., Zanchin, N.I., Barbosa, J.A. and Kobarg, J. (2010) 'A draft of the human septin interactome', *PLoS One*, 5(11), p. e13799.

Nasmyth, K. and Haering, C.H. (2005) 'The structure and function of SMC and kleisin complexes', *Annu Rev Biochem*, 74, pp. 595-648.

Okubo, S., Hara, F., Tsuchida, Y., Shimotakahara, S., Suzuki, S., Hatanaka, H., Yokoyama, S., Tanaka, H., Yasuda, H. and Shindo, H. (2004) 'NMR structure of the N-terminal domain of SUMO ligase PIAS1 and its interaction with tumor suppressor p53 and A/T-rich DNA oligomers', *J Biol Chem*, 279(30), pp. 31455-61.

Oliva, A., Rosebrock, A., Ferrezuelo, F., Pyne, S., Chen, H., Skiena, S., Futcher, B. and Leatherwood, J. (2005) 'The cell cycle-regulated genes of Schizosaccharomyces pombe', *PLoS Biol*, 3(7), p. e225.

Orth, K., Xu, Z., Mudgett, M.B., Bao, Z.Q., Palmer, L.E., Bliska, J.B., Mangel, W.F., Staskawicz, B. and Dixon, J.E. (2000) 'Disruption of signaling by Yersinia effector YopJ, a ubiquitin-like protein protease', *Science*, 290(5496), pp. 1594-7.

Otomo, C., Metlagel, Z., Takaesu, G. and Otomo, T. (2013) 'Structure of the human ATG12~ATG5 conjugate required for LC3 lipidation in autophagy', *Nat Struct Mol Biol*, 20(1), pp. 59-66.

Owerbach, D., McKay, E.M., Yeh, E.T., Gabbay, K.H. and Bohren, K.M. (2005) 'A proline-90 residue unique to SUMO-4 prevents maturation and sumoylation', *Biochem Biophys Res Commun*, 337(2), pp. 517-20.

Page, B.D. and Snyder, M. (1993) 'Chromosome segregation in yeast', *Annu Rev Microbiol*, 47, pp. 231-61.

Pampin, M., Simonin, Y., Blondel, B., Percherancier, Y. and Chelbi-Alix, M.K. (2006) 'Cross talk between PML and p53 during poliovirus infection: implications for antiviral defense', *J Virol*, 80(17), pp. 8582-92.

Parker, J.L. and Ulrich, H.D. (2012) 'A SUMO-interacting motif activates budding yeast ubiquitin ligase Rad18 towards SUMO-modified PCNA', *Nucleic Acids Res*, 40(22), pp. 11380-8.

Parker, J.L., Bucceri, A., Davies, A.A., Heidrich, K., Windecker, H. and Ulrich, H.D. (2008) 'SUMO modification of PCNA is controlled by DNA', *Embo j*, 27(18), pp. 2422-31.

Pennella, M.A., Liu, Y., Woo, J.L., Kim, C.A. and Berk, A.J. (2010) 'Adenovirus E1B 55-kilodalton protein is a p53-SUMO1 E3 ligase that represses p53 and stimulates its nuclear export through interactions with promyelocytic leukemia nuclear bodies', *J Virol*, 84(23), pp. 12210-25.

Peters, J.M. (2006) 'The anaphase promoting complex/cyclosome: a machine designed to destroy', *Nat Rev Mol Cell Biol*, 7(9), pp. 644-56.

Pfander, B., Moldovan, G.L., Sacher, M., Hoege, C. and Jentsch, S. (2005) 'SUMO-modified PCNA recruits Srs2 to prevent recombination during S phase', *Nature*, 436(7049), pp. 428-33.

Pichler, A., Gast, A., Seeler, J.S., Dejean, A. and Melchior, F. (2002) 'The nucleoporin RanBP2 has SUMO1 E3 ligase activity', *Cell*, 108(1), pp. 109-20.

Pichler, A., Knipscheer, P., Oberhofer, E., van Dijk, W.J., Korner, R., Olsen, J.V., Jentsch, S., Melchior, F. and Sixma, T.K. (2005) 'SUMO modification of the ubiquitin-conjugating enzyme E2-25K', *Nat Struct Mol Biol*, 12(3), pp. 264-9.

Pinto, M.P., Carvalho, A.F., Grou, C.P., Rodriguez-Borges, J.E., Sa-Miranda, C. and Azevedo, J.E. (2012) 'Heat shock induces a massive but differential inactivation of SUMO-specific proteases', *Biochim Biophys Acta*, 1823(10), pp. 1958-66.

Pirkkala, L., NykÄNen, P. and Sistonen, L.E.A. (2001) 'Roles of the heat shock transcription factors in regulation of the heat shock response and beyond', *The FASEB Journal*, 15(7), pp. 1118-1131.

Prudden, J., Pebernard, S., Raffa, G., Slavin, D.A., Perry, J.J., Tainer, J.A., McGowan, C.H. and Boddy, M.N. (2007) 'SUMO-targeted ubiquitin ligases in genome stability', *Embo j*, 26(18), pp. 4089-101.

Psakhye, I. and Jentsch, S. (2012) 'Protein group modification and synergy in the SUMO pathway as exemplified in DNA repair', *Cell*, 151(4), pp. 807-20.

Purtill, F.S., Whitehall, S.K., Williams, E.S., McInerny, C.J., Sharrocks, A.D. and Morgan, B.A. (2011) 'A homeodomain transcription factor regulates the DNA replication checkpoint in yeast', *Cell Cycle*, 10(4), pp. 664-670.

Reindle, A., Belichenko, I., Bylebyl, G.R., Chen, X.L., Gandhi, N. and Johnson, E.S. (2006) 'Multiple domains in Siz SUMO ligases contribute to substrate selectivity', *J Cell Sci*, 119(Pt 22), pp. 4749-57.

Reverter, D. and Lima, C.D. (2004) 'A basis for SUMO protease specificity provided by analysis of human Senp2 and a Senp2-SUMO complex', *Structure*, 12(8), pp. 1519-31.

Ribar, B., Grallert, A., Olah, E. and Szallasi, Z. (1999) 'Deletion of the sep1(+) forkhead transcription factor homologue is not lethal but causes hyphal growth in Schizosaccharomyces pombe', *Biochem Biophys Res Commun*, 263(2), pp. 465-74.

Ribet, D., Hamon, M., Gouin, E., Nahori, M.A., Impens, F., Neyret-Kahn, H., Gevaert, K., Vandekerckhove, J., Dejean, A. and Cossart, P. (2010) 'Listeria monocytogenes impairs SUMOylation for efficient infection', *Nature*, 464(7292), pp. 1192-5.

Roberts-Galbraith, R.H., Chen, J.S., Wang, J. and Gould, K.L. (2009) 'The SH3 domains of two PCH family members cooperate in assembly of the Schizosaccharomyces pombe contractile ring', *J Cell Biol*, 184(1), pp. 113-27.

Rodriguez, M.S., Dargemont, C. and Hay, R.T. (2001) 'SUMO-1 conjugation *in vivo* requires both a consensus modification motif and nuclear targeting', *J Biol Chem*, 276(16), pp. 12654-9.

Rouiller, I., Xu, X.P., Amann, K.J., Egile, C., Nickell, S., Nicastro, D., Li, R., Pollard, T.D., Volkmann, N. and Hanein, D. (2008) 'The structural basis of actin filament branching by the Arp2/3 complex', *J Cell Biol*, 180(5), pp. 887-95.

Rustici, G., Mata, J., Kivinen, K., Lio, P., Penkett, C.J., Burns, G., Hayles, J., Brazma, A., Nurse, P. and Bahler, J. (2004) 'Periodic gene expression program of the fission yeast cell cycle', *Nat Genet*, 36(8), pp. 809-17.

Ryan, C.J., Roguev, A., Patrick, K., Xu, J., Jahari, H., Tong, Z., Beltrao, P., Shales, M., Qu, H., Collins, S.R., Kliegman, J.I., Jiang, L., Kuo, D., Tosti, E., Kim, H.S., Edelmann, W., Keogh, M.C., Greene, D., Tang, C., Cunningham, P., Shokat, K.M., Cagney, G., Svensson, J.P., Guthrie, C., Espenshade, P.J., Ideker, T. and Krogan, N.J. (2012) 'Hierarchical modularity and the evolution of genetic interactomes across species', *Mol Cell*, 46(5), pp. 691-704.

Saibil, H. (2013) 'Chaperone machines for protein folding, unfolding and disaggregation', *Nature reviews. Molecular cell biology*, 14(10), pp. 630-642.

Sabo, A., Doni, M. and Amati, B. (2014) 'SUMOylation of Myc-family proteins', *PLoS One*, 9(3), p. e91072.

Sacher, M., Pfander, B., Hoege, C. and Jentsch, S. (2006) 'Control of Rad52 recombination activity by double-strand break-induced SUMO modification', *Nat Cell Biol*, 8(11), pp. 1284-90.

Sahin, U., Lallemand-Breitenbach, V. and de The, H. (2014) 'PML nuclear bodies: regulation, function and therapeutic perspectives', *J Pathol*, 234(3), pp. 289-91.

Saitoh, H. and Hinchey, J. (2000) 'Functional heterogeneity of small ubiquitin-related protein modifiers SUMO-1 versus SUMO-2/3', *J Biol Chem*, 275(9), pp. 6252-8.

Saitoh, H., Pizzi, M.D. and Wang, J. (2002) 'Perturbation of SUMOlation enzyme Ubc9 by distinct domain within nucleoporin RanBP2/Nup358', *J Biol Chem*, 277(7), pp. 4755-63.

Sale, J.E. (2012) 'Competition, collaboration and coordination--determining how cells bypass DNA damage', *J Cell Sci*, 125(Pt 7), pp. 1633-43.

Sampson, D.A., Wang, M. and Matunis, M.J. (2001) 'The small ubiquitin-like modifier-1 (SUMO-1) consensus sequence mediates Ubc9 binding and is essential for SUMO-1 modification', *J Biol Chem*, 276(24), pp. 21664-9.

Sarkar, K., Sadhukhan, S., Han, S.S. and Vyas, Y.M. (2015) 'SUMOylation-disrupting WAS mutation converts WASp from a transcriptional activator to a repressor of NF-kappaB response genes in T cells', *Blood*, 126(14), pp. 1670-82.

Schaerer-Brodbeck, C. and Riezman, H. (2000) 'Saccharomyces cerevisiae Arc35p works through two genetically separable calmodulin functions to regulate the actin and tubulin cytoskeletons', *J Cell Sci*, 113 (Pt 3), pp. 521-32.

Schaerer-Brodbeck, C. and Riezman, H. (2003) 'Genetic and biochemical interactions between the Arp2/3 complex, Cmd1p, casein kinase II, and Tub4p in yeast', *FEMS Yeast Res*, 4(1), pp. 37-49.

Schatz, P.J., Solomon, F. and Botstein, D. (1988) 'Isolation and characterization of conditional-lethal mutations in the TUB1 alpha-tubulin gene of the yeast Saccharomyces cerevisiae', *Genetics*, 120(3), pp. 681-95.

Schiestl, R.H. and Gietz, R.D. (1989) 'High efficiency transformation of intact yeast cells using single stranded nucleic acids as a carrier', *Curr Genet*, 16(5-6), pp. 339-46.

Schimmel, J., Eifler, K., Sigurethsson, J.O., Cuijpers, S.A., Hendriks, I.A., Verlaan-de Vries, M., Kelstrup, C.D., Francavilla, C., Medema, R.H., Olsen, J.V. and Vertegaal, A.C. (2014) 'Uncovering SUMOylation dynamics during cell-cycle progression reveals FoxM1 as a key mitotic SUMO target protein', *Mol Cell*, 53(6), pp. 1053-66.

Schindelin, J., Arganda-Carreras, I., Frise, E., Kaynig, V., Longair, M., Pietzsch, T., Preibisch, S., Rueden, C., Saalfeld, S., Schmid, B., Tinevez, J.Y., White, D.J., Hartenstein, V., Eliceiri, K., Tomancak, P. and Cardona, A. (2012) 'Fiji: an open-source platform for biological-image analysis', *Nat Methods*, 9(7), pp. 676-82.

Schwienhorst, I., Johnson, E.S. and Dohmen, R.J. (2000) 'SUMO conjugation and deconjugation', *Molecular and General Genetics MGG*, 263(5), pp. 771-786.

Seet, B.T., Dikic, I., Zhou, M.M. and Pawson, T. (2006) 'Reading protein modifications with interaction domains', *Nat Rev Mol Cell Biol*, 7(7), pp. 473-83.

Seufert, W., Futcher, B. and Jentsch, S. (1995) 'Role of a ubiquitin-conjugating enzyme in degradation of S- and M-phase cyclins', *Nature*, 373(6509), pp. 78-81.

Shao, R., Zhang, F.P., Tian, F., Anders Friberg, P., Wang, X., Sjoland, H. and Billig, H. (2004) 'Increase of SUMO-1 expression in response to hypoxia: direct interaction with HIF-1alpha in adult mouse brain and heart *in vivo*', *FEBS Lett*, 569(1-3), pp. 293-300.

Shih, H.P., Hales, K.G., Pringle, J.R. and Peifer, M. (2002) 'Identification of septin-interacting proteins and characterization of the Smt3/SUMO-conjugation system in Drosophila', *J Cell Sci*, 115(Pt 6), pp. 1259-71.

Shimada, M., Yamada-Namikawa, C., Murakami-Tonami, Y., Yoshida, T., Nakanishi, M., Urano, T., Murakami, H. (2008) 'Cdc2p controls the forkhead transcription factor Fkh2p by phosphorylation during sexual differentiation in fission yeast' *EMBO J,* (27)1, pp.132-42.

Shirayama, M., Toth, A., Galova, M. and Nasmyth, K. (1999) 'APC(Cdc20) promotes exit from mitosis by destroying the anaphase inhibitor Pds1 and cyclin Clb5', *Nature*, 402(6758), pp. 203-7.

Shrivastav, M., De Haro, L.P. and Nickoloff, J.A. (2008) 'Regulation of DNA double-strand break repair pathway choice', *Cell Res*, 18(1), pp. 134-47.

Singh, R.K., Gonzalez, M., Kabbaj, M.H. and Gunjan, A. (2012) 'Novel E3 ubiquitin ligases that regulate histone protein levels in the budding yeast Saccharomyces cerevisiae', *PLoS One*, 7(5), p. e36295.

Skilton, A., Ho, J.C., Mercer, B., Outwin, E. and Watts, F.Z. (2009) 'SUMO chain formation is required for response to replication arrest in *S. pombe*', *PLoS One*, 4(8), p. e6750.

Somer, L., Shmulman, O., Dror, T., Hashmueli, S., Kashi, Y. (2002) 'The eukaryote chaperonin CCT is a cold shock protein in Saccharomyces cerevisiae', *Cell Stress Chaperones*, 7(1), pp. 47-54.

Song, J., Durrin, L.K., Wilkinson, T.A., Krontiris, T.G. and Chen, Y. (2004) 'Identification of a SUMO-binding motif that recognizes SUMO-modified proteins', *Proc Natl Acad Sci U S A*, 101(40), pp. 14373-8.

Song, J.G., Xie, H.H., Li, N., Wu, K., Qiu, J.G., Shen, D.M. and Huang, C.J. (2015) 'SUMO-specific protease 6 promotes gastric cancer cell growth via deSUMOylation of FoxM1', *Tumour Biol*, 36(12), pp. 9865-71.

Srikumar, T., Lewicki, M.C. and Raught, B. (2013) 'A global *S. cerevisiae* small ubiquitin-related modifier (SUMO) system interactome', *Mol Syst Biol*, 9, p. 668.

Stehmeier, P. and Muller, S. (2009) 'Phospho-regulated SUMO interaction modules connect the SUMO system to CK2 signaling', *Mol Cell*, 33(3), pp. 400-9.

Strunnikov, A.V., Aravind, L. and Koonin, E.V. (2001) 'Saccharomyces cerevisiae SMT4 encodes an evolutionarily conserved protease with a role in chromosome condensation regulation', *Genetics*, 158(1), pp. 95-107.

Styrkarsdottir, U., Egel, R. and Nielsen, O. (1993) 'The smt-0 mutation which abolishes mating-type switching in fission yeast is a deletion', *Curr Genet*, 23(2), pp. 184-6.

Su, X.A., Dion, V., Gasser, S.M. and Freudenreich, C.H. (2015) 'Regulation of recombination at yeast nuclear pores controls repair and triplet repeat stability', *Genes Dev*, 29(10), pp. 1006-17.

Suarez, M.B., Alonso-Nunez, M.L., del Rey, F., McInerny, C.J. and Vazquez de Aldana, C.R. (2015) 'Regulation of Ace2-dependent genes requires components of the PBF complex in Schizosaccharomyces pombe', *Cell Cycle*, 14(19), pp. 3124-37.

Sun, H. and Hunter, T. (2012) 'Poly-small ubiquitin-like modifier (PolySUMO)-binding proteins identified through a string search', *J Biol Chem*, 287(50), pp. 42071-83.

Sung, M.K., Ha, C.W. and Huh, W.K. (2008) 'A vector system for efficient and economical switching of C-terminal epitope tags in Saccharomyces cerevisiae', *Yeast*, 25(4), pp. 301-11.

Sung, M.K., Lim, G., Yi, D.G., Chang, Y.J., Yang, E.B., Lee, K. and Huh, W.K. (2013) 'Genome-wide bimolecular fluorescence complementation analysis of SUMO interactome in yeast', *Genome Res*, 23(4), pp. 736-46.

Sydorskyy, Y., Srikumar, T., Jeram, S.M., Wheaton, S., Vizeacoumar, F.J., Makhnevych, T., Chong, Y.T., Gingras, A.C. and Raught, B. (2010) 'A novel mechanism for SUMO system control: regulated Ulp1 nucleolar sequestration', *Mol Cell Biol*, 30(18), pp. 4452-62.

Szilagyi, Z., Banyai, G., Lopez, M.D., McInerny, C.J., Gustafsson, C.M. (2012) 'Cyclin-dependent kinase 8 regulates mitotic commitment in fission yeast' *Mol Cell Biol* 32(11), pp. 2099-109.

Takahashi, Y., Iwase, M., Konishi, M., Tanaka, M., Toh-e, A. and Kikuchi, Y. (1999) 'Smt3, a SUMO-1 Homolog, Is Conjugated to Cdc3, a Component of Septin Rings at the Mother-Bud Neck in Budding Yeast', *Biochemical and Biophysical Research Communications*, 259(3), pp. 582-587.

Takahashi, Y., Iwase, M., Strunnikov, A.V. and Kikuchi, Y. (2008) 'Cytoplasmic sumoylation by PIAS-type Siz1-SUMO ligase', *Cell Cycle*, 7(12), pp. 1738-44.

Takahashi, Y., Kahyo, T., Toh, E.A., Yasuda, H. and Kikuchi, Y. (2001a) 'Yeast Ull1/Siz1 is a novel SUMO1/Smt3 ligase for septin components and functions as an adaptor between conjugating enzyme and substrates', *J Biol Chem*, 276(52), pp. 48973-7.

Takahashi, Y., Mizoi, J., Toh, E.A. and Kikuchi, Y. (2000) 'Yeast Ulp1, an Smt3-specific protease, associates with nucleoporins', *J Biochem*, 128(5), pp. 723-5.

Takahashi, Y., Toh, E.A. and Kikuchi, Y. (2003) 'Comparative analysis of yeast PIAS-type SUMO ligases *in vivo* and *in vitro*', *J Biochem*, 133(4), pp. 415-22.

Takahashi, Y., Toh, E.A. and Kikuchi, Y. (2001) 'A novel factor required for the SUMO1/Smt3 conjugation of yeast septins', *Gene*, 275(2), pp. 223-31.

Talamillo, A., Sanchez, J., Cantera, R., Perez, C., Martin, D., Caminero, E. and Barrio, R. (2008) 'Smt3 is required for Drosophila melanogaster metamorphosis', *Development*, 135(9), pp. 1659-68.

Tanaka, K., Nishide, J., Okazaki, K., Kato, H., Niwa, O., Nakagawa, T., Matsuda, H., Kawamukai, M. and Murakami, Y. (1999) 'Characterization of a fission yeast SUMO-1 homologue, pmt3p, required for multiple nuclear events, including the control of telomere length and chromosome segregation', *Mol Cell Biol*, 19(12), pp. 8660-72.

Tatham, M.H., Jaffray, E., Vaughan, O.A., Desterro, J.M., Botting, C.H., Naismith, J.H. and Hay, R.T. (2001) 'Polymeric chains of SUMO-2 and SUMO-3 are conjugated to protein substrates by SAE1/SAE2 and Ubc9', *J Biol Chem*, 276(38), pp. 35368-74.

Taylor, D.L., Ho, J.C., Oliver, A. and Watts, F.Z. (2002) 'Cell-cycle-dependent localisation of Ulp1, a Schizosaccharomyces pombe Pmt3 (SUMO)-specific protease', *J Cell Sci*, 115(Pt 6), pp. 1113-22.

Tong, A.H. and Boone, C. (2006) 'Synthetic genetic array analysis in Saccharomyces cerevisiae', *Methods Mol Biol*, 313, pp. 171-92.

Tong, A.H., Evangelista, M., Parsons, A.B., Xu, H., Bader, G.D., Page, N., Robinson, M., Raghibizadeh, S., Hogue, C.W., Bussey, H., Andrews, B., Tyers, M. and Boone, C. (2001) 'Systematic genetic analysis with ordered arrays of yeast deletion mutants', *Science*, 294(5550), pp. 2364-8.

Truong, K., Lee, T.D. and Chen, Y. (2012) 'Small ubiquitin-like modifier (SUMO) modification of E1 Cys domain inhibits E1 Cys domain enzymatic activity', *J Biol Chem*, 287(19), pp. 15154-63.

Urulangodi, M., Sebesta, M., Menolfi, D., Szakal, B., Sollier, J., Sisakova, A., Krejci, L. and Branzei, D. (2015) 'Local regulation of the Srs2 helicase by the SUMO-like domain protein Esc2 promotes recombination at sites of stalled replication', *Genes Dev*, 29(19), pp. 2067-80.

Uzunova, K., Gottsche, K., Miteva, M., Weisshaar, S.R., Glanemann, C., Schnellhardt, M., Niessen, M., Scheel, H., Hofmann, K., Johnson, E.S., Praefcke, G.J. and Dohmen, R.J. (2007) 'Ubiquitin-dependent proteolytic control of SUMO conjugates', *J Biol Chem*, 282(47), pp. 34167-75.

Van Damme, E., Laukens, K., Dang, T.H. and Van Ostade, X. (2010) 'A manually curated network of the PML nuclear body interactome reveals an important role for PML-NBs in SUMOylation dynamics', *Int J Biol Sci*, 6(1), pp. 51-67.

Veal, E.A., Day, A.M. and Morgan, B.A. (2007) 'Hydrogen peroxide sensing and signaling', *Mol Cell*, 26(1), pp. 1-14.

Veaute, X., Jeusset, J., Soustelle, C., Kowalczykowski, S.C., Le Cam, E. and Fabre, F. (2003) 'The Srs2 helicase prevents recombination by disrupting Rad51 nucleoprotein filaments', *Nature*, 423(6937), pp. 309-12.

Vermeulen, K., Van Bockstaele, D.R. and Berneman, Z.N. (2003) 'The cell cycle: a review of regulation, deregulation and therapeutic targets in cancer', *Cell Prolif*, 36(3), pp. 131-49.

Vertegaal, A.C., Ogg, S.C., Jaffray, E., Rodriguez, M.S., Hay, R.T., Andersen, J.S., Mann, M. and Lamond, A.I. (2004) 'A proteomic study of SUMO-2 target proteins', *J Biol Chem*, 279(32), pp. 33791-8.

Vigodner, M., Shrivastava, V., Gutstein, L.E., Schneider, J., Nieves, E., Goldstein, M., Feliciano, M. and Callaway, M. (2013) 'Localization and identification of sumoylated proteins in human sperm: excessive sumoylation is a marker of defective spermatozoa', *Hum Reprod*, 28(1), pp. 210-23.

Voth, W.P., Yu, Y., Takahata, S., Kretschmann, K.L., Lieb, J.D., Parker, R.L., Milash, B. and Stillman, D.J. (2007) 'Forkhead proteins control the outcome of transcription factor binding by antiactivation', *Embo j*, 26(20), pp. 4324-34.

Wan, J., Subramonian, D. and Zhang, X.D. (2012) 'SUMOylation in control of accurate chromosome segregation during mitosis', *Curr Protein Pept Sci*, 13(5), pp. 467-81.

Wang, C., Tao, W., Ni, S., Chen, Q., Zhao, Z., Ma, L., Fu, Y. and Jiao, Z. (2015) 'Tumor-suppressive microRNA-145 induces growth arrest by targeting SENP1 in human prostate cancer cells', *Cancer Sci*, 106(4), pp. 375-82.

Wang, J., Taherbhoy, A.M., Hunt, H.W., Seyedin, S.N., Miller, D.W., Miller, D.J., Huang, D.T. and Schulman, B.A. (2010) 'Crystal structure of UBA2(ufd)-Ubc9: insights into E1-E2 interactions in Sumo pathways', *PLoS One*, 5(12), p. e15805.

Warren, D.T., Andrews, P.D., Gourlay, C.W. and Ayscough, K.R. (2002) 'Sla1p couples the yeast endocytic machinery to proteins regulating actin dynamics', *J Cell Sci*, 115(Pt 8), pp. 1703-15.

Wasch, R. and Cross, F.R. (2002) 'APC-dependent proteolysis of the mitotic cyclin Clb2 is essential for mitotic exit', *Nature*, 418(6897), pp. 556-62.

Watts, F.Z. (2013) 'Starting and stopping SUMOylation. What regulates the regulator?', *Chromosoma*, 122(6), pp. 451-63.

Weeraratna, A.T., Kalehua, A., Deleon, I., Bertak, D., Maher, G., Wade, M.S., Lustig, A., Becker, K.G., Wood, W., 3rd, Walker, D.G., Beach, T.G. and Taub, D.D. (2007) 'Alterations in immunological and neurological gene expression patterns in Alzheimer's disease tissues', *Exp Cell Res*, 313(3), pp. 450-61.

Weger, S., Hammer, E. and Heilbronn, R. (2005) 'Topors acts as a SUMO-1 E3 ligase for p53 *in vitro* and *in vivo*', *FEBS Lett*, 579(22), pp. 5007-12.

Wei, L. and Zhao, X. (2016) 'A new MCM modification cycle regulates DNA replication initiation', *Nat Struct Mol Biol*, 23(3), pp. 209-16.

Wen, D., Xu, Z., Xia, L., Liu, X., Tu, Y., Lei, H., Wang, W., Wang, T., Song, L., Ma, C., Xu, H., Zhu, W., Chen, G. and Wu, Y. (2014) 'Important role of SUMOylation of Spliceosome factors in prostate cancer cells', *J Proteome Res*, 13(8), pp. 3571-82.

Westerbeck, J.W., Pasupala, N., Guillotte, M., Szymanski, E., Matson, B.C., Esteban, C. and Kerscher, O. (2014) 'A SUMO-targeted ubiquitin ligase is involved in the degradation of the nuclear pool of the SUMO E3 ligase Siz1', *Mol Biol Cell*, 25(1), pp. 1-16.

Wierstra, I. (2013) 'FOXM1 (Forkhead box M1) in tumorigenesis: overexpression in human cancer, implication in tumorigenesis, oncogenic functions, tumor-suppressive properties, and target of anticancer therapy', *Adv Cancer Res*, 119, pp. 191-419.

Wimmer, P., Schreiner, S. and Dobner, T. (2012) 'Human pathogens and the host cell SUMOylation system', *J Virol*, 86(2), pp. 642-54.

Windecker, H. and Ulrich, H.D. (2008) 'Architecture and assembly of poly-SUMO chains on PCNA in Saccharomyces cerevisiae', *J Mol Biol*, 376(1), pp. 221-31.

Winter, D., Choe, E., Li, R. (1999) 'Genetic dissection of the budding yeast Arp2/3 complex: A comparison of the in vivo and structural roles of the individual subunits', *Proc Natl Acad Sci U S A*, 96(13), pp. 7288-7293.

Winter, D., Podtelejnikov, A.V., Mann, M. and Li, R. (1997) 'The complex containing actin-related proteins Arp2 and Arp3 is required for the motility and integrity of yeast actin patches', *Curr Biol*, 7(7), pp. 519-29.

Witty, J., Aguilar-Martinez, E. and Sharrocks, A.D. (2010) 'SENP1 participates in the dynamic regulation of Elk-1 SUMOylation', *Biochem J*, 428(2), pp. 247-54.

Wohlschlegel, J.A., Johnson, E.S., Reed, S.I. and Yates, J.R., 3rd (2004) 'Global analysis of protein sumoylation in Saccharomyces cerevisiae', *J Biol Chem*, 279(44), pp. 45662-8.

Wu, F., Zhu, S., Ding, Y., Beck, W.T. and Mo, Y.Y. (2009) 'MicroRNA-mediated regulation of Ubc9 expression in cancer cells', *Clin Cancer Res*, 15(5), pp. 1550-7.

Xu, J., He, Y., Qiang, B., Yuan, J., Peng, X. and Pan, X.M. (2008a) 'A novel method for high accuracy sumoylation site prediction from protein sequences', *BMC Bioinformatics*, 9, p. 8.

Xu, Z., Lam, L.S., Lam, L.H., Chau, S.F., Ng, T.B. and Au, S.W. (2008b) 'Molecular basis of the redox regulation of SUMO proteases: a protective mechanism of intermolecular disulfide linkage against irreversible sulfhydryl oxidation', *FASEB J*, 22(1), pp. 127-37.

Yang, S.H. and Sharrocks, A.D. (2004) 'SUMO promotes HDAC-mediated transcriptional repression', *Mol Cell*, 13(4), pp. 611-7.

Yang, S.H. and Sharrocks, A.D. (2005) 'PIASx acts as an Elk-1 coactivator by facilitating derepression', *Embo j*, 24(12), pp. 2161-71.

Yang, S.H., Galanis, A., Witty, J. and Sharrocks, A.D. (2006) 'An extended consensus motif enhances the specificity of substrate modification by SUMO', *EMBO J*, 25(21), pp. 5083-93.

Yang, S.H., Jaffray, E., Hay, R.T. and Sharrocks, A.D. (2003) 'Dynamic interplay of the SUMO and ERK pathways in regulating Elk-1 transcriptional activity', *Mol Cell*, 12(1), pp. 63-74.

Yang, W., Sheng, H., Warner, D.S. and Paschen, W. (2008) 'Transient focal cerebral ischemia induces a dramatic activation of small ubiquitin-like modifier conjugation', *J Cereb Blood Flow Metab*, 28(5), pp. 892-6.

Yeh, E.T.H. (2009) 'SUMOylation and De-SUMOylation: Wrestling with Life's Processes', *The Journal of Biological Chemistry*, 284(13), pp. 8223-8227.

Yeh, J. and Haarer, B.K. (1996) 'Profilin is required for the normal timing of actin polymerization in response to thermal stress', *FEBS Lett*, 398(2-3), pp. 303-7.

Yoo, Y., Wu, X. and Guan, J.L. (2007) 'A novel role of the actin-nucleating Arp2/3 complex in the regulation of RNA polymerase II-dependent transcription', *J Biol Chem*, 282(10), pp. 7616-23.

Yunus, A.A. and Lima, C.D. (2009) 'Structure of the Siz/PIAS SUMO E3 Ligase Siz1 and Determinants Required for SUMO Modification of PCNA', *Molecular Cell*, 35(5), pp. 669-682.

Zeman, M.K. and Cimprich, K.A. (2014) 'Causes and consequences of replication stress', *Nat Cell Biol*, 16(1), pp. 2-9.

Zhang, J., Yuan, C., Wu, J., Elsayed, Z. and Fu, Z. (2015) 'Polo-like kinase 1-mediated phosphorylation of Forkhead box protein M1b antagonizes its SUMOylation and facilitates its mitotic function', *J Biol Chem*, 290(6), pp. 3708-19.

Zhang, N., Wu, X., Yang, L., Xiao, F., Zhang, H., Zhou, A., Huang, Z. and Huang, S. (2012) 'FoxM1 inhibition sensitizes resistant glioblastoma cells to temozolomide by downregulating the expression of DNA-repair gene Rad51', *Clin Cancer Res*, 18(21), pp. 5961-71.

Zhang, Y.Q. and Sarge, K.D. (2008) 'Sumoylation of amyloid precursor protein negatively regulates Abeta aggregate levels', *Biochem Biophys Res Commun*, 374(4), pp. 673-8.

Zhao, X. and Blobel, G. (2005) 'A SUMO ligase is part of a nuclear multiprotein complex that affects DNA repair and chromosomal organization', *Proc Natl Acad Sci U S A*, 102(13), pp. 4777-82.

Zhao, Y., Kwon, S.W., Anselmo, A., Kaur, K. and White, M.A. (2004) 'Broad spectrum identification of cellular small ubiquitin-related modifier (SUMO) substrate proteins', *J Biol Chem*, 279(20), pp. 20999-1002.

Zhou, H., Monack, D.M., Kayagaki, N., Wertz, I., Yin, J., Wolf, B. and Dixit, V.M. (2005) 'Yersinia virulence factor YopJ acts as a deubiquitinase to inhibit NF-κB activation', *The Journal of Experimental Medicine*, 202(10), pp. 1327-1332.

Zhou, W., Ryan, J.J. and Zhou, H. (2004) 'Global analyses of sumoylated proteins in Saccharomyces cerevisiae. Induction of protein sumoylation by cellular stresses', *J Biol Chem*, 279(31), pp. 32262-8.

Zilahi, E., Salimova, E., Simanis, V. and Sipiczki, M. (2000) 'The *S. pombe* sep1 gene encodes a nuclear protein that is required for periodic expression of the cdc15 gene', *FEBS Lett*, 481(2), pp. 105-8.